DISS. ETH NO. 27102

Bacterial Sensing in the Intestinal Mucosa and Consequences Thereof

A Thesis submitted to attain the degree of

DOCTOR of SCIENCE ETH ZURICH

(Dr. sc. ETH Zurich)

presented by

Annika Hausmann

M. Sc. Molecular Medicine, Universität Freiburg

Born May 1989 in Cologne

Citizen of Germany

Accepted on the recommendation of

Prof. Dr. Wolf-Dietrich Hardt

Prof. Dr. Mikael Sellin

Prof. Dr. Kevin Maloy

Dr. Roman Spörri

2020

Like what you do, and you will do your best

- *Katherine Johnson*

TABLE OF CONTENTS

SUMMARY

The innate immune system confers fast protection from pathogenic threats. To achieve this task, it relies on invariant pattern recognition receptors (PRRs), which bind conserved microbe-associated patterns. At systemic sites, which are naturally devoid of bacteria, inflammation efficiently clears microbial intruders upon detection. By contrast, the intestinal mucosa represents an interesting exception. Its localization at the interface between the sterile host body compartment and the intestinal lumen containing high densities of commensal bacteria requires specific regulatory mechanisms to ensure peaceful coexistence with the commensal microbiota, and protection from enteropathogens at the same time. To date, it remains incompletely understood how the regulation of bacterial sensing in the intestinal mucosa facilitates the differentiation between pathogenic and commensal bacteria.

In this work, I have employed the model enteropathogen *Salmonella* Typhimurium (*S*. Tm) to probe and dissect innate immune responses in the intestinal mucosa, focusing on the roles of the PRRs TLR4 and NLRC4.

I found that intestinal epithelial cells (IECs) in the adult, homeostatic mucosa do not directly sense LPS via TLR4 and instead form an extracellular LPS-inert physical barrier to prevent bacterial translocation into the lamina propria. Sentinel $CD11b^{+}$ $CD103^{-}$ mononuclear phagocytes, by contrast, stretch out in the intercrypt lamina propria underneath the epithelium and react swiftly with TNF production upon TLR4 stimulation. This induces localized epithelial NFκB activation, which results in the secretion of direct epithelial immune effectors such as C3 and Reg3γ, and of chemokines for the recruitment of immune cells.

Previous work established the NAIP/NLRC4 inflammasome as an important epithelial-intrinsic protection for the restriction of mucosal *S*. Tm loads by expulsion of infected IECs. *Nlrc4*$^{-/-}$ mice also carry increased *S*. Tm loads in their mLN. Immune cell NAIP/NLRC4 was implicated in the restriction of intracellular pathogens before, which suggested that immune cells might be responsible for this systemic NAIP/NLRC4-mediated protection. By contrast, *S*. Tm evades immune cell NAIP/NLRC4 detection by rapid downregulation of the NAIP/NLRC4 ligands flagella and TTSS-1 upon entry into the intestinal mucosa. Therefore, while immune cell NAIP/NLRC4 has a protective potential to restrict intracellular *S*. Tm replication, *S*. Tm evades this restriction. The necessity of the flagella and TTSS-1 for epithelial invasion, by contrast, prevents the evasion of epithelial NAIP/NLRC4 recognition and therefore positions IECs ideally for the NAIP/NLRC4-mediated restriction of mucosal *S*. Tm loads. NAIP/NLRC4-mediated expulsion of infected IECs consequently controls the migration of *S*. Tm to systemic sites and ultimately protects from increased systemic pathogen loads.

The two PRRs analyzed here fulfill their protective functions in compartments of the intestinal mucosa, which are usually devoid of bacteria: the lamina propria (TLR4) and the host cell cytosol (NLRC4). In conclusion, they employ the pathogen-associated feature of invasiveness to differentiate between commensal and harmful bacteria. The equipment of physiologically bacteria-free compartments of the mucosa with PRRs thereby enables the detection of enteropathogen invasion and/or sensing of barrier malfunctions while preventing immune activation by commensals.

Finally, I have assessed the potential of organoids as an *ex vivo* model to assess IEC physiology and function. Recently, intestinal epithelial organoids have emerged as a relevant model system. In the presented work, I have validated organoids as a realistic, reproducible model for IECs *in vivo*, and I have shown that their physiology in homeostasis and upon TNF stimulation is largely independent of donor-derived microbiota imprints. This will be the basis for future mechanistic work on the role of IECs in pathogen defense.

Several features complicate the analysis of host-microbe interactions in the intestine: i) their complex, reciprocal spatiotemporal kinetics, ii) the sensitivity to microbiota changes, and iii) the need for good model systems to identify and quantify the contribution of specific cell types to host-microbe interactions. In the presented work, I discuss the applicability of mechanistic mathematical models in combination with genetic tagging approaches to decipher the complex interactions of host-microbe relationships and emphasize the importance of *in vivo* models to confirm the relevance of identified mechanisms. Furthermore, I discuss the importance of controlling for microbiota differences by the use of wild type littermate controls for transgenic mice.

My findings advance our understanding of bacterial sensing in the intestinal mucosa during *S*. Tm infection and establish versatile *in vivo* and *ex vivo* systems for assessing the contributions of different cell types to host-microbe crosstalk. This is an important step towards deciphering the complex network which regulates intestinal homeostasis and protects the intestinal mucosa from bacterial infection.

ZUSAMMENFASSUNG

Das angeborene Immunsystem bietet einen schnell reagierenden Schutz vor pathogenen Bedrohungen. Die Basis dafür sind Mustererkennungsrezeptoren, die konservierte, mikroben-assoziierte Strukturen erkennen. In systemischen Organen des Wirts, die phsyiologisch keine Bakterien enthalten, können bakterielle Eindringlinge somit schnell und effizient durch eine Immunantwort eliminiert werden. Die Darmmukosa stellt dagegen eine interessante Ausnahme dar. Ihre Lokalisation zwischen dem sterilen Wirts-Kompartiment und dem mit kommensalen Bakterien gefüllten Darmlumen erfordert spezifische regulierende Mechanismen, um eine friedliche Koexistenz mit der Mikrobiota bei gleichzeitigem Schutz vor Enteropathogenen zu ermöglichen. Bis heute ist nicht vollständig verstanden, wie die Regulation von bakterieller Detektion in der Darmmukosa die Unterscheidung von kommensalen und pathogenen Bakterien ermöglicht.

In der vorliegenden Arbeit habe ich das Modellenteropathogen *Salmonella* Typhimurium (*S*. Tm) verwendet, um angeborene Immunantworten in der Darmmukosa zu aktivieren und ihre Komponenten zu analysieren. Dabei habe ich mich auf die Mustererkennungsrezeptoren TLR4 und NLRC4 fokussiert.

Ich habe herausgefunden, dass Darmepithelzellen in der adulten, homöostatischen Darmmukosa LPS nicht direkt über TLR4 detektieren. Im Gegenteil bilden sie eine physikalische, für extrazelluläres LPS inaktive, Barriere, um bakterielle Invasion in die Lamina Propria zu verhindern. Stattdessen ist die Darmmukosa mit $CD11b^{+}$ $CD103^{-}$ mononukleären Wächterphagozyten ausgestattet, die ausgestreckt in der Lamina Propria zwischen den Krypten in unmittelbarer Nähe zum Epithel liegen. Diese reagieren schnell mit der Produktion von TNF auf die Stimulation mit LPS. Dies führt zu einer lokalen Aktivierung des NFκB-Signalwegs in Darmepithelizellen, die daraufhin direkte Immuneffektoren wie C3 und Reg3γ sekretieren sowie Chemokine, um Immunzellen zu rekrutieren.

Vorherige Studien haben NAIP/NLRC4 als einen wichtigen, epithel-intrinsischen Schutzeffektor identifiziert, der eine mukosale *S*. Tm Akkumulation durch das Ausstoβen infizierter Darmepithelzellen aus dem Epithelverband verhindert. *Nlrc4*$^{-/-}$ Mäuse haben nicht nur erhöhte Pathogenlasten in der Darmmuksoa, sondern auch in den mesenterischen Lymphknoten. Immunzell-NAIP/NLRC4 soll auch eine Rolle in der Kontrolle intrazellulärer Pathogene spielen und könnte dementsprechend in diese systemische Kontrolle der Pathogenlast involviert sein. *S*. Tm reguliert allerdings die Expression von Flagellen und dem Typ-Drei-Sekretionssystem - den Molekülen die durch NAIP/NLRC4 erkannt werden - herunter, sobald sie die Darmmukosa invadiert haben. Dadurch verhindert *S*. Tm die Detektion durch Immunzellen, obwohl diese durchaus das Potential haben, *S*. Tm über NAIP/NLRC4 zu detektieren. Die Notwendigkeit für *S*. Tm, Flagellen und das Typ-3-Sekretionssystem für die Invasion in Darmepthelzellen zu exprimieren, verhindert dagegen das Ausweichen der Detektion durch epitheliales NAIP/NLRC4 und positioniert die Darmepithelzellen ideal für eine effiziente Detektion von *S*. Tm. Das Ausstoβen infizierter Darmepithelzellen über NAIP/NLRC4 kontrolliert dadurch die systemische Migration von *S*. Tm und schützt somit letzlich vor hohen systemischen Pathogenlasten.

Die beiden hier analysierten Mustererkennungsrezeptoren führen ihre schützenden Funktionen in Kompartimenten der Mukosa aus, die physiologisch frei von Bakterien sind: die Lamina Propria (TLR4) und das Zytosol von Wirtszellen (NLRC4). Sie nutzen also die Pathogen-assoziierte Eigenschaft der Invasion als

Unterscheidungsmerkmal zwischen kommensalen und pathogenen Bakterien. Die Ausrüstung von physiologisch bakterienfreien Kompartimenten der Darmmukosa mit Mustererkennungsrezeptoren ermöglicht somit die Detektion von Enteropathogen-Angriffen und/oder Barrieredefekten und verhindert gleichzeitig eine Immunaktivierung durch kommensale Bakterien.

Schlussendlich habe ich das Potential von Organoiden als *ex vivo* Modell zur Untersuchung von Epithelzellphysiologie und -funktion analysiert. Darmepithelorganoide etablieren sich mehr und mehr als relevantes Modellsystem. In der vorliegenden Arbeit habe ich Organoide als realistisches, reproduzierbares Modell validiert, dessen Physiologie in Homöostase und nach TNF Stimulation weitgehend unabhängig von der Mikrobiota der Donoren ist. Dies ist die Basis für die zukünftige, mechanistische Untersuchung der Rolle von Darmepithelzellen in der Interkation mit Mikroben.

Mehrere Eigenschaften erschweren die Analyse von Wirt-Bakterien Interaktionen im Darm: i) ihre komplexe, reziproke raumzeitliche Kinetik, ii) die Sensitivität für Veränderungen der Mikrobiota, und iii) der Bedarf an guten Modellsystemen, die die Identifizierung und Quantifizierung der Beiträge verschiedener Zellytpen zu Immunantworten erlauben. In der vorliegenden Arbeit diskutiere ich die Anwendbarkeit von mechanistischen mathematischen Modellen in Kombination mit neutralen genetischen Markierungen, um die komplexen Zusammenhänge in Wirt-Bakterien Interaktionen zu entziffern, und betone die Wichtigkeit von *in vivo* Modellen, um die Relevanz identifizierter Mechanismen zu bestätigen. Desweiteren diskutiere ich die Wichtigkeit der Kontrolle von Mikrobiota-Unterschieden in transgenen Mäusen durch Wildtypgeschwister.

Meine Erkenntnisse erweitern das Verständnis der bakteriellen Detektion in *S*. Tm Infektionen, und etablieren vielseitige *in vivo* und *ex vivo* Modelle zur Identifikation des Beitrages von verschiedenen Zelltypen zur Kommunikation zwischen Wirt und Mikroben. Dies ist ein wichtiger Schritt zur Entzifferung des komplexen Netzwerkes, das Darmhomöostase und den Schutz vor bakteriellen Infektionen ermöglicht.

CHAPTER 1 - GENERAL INTRODUCTION

The content of this chapter was partially adapted (as indicated) from the following publication:

The Interplay between *Salmonella enterica* Serovar Typhimurium and the Intestinal Mucosa during Oral Infection

Annika Hausmann[1] and Wolf-Dietrich Hardt[1]

Author Affiliations:

[1]Institute of Microbiology, D-BIOL, ETH Zurich, Zurich, Switzerland

Author Contributions:

AH and WDH designed the scope of the review. AH wrote the manuscript with corrections and suggestions by WDH.

Published in Microbiology Spectrum, 05.04.2019. Doi: 10.1128/microbiolspec.BAI-0004-2019

Sections adapted from that manuscript are clearly indicated with "adapted from Hausmann and Hardt, Microbiology Spectrum"

THE IMMUNE SYSTEM OF THE INTESTINAL MUCOSA

(adapted from Hausmann and Hardt, Microbiology Spectrum 2019)

The gastrointestinal tract mediates the uptake of nutrients and water. After pre-digestion in the stomach, the intestine - consisting of small intestine, cecum and colon - breaks up food particles into nutrients and absorbs them. In addition to host-secreted digestive enzymes, microbes within the intestine break down food molecules and thereby enable the full utilization of food-derived nutrients (Figure 1) (Samuel and Gordon, 2006). These microbes form the microbiota, which contributes not only to digestion, but also to maturation of the immune system (Gomez de Agüero et al., 2016; Trompette et al., 2018) and protection from colonization with enteropathogens ("colonizkation resistance" (CR) (Stecher and Hardt, 2008; Stecher et al., 2007)) and affects host physiology (Samuel and Gordon, 2006). The microbiota is therefore highly beneficial for its hosts. In spite of these beneficial effects, commensals share conserved molecules with pathogenic bacteria. This creates a critical detection problem for the mucosal immune system at the interface between the sterile compartment of the host`s body and the gut luminal environment containing the microbiota. Pathogens are regularly ingested, requiring immune surveillance of the intestine to avoid infections. However, no immune response is mounted against commensals in healthy individuals (Corridoni et al., 2018). Thus, the intestine provides a fascinating system to study how the delicate balance of peaceful co-habitation with the commensal microbiota is maintained and how specific defense against pathogen attack is achieved (Mowat and Agace, 2014).

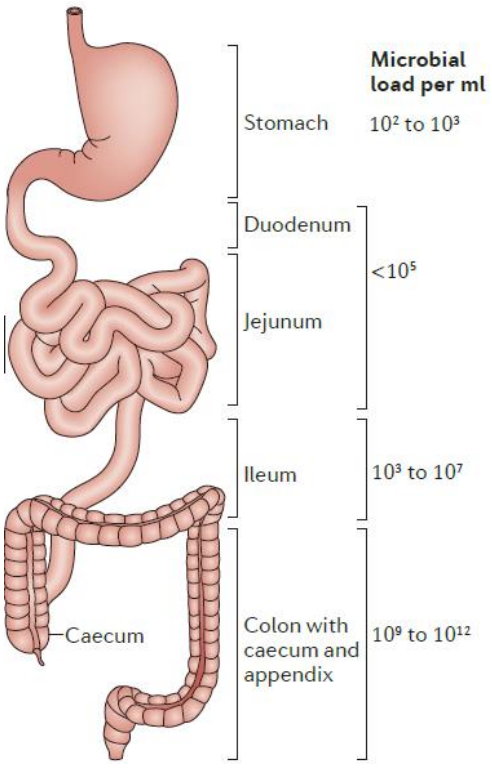

Figure 1 ***The structure of the gastrointestinal tract*** *and varying microbial densities along the intestinal axis. Adapted from Mowat and Agace, 2014*

COMPONENTS OF THE INTESTINAL IMMUNE SYSTEM

(adapted from Hausmann and Hardt, Microbiology Spectrum 2019 as indicated)

MICROBIOTA

The intestinal microbiota, consisting of bacteria, viruses, fungi and protozoa (Ducarmon et al., 2019), colonizes the intestinal lumen and engages in a symbiotic relationship with the host (Figure 2). Bacteria are the best-studied component of the microbiota. Bacterial density varies along the intestinal tract and is highest in the colon, where it reaches levels of ~10^{11} bacteria/ml content (Sender et al., 2016).

The microbiota trains and modulates the immune system within and beyond the mucosa (Cahenzli et al., 2013). Microbiota-derived soluble metabolites reach distant sites via the blood stream, where they impact host defense against bacterial (McDonald et al., 2020) and viral (Trompette et al., 2018) infections, as well as predisposition for allergy and chronic inflammatory diseases (Gollwitzer and Marsland, 2015; Gollwitzer et al., 2014; Gomez de Agüero et al., 2016; Trompette et al., 2014).

Besides its influence on host cells, the microbiota also directly protects from enteropathogen colonization by providing CR (Kreuzer and Hardt, 2020; Wotzka et al., 2017). Several mechanisms contribute to this phenomenon: i) inhibition of enteropathogens via microbiota-derived metabolites such as short chain fatty acids (SCFAs) (Hung et al., 2013; Jacobson et al., 2018) or secondary bile acids (Thanissery et al., 2017; Watanabe et al., 2017), ii) direct killing of enteropathogens by microbiota members via bacteriocins or the Type six secretion system (Ross et al., 2019; Sassone-Corsi et al., 2016), iii) depletion of specific enteropathogens by bacteriophages present in the microbiota (Duan et al., 2019; Yen et al., 2017) and iv) depletion of nutrients by the microbiota (Maltby et al., 2013; Momose et al., 2008). CR requires an intact microbiota. Perturbances of the microbiota, e.g. by antibiotic treatment (Barthel et al., 2003), diet shifts (Wotzka et al., 2019) or inflammation (Stecher et al., 2007) can alleviate CR and result in higher susceptibility to enteropathogen infection (see below).

Taken together, the microbiota has a complex impact on the intestinal environment. Consequently, microbiota differences result in differences in CR (Brugiroux et al., 2016). Oral infections are therefore highly sensitive to microbiota variations, which makes the control of microbiota-mediated effects imperative for the design of conclusive studies of host-microbe interaction (Mamantopoulos et al., 2018).

MUCUS LAYER

(adapted from Hausmann and Hardt, Microbiology Spectrum 2019)

Goblet cells produce mucins (mainly MUC2), gel-forming glycoproteins, to build the mucus layer (Johansson and Hansson, 2016). The mucus layer is best characterized in the murine colon, where it is organized in two layers. The inner layer close to the epithelium is ~50 µm thick, viscous, dense in MUC2 and devoid of bacteria. Bacteria populate and degrade the outer mucus layer, which is ~100 µm thick (Figure 2). Together, the two mucus layers act as a protective filter which keeps bacteria at a distance while allowing free diffusion of amino acids, sugars and small molecular compounds (Johansson et al., 2008, 2011).

Muc2$^{-/-}$ mice are unable to produce a mucus layer. They remain healthy if held under germ-free conditions. Upon colonization with a pathogen-free microbiota, bacteria engage in direct contact with the epithelium. Under these conditions, *Muc2*$^{-/-}$ mice develop colitis by 7 weeks of age and are predisposed to

colon cancer (Johansson et al., 2008). This underlines the importance of mucus for the maintenance of intestinal homeostasis in the context of a commensal microbiota. Interestingly, a dense mucus layer exists only in the colon and the stomach. By contrast, the mucus in the small intestine is organized discontinuously in clouds between the villi (Johansson et al., 2011) and the cecal mucus localizes specifically in the crypts within the epithelium, leaving the epithelium between crypts unprotected. Interestingly, this difference between the cecal and colonic mucus layer contributes to the different *Salmonella* Typhimurium (*S*. Tm) invasion rates into these tissues during oral infection (Furter et al., 2019).

The colonic epithelium is equipped with sentinel goblet cells located in the apical part of the crypts to specifically detect breaches of the mucus layer. These cells recognize pathogen associated molecular patterns (PAMPs) of bacterial intruders in the inner mucus layer via toll-like receptors (TLRs) and the nucleotide-binding oligomerization domain (NOD) like receptor (NLR) family pyrin domain containing (NLRP) 6 inflammasome. They react by signaling via gap junctions to induce coordinated mucus secretion, pushing the intruding bacteria away from the epithelial surface (Birchenough et al., 2016; Wlodarska et al., 2014). Global mucus secretion is triggered by Interferon (IFN)γ signaling, which is abundant during mucosal *S*. Tm infection (Klose et al., 2013; Songhet et al., 2011). Taken together, this emphasizes the crucial role of mucus architecture and its shielding functions in protection from pathogenic threats, which can be tuned in response to defined stimuli.

ANTIMICROBIAL PEPTIDES

(adapted from Hausmann and Hardt, Microbiology Spectrum 2019)

Another factor in the maintenance of intestinal microbial homeostasis and the defense against pathogens are antimicrobial peptides (AMPs). Intestinal epithelial cells (IECs) express several different AMPs, including defensins, cathelicidins, Lipocalin and the lectin-family Reg3. Low levels of AMPs expressed in the unperturbed mucosa promote homeostasis, i.e. by maintaining a favorable microbiota composition and by preventing microbiota penetration of the epithelial barrier (Figure 2) (Cullen et al., 2015; Miki et al., 2017a). Lipocalin and the Reg3 lectins are strongly induced upon bacterial infection (Miki et al., 2017b; Raffatellu et al., 2009; Stelter et al., 2011). Intestinal dendritic cells (DCs) contribute to this response. Upon sensing of microbial products (e.g. flagellin), they elicit a signaling cascade involving Interleukin (IL)23, innate lymphoid cells (ILCs) and IL22, a strong inducer of AMP production in IECs (see below) (Kinnebrew et al., 2012). Thus, the AMP-mediated chemical barrier is tunable in response to infection.

AMPs play main roles in the defense against a variety of intestinal pathogens (Brandl et al., 2007; Dessein et al., 2009; Loonen et al., 2014; Miki and Hardt, 2013; Zheng et al., 2008). However, in some cases, AMP production can also promote, instead of preventing, disease. In oral *S*. Tm infections, Reg3β delays remission from acute *S*. Tm enterocolitis by suppressing the regrowth of certain microbiota species, especially *Bacteroides* spp. (Miki et al., 2017b). While *S*. Tm is resistant to Reg3β and Lipocalin (Miki et al., 2017b; Raffatellu et al., 2009), key members of the microbiota are highly susceptible. Thus, by eliciting an antibacterial response program, the host keeps the intestinal niche open for *S*. Tm through depletion of the resident microbiota.

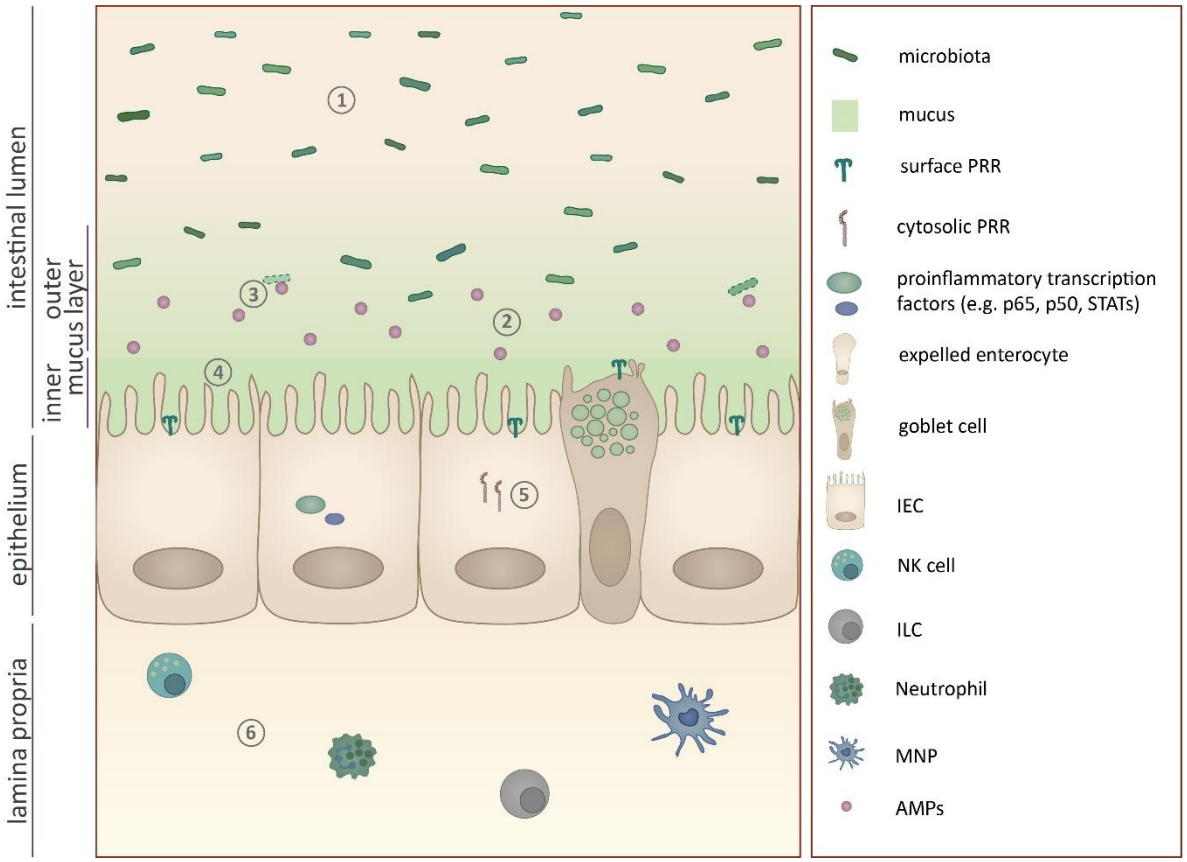

Figure 2 ***Innate immune mechanisms in the intestinal mucosa under homeostasis.*** *The innate immune system of the intestinal mucosa is organized in several layers. This comprises 1) the occupation of the intestinal lumen by the microbiota, 2) the mucus layer containing 3) AMPs, and 4) the epithelium equipped with 5) PRRs for recognition of intracellular bacteria as physical barriers between intestinal lumen and sterile lamina propria, which is surveilled by 6) immune cells. Adapted from Hausmann and Hardt 2019.*

INTESTINAL EPITHELIAL CELLS

The intestinal epithelium consists of a single layer of IECs, which lines the intestine along the whole cephalocaudal axis (Figure 2) (Mowat and Agace, 2014). The basal membrane anchors IECs in the mucosa. Cell-cell connections by tight junctions prevent leakage of luminal content into the mucosa and thereby ensure epithelial barrier function. Apically, the epithelial plasma membrane forms protrusions which enlarge the luminal epithelial surface for efficient exchange of water, metabolites, enzymes and antibacterial factors between the intestinal mucosa and the lumen. This surface enlargement is especially pronounced in the small intestine, where the epithelium forms long protrusions, villi, into the intestinal lumen. In accordance, the small intestine is the major site of secretion of digestive enzymes and nutrient absorption (Mowat and Agace, 2014). Between the villi, the epithelium forms invaginations, which are called crypts. These crypts exist along the whole axis of the intestine, while villi are only present in the small intestine. Leucine-rich repeat-containing G-protein coupled receptor (Lgr)5^{+} stem cells ensuring the constant renewal of the epithelium reside in the bottom of those crypts and give rise to transient amplifying cells (Barker et al., 2007). These transient amplifying cells proliferate and differentiate into IEC subtypes while migrating upwards along the crypt axis (Gehart and Clevers, 2019; Marshman et al., 2002). This dynamic process of proliferation, maturation, and shedding of mature IECs at the apical side of the

crypt into the intestinal lumen ensures constant epithelial renewal (Figure 3) (Gehart and Clevers, 2019; Santos et al., 2018). This renewal of the apical crypt part typically takes ~4d.

The epithelium harbors a variety of IEC subtypes. Besides nutrient absorption and simply constituting a physical barrier between intestinal lumen and mucosa, IECs actively contribute to digestion and antibacterial responses (Maloy and Powrie, 2011). Enterocytes absorb nutrients and water and perform metabolic and digestive functions. Mature enterocytes in the upper part of the crypt metabolize microbiota-derived SCFAs by oxygen consuming β-oxidation and thereby contribute to an anaerobic environment in the intestinal lumen. Enterocytes close to the crypt base, by contrast, anaerobically ferment glucose to lactate (Allaire et al., 2018). Goblet cells produce mucins to form the protective mucus layer, which shields the epithelium from direct contact with the luminal microbes. Goblet cell abundance increases along the intestinal tract, reaching the highest density in the colon where they make up up to 25% of IECs (Allaire et al., 2018; Mowat and Agace, 2014; Peterson and Artis, 2014). Paneth cells specifically localize in the crypt base of the small intestine. In contrast to the remaining IEC subtypes, they migrate downwards the crypt upon differentiation and are long-lived. At the crypt base they contribute to the maintenance of the stem cell niche, e.g. by secretion of the stem cell factor Wnt (Santos et al., 2018). Furthermore, Paneth cells produce antimicrobial peptides like Reg3γ, Lysozyme and defensins, which protect the stem cell niche from bacterial threats and contribute to epithelial barrier function (Peterson and Artis, 2014). Enteroendocrine cells represent the link between the central and the enteric nerve system and regulate digestive functions through the secretion of hormones (Veiga-Fernandes and Mucida, 2016). Tuft cells locally differentiate into distinct subsets and protect from helminth infection (Haber et al., 2017; von Moltke et al., 2016; Nadjsombati et al., 2018), while M-cells are specifically present in the dome epithelium associated with the Peyer`s Patches. Here, they take up luminal antigens for antigen presentation and thereby shape adaptive immune responses in the intestine (Mabbott et al., 2013).

The barrier function of the epithelium is adaptable. For the fine-tuning of these barrier functions, IECs rely on innate immune PRRs like TLRs and NLRs for sensing of microbial contact (Figure 2). It has however remained controversial, whether IECs directly perceive these signals. Alternatively, bacterial sensing might occur by immune cells in the lamina propria, which relay the information to IECs.

In line with the differences in microbial density along the intestinal tract, epithelial expression of TLRs varies along the intestinal axis and with regard to subcellular localization (Kayisoglu et al., 2020; Price et al., 2018). These regional differences seem, at least for TLR4, determined pre-birth and independent of microbiota exposure (Kayisoglu et al., 2020). There is evidence for *Tlr4* gene (Kayisoglu et al., 2020; Price et al., 2018) and protein expression in the colon (Price et al., 2018) and the small intestine (Hornef et al., 2002). The functional relevance of epithelial TLR4 with regard to LPS responsiveness remains however controversial (Hornef et al., 2003; Kayisoglu et al., 2020; Lotz et al., 2006; Price et al., 2018) (Chapter 3). Similarly, contradictory reports exist for a functional role of epithelial TLR5 in response to Flagellin (Fulde et al., 2018; Kayisoglu et al., 2020; Price et al., 2018). The dynamic expression of epithelial TLRs during development and adulthood (Fulde et al., 2018; Lotz et al., 2006), the contribution of immune cells to mucosal expression of PRRs, the difficulty to stain for TLRs (Price et al., 2018), as well as the use of *in vitro* models which incompletely recapitulate *in vivo* structures (see Chapters 3 and 5) contribute to these ambivalent observations.

The functional relevance of epithelial NLRs is similarly controversial. Recent evidence suggests that IECs express NLR family caspase recruitment domain (CARD)-containing protein (NLRC) 4 and its NLR family apoptosis inhibitory protein (NAIP) sensors, NLRP6, and the downstream effectors apoptosis-

associated speck-like protein containing a CARD (ASC) and Caspase-1. NLRP3 and IL1β, by contrast, seem to be absent in IECs (Sellin et al., 2014; Winsor et al., 2019) (Chapter 5), while the exposure to inflammatory cytokines induces expression of Caspase-11 (Chapter 5). Constitutive epithelial expression of IL18 contributes to the maintenance of homeostasis through induction of regulatory T (T_{reg})-cells (Harrison et al., 2015). In the context of oral enteropathogen infection, epithelial NAIP/NLRC4 protects from *S*. Tm (Rauch et al., 2017; Sellin et al., 2014) (Chapter 4) and *Citrobacter rodentium* (Nordlander et al., 2014) infection (see below for a detailed introduction into inflammasome functions). Potential regional differences in epithelial NLR expression as described for TLRs remain to be investigated.

Given their specific anatomical localization in direct contact with the microbiota in the intestinal lumen (Figure 2), it remains unclear how IECs regulate PRR activation to avoid overstimulation. This might involve the expression of inhibitory molecules triggering negative feedback loops (Vereecke et al., 2010, 2014) and spatial segregation of PRR expression on IECs (Lee et al., 2006).

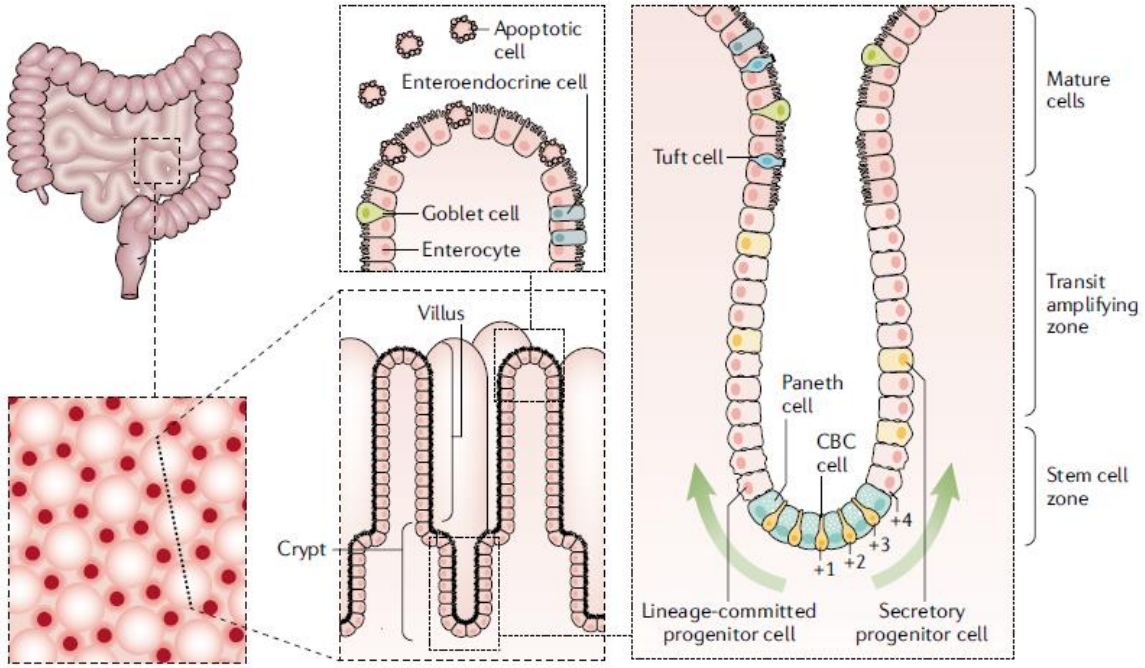

Figure 3 ***Structure of the small intestinal epithelium.*** *Each crypt harbors ~15 stem cells (crypt base columnar cells (CBC)), which are embedded between Paneth cells. These stem cells give rise to lineage-committed transient amplifying progenitor cells, which divide rapidly and migrate further up the crypt during differentiation into the different mature IEC subsets. Apoptotic IECs at the apical end of the crypt/villus slough into the intestinal lumen. Published in Gehart and Clevers, 2019.*

PROFESSIONAL IMMUNE CELLS

Mucosal immune cells have the challenging task to provide protection against pathogenic threats and to actively induce tolerogenic responses towards luminal antigens derived e.g. from commensal bacteria and food components at the same time. Anatomical structures of the intestinal mucosa facilitate this task. The biggest fraction of intestinal immune cells resides in the lamina propria and submucosa. The epithelium

shields these sterile compartments from the bacteria in the intestinal lumen, and thereby prevents direct contact of the immune cells with the luminal microbes (Figure 2) (Mowat and Agace, 2014).

Sites specifically dedicated to immune cell priming exist along the length of the intestine as organized lymphoid cell aggregates (gut-associated lymphoid tissue, GALT). They comprise the Peyer`s (small intestine), cecal (cecum) and colonic (colon) patches (Cornes, 1965; Owen et al., 1991; Perry and Sharp, 1988), as well smaller aggregates, referred to as isolated lymphoid follicles (ILFs) (Herbrand et al., 2008; Pabst et al., 2005). These ILFs are distributed in small intestine, cecum and colon. GALT consists of lymphoid cell accumulations, harboring T- and B-cells, in the mucosa and submucosa (Mowat and Agace, 2014). These areas are covered by dome/follicle associated epithelium, which contains M-cells (Mabbott et al., 2013), specialized IECs with the ability to take up luminal antigens and transfer them to DCs for antigen presentation within the follicles (Mabbott et al., 2013; Mowat and Agace, 2014). GALT is therefore an important site for T-cell priming and production of Immunoglobulin (Ig)A (Figure 4) (Lee et al., 2008; Masahata et al., 2014).

Immune effector cells, by contrast, are dispersed throughout the epithelium and the lamina propria. The epithelium is colonized by intraepithelial lymphocytes (consisting of conventional and γδ T-cells, as well as natural killer T-cells (Mowat and Agace, 2014)). This heterogeneous cell group contributes to tissue homeostasis and pathogen clearance via innate and adaptive immune functions (Figure 4) (Peterson and Artis, 2014; Sheridan and Lefrançois, 2010).

Besides B- and T-cells, the homeostatic lamina propria contains an array of innate immune cells. These include ILCs, granulocytes, mast cells, and mononuclear phagocytes (MPs) (Mowat and Agace, 2014). Innate immune cells are first responders in the case of a pathogen attack, but also contribute to a tolerogenic tissue environment and thereby to tissue homeostasis (Figure 4) (Kayama and Takeda, 2016).

The group of MPs comprises macrophages and DCs. The plasticity of this cell group in combination with overlapping marker expression complicated the classification of mucosal MPs into those two subcategories (Joeris et al., 2017). Nonetheless, the role of intestinal MPs as central coordinators of mucosal homeostasis, bacterial defense, inflammation and tissue repair is well established (Joeris et al., 2017). Their ability to ingest and present antigens to induce adaptive B- and T-cell responses (Cerovic et al., 2014; Koscsó et al., 2020; Macpherson and Uhr, 2004), and the equipment with innate PRRs and bactericidal mechanisms (Kinnebrew et al., 2012; Monteleone et al., 2008; Smythies et al., 2005) places them at the interface of the innate and the adaptive immune system. In the scope of this work, I will focus on the innate immune functions of MPs.

Macrophages are sessile cells, which seed the intestinal tissue during embryogenesis. A small population of long lived tissue-resident cluster of differentiation (CD)4^+ $Tim4^+$ macrophages is locally maintained independently of CCR2-mediated immigration of $Ly6C^{hi}$ monocytes into the tissue (Shaw et al., 2018). By contrast, the larger fraction of intestinal macrophages is constantly replaced by blood-derived $Ly6C^{hi}$ monocytes (Bain et al., 2013). Consequently, and in contrast to other tissues (Theret et al., 2019), the adult intestinal macrophage population is majorly of hematopoietic origin (Mowat et al., 2017). Incoming monocytes mature into intestinal tissue macrophages by downregulating Ly6C and upregulating MHCII, CD64, F4/80, CX_3CR1 and CD11c (Bain et al., 2013; Tamoutounour et al., 2012).

Intestinal macrophages have a high phagocytic activity. Their repertoire of receptors for the uptake of apoptotic cells and opsonized microbes in combination with high bactericidal activity makes them efficient scavengers, which silently remove e.g. translocated bacteria (Smythies et al., 2005). This silent scavenging

is achieved by the general anergy of macrophages towards TLR stimulation. In contrast to macrophages from other tissues, intestinal macrophages do not produce ROS, NO or pro-inflammatory cytokines in response to TLR activation (Mowat et al., 2017). This anergy is mediated via IL10 and transforming growth factor (TGF)β (Bain et al., 2013; Schridde et al., 2017). In line with this, the loss of IL10R signaling in macrophages can trigger inflammatory bowel disease (IBD) (Zigmond et al., 2014). Besides intestinal macrophages, forkhead box protein (FoxP)3$^+$ T_{reg}-cells depend on IL10 signaling (Murai et al., 2009). Both macrophages and T_{reg}-cells secrete and sense IL10 in the intestinal mucosa, presenting a positive feedback loop of tolerogenic signaling.

Intestinal DCs constantly sample their environment for self and foreign (food, microbiota, pathogen) antigens by phagocytosis of apoptotic cells, transepithelial sampling via dendrites, goblet-cell associated antigen passage or via M-cells (Joeris et al., 2017). Upon antigen uptake and TLR stimulation, intestinal DCs upregulate costimulatory molecules and CCR7, which allows them to migrate to the mesenteric lymph nodes (mLN) to induce adaptive immune responses. DCs are well equipped with TLRs. Similarly to intestinal macrophages, IL10 controls the expression of pro-inflammatory cytokines upon TLR stimulation in DCs (Monteleone et al., 2008).

Classical DCs (cDCs) are defined by their dependence on FMS-like tyrosine kinase 3 ligand (Flt3L) for expansion and can be divided into two subgroups, which are differentiated by the expression of XCR1 (cDC1) and signal regulatory protein (SIRP)α (cDC2) (Joeris et al., 2017). The surface markers CD103 and CD11b help to further subdivide these subsets. While the cDC1 subset consists almost entirely of CD103$^+$ CD11b$^-$ CX_3CR1^- cells, the cDC2 subset is more heterogeneous. It comprises CD103$^+$ CD11b$^+$ and CD103$^-$ CD11b$^+$ cells (Joeris et al., 2017). Notably, the CD103$^-$ CD11b$^+$ subset shares a number of surface markers with intestinal macrophages. The expression of F4/80 and CD64 on macrophages, but not on CD103$^-$ CD11b$^+$ cDC2s distinguishes these two cell types (Scott et al., 2015).

Generally, the cDC1 subset is associated with tolerogenic responses and with the ability to induce T_{reg}-cells via retinoic acid (Coombes et al., 2007; Schlickum et al., 2008; Sun et al., 2007). Furthermore, cDC1s have a protective effect against dextrane sodium sulphate-colitis by inducing anti-inflammatory responses in IECs (Muzaki et al., 2015).

The cDC2 subsets, by contrast, appear more immunogenic. In this context, CD103$^+$ CD11b$^+$ DCs activate ILCs via IL23 to induce AMP production in IECs upon bacterial sensing via TLR5 (Kinnebrew et al., 2012). CX_3CR1^+ DCs form transepithelial dendrites via G protein-coupled receptor (GPR)31 into the intestinal lumen to sample bacteria (Morita et al., 2019; Niess et al., 2005). This process contributes to the uptake of *S*. Tm during early oral infection ("alternative pathway", see Chapter 1.2.2). Upon bacterial engulfment, DC subsets transport *S*. Tm to the mLN, where they reside in macrophages (Bravo-Blas et al., 2019; Hapfelmeier et al., 2008).

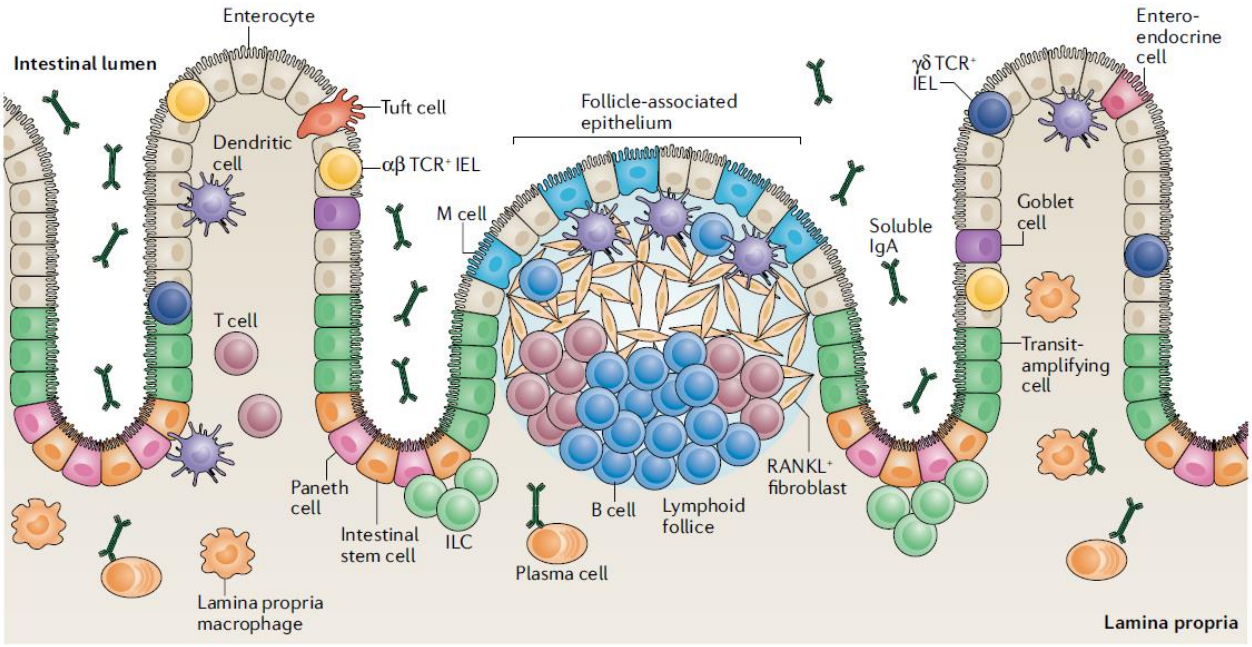

Figure 4 ***Immune cells in the intestinal mucosa.*** *IELs colonize the intestinal epithelium, whereas MPs, T- and B-cells reside in the lamina propria. M-cells within the follicle-associated epithelium shielding lymphoid follicles sample luminal antigens and pass them on to DCs for antigen presentation to B- and T-cells. Published in Bar-Ephraim et al., 2020*

PATTERN RECOGNITION RECEPTORS - BACTERIAL RECOGNITION IN THE INTESTINAL MUCOSA

(adapted from Hausmann and Hardt, Microbiology Spectrum 2019 as indicated)

PRRs are invariable receptors of the innate immune system. Consequently, they are not adaptable to specific pathogens which are encountered during the lifetime of an organism and therefore rely on the recognition of conserved microbial structures. The broad expression patterns of PRR ligands on large groups of microbes allow efficient detection of microbial threats by a small set of pre-defined receptors (Charles A Janeway et al., 2001). This principle intuitively applies to systemic body sites, in which microbes are absent except during infection events or leakage through barrier damage like a skin wound. At these sites, microbial components do not occur naturally and are therefore a sign of disturbance which require an immune response.

Mucosal surfaces, by contrast, are constantly exposed to microbes. This applies especially to the intestinal mucosa, which is in direct contact with the microbiota in the intestinal lumen. The context and consequences of PRR activation at systemic sites are therefore quite different to those at mucosal surfaces. As commensal and pathogenic bacteria share molecular patterns which are recognized by PRRs, it is still not entirely clear how the innate intestinal immune system is able to avoid PRR stimulation by beneficial bacteria, and provide protection against pathogen colonization at the same time. Chronic inflammatory diseases of the intestinal mucosa like IBD are in part driven by aberrant commensal bacterial recognition via PRRs and illustrate how delicate the balance between homeostasis and inflammation is (Maloy and Powrie, 2011).

TOLL-LIKE RECEPTORS

TLR-MEDIATED LIGAND BINDING

TLRs, like other innate PRRs, evolved to recognize conserved structures expressed by microorganisms. Conditioned by their localization at the plasma membrane or in endosomes, they screen extracytosolic spaces. TLRs present at the plasma membrane bind to microbial cell surface components: TLR4 recognizes Lipopolysaccharide (LPS) (Poltorak et al., 1998), TLR5 flagellin (Gewirtz et al., 2001; Hayashi et al., 2001) and TLR1, 2 and 6 (Kang et al., 2009; Takeuchi et al., 1999, 2001, 2002) bind to bacterial lipoproteins (Figure 5). By contrast, endosomal TLRs specialize in binding of nucleic acids. TLR3 binds to double-stranded (ds)RNA (Alexopoulou et al., 2001), TLR7 and 8 to single stranded (ss)RNA (Diebold et al., 2004; Heil et al., 2004; Hemmi et al., 2002), TLR9 recognizes ssDNA in association with unmethylated CpG (Hemmi et al., 2000) and TLR13 binds to bacterial ribosomal RNA (Hidmark et al., 2012) (Figure 5). Ligand binding occurs directly via leucine-rich-repeat regions of the ectodomains (Jin and Lee, 2008) and usually involves homodimerization of the ectodomains (Fitzgerald and Kagan, 2020).

In the case of TLR4, one homodimer interacts with two molecules of LPS - specifically with the Lipid A component of LPS (Park et al., 2009). This is exploited by well-adapted pathogens like *S*. Tm, which can modify their LPS by the addition of an O-Antigen to shield Lipid A and thereby down-modulate detection by TLR4 (Duerr et al., 2009). Lipid A by itself has a low affinity to TLR4, resulting in a high threshold for direct binding of Lipid A to the receptor (Picard et al., 2010). LPS binding proteins facilitate high-sensitivity detection of LPS. LPS binding protein (LBP) is a secreted protein, which associates with bacterial membranes or LPS micelles and mediates binding of CD14 to LPS. CD14 exists in a soluble and a membrane bound state, and transfers LPS to myeloid differentiation factor (MD)2 (Frey et al., 1992; Lee et al., 1993; Wright et al., 1990). MD2 stably interacts with the TLR4 ectodomain. This TLR4-MD2 heterodimer represents the actual functional LPS receptor (Gioannini et al., 2004; Ryu et al., 2017). The transfer of LPS to MD2 induces dimerization of TLR4, thereby activating downstream signaling (Latz et al., 2007).

Importantly, the dependence of LPS detection on LPS binding proteins allows the regulation of LPS sensitivity (Gioannini and Weiss, 2007). Many cell types express TLR4 and MD2, but only some co-express CD14. Cells lacking CD14 expression have low LPS responsiveness. This seems to apply, e.g., to IECs and endothelial cells (Haziot et al., 1993; Kayisoglu et al., 2020). LPS sensitivity of those cells can potentially be increased by expression of soluble CD14 by other cells (Fitzgerald and Kagan, 2020).

TLRs contribute indirectly (by promoting epithelial homeostasis (Rakoff-Nahoum et al., 2004)) and directly (by inducing antibacterial responses (Medzhitov and Janeway, 2000)) to protection from pathogens. While global defects in TLR signaling increase susceptibility to *S*. Tm infection (Sivick et al., 2014), TLR deficiency can counterintuitively also protect from *S*. Tm infection. TLR signaling via TLR2, 4 and 9 induces endosomal acidification, a signal for *S*. Tm to switch on its intracellular survival program (see below). Consequently, bone marrow-derived macrophages (BMDMs) of *Tlr2x4x9*$^{-/-}$ mice are less permissive for *S*. Tm growth (Arpaia et al., 2011). *In vivo* experiments however only partially recapitulated those results (Arpaia et al., 2011; Sivick et al., 2014; Talbot et al., 2009), highlighting the importance of the identification of contributions of cellular subsets to TLR-mediated responses in tissue contexts.

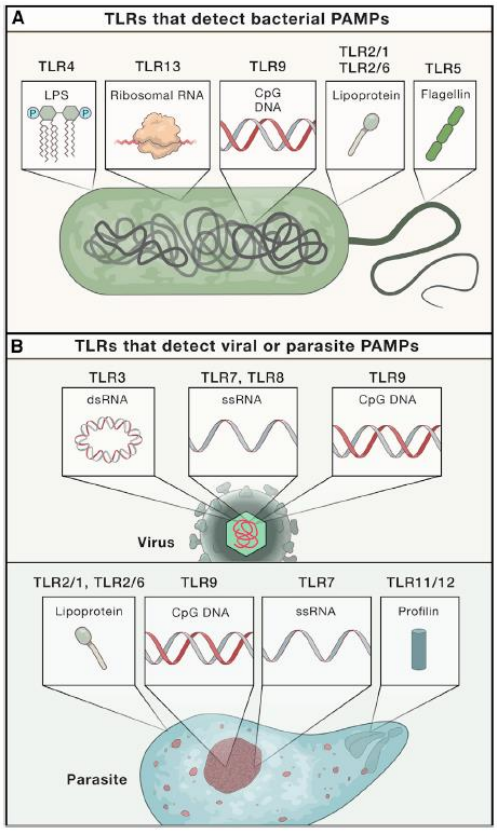

Figure 5 ***The detection of conserved microbial structures by different TLRs.*** *Published in Fitzgerald and Kagan, 2020.*

INITIATION OF DOWNSTREAM SIGNALING

Dimerization of the TLR4 ectodomains coincides with a dimerization of the cytosolic Toll/interleukin-1 receptor homology (TIR) domains of TLR4. These TIR domains function as adaptors for the assembly of supramolecular organizing centers (SMOCs) (Lin et al., 2010; Motshwene et al., 2009). Two distinct SMOCs mediate downstream signaling of TLRs. The myddosome mediates downstream signaling of all TLRs except for TLR3 (Motshwene et al., 2009). TIR-containing adaptor protein (TIRAP)/myeloid differentiation primary response 88 (MyD88)-adaptor-like (MAL) is a membrane protein, which screens the inner membrane leaflet for dimerized TIR domains and binds to them (Fitzgerald et al., 2001; Horng et al., 2001; Kagan and Medzhitov, 2006), which induces binding of MyD88, Interleukin-1 receptor associated kinase (IRAK) family members and TNF receptor associated factor (TRAF)6 (Bonham et al., 2014). TRAF6 activates TGFβ-activated kinase (TAK)1, which mediates activation of nuclear factor kappa-light-chain-enhancer of activated B-cells (NFκB) signaling via the inhibitor of κB (iκB) kinase (IKK) complex as well as activation of mitogen-activated protein kinase (MAPK) signaling via activator protein (AP-1) (Figure 6) (Emmerich et al., 2013; Wang et al., 2001). Experiments in *Myd88*$^{-/-}$ animals revealed a second downstream signaling pathway for TLR3 and 4, mediated by the triffosome (Yamamoto et al., 2003). In this case, TIR-domain containing adapter-inducing interferon β (TRIF)-related adaptor molecule (TRAM) initiates the recruitment of TRIF and TRAF3/6 upon binding to the dimerized TIR domains (Fitzgerald et al., 2003; Hoebe et al., 2003; Yamamoto et al., 2003). Similarly to myddosome assembly, this initiates NFκB and MAPK signaling. Additionally, triffosome mediated TLR signaling induces interferon regulated factor (IRF)3 activation (Figure 6) (Fitzgerald and Kagan, 2020). The assembly of the triffosome is likely restricted to the

endosomal compartment, leading to a slightly delayed response compared to MyD88-relayed activation (Fitzgerald and Kagan, 2020).

Several pathways related to microbial detection and immune responses use SMOCs for signal transmission and cellular activation (Fitzgerald and Kagan, 2020). This likely serves to provide a certain threshold for the activation of enzymes, leading to an all-or-nothing response (Sung et al., 2014). Accordingly, increased doses of PAMPs induce similar activation at single cell level with regard to NFκB activation and cytokine production. Instead, they trigger activation of a larger number of cells (Fischer et al., 2019). Cellular responses to TLR activation seem therefore to be designed for the induction of all-or-nothing responses (Fitzgerald and Kagan, 2020).

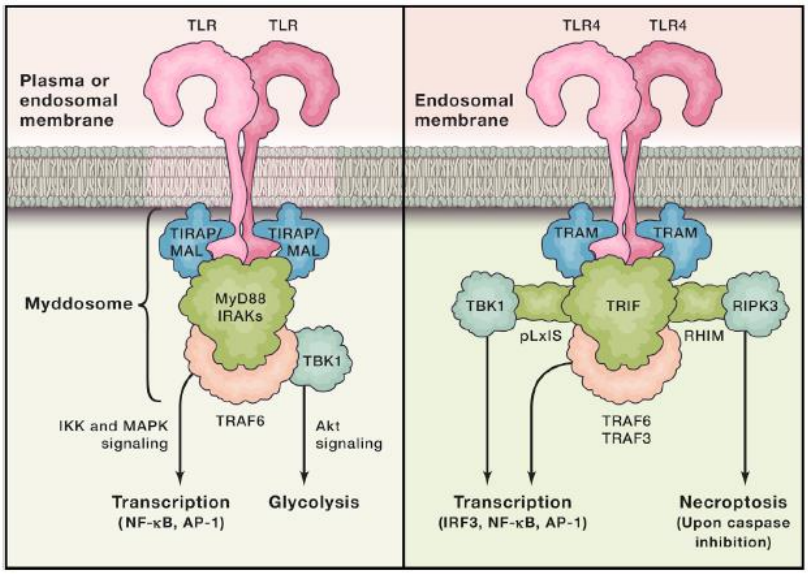

Figure 6 ***Downstream signaling of TLRs.*** *The myddosome relays signaling of all TLRs except TLR3 (left side). TLR3 and 4 can alternatively signal via the triffosome (right side). Published in Fitzgerald and Kagan, 2020.*

THE NFKB SIGNALING PATHWAY

TLR stimulation activates NFκB, MAPK and IRF3 signaling. For the scope of this work, I will focus here on NFκB signaling. The family of NFκB transcription factors comprises p50, p52, p65 (RelA), RelB and c-Rel (Wullaert et al., 2011). In a resting cell, IκB sequesters these transcription factors in the cytosol. Upon activation of TLRs or the receptors of the pro-inflammatory cytokines IL1β or TNF, TAK1 activates IKK, which phosphorylates IκB and thereby induces its degradation (Adachi et al., 1998; Fitzgerald and Kagan, 2020; Fitzgerald et al., 2003; Hayden and Ghosh, 2014; Muzio et al., 1997; Yamamoto et al., 2003). This allows the translocation of NFκB transcription factor dimers, typically heterodimers of p50 and p65, to the nucleus (Figure 7). Here, they bind NFκB consensus DNA sequences to regulate the transcription of immune response genes. NFκB target genes include inflammation-associated genes like cytokines, chemokines and adhesion molecules, but also factors involved in proliferation and survival (Bollrath and Greten, 2009; Kreuz et al., 2001; Micheau et al., 2001; Wang et al., 1998; Wullaert et al., 2011).

Consequently, the outcomes of NFκB activation are highly ambiguous and modulate cellular responses to a defined stimulus. An example by Wullaert et al. (Wullaert et al., 2011) illustrates this ambiguity. The binding of TNF by TNFR1 activates Caspase-8, which triggers apoptosis. At the same time, activation of

NFκB transcriptional regulation and AP-1 mediated MAPK signaling induces the production of anti-apoptotic factors. This ultimately results in survival of cells with active NFκB signaling. In this manner the presence or absence of NFκB signaling within a cell can modulate the cell-intrinsic consequences of receptor stimulation.

Due to its dual role, the NFκB signaling pathway is implicated in a variety of inflammatory diseases. Both the overstimulation and the lack of NFκB signaling can trigger chronic inflammation (Liu et al., 2017; Wullaert et al., 2011). The detrimental effect of a lack or inhibition of NFκB is specifically pronounced in IECs (Dheer et al., 2016; Guma et al., 2011; Vereecke et al., 2010, 2014; Vlantis et al., 2011), making them highly susceptible to apoptosis (Vlantis et al., 2016). This contributes, at least in part, to deregulated responses to microbial stimuli and thereby to chronic inflammatory diseases like IBD (Rogler et al., 1998; Zhang et al., 2006a).

A common virulence strategy of pathogens is the modulation of inflammatory responses. As a central coordinator of inflammation, several pathogens secrete virulence factors targeting the NFκB pathway to control infection-induced inflammation (see Chapter below).

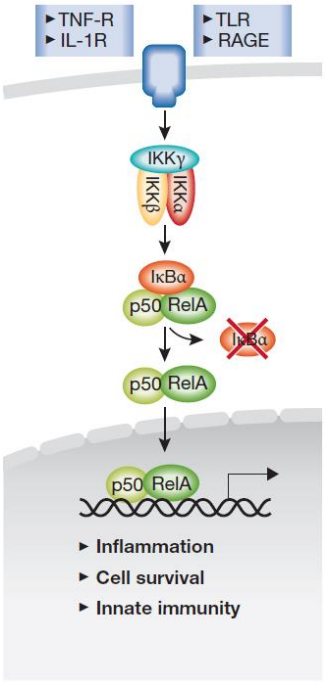

Figure 7 ***Canonical NFκB signaling.*** *TLR, TNF or IL1 receptor activation induces the degradation of IκB and enables the translocation of NFκB transcription factors to the nucleus. Adapted from Bollrath and Greten, 2009.*

NOD-LIKE RECEPTORS
(adapted from Hausmann and Hardt, Microbiology Spectrum 2019)

NLRs are an important element of the innate immune system (Broz, 2019; Broz and Dixit, 2016). The cytosolic PRRs recognize conserved microbial structures or cellular damage. Recognition events typically activate downstream caspases, promote cytokine release and elicit a specific type of cell death termed pyroptosis (Broz and Dixit, 2016). The NAIP/NLRC4 inflammasome detects flagella (Franchi et al., 2006;

Miao et al., 2006) and subunits of the Type three secretion system (TTSS)-1 apparatus of bacteria (Kofoed and Vance, 2011; Zhao et al., 2011). NLRP1 and the Pyrin inflammasome detect bacterial toxins (Boyden and Dietrich, 2006; Xu et al., 2014), the absent in melanoma 2 (Aim2) inflammasome is sensitive to double stranded DNA in the cytosol (Fernandes-Alnemri et al., 2010; Rathinam et al., 2010) and NLRP3 is activated upon recognition of microbial stimuli and/or cellular damage (Muñoz-Planillo et al., 2013). Cytosolic binding of LPS by Caspase-11 leads to non-canonical induction of pyroptosis and activates Caspase-1 via indirect induction of NLRP3 (Figure 8) (Kayagaki et al., 2011). Thereby, inflammasomes are mounting defense in response to cytoplasmic evidence of infection.

Recent studies revealed a major role of inflammasomes in the epithelial defense against enteropathogen infection. In streptomycin pretreated mice, defects in the NLRC4 inflammasome lead to 100-fold increased *S*. Tm loads in the cecal epithelium. This effect partially depends on Caspase-1 and relies on the expulsion of infected IECs from the epithelium (Rauch et al., 2017; Sellin et al., 2014).

Observations in mice infected with *S*. Tm suggest that infected IECs are expelled from the epithelium and undergo cell death in the intestinal lumen (Knodler et al., 2014; Sellin et al., 2014). The dependence of infected IEC expulsion on the NLRC4-inflammasome has recently been verified by an elegant genetic reconstitution of NLRC4 specifically in IECs of *S*. Tm or FlaTox-treated mice (Rauch et al., 2017). FlaTox is a bioengineered AB-toxin. The *Legionella pneumophila* flagellin (FlaA), a strong stimulator of the NAIP/NLRC4 inflammasome, is fused to the N-terminal domain of *Bacillus anthracis* lethal factor (LFn). In combination with the anthrax protective antigen channel (PA), FlaA is delivered into the cytosol. FlaTox can be used for sterile activation of the NLRC4 inflammasome (von Moltke et al., 2012). This is highly elegant, as it avoids confounding effects elicited by the innate immune recognition of other bacterial factors present during an infection with pathogen cells. In FlaTox-treated mice, NLRC4 was confirmed as the key inducer of the IEC expulsion defense. In spite of epithelium-wide NLRC4 activation, the epithelial layer remains intact for at least 60 min, as neighboring IECs seal voids left by epithelial expulsion through the formation of "actin purse-strings" around the expelled IEC (Rauch et al., 2017).

FlaTox treatment revealed the downstream signaling of NLRC4 activation in the cecal mucosa of mice, which occurs via two parallel signaling pathways. One pathway involves Caspase-1, Gasdermin D, secretion of the pro-inflammatory cytokine IL18 and a pyroptosis-like epithelial cell death. The parallel pathway requires ASC and Caspase-8 and elicits expulsion via an apoptosis-like epithelial cell death with little IL18 release (Rauch et al., 2017). The key role of Caspase-8 was later confirmed by IEC-specific ablation (Hefele et al., 2018). Moreover, this work identified a modulating function of receptor-interacting serine/threonine-protein kinase 3 (RipK3) and mixed lineage kinase domain-like protein (Mlkl), suggesting that Caspase-8, RipK3 and Mlkl cooperate in defining whether apoptosis or necroptosis dominate this second enterocyte cell death pathway upon NLRC4 activation (Hefele et al., 2018).

Recent efforts to dissect the connectivity of host cell death pathways in response to intracellular infection confirmed the central role of Caspase-1 and Caspase-8 in *S*. Tm infected BMDMs and *in vivo* (Doerflinger et al., 2020). Specifically, Caspase-1 functions as a master regulator of infection-induced cell death, comprising pyroptosis, apoptosis and necroptosis. In the absence of Caspase-1, Caspase-8 coordinates this induction through a highly connected and flexible crosstalk between initiators and executers of cell death. This analysis revealed a redundantly wired network, which ensures the suicide of infected macrophages even in the absence of any known cell death executers, as long as Caspase-1 and/or Caspase-8 are present and functional (Doerflinger et al., 2020). The complex wiring of cell death induction is likely a result of a long history of coevolution between host and pathogen, requiring constant adaptation. It remains to be

shown if the flexible roles of initiators and executers of cell death pathways are also relevant in other cell types targeted by intracellular pathogens, like IECs.

In BMDMs, the binding of cytosolic LPS by Caspase-11 induces non-canonical inflammasome activation resulting in pyroptosis (Kayagaki et al., 2011). Whether this Caspase-11-mediated cell death of infected cells plays a role in IECs however remains controversial. Several studies tested the importance of Caspase-11 in the context of epithelial *S*. Tm infection and found contradictory results (Knodler et al., 2014; Sellin et al., 2014). Sellin et al. show that Caspase-11 plays no role in the control of cecal tissue loads in *S*. Tm infection, whereas Knodler and colleagues observed increased pathogen loads in the cecal tissue at seven days of infection. To conclusively interpret these data, further experiments assessing the initial 24h after infection in littermate-controlled experimental settings will be of great value (Chapter 4).

Generally, it appears that Caspase-11 - at least in BMDMs - confers resistance against cytosolic bacteria, like the naturally cytosolic pathogen *Burkholderia thailandensis* as well as the cytosolic escaper mutants of *S*. Tm (*ΔsifA*) and *Legionella pneumophila* (*ΔsdhA*) (Aachoui et al., 2013). Interestingly, the cytosolic pathogen *Francisella novicida* expresses a tetra-acylated Lipid A (which is not detected by Caspase-11), instead of penta- or hexa-acylated Lipid A which binds to Caspase-11. This might represent a mechanism of immune-evasion for this naturally cytosolic bacterium (Hagar et al., 2013). To date, it remains unclear whether LPS-recognition by inflammasomes contributes to epithelial defense and whether stealthy LPS modifications might offer ways to avoid recognition.

In conclusion, NLRC4-driven defenses reduce pathogen loads in the gut tissue by eliciting Caspase-mediated expulsion of infected enterocytes. The role of Caspase-11 in this process is not fully understood. In parallel, the NLRC4-mediated response induces profound pro-inflammatory signals which recruit granulocytes, mature natural killer (NK)-cells, macrophages and DCs to clear remaining pathogens from the gut tissue (Müller et al., 2016; Sellin et al., 2014, 2018). Which downstream signaling pathways (via Caspase-1 or via Caspase-8; death by pyroptosis, necroptosis or apoptosis) dominate the defense against *S*. Tm and how different cell types orchestrate inflammasome-mediated antibacterial defense will remain an important topic for further work (Chapter 4).

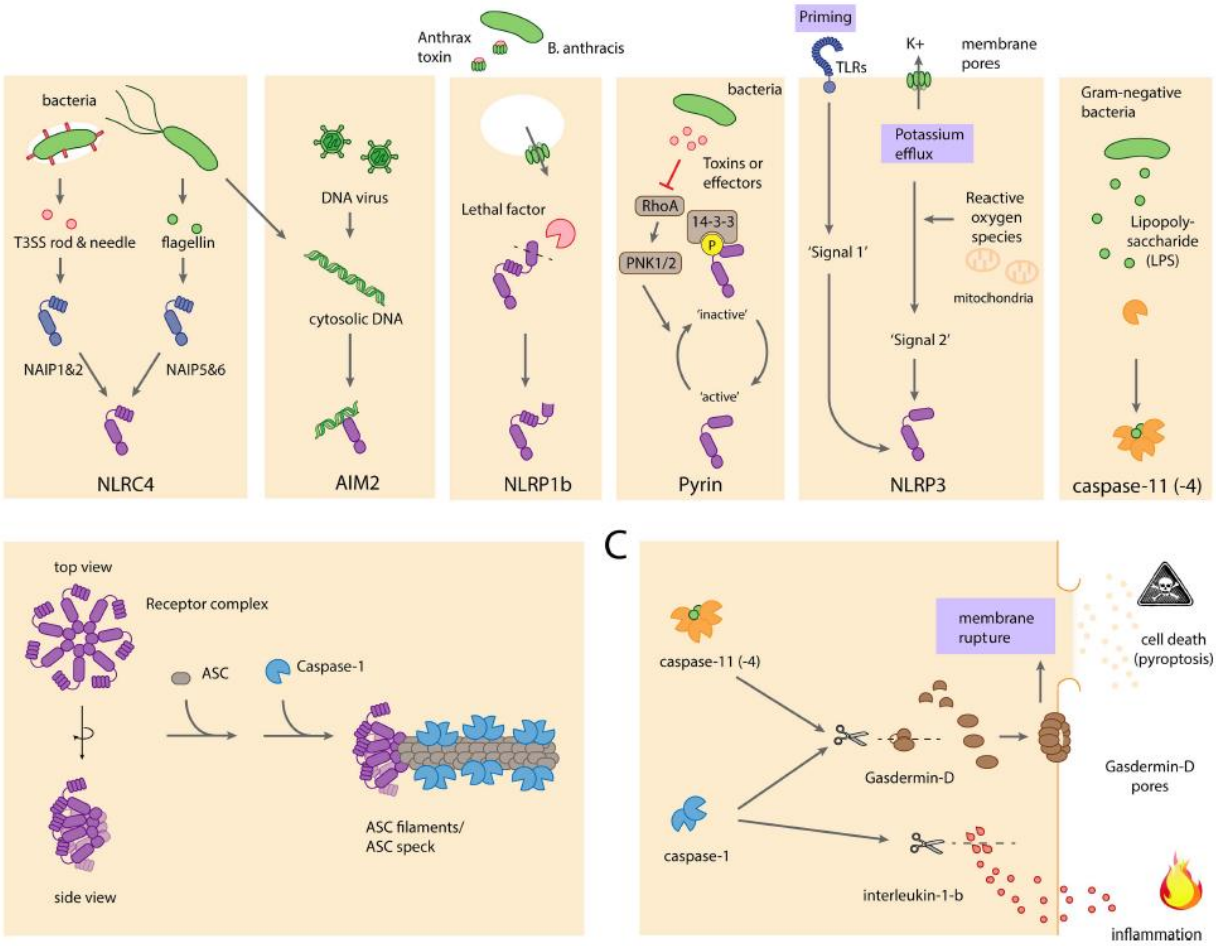

Figure 8 ***Overview on inflammasomes, their stimuli and consequences of their activation.*** *Published in Broz, 2019.*

SALMONELLA TYPHIMURIUM INFECTION OF THE INTESTINAL MUCOSA

(*adapted from Hausmann and Hardt, Microbiology Spectrum 2019)*

HEALTH IMPACT OF *S.* TM INFECTION

(adapted from Hausmann and Hardt, Microbiology Spectrum 2019)

S. Tm is a major health issue. As one of the top causes of diarrheal disease burden worldwide (Kirk et al., 2015), the foodborne pathogen usually causes self-limiting gastroenteritis accompanied by fever, abdominal pain and nausea. In children, elderly and immunocompromised persons, infection with *S*. Tm can even be life-threatening (Tsolis et al., 2011). *S.* Tm is a versatile, gram-negative pathogen for the study of host-pathogen interactions. It is able to cope with the host response and exploits defense mechanisms to its advantage. The well-characterized kinetics of the infection in standardized models enable detailed studies of host-*S*. Tm interaction.

EARLY KINETICS OF ORAL *S.* TM INFECTION

(adapted from Hausmann and Hardt, Microbiology Spectrum 2019)

S. Tm infection of streptomycin-pretreated mice is a model for non-typhoidal *Salmonella* diarrhea. In this model, CR is alleviated by streptomycin (Barthel et al., 2003; Bohnhoff and Miller, 1962; Bohnhoff et al., 1954). This leads to efficient colonization of the intestinal lumen within 4-6h after intragastrical inoculation. The disease is characterized by strong inflammation of the cecal mucosa, expulsion of infected epithelial cells and the recruitment of neutrophils and NK cells (Barthel et al., 2003). The robust disease induction in this model allows a detailed analysis of the underlying mechanisms, including the function of virulence factors in tissue invasion. It allows studying innate defenses protecting the gut, like host responses that mount the characteristic gut inflammation, pathogen clearance by microbiota re-growth, as well as O-antigen specific secretory IgA at the end of an acute infection (Wotzka et al., 2017).

In the streptomycin mouse model, the cecum is well established as the major site of *S*. Tm invasion (Barthel et al., 2003; Furter et al., 2019). So far, it is not well understood, why *S*. Tm preferentially targets this site of the murine intestine. We speculate that this might be due to its particular anatomical features (e.g. low flow rate of the content of this dead-ended side-arm of the gut), metabolite availability or environmental signals that trigger virulence factor expression. Furthermore, the sparse decoration of the cecal mucosa with mucus might allow easier epithelial invasion compared to the colon (Furter et al., 2019). Around 2h after intragastrical inoculation, *S*. Tm reaches the murine cecum and grows up to a density of 10^9 bacteria/g cecal content within the next 4-6h (Barthel et al., 2003; Sellin et al., 2014).

By 8-12 h, *S*. Tm invasion into the mucosa yields pathogen densities of $>10^6$ bacteria/g cecal tissue. Three mechanisms were suggested to drive this tissue invasion: 1) active invasion of IECs by *S*. Tm ("classical pathway"), 2) uptake by phagocytes sampling the intestinal lumen ("alternative pathway") and 3) uptake of *S*. Tm by M cells. The latter occurs mainly in the Peyer's patches of the small intestine and possibly in the cecal patch at the tip of the cecum. We will not discuss this in detail but describe the former two mechanisms which explain the infection of the cecal absorptive mucosa, instead.

Active IEC invasion via the classical pathway is promoted by the *Salmonella* pathogenicity island (SPI)-1 encoded TTSS-1, the *sii* adhesin and the flagella (Gerlach et al., 2007; Hapfelmeier et al., 2005; Stecher et al., 2008) (Figure 9). The expression of SPI-1 occurs in response to environmental signals in the intestinal lumen, which induce a regulatory feed-forward loop ensuring that the invasion machinery is "trigger-ready" before the pathogen actually reaches the gut epithelium.

Flagella mediate bacterial motility. During orogastric *S*. Tm infection, they are crucial for active swimming towards the intestinal epithelium as well as for attachment to IECs (Kaiser et al., 2012; Maier et al., 2013; Stecher et al., 2004, 2008; Wangdi et al., 2014). Importantly, flagella are co-expressed with TTSS-1 (Golubeva et al., 2012). TTSS-1 is a needle-like complex, which allows injection of a virulence factor cocktail ("effector proteins") into the cytosol of the host cell (Galán and Waksman, 2018; Galán et al., 2014). In the host cellular cytosol, these effector proteins trigger cytoskeletal rearrangements and bacterial uptake. SipA, SopB, SopE and SopE2 cooperate to induce Rho GTPase activation and Arp2/3 dependent rearrangements of the actin cytoskeleton (Hardt et al., 1998; Srikanth et al., 2011). This process is well characterized in HeLa cells where it leads to a membrane-ruffle dependent uptake of the bacterial cell (Zhou et al., 1999a, 1999b). Similar observations were made during M-cell invasion in the murine small intestine and in the classical orogastric infection experiments in opium-treated guinea pigs (Takeuchi, 1967). Recent work however suggests that epithelial invasion *in vivo* does not induce ruffle formation (Fattinger et al., 2020). *S*. Tm entry into epithelial cells initiates early intestinal inflammation. From here, the bacterium penetrates into deeper layers of the mucosal tissue and systemic organs (Hapfelmeier et al., 2005; Müller et al., 2012; Zhang et al., 2018) (Figure 9).

S. Tm mutants lacking a functional TTSS-1 apparatus (e.g. *ΔinvG*) rely on sampling by phagocytes from the intestinal lumen to breach the epithelial barrier ("alternative pathway"; Figure 9) (Hapfelmeier et al., 2008). It is likely that classical and alternative pathways operate in parallel during infections with wild type *S*. Tm.

Once taken up by the host cell, *S*. Tm resides within a *Salmonella* containing vacuole (SCV; Figure 9). The SCV is an endosomal compartment that is actively modified by the bacterium. Early SCV biogenesis is controlled mainly by the TTSS-1 (Knodler and Steele-Mortimer, 2005; Knodler et al., 2003; Kreibich et al., 2015; Steele-Mortimer et al., 2002; Zhang et al., 2018). Throughout the maturation process, acidification of the SCV leads to SPI-2 mediated induction of TTSS-2 (Figure 10), which contributes to later stages of SCV maintenance. SPI-1 and SPI-2 effectors (e.g. SipA, SopB, SopE, SpiC, SipC and SifA) stabilize the SCV membrane and control SCV fusion with the endocytic pathway of the host cell (Steele-Mortimer, 2008). Accordingly, SCVs display altered surface markers compared to classical lysosomes. They are positive for Lamp1 and vATPase, but lack cathepsins and Mannose-6-phosphate receptors (Steele-Mortimer, 2008).

SPI-2 can promote intracellular replication and survival of *S*. Tm both *in vitro* and *in vivo* by controlling the fusion of lysosomes with the SCV, suppression of iNOS- and NADPH oxidase-induced bactericidal effects as well as inhibition of apoptosis. This is well-established in macrophages *in vitro* and *in vivo*, but may also be of relevance for *S*. Tm growth within other cell types *in vivo* (Hensel et al., 1995; Shea et al., 1996; Waterman and Holden, 2003).

SPI-1 expression is downregulated immediately after host cell invasion. However, in HeLa cells its expression resumes after 6h of infection (Hautefort et al., 2008). This reinduction goes along with an induction of flagellar gene expression and might also happen *in vivo* (Laughlin et al., 2014). The switch to an invasive phenotype is specifically observed in HeLa cells (not in BMDMs) and strongly correlates with

cytosolic escape from the SCV and hyperreplication in the nutrient rich cytosol (Brumell et al., 2002; Hautefort et al., 2008; Knodler et al., 2010). In line with this, HeLa cells infected with *sifA* mutants - which lack a main stabilizer of the SCV membrane - harbor high loads of cytosolic *S*. Tm already at early stages of the infection. BMDMs, in contrast, are not permissive for cytosolic hyperreplication of *S*. Tm, which might be due to different PRR expression patterns in these two cell types (e.g.: Caspase-11; as above) (Thurston et al., 2016).

These fluctuations in SPI-1 gene expression in epithelial cells might represent a cycle of invasion, replication, expulsion and reinfection that could also happen in the intestinal mucosa of infected mice. *S*. Tm might make use of the protected niche of the SCV to adapt to an intracellular life style. It switches on TTSS-2 in enterocytes and replicates moderately within these cells. Escape from the SCV appears to be detected by the chemo-sensors of the NLRC4-inflammasome, leading to expulsion of infected enterocytes into the gut lumen (see above; Figures 9 and 10). Back in the lumen, TTSS-1 and flagella may ideally prepare the *S*. Tm cell for the next round of enterocyte invasion (Knodler et al., 2010; Laughlin et al., 2014; Sellin et al., 2014). Clearly, this hypothesis can only be tested *in vivo*, when the pathogen faces the multi-layered architecture of the intestinal defenses.

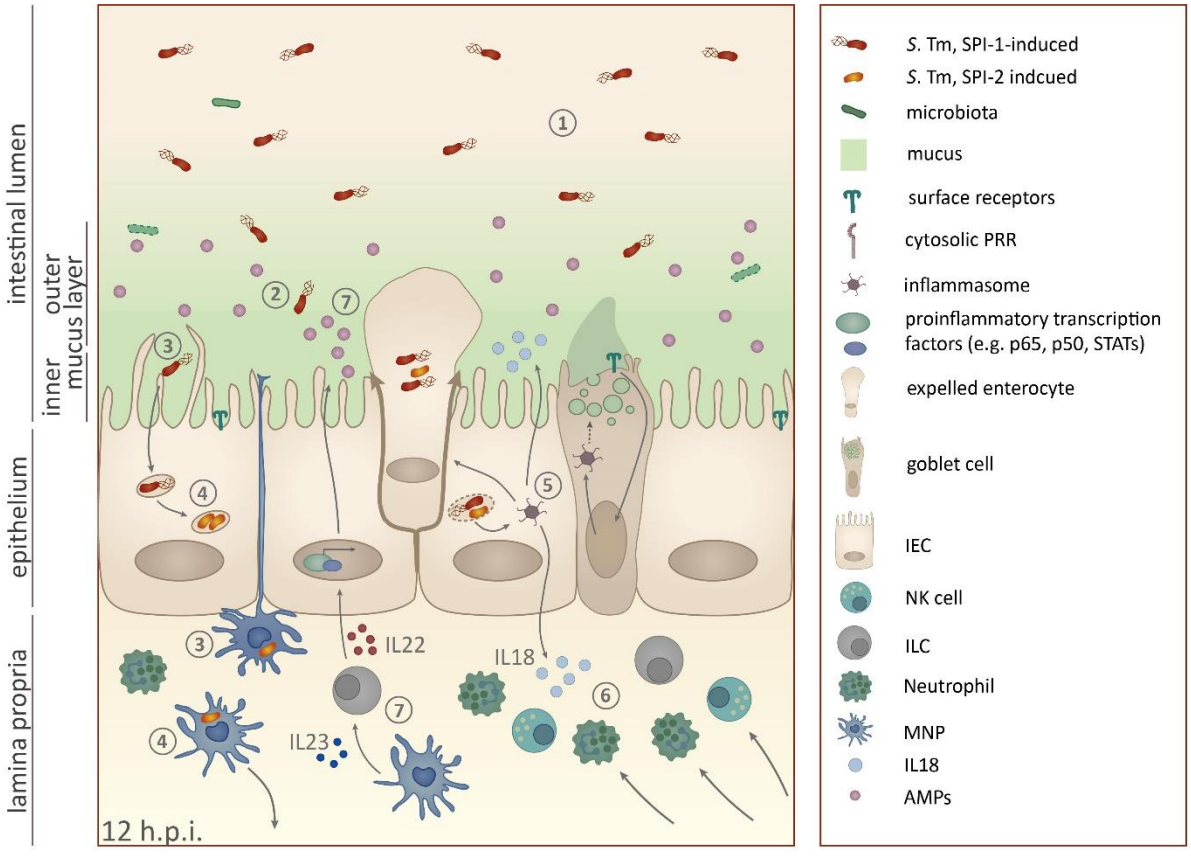

Figure 9 ***Innate immune mechanisms during early oral infection with S. Tm.*** *Upon CR disturbance, S. Tm colonizes the intestinal lumen 1), uses the flagella to swim through the mucus layer 2) towards the epithelium, where it triggers TTSS-1 mediated uptake into IECs or is taken up from the lumen by MPs 3). Intracellular S. Tm reside within the SCV and switch on SPI-2 expression 4). NLRs detect cytosolic escape of S. Tm 5), which induces the expulsion of*

infected IECs and secretion of IL18 to attract immune cells 6). Detection of microbial compounds by MPs enhance AMP production by IECs 7). Adapted from Hausmann and Hardt, 2019.

DOWNSTREAM ELICITATION OF MUCOSAL INFLAMMATION
(adapted from Hausmann and Hardt, Microbiology Spectrum 2019)

Besides expulsion of infected IECs, assembly of the NAIP/NLRC4 inflammasome leads to activation and secretion of IL1β and IL18. Both cytokines are produced as inactive precursors (pro-IL1β and pro-IL18), that are activated upon cleavage by Caspase-1 and Caspase-11. IL18 secretion by IECs is mainly regulated at the protein level. It is constantly produced and secreted at low levels by IECs during homeostatic conditions (Harrison et al., 2015; Winsor et al., 2019). IL1β, in contrast, seems to be further regulated on a transcriptional level, leading to a specific upregulation of *Il1b* mRNA levels in response to microbial stimuli (Sellin et al., 2014). The contribution of IECs to IL1β secretion is thought to be minor (Thinwa et al., 2014; Winsor et al., 2019; Wlodarska et al., 2014). Nevertheless, the infected mucosa features elevated levels of both IL18 and IL1β. IL18 is crucial for induction of inflammation within the first 12h after oral infection, while IL1β is dispensable for the mounting of inflammation at early time points after oral *S*. Tm infection (Müller et al., 2016) (Figure 9). IL18-mediated inflammation was shown to require Caspase-1 (most likely within IECs), with a contribution of immune cells in the intestinal mucosa (Müller et al., 2016; Sellin et al., 2018).

IL18 recruits neutrophils and mature NK cells into the cecal lamina propria (Figure 9). NK cells express Perforin, which plays a major role in the swift induction of mucosal inflammation. Interestingly, this IL18 mediated NK cell-elicited mucosal inflammation is neither required for the control of local nor of systemic bacterial loads in the first 12h of infection. This indicates that the early host response against oral *S*. Tm infection relies mainly on the NAIP/NLRC4-mediated expulsion of infected IECs, not on the recruited phagocytes (Müller et al., 2016; Sellin et al., 2014, 2018). Strikingly, the induction of mucosal inflammation seems to have - during early infection - no obvious benefit for the host. By contrast, it might even hinder pathogen clearance at later stages of the infection cycle by contributing to antimicrobial responses that repress regrowth of the microbiota (Dolowschiak et al., 2016; Miki et al., 2017a, 2017b; Raffatellu et al., 2009).

The inflamed mucosa also attracts neutrophils via IL18 and IL1β, most likely through induction of chemokines. Neutrophils limit pathogen loads both in the mucosa as well as in the intestinal lumen at later stages of infection (Maier et al., 2014; Müller et al., 2016). Pathogen clearance by neutrophils is mediated indirectly (via cytokine mediated recruitment of further phagocytes) and directly via phagocytosis and intracellular killing of pathogens (Müller et al., 2016). Macrophages contribute to pathogen phagocytosis. In case of pathogens like *Chromobacterium violaceum* or *S*. Tm, these infected macrophages tend to undergo pyroptosis upon phagocytosis, thus forming so-called PITs (pore-induced intracellular traps). These PITs retain surviving bacteria and are taken up by neutrophils, which kill the entrapped bacteria in a NADPH-oxidase dependent way (Jorgensen et al., 2016a, 2016b). This is well established for systemic infection. However, it remains to be shown whether this mechanism also contributes to pathogen clearance from the *S*. Tm infected gut tissue.

Inflammatory processes in the mucosa are to some extent self-sustained. The remission after antibiotic treatment of intestinal *S*. Tm infections is slowed down by IFNγ signaling, a prominent by-product of mucosal inflammation (Dolowschiak et al., 2016). Treatment of *S*. Tm infected mice with ciprofloxacin

eliminates pathogen cells from the intestinal lumen within a few hours. However, a small antibiotic-tolerant fraction of bacteria remains in the mucosal tissue and in the mLN (persisters; Figure 10) (Claudi et al., 2014; Kaiser et al., 2013). This may further prolong IFNγ-driven defenses in the mucosa tissue, slowing down the clearance of granulocytes from the gut and inhibiting the polarization of lamina propria phagocytes towards a homeostatic phenotype (Dolowschiak et al., 2016). Overall, such prolonged signaling slows down remission and might contribute to gastrointestinal disorders after enteropathogen colonization, and increase susceptibility to subsequent infections (Yang et al., 2017).

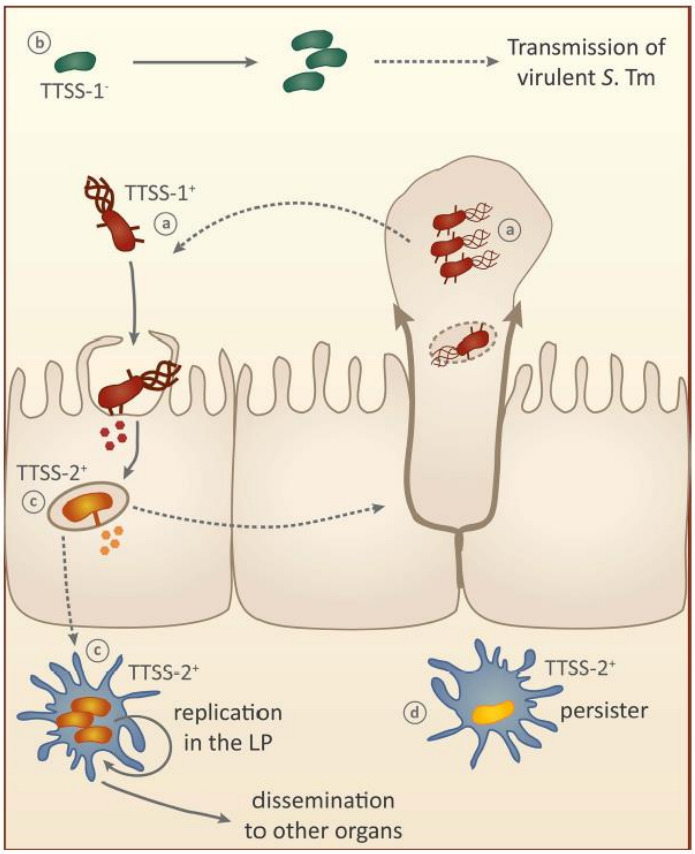

Figure 10 ***Different S. Tm phenotypes are required at different stages of infection.*** *a) TTSS-1⁺, flagella⁺,TTSS-2⁻; required for active invasion into host cells. b) TTSS-1⁺, in vitro flagella⁻ (Sturm et al., 2011),TTSS-2⁻, fast growing; ensures transmission, c) TTSS-1⁻, flagella⁻, TTSS-2⁺, fast growing; intracellular survival, d) TTSS-1⁻, flagella⁻, TTSS-2⁺, slow growing; antibiotic tolerance ("persisters"). Published in Hausmann and Hardt, 2019.*

MODULATION OF HOST RESPONSES BY DIFFERENTIAL VIRULENCE FACTOR EXPRESSION
(adapted from Hausmann and Hardt, Microbiology Spectrum 2019)

Coevolution tends to result in a fine-tuned adaptation of pathogens to their hosts (Diard and Hardt, 2017a). *S.* Tm provides a well-studied example of complementary adaptations to avoid innate immune defenses, i.e. the expression of virulence factors disrupting innate immune signaling and the down-

regulation of PAMPs. The modulation of host responses via virulence factors appears to be common to many pathogenic bacteria (Table 1). This has recently been reviewed in detail (Pinaud et al., 2018).

Common targets of immune modulation are components of the NFκB and cell death pathways, which are tightly interlinked to regulate survival versus death and which elicit (or avoid) the production and release of pro-inflammatory cytokines (Blaser et al.). The NFκB pathway integrates a variety stimuli to induce pro-inflammatory signaling. Indeed, *S*. Tm expresses a variety of effector proteins targeting the NFκB signaling pathway (Table 2). One striking example are the effector proteins PipA, GogA and GtgA, which are injected into host cells via TTSS-1 and/or TTSS-2. They redundantly block the NFκB signaling pathway by cleaving p65 and RelB. Interestingly, these NFκB transcription factors are targeted directly inside the nucleus. This implies that a short triggering of pro-inflammatory downstream mechanisms is permitted. After one cycle of induction, the inflammatory response is shut down by PipA, GogA and GtgA. This may help to reduce gut tissue pathology and prevents an overwhelming immune response. By contrast, an *S*. Tm mutant lacking PipA, GogA and GtgA elicits more pronounced enteropathy and host death (Sun et al., 2016). Future work will have to address if PipA, GogA and GtgA are blocking NFκB signaling in infected IECs (and may delay their demise) or in lamina propria phagocytes.

A second important adaptation to achieve successful gut infection resides in the tight regulation of virulence factor gene expression. Numerous studies have established an elaborate network of transcriptional and post-transcriptional controls that allow the pathogen to deduce its exact location within the host and to trigger the appropriate virulence factors for survival in that niche and/or to prepare the next step of the infection process (Kröger et al., 2013; Saini et al., 2010; Westermann et al., 2016). This creates pathogen cells with distinct virulence gene expression patterns at the different sites of the host.

In the gut lumen, the pathogen forms (at least) two distinct phenotypes, TTSS-1$^+$ and TTSS-1$^-$ (Figure 10). According to the division of labor hypothesis proposed by Diard et al. (Diard et al., 2013), both phenotypes play a key role in the life-cycle of *S*. Tm. The TTSS-1$^+$ phenotype expresses flagella (to reach the epithelium), the invasion-mediating TTSS-1 apparatus and a cocktail of TTSS-1 effector proteins to be deployed as soon as the pathogen docks to an epithelial cell. This mediates invasion into the host cell (Ackermann et al., 2008; Diard et al., 2013; Hautefort et al., 2008; Schlumberger et al., 2005; Sturm et al., 2011; Winnen et al., 2008) (Figure 10). The TTSS-1$^+$ population is thus poised to invade the epithelium and triggers pronounced inflammation. However, the expression of TTSS-1 is associated with a reduced growth rate due to fitness-costs (Diard et al., 2013; Sturm et al., 2011). In contrast, the TTSS-1$^-$ phenotype does not express TTSS-1, remains in the gut lumen and blooms in the milieu of the infected gut (Figure 10). This stabilizes *S*. Tm virulence by preventing overgrowth of avirulent mutants that spontaneously emerge from the *S*. Tm population during infection. These mutants are genetically unable to express the TTSS-1$^+$ phenotype and are fast-growing. This represents an advantage in the inflamed gut of infected hosts, but a major disadvantage upon transmission to the next hosts as these mutants are unable to trigger inflammation on their own (Diard and Hardt, 2017b; Diard et al., 2014). The fast growing TTSS-1$^-$ phenotype therefore keeps avirulent mutants at bay by competing against them for the same niche in the gut. This is thought to ensure the transmission of virulent genotypes upon chronic infection (Diard and Hardt, 2017b; Diard et al., 2013) (Figure 10).

After arrival in the gut tissue, most *S*. Tm cells switch off TTSS-1 and flagella gene expression and trigger TTSS-2 expression instead (Figure 10). This may partially help to avoid stimulation of the NLRC4 inflammasome (Chapter 4). TTSS-2 effector proteins may help to further dampen such innate immune

responses and promote intracellular survival (Hapfelmeier et al., 2005). Interestingly, some of the tissue-resident *S*. Tm cells re-initiate TTSS-1 and flagellar gene expression (Laughlin et al., 2014), probably in preparation for reinvasion of the epithelium. Other *S*. Tm cells appear to enter into a slow-growing state of persistence (TTSS-1$^-$, TTSS-2$^+$; some populations may also feature no/low TTSS-2 expression; extremely slow growth; Figure 10) which creates a tissue-lodged pathogen reservoir that can survive antibiotics therapy for >10 days and re-seed the host's gut lumen as soon as the therapy is discontinued (Bakkeren et al., 2019; Claudi et al., 2014; Diard et al., 2014; Kaiser et al., 2013). Another *S*. Tm phenotype (i.e. TTSS-1$^-$, TTSS-2$^+$, fast growth) forms inside phagocytes and may promote pathogen growth in the lamina propria, boosting dissemination to other organs upon migration of infected cells to systemic sites (Bravo-Blas et al., 2019; Carden et al., 2017; Hapfelmeier et al., 2008; Hensel et al., 1995; Kaiser et al., 2013; Müller et al., 2012).

Owing to the multitude of different phagocyte populations that take up *S*. Tm in the gut tissue (Hapfelmeier et al., 2008; Müller et al., 2012), the time-dependence of SCV maturation, and the different defenses faced within particular host cells, the spectrum of stimuli and of the resulting *S*. Tm phenotypes is likely much more diverse than depicted in Figure 10 (Bumann and Cunrath, 2017; Kreibich and Hardt, 2015). Phenotypic heterogeneity and the cooperation between different pathogen subpopulations is likely of key importance for disease progression, pathogen blooms in the infected gut and for successful transmission within the host population.

Table 1 ***Examples of host response-modulating virulence factors of a variety of pathogenic bacteria.***

Effector	Target molecule	Target pathway	Type of interaction	Outcome of interaction	System	Organism	Reference
YopM	pyrin inflammasome	pyrin inflammasome	inhibition	anti-inflammatory	*in vivo*	*Yersinia*	(Chung et al., 2016; Ratner et al., 2016)
YopH	IL18 secretion	Inflammasome downstream signaling	inhibition	anti-inflammatory	*in vitro*	*Yersinia*	(Thinwa et al., 2014)
NleF	Caspase-4, -8, -9	Caspase-mediated cell death	inhibition	anti-apoptotic	*in vitro*	*Escherichia coli*	(Blasche et al., 2013)
OspC3	Caspase-4	Caspase-mediated cell death	inhibition	anti-apoptotic	*in vivo (guinea pig)*	*Shigella*	(Kobayashi et al., 2013)
IpaH9.8	IKK	NFκB signaling	promotes ubiquitination of NEMO	anti-inflammatory	*in vitro*	*Shigella*	(Ashida et al., 2010)
NleB1	FADD	Caspase-8-mediated cell death	inhibition	anti-apoptotic	*in vivo*	*Citrobacter rodentium*	(El Qaidi et al., 2017; Li et al., 2013; Pearson et al., 2013; Scott et al., 2017)

Table 2 ***S. Tm virulence factors that modulate the host immune response.***

Effector	Target molecule	Target pathway	Type of interaction	Outcome of interaction	System	Reference
SseK1, SseK3	FADD, TRADD	TNFα-induced NFκB signaling	inactivation by arginie-GlcNAcylation	inhibition of necroptosis (apoptosis not affected)	In vitro	(Günster et al., 2017)
AvrA	IκBa, MKK4, MKK7	NFκB, JNK, MAPK- signaling	inactivation by acetylation	anti-inflammatory and anti-apoptotic	in vitro, in vivo	(Collier-Hyams et al., 2002; Ye et al., 2007)
GogB	Scf unbiquitin ligase complex (Skp1, FBOX22)	IκB degradation and MAPK signaling	inhibition	anti-inflammatory	In vitro, in vivo	(Pilar et al., 2012)
SpvC	ERK, p38, JNK	MAPK	phosphothreonine lyase, inhibition	anti-inflammatory	in vitro, in vivo	(Haneda et al., 2012; Li et al., 2007; Mazurkiewicz et al., 2008; Zhu et al., 2007)
SseL	IκBa?	NFκB signaling, autophagy	inactivation by deubiquitinylation	anti-inflammatory	In vitro, in vivo	(Le Negrate et al., 2008; Mesquita et al., 2012, 2013)
SspH1	PKN1	NFκB signaling	Inhibition by E3 unibuitin ligation	anti-inflammatory	in vitro	(Haraga and Miller, 2003, 2006; Keszei et al., 2014)
SpvD	Xpo2	NFκB nuclear translocation	Inhibition of importin-mediated nuclear import, deconjugation	anti-inflammatory	in vitro, small in vivo effect	(Rolhion et al., 2016)
PipA	p65 and RelB, redunant	NFκB signaling	inhibition	anti-inflammatory	In vitro, in vivo	(Sun et al., 2016)
GogA						
GtgA						
SopB	Nlrc4 inflammasome pathway?	inflammasome activation	inhibition	anti-inflammatory	in vitro	(Hu et al., 2017)
SopA	TRIM56 and TRIM65	IFNb signaling	HECT-like E3 ligase, stimulation	pro-inflammatory	In vitro	(Diao et al., 2008; Fiskin et al., 2017; Kamanova et al., 2016; Zhang et al., 2006b)

RECENT ADVANCES IN THE ANALYSIS OF HOST-MICROBE INTERACTION

(adapted from Hausmann and Hardt, Microbiology Spectrum 2019)

Host-bacteria interactions are multilayered and dynamic. Several characteristics of the host-bacteria interaction contribute to this feature: i) organ complexity - organs harbor a variety of host cell types with specific functions and localizations, which have distinct roles in the response to bacterial exposure (see above), ii) host complexity - different organs within one host present different microenvironments, which shape, and are shaped by, host-bacteria interaction. These effects are direct (e.g. during a systemic infection (Kurtz et al., 2017)) or indirect (e.g. by production of soluble metabolites by the microbiota (Trompette et al., 2018)), iii) bacterial population complexity - bacterial populations often present phenotypic heterogeneity, which enables a dynamic adaptation to different environmental conditions, and thereby to different steps of the host-bacteria interaction (see above), iv) bacteria-bacteria interaction *within-host* - the commensal bacteria present in a host, e.g. as part of the intestinal microbiota, interact with newly arriving strains and influence the outcome of this interaction e.g. by nutrient competition, direct bacteria-bacteria interaction or modulation of virulence factors expression (see above), v) the spatiotemporal dynamics of these processes, given by the reciprocal nature of interactions between host and bacterial cells at any given time (Chapter 2). This complexity poses challenges to the analysis of host-bacteria interactions, especially in pinpointing contributions of specific cell types or phenotypic subpopulations. Recent advances have yielded tools to specifically dissect the spatiotemporal dynamics of host-microbe interaction.

Cell culture models are useful tools to reduce complexity and analyze individual host-microbe interaction in a controlled system. They therefore have great value for the detailed analysis of molecular signaling mechanisms and contributed to the understanding of the disease/infection-promoting capacity of several virulence factors (Andritschke et al., 2016; Di Martino et al., 2019; Kreibich et al., 2015). While protocols for cultivation of immune cells exist for decades (Sallusto and Lanzavecchia, 1994; Stone and Takemoto, 1970), the maintenance of primary epithelial cells in culture had remained challenging until recently. This resulted in the generation of a number of immortalized epithelial cell lines (Bens et al., 1996; Fogh and Trempe, 1975; Fogh et al., 1977; Scherer et al., 1953), in which oncogenes/the lack of tumor suppressor genes maintain proliferative capacity. However, immortalized cell lines are unlikely to represent a realistic model for short-lived IECs - in particular for studies involving cell death. Recently developed protocols for the isolation, maintenance and differentiation of intestinal epithelial stem cells as intestinal organoids (Sato et al., 2009) provide an attractive alternative. These organoids recapitulate the tissue architecture of the epithelium *in vivo* and display cellular heterogeneity (Figure 11) (Bar-Ephraim et al., 2020). Consequently, intestinal organoids become established as a model for the analysis of bacterial infection of the epithelium (Co et al., 2019; Foulke-Abel et al., 2014; Holly et al., 2020; Mitchell et al., 2020; Sun, 2017; Yin and Zhou, 2018; Zhang et al., 2014). It however remained unclear, to which extent organoids mimic their tissue of origin, and how the donor microbiota would impact this phenotype. We addressed this in a systematic study described in Chapter 5.

While cell culture systems enable precise identification and quantification of mechanisms of microbe interactions with specific cell types, they often fail to recapitulate complex tissue environments *in vivo*. Therefore, the full relevance of mechanisms discovered *in vitro* can only be verified in animal models (Fattinger et al., 2020). This makes robust animal models indispensable for translatable insights on the reciprocal relationship between microbes and hosts. In the last years it became evident that microbiota

shifts in separately held mice can have substantial effects on phenotypes in studies of host-microbe interaction, and that co-housing for up to eight weeks is not sufficient to neutralize these shifts (Mamantopoulos et al., 2017; Robertson et al., 2019; Stappenbeck and Virgin, 2016) (Chapter 4). Wild type littermate controls for transgenic animals to normalize for microbiota shifts are therefore one key component of robust animal models in the context of host-microbe interaction (Mamantopoulos et al., 2018).

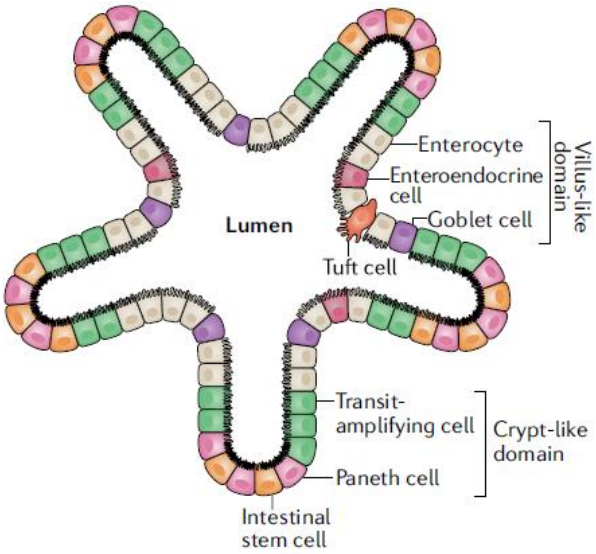

Figure 11 ***Schematic drawing of a small intestinal organoid.*** *Organoids recapitulate tissue architecture and cellular differentiation in culture. Published in Bar-Ephraim et al., 2020.*

The spatiotemporal dynamics of host-microbe interactions *in vivo* make them difficult to study. Conventional methods for the read out of bacterial population size and quantification of immune responses were designed to provide snap shot information at the time point of analysis. Due to the dynamic nature of bacterial colonization they therefore do not provide fully conclusive information about population kinetics prior to analysis. The use of genetic barcoding strategies in combination with mathematical modeling enables mechanistic and quantitative analyses of these relationships, and provides information on events which took place before the time point of analysis (Abel et al., 2015; Grant et al., 2008). These approaches are elaborated in Chapter 2 and applied in Chapter 4.

AIMS OF THE PRESENTED THESIS

PRRs initiate mucosal immune responses to contain enteropathogen infections. These PRRs bind to conserved bacterial structures, which are also present on commensal bacteria of the microbiota. At systemic sites, which are normally devoid of bacteria, PRR activation triggers pronounced inflammatory responses to clear the bacterial intruder. The omnipresence of commensal bacteria (carrying potential PRR stimuli) in the intestine, by contrast, poses a particular challenge to the innate mucosal immune system. Specific mechanisms in the intestinal mucosa have to ensure tolerance to commensals to avoid overstimulation and chronic inflammation. At the same time, the mucosal immune system cannot be completely blind to bacterial triggers, as enteropathogens are regularly ingested and pose a severe threat. Therefore, a fine-tuned system of regulatory mechanisms must exist to specifically mount innate immune responses to enteropathogens, but not to commensals. Several mechanisms contributing to this were identified, but it still remains unclear how PRRs mediate antibacterial defenses specifically in response to pathogenic threats.

In my PhD thesis, I used the model enteropathogen *S*. Tm as a probe to study mucosal defenses. *S*. Tm is well suited for this analysis, as it offers several in-depth characterized models of oral and systemic infection to decipher the contributions of specific PRRs and cell types to defense. Understanding which features of a pathogen result in their recognition by the innate mucosal immune system and the mounting of an immune response can aid in understanding tolerance towards commensal bacteria and its breakdown in inflammatory diseases of the intestine.

In a first approach I have addressed how sensing of bacterial LPS via TLR4 is wired in the intestinal mucosa. Specifically, I have analyzed direct versus indirect activation of epithelial NFκB signaling by LPS and *S*. Tm exposure. These data are presented in Chapter 3.

The role of epithelial NAIP/NLRC4 in protection from *S*. Tm infection is well established. However, it remained unclear at how it is implicated in the protection from systemic pathogen spread. This has been addressed in a further project, in which I have analyzed the impact of inflammasome components in immune cells and IECs in the protection from systemic spread during oral *S*. Tm infection. To differentiate between epithelial and immune cell contributions, we used an approach employing barcoded bacteria and mathematical modeling. This approach is elaborated in detail in Chapter 2 and the results are presented in Chapter 4.

Deciphering the contributions of different cell types to an immune response requires reliable models for these studies. Intestinal organoids emerge as a model to analyze epithelial responses to bacterial infection. However, it had remained unclear to which degree organoids recapitulate their tissue of origin. I have addressed this question in Chapter 5. A huge confounding factor in studies of host-microbe interactions are microbiota shifts in separately maintained transgenic mouse lines, which can be controlled for with littermate wild type control mice. Therefore, I have also analyzed the influence of the donor microbiota on organoid phenotypes, to assess the requirement for littermate control organoids.

In combination, these approaches should help to decipher the contributions of specific PRRs and cell types in the intestinal mucosa and beyond to the response to oral infection with *S*. Tm in order to identify general principles of the regulation of innate bacterial sensing in the intestinal mucosa.

REFERENCES

Aachoui, Y., Leaf, I.A., Hagar, J.A., Fontana, M.F., Campos, C.G., Zak, D.E., Tan, M.H., Cotter, P.A., Vance, R.E., Aderem, A., et al. (2013). Caspase-11 protects against bacteria that escape the vacuole. Science *339*, 975–978.

Abel, S., Wiesch, P.A. zur, Davis, B.M., and Waldor, M.K. (2015). Analysis of Bottlenecks in Experimental Models of Infection. PLOS Pathog. *11*, e1004823.

Ackermann, M., Stecher, B., Freed, N.E., Songhet, P., Hardt, W.-D., and Doebeli, M. (2008). Self-destructive cooperation mediated by phenotypic noise. Nature *454*, 987–990.

Adachi, O., Kawai, T., Takeda, K., Matsumoto, M., Tsutsui, H., Sakagami, M., Nakanishi, K., and Akira, S. (1998). Targeted disruption of the MyD88 gene results in loss of IL-1- and IL-18-mediated function. Immunity *9*, 143–150.

Alexopoulou, L., Holt, A.C., Medzhitov, R., and Flavell, R.A. (2001). Recognition of double-stranded RNA and activation of NF-kappaB by Toll-like receptor 3. Nature *413*, 732–738.

Allaire, J.M., Crowley, S.M., Law, H.T., Chang, S.-Y., Ko, H.-J., and Vallance, B.A. (2018). The Intestinal Epithelium: Central Coordinator of Mucosal Immunity. Trends Immunol. *39*, 677–696.

Andritschke, D., Dilling, S., Emmenlauer, M., Welz, T., Schmich, F., Misselwitz, B., Rämö, P., Rottner, K., Kerkhoff, E., Wada, T., et al. (2016). A Genome-Wide siRNA Screen Implicates Spire1/2 in SipA-Driven Salmonella Typhimurium Host Cell Invasion. PLoS ONE *11*.

Arpaia, N., Godec, J., Lau, L., Sivick, K.E., McLaughlin, L.M., Jones, M.B., Dracheva, T., Peterson, S.N., Monack, D.M., and Barton, G.M. (2011). TLR signaling is required for Salmonella typhimurium virulence. Cell *144*, 675–688.

Ashida, H., Kim, M., Schmidt-Supprian, M., Ma, A., Ogawa, M., and Sasakawa, C. (2010). A bacterial E3 ubiquitin ligase IpaH9.8 targets NEMO/IKKgamma to dampen the host NF-kappaB-mediated inflammatory response. Nat. Cell Biol. *12*, 66–73; sup pp 1-9.

Bain, C.C., Scott, C.L., Uronen-Hansson, H., Gudjonsson, S., Jansson, O., Grip, O., Guilliams, M., Malissen, B., Agace, W.W., and Mowat, A.M. (2013). Resident and pro-inflammatory macrophages in the colon represent alternative context-dependent fates of the same Ly6C hi monocyte precursors. Mucosal Immunol. *6*, 498–510.

Bakkeren, E., Huisman, J.S., Fattinger, S.A., Hausmann, A., Furter, M., Egli, A., Slack, E., Sellin, M.E., Bonhoeffer, S., Regoes, R.R., et al. (2019). Salmonella persisters promote the spread of antibiotic resistance plasmids in the gut. Nature *573*, 276–280.

Bar-Ephraim, Y.E., Kretzschmar, K., and Clevers, H. (2020). Organoids in immunological research. Nat. Rev. Immunol. *20*, 279–293.

Barker, N., van Es, J.H., Kuipers, J., Kujala, P., van den Born, M., Cozijnsen, M., Haegebarth, A., Korving, J., Begthel, H., Peters, P.J., et al. (2007). Identification of stem cells in small intestine and colon by marker gene Lgr5. Nature *449*, 1003–1007.

Barthel, M., Hapfelmeier, S., Quintanilla-Martínez, L., Kremer, M., Rohde, M., Hogardt, M., Pfeffer, K., Rüssmann, H., and Hardt, W.-D. (2003). Pretreatment of Mice with Streptomycin Provides a Salmonella enterica Serovar Typhimurium Colitis Model That Allows Analysis of Both Pathogen and Host. Infect. Immun. *71*, 2839–2858.

Bens, M., Bogdanova, A., Cluzeaud, F., Miquerol, L., Kerneis, S., Kraehenbuhl, J.P., Kahn, A., Pringault, E., and Vandewalle, A. (1996). Transimmortalized mouse intestinal cells (m-ICc12) that maintain a crypt phenotype. Am. J. Physiol. *270*, C1666-1674.

Birchenough, G.M.H., Nyström, E.E.L., Johansson, M.E.V., and Hansson, G.C. (2016). A sentinel goblet cell guards the colonic crypt by triggering Nlrp6-dependent Muc2 secretion. Science *352*, 1535–1542.

Blasche, S., Mörtl, M., Steuber, H., Siszler, G., Nisa, S., Schwarz, F., Lavrik, I., Gronewold, T.M.A., Maskos, K., Donnenberg, M.S., et al. (2013). The E. coli effector protein NleF is a caspase inhibitor. PloS One *8*, e58937.

Blaser, H., Dostert, C., Mak, T.W., and Brenner, D. TNF and ROS Crosstalk in Inflammation. Trends Cell Biol. *0*.

Bohnhoff, M., and Miller, C.P. (1962). Enhanced Susceptibility to Salmonella Infection in Streptomycin-Treated Mice. J. Infect. Dis. *111*, 117–127.

Bohnhoff, M., Drake, B.L., and Miller, C.P. (1954). Effect of streptomycin on susceptibility of intestinal tract to experimental Salmonella infection. Proc. Soc. Exp. Biol. Med. Soc. Exp. Biol. Med. N. Y. N *86*, 132–137.

Bollrath, J., and Greten, F.R. (2009). IKK/NF-κB and STAT3 pathways: central signalling hubs in inflammation-mediated tumour promotion and metastasis. EMBO Rep. *10*, 1314–1319.

Bonham, K.S., Orzalli, M.H., Hayashi, K., Wolf, A.I., Glanemann, C., Weninger, W., Iwasaki, A., Knipe, D.M., and Kagan, J.C. (2014). A promiscuous lipid-binding protein diversifies the subcellular sites of toll-like receptor signal transduction. Cell *156*, 705–716.

Boyden, E.D., and Dietrich, W.F. (2006). Nalp1b controls mouse macrophage susceptibility to anthrax lethal toxin. Nat. Genet. *38*, 240–244.

Brandl, K., Plitas, G., Schnabl, B., DeMatteo, R.P., and Pamer, E.G. (2007). MyD88-mediated signals induce the bactericidal lectin RegIII gamma and protect mice against intestinal Listeria monocytogenes infection. J. Exp. Med. *204*, 1891–1900.

Bravo-Blas, A., Utriainen, L., Clay, S.L., Kästele, V., Cerovic, V., Cunningham, A.F., Henderson, I.R., Wall, D.M., and Milling, S.W.F. (2019). Salmonella enterica Serovar Typhimurium Travels to Mesenteric Lymph Nodes Both with Host Cells and Autonomously. J. Immunol. Baltim. Md 1950 *202*, 260–267.

Broz, P. (2019). Recognition of Intracellular Bacteria by Inflammasomes. Microbiol. Spectr. *7*.

Broz, P., and Dixit, V.M. (2016). Inflammasomes: mechanism of assembly, regulation and signalling. Nat. Rev. Immunol. *16*, 407–420.

Brugiroux, S., Beutler, M., Pfann, C., Garzetti, D., Ruscheweyh, H.-J., Ring, D., Diehl, M., Herp, S., Lötscher, Y., Hussain, S., et al. (2016). Genome-guided design of a defined mouse microbiota that confers colonization resistance against Salmonella enterica serovar Typhimurium. Nat. Microbiol. *2*, 16215.

Brumell, J.H., Tang, P., Zaharik, M.L., and Finlay, B.B. (2002). Disruption of the Salmonella-containing vacuole leads to increased replication of Salmonella enterica serovar typhimurium in the cytosol of epithelial cells. Infect. Immun. *70*, 3264–3270.

Bumann, D., and Cunrath, O. (2017). Heterogeneity of Salmonella-host interactions in infected host tissues. Curr. Opin. Microbiol. *39*, 57–63.

Cahenzli, J., Köller, Y., Wyss, M., Geuking, M.B., and McCoy, K.D. (2013). Intestinal Microbial Diversity during Early-Life Colonization Shapes Long-Term IgE Levels. Cell Host Microbe *14*, 559–570.

Carden, S.E., Walker, G.T., Honeycutt, J., Lugo, K., Pham, T., Jacobson, A., Bouley, D., Idoyaga, J., Tsolis, R.M., and Monack, D. (2017). Pseudogenization of the Secreted Effector Gene sseI Confers Rapid Systemic Dissemination of S. Typhimurium ST313 within Migratory Dendritic Cells. Cell Host Microbe *21*, 182–194.

Cerovic, V., Bain, C.C., Mowat, A.M., and Milling, S.W.F. (2014). Intestinal macrophages and dendritic cells: what's the difference? Trends Immunol. *35*, 270–277.

Charles A Janeway, J., Travers, P., Walport, M., and Shlomchik, M.J. (2001). Receptors of the innate immune system. Immunobiol. Immune Syst. Health Dis. 5th Ed.

Chung, L.K., Park, Y.H., Zheng, Y., Brodsky, I.E., Hearing, P., Kastner, D.L., Chae, J.J., and Bliska, J.B. (2016). The Yersinia Virulence Factor YopM Hijacks Host Kinases to Inhibit Type III Effector-Triggered Activation of the Pyrin Inflammasome. Cell Host Microbe *20*, 296–306.

Claudi, B., Spröte, P., Chirkova, A., Personnic, N., Zankl, J., Schürmann, N., Schmidt, A., and Bumann, D. (2014). Phenotypic variation of Salmonella in host tissues delays eradication by antimicrobial chemotherapy. Cell *158*, 722–733.

Co, J.Y., Margalef-Català, M., Li, X., Mah, A.T., Kuo, C.J., Monack, D.M., and Amieva, M.R. (2019). Controlling Epithelial Polarity: A Human Enteroid Model for Host-Pathogen Interactions. Cell Rep. *26*, 2509-2520.e4.

Collier-Hyams, L.S., Zeng, H., Sun, J., Tomlinson, A.D., Bao, Z.Q., Chen, H., Madara, J.L., Orth, K., and Neish, A.S. (2002). Cutting edge: Salmonella AvrA effector inhibits the key proinflammatory, anti-apoptotic NF-kappa B pathway. J. Immunol. Baltim. Md 1950 *169*, 2846–2850.

Coombes, J.L., Siddiqui, K.R.R., Arancibia-Cárcamo, C.V., Hall, J., Sun, C.-M., Belkaid, Y., and Powrie, F. (2007). A functionally specialized population of mucosal CD103+ DCs induces Foxp3+ regulatory T cells via a TGF-β– and retinoic acid–dependent mechanism. J. Exp. Med. *204*, 1757–1764.

Cornes, J.S. (1965). Number, size, and distribution of Peyer's patches in the human small intestine: Part I The development of Peyer's patches. Gut *6*, 225–229.

Corridoni, D., Chapman, T., Ambrose, T., and Simmons, A. (2018). Emerging Mechanisms of Innate Immunity and Their Translational Potential in Inflammatory Bowel Disease. Front. Med. *5*, 32.

Cullen, T.W., Schofield, W.B., Barry, N.A., Putnam, E.E., Rundell, E.A., Trent, M.S., Degnan, P.H., Booth, C.J., Yu, H., and Goodman, A.L. (2015). Gut microbiota. Antimicrobial peptide resistance mediates resilience of prominent gut commensals during inflammation. Science *347*, 170–175.

Dessein, R., Gironella, M., Vignal, C., Peyrin-Biroulet, L., Sokol, H., Secher, T., Lacas-Gervais, S., Gratadoux, J.-J., Lafont, F., Dagorn, J.-C., et al. (2009). Toll-like receptor 2 is critical for induction of Reg3 beta expression and intestinal clearance of Yersinia pseudotuberculosis. Gut *58*, 771–776.

Dheer, R., Santaolalla, R., Davies, J.M., Lang, J.K., Phillips, M.C., Pastorini, C., Vazquez-Pertejo, M.T., and Abreu, M.T. (2016). Intestinal Epithelial Toll-Like Receptor 4 Signaling Affects Epithelial Function and Colonic Microbiota and Promotes a Risk for Transmissible Colitis. Infect. Immun. *84*, 798–810.

Di Martino, M.L., Ek, V., Hardt, W.-D., Eriksson, J., and Sellin, M.E. (2019). Barcoded Consortium Infections Resolve Cell Type-Dependent Salmonella enterica Serovar Typhimurium Entry Mechanisms. MBio *10*.

Diao, J., Zhang, Y., Huibregtse, J.M., Zhou, D., and Chen, J. (2008). Crystal structure of SopA, a Salmonella effector protein mimicking a eukaryotic ubiquitin ligase. Nat. Struct. Mol. Biol. *15*, 65–70.

Diard, M., and Hardt, W.-D. (2017a). Evolution of bacterial virulence. FEMS Microbiol. Rev. *41*, 679–697.

Diard, M., and Hardt, W.-D. (2017b). Basic Processes inSalmonella-Host Interactions: Within-Host Evolution and the Transmission of the Virulent Genotype. Microbiol. Spectr. *5*.

Diard, M., Garcia, V., Maier, L., Remus-Emsermann, M.N.P., Regoes, R.R., Ackermann, M., and Hardt, W.-D. (2013). Stabilization of cooperative virulence by the expression of an avirulent phenotype. Nature *494*, 353–356.

Diard, M., Sellin, M.E., Dolowschiak, T., Arnoldini, M., Ackermann, M., and Hardt, W.-D. (2014). Antibiotic treatment selects for cooperative virulence of Salmonella typhimurium. Curr. Biol. CB *24*, 2000–2005.

Diebold, S.S., Kaisho, T., Hemmi, H., Akira, S., and Reis e Sousa, C. (2004). Innate antiviral responses by means of TLR7-mediated recognition of single-stranded RNA. Science *303*, 1529–1531.

Doerflinger, M., Deng, Y., Whitney, P., Salvamoser, R., Engel, S., Kueh, A.J., Tai, L., Bachem, A., Gressier, E., Geoghegan, N.D., et al. (2020). Flexible Usage and Interconnectivity of Diverse Cell Death Pathways Protect against Intracellular Infection. Immunity.

Dolowschiak, T., Mueller, A.A., Pisan, L.J., Feigelman, R., Felmy, B., Sellin, M.E., Namineni, S., Nguyen, B.D., Wotzka, S.Y., Heikenwalder, M., et al. (2016). IFN-γ Hinders Recovery from Mucosal Inflammation during Antibiotic Therapy for Salmonella Gut Infection. Cell Host Microbe *20*, 238–249.

Duan, Y., Llorente, C., Lang, S., Brandl, K., Chu, H., Jiang, L., White, R.C., Clarke, T.H., Nguyen, K., Torralba, M., et al. (2019). Bacteriophage targeting of gut bacterium attenuates alcoholic liver disease. Nature *575*, 505–511.

Ducarmon, Q.R., Zwittink, R.D., Hornung, B.V.H., Schaik, W. van, Young, V.B., and Kuijper, E.J. (2019). Gut Microbiota and Colonization Resistance against Bacterial Enteric Infection. Microbiol. Mol. Biol. Rev. *83*.

Duerr, C.U., Zenk, S.F., Chassin, C., Pott, J., Gütle, D., Hensel, M., and Hornef, M.W. (2009). O-antigen delays lipopolysaccharide recognition and impairs antibacterial host defense in murine intestinal epithelial cells. PLoS Pathog. *5*, e1000567.

El Qaidi, S., Chen, K., Halim, A., Siukstaite, L., Rueter, C., Hurtado-Guerrero, R., Clausen, H., and Hardwidge, P.R. (2017). NleB/SseK effectors fromCitrobacter rodentium,Escherichia coli, andSalmonella entericadisplay distinct differences in host substrate specificity. J. Biol. Chem. *292*, 11423–11430.

Emmerich, C.H., Ordureau, A., Strickson, S., Arthur, J.S.C., Pedrioli, P.G.A., Komander, D., and Cohen, P. (2013). Activation of the canonical IKK complex by K63/M1-linked hybrid ubiquitin chains. Proc. Natl. Acad. Sci. *110*, 15247–15252.

Fattinger, S.A., Böck, D., Di Martino, M.L., Deuring, S., Samperio Ventayol, P., Ek, V., Furter, M., Kreibich, S., Bosia, F., Müller-Hauser, A.A., et al. (2020). Salmonella Typhimurium discreet-invasion of the murine gut absorptive epithelium. PLoS Pathog. *16*, e1008503.

Fernandes-Alnemri, T., Yu, J.-W., Juliana, C., Solorzano, L., Kang, S., Wu, J., Datta, P., McCormick, M., Huang, L., McDermott, E., et al. (2010). The AIM2 inflammasome is critical for innate immunity to Francisella tularensis. Nat. Immunol. *11*, 385–393.

Fischer, C., Metsger, M., Bauch, S., Vidal, R., Böttcher, M., Grote, P., Kliem, M., and Sauer, S. (2019). Signals trigger state-specific transcriptional programs to support diversity and homeostasis in immune cells. Sci. Signal. *12*.

Fiskin, E., Bhogaraju, S., Herhaus, L., Kalayil, S., Hahn, M., and Dikic, I. (2017). Structural basis for the recognition and degradation of host TRIM proteins by Salmonella effector SopA. Nat. Commun. *8*, 14004.

Fitzgerald, K.A., and Kagan, J.C. (2020). Toll-like Receptors and the Control of Immunity. Cell *180*, 1044–1066.

Fitzgerald, K.A., Palsson-McDermott, E.M., Bowie, A.G., Jefferies, C.A., Mansell, A.S., Brady, G., Brint, E., Dunne, A., Gray, P., Harte, M.T., et al. (2001). Mal (MyD88-adapter-like) is required for Toll-like receptor-4 signal transduction. Nature *413*, 78–83.

Fitzgerald, K.A., Rowe, D.C., Barnes, B.J., Caffrey, D.R., Visintin, A., Latz, E., Monks, B., Pitha, P.M., and Golenbock, D.T. (2003). LPS-TLR4 signaling to IRF-3/7 and NF-kappaB involves the toll adapters TRAM and TRIF. J. Exp. Med. *198*, 1043–1055.

Fogh, J., and Trempe, G. (1975). New Human Tumor Cell Lines. In Human Tumor Cells in Vitro, J. Fogh, ed. (Boston, MA: Springer US), pp. 115–159.

Fogh, J., Wright, W.C., and Loveless, J.D. (1977). Absence of HeLa cell contamination in 169 cell lines derived from human tumors. J. Natl. Cancer Inst. *58*, 209–214.

Foulke-Abel, J., In, J., Kovbasnjuk, O., Zachos, N.C., Ettayebi, K., Blutt, S.E., Hyser, J.M., Zeng, X.-L., Crawford, S.E., Broughman, J.R., et al. (2014). Human enteroids as an ex-vivo model of host–pathogen interactions in the gastrointestinal tract. Exp. Biol. Med. *239*, 1124–1134.

Franchi, L., Amer, A., Body-Malapel, M., Kanneganti, T.-D., Özören, N., Jagirdar, R., Inohara, N., Vandenabeele, P., Bertin, J., Coyle, A., et al. (2006). Cytosolic flagellin requires Ipaf for activation of caspase-1 and interleukin 1β in salmonella-infected macrophages. Nat. Immunol. *7*, 576–582.

Frey, E.A., Miller, D.S., Jahr, T.G., Sundan, A., Bazil, V., Espevik, T., Finlay, B.B., and Wright, S.D. (1992). Soluble CD14 participates in the response of cells to lipopolysaccharide. J. Exp. Med. *176*, 1665–1671.

Fulde, M., Sommer, F., Chassaing, B., van Vorst, K., Dupont, A., Hensel, M., Basic, M., Klopfleisch, R., Rosenstiel, P., Bleich, A., et al. (2018). Neonatal selection by Toll-like receptor 5 influences long-term gut microbiota composition. Nature *560*, 489–493.

Furter, M., Sellin, M.E., Hansson, G.C., and Hardt, W.-D. (2019). Mucus Architecture and Near-Surface Swimming Affect Distinct Salmonella Typhimurium Infection Patterns along the Murine Intestinal Tract. Cell Rep. *27*, 2665-2678.e3.

Galán, J.E., and Waksman, G. (2018). Protein-Injection Machines in Bacteria. Cell *172*, 1306–1318.

Galán, J.E., Lara-Tejero, M., Marlovits, T.C., and Wagner, S. (2014). Bacterial type III secretion systems: specialized nanomachines for protein delivery into target cells. Annu. Rev. Microbiol. *68*, 415–438.

Gehart, H., and Clevers, H. (2019). Tales from the crypt: new insights into intestinal stem cells. Nat. Rev. Gastroenterol. Hepatol. *16*, 19–34.

Gerlach, R.G., Jäckel, D., Stecher, B., Wagner, C., Lupas, A., Hardt, W.-D., and Hensel, M. (2007). Salmonella Pathogenicity Island 4 encodes a giant non-fimbrial adhesin and the cognate type 1 secretion system. Cell. Microbiol. *9*, 1834–1850.

Gewirtz, A.T., Navas, T.A., Lyons, S., Godowski, P.J., and Madara, J.L. (2001). Cutting edge: bacterial flagellin activates basolaterally expressed TLR5 to induce epithelial proinflammatory gene expression. J. Immunol. Baltim. Md 1950 *167*, 1882–1885.

Gioannini, T.L., and Weiss, J.P. (2007). Regulation of interactions of Gram-negative bacterial endotoxins with mammalian cells. Immunol. Res. *39*, 249–260.

Gioannini, T.L., Teghanemt, A., Zhang, D., Coussens, N.P., Dockstader, W., Ramaswamy, S., and Weiss, J.P. (2004). Isolation of an endotoxin-MD-2 complex that produces Toll-like receptor 4-dependent cell activation at picomolar concentrations. Proc. Natl. Acad. Sci. U. S. A. *101*, 4186–4191.

Gollwitzer, E.S., and Marsland, B.J. (2015). Impact of Early-Life Exposures on Immune Maturation and Susceptibility to Disease. Trends Immunol.

Gollwitzer, E.S., Saglani, S., Trompette, A., Yadava, K., Sherburn, R., McCoy, K.D., Nicod, L.P., Lloyd, C.M., and Marsland, B.J. (2014). Lung microbiota promotes tolerance to allergens in neonates via PD-L1. Nat. Med. *20*, 642–647.

Golubeva, Y.A., Sadik, A.Y., Ellermeier, J.R., and Slauch, J.M. (2012). Integrating global regulatory input into the Salmonella pathogenicity island 1 type III secretion system. Genetics *190*, 79–90.

Gomez de Agüero, M., Ganal-Vonarburg, S.C., Fuhrer, T., Rupp, S., Uchimura, Y., Li, H., Steinert, A., Heikenwalder, M., Hapfelmeier, S., Sauer, U., et al. (2016). The maternal microbiota drives early postnatal innate immune development. Science *351*, 1296–1302.

Grant, A.J., Restif, O., McKinley, T.J., Sheppard, M., Maskell, D.J., and Mastroeni, P. (2008). Modelling within-host spatiotemporal dynamics of invasive bacterial disease. PLoS Biol. *6*, e74.

Guma, M., Stepniak, D., Shaked, H., Spehlmann, M.E., Shenouda, S., Cheroutre, H., Vicente-Suarez, I., Eckmann, L., Kagnoff, M.F., and Karin, M. (2011). Constitutive intestinal NF-κB does not trigger destructive inflammation unless accompanied by MAPK activation. J. Exp. Med. *208*, 1889–1900.

Günster, R.A., Matthews, S.A., Holden, D.W., and Thurston, T.L.M. (2017). SseK1 and SseK3 Type III Secretion System Effectors Inhibit NF-κB Signaling and Necroptotic Cell Death in Salmonella-Infected Macrophages. Infect. Immun. *85*.

Haber, A.L., Biton, M., Rogel, N., Herbst, R.H., Shekhar, K., Smillie, C., Burgin, G., Delorey, T.M., Howitt, M.R., Katz, Y., et al. (2017). A single-cell survey of the small intestinal epithelium. Nature *551*, 333–339.

Hagar, J.A., Powell, D.A., Aachoui, Y., Ernst, R.K., and Miao, E.A. (2013). Cytoplasmic LPS activates caspase-11: implications in TLR4-independent endotoxic shock. Science *341*, 1250–1253.

Haneda, T., Ishii, Y., Shimizu, H., Ohshima, K., Iida, N., Danbara, H., and Okada, N. (2012). Salmonella type III effector SpvC, a phosphothreonine lyase, contributes to reduction in inflammatory response during intestinal phase of infection. Cell. Microbiol. *14*, 485–499.

Hapfelmeier, S., Stecher, B., Barthel, M., Kremer, M., Müller, A.J., Heikenwalder, M., Stallmach, T., Hensel, M., Pfeffer, K., Akira, S., et al. (2005). The Salmonella pathogenicity island (SPI)-2 and SPI-1 type III secretion systems allow Salmonella serovar typhimurium to trigger colitis via MyD88-dependent and MyD88-independent mechanisms. J. Immunol. Baltim. Md 1950 *174*, 1675–1685.

Hapfelmeier, S., Müller, A.J., Stecher, B., Kaiser, P., Barthel, M., Endt, K., Eberhard, M., Robbiani, R., Jacobi, C.A., Heikenwalder, M., et al. (2008). Microbe sampling by mucosal dendritic cells is a discrete, MyD88-independent step in DeltainvG S. Typhimurium colitis. J. Exp. Med. *205*, 437–450.

Haraga, A., and Miller, S.I. (2003). A Salmonella enterica serovar typhimurium translocated leucine-rich repeat effector protein inhibits NF-kappa B-dependent gene expression. Infect. Immun. *71*, 4052–4058.

Haraga, A., and Miller, S.I. (2006). A Salmonella type III secretion effector interacts with the mammalian serine/threonine protein kinase PKN1. Cell. Microbiol. *8*, 837–846.

Hardt, W.D., Chen, L.M., Schuebel, K.E., Bustelo, X.R., and Galán, J.E. (1998). S. typhimurium encodes an activator of Rho GTPases that induces membrane ruffling and nuclear responses in host cells. Cell *93*, 815–826.

Harrison, O.J., Srinivasan, N., Pott, J., Schiering, C., Krausgruber, T., Ilott, N.E., and Maloy, K.J. (2015). Epithelial-derived IL-18 regulates Th17 cell differentiation and Foxp3^{+} Treg cell function in the intestine. Mucosal Immunol. *8*, 1226–1236.

Hautefort, I., Thompson, A., Eriksson-Ygberg, S., Parker, M.L., Lucchini, S., Danino, V., Bongaerts, R.J.M., Ahmad, N., Rhen, M., and Hinton, J.C.D. (2008). During infection of epithelial cells Salmonella enterica

serovar Typhimurium undergoes a time-dependent transcriptional adaptation that results in simultaneous expression of three type 3 secretion systems. Cell. Microbiol. *10*, 958–984.

Hayashi, F., Smith, K.D., Ozinsky, A., Hawn, T.R., Yi, E.C., Goodlett, D.R., Eng, J.K., Akira, S., Underhill, D.M., and Aderem, A. (2001). The innate immune response to bacterial flagellin is mediated by Toll-like receptor 5. Nature *410*, 1099–1103.

Hayden, M.S., and Ghosh, S. (2014). Regulation of NF-κB by TNF family cytokines. Semin. Immunol. *26*, 253–266.

Haziot, A., Rong, G.W., Silver, J., and Goyert, S.M. (1993). Recombinant soluble CD14 mediates the activation of endothelial cells by lipopolysaccharide. J. Immunol. Baltim. Md 1950 *151*, 1500–1507.

Hefele, M., Stolzer, I., Ruder, B., He, G.-W., Mahapatro, M., Wirtz, S., Neurath, M.F., and Günther, C. (2018). Intestinal epithelial Caspase-8 signaling is essential to prevent necroptosis during Salmonella Typhimurium induced enteritis. Mucosal Immunol.

Heil, F., Hemmi, H., Hochrein, H., Ampenberger, F., Kirschning, C., Akira, S., Lipford, G., Wagner, H., and Bauer, S. (2004). Species-specific recognition of single-stranded RNA via toll-like receptor 7 and 8. Science *303*, 1526–1529.

Hemmi, H., Takeuchi, O., Kawai, T., Kaisho, T., Sato, S., Sanjo, H., Matsumoto, M., Hoshino, K., Wagner, H., Takeda, K., et al. (2000). A Toll-like receptor recognizes bacterial DNA. Nature *408*, 740–745.

Hemmi, H., Kaisho, T., Takeuchi, O., Sato, S., Sanjo, H., Hoshino, K., Horiuchi, T., Tomizawa, H., Takeda, K., and Akira, S. (2002). Small anti-viral compounds activate immune cells via the TLR7 MyD88-dependent signaling pathway. Nat. Immunol. *3*, 196–200.

Hensel, M., Shea, J.E., Gleeson, C., Jones, M.D., Dalton, E., and Holden, D.W. (1995). Simultaneous identification of bacterial virulence genes by negative selection. Science *269*, 400–403.

Herbrand, H., Bernhardt, G., Förster, R., and Pabst, O. (2008). Dynamics and function of solitary intestinal lymphoid tissue. Crit. Rev. Immunol. *28*, 1–13.

Hidmark, A., von Saint Paul, A., and Dalpke, A.H. (2012). Cutting edge: TLR13 is a receptor for bacterial RNA. J. Immunol. Baltim. Md 1950 *189*, 2717–2721.

Hoebe, K., Janssen, E.M., Kim, S.O., Alexopoulou, L., Flavell, R.A., Han, J., and Beutler, B. (2003). Upregulation of costimulatory molecules induced by lipopolysaccharide and double-stranded RNA occurs by Trif-dependent and Trif-independent pathways. Nat. Immunol. *4*, 1223–1229.

Holly, M.K., Han, X., Zhao, E.J., Crowley, S.M., Allaire, J.M., Knodler, L.A., Vallance, B.A., and Smith, J.G. (2020). Salmonella enterica Infection of Murine and Human Enteroid-Derived Monolayers Elicits Differential Activation of Epithelium-Intrinsic Inflammasomes. Infect. Immun. *88*.

Hornef, M.W., Frisan, T., Vandewalle, A., Normark, S., and Richter-Dahlfors, A. (2002). Toll-like receptor 4 resides in the Golgi apparatus and colocalizes with internalized lipopolysaccharide in intestinal epithelial cells. J. Exp. Med. *195*, 559–570.

Hornef, M.W., Normark, B.H., Vandewalle, A., and Normark, S. (2003). Intracellular recognition of lipopolysaccharide by toll-like receptor 4 in intestinal epithelial cells. J. Exp. Med. *198*, 1225–1235.

Horng, T., Barton, G.M., and Medzhitov, R. (2001). TIRAP: an adapter molecule in the Toll signaling pathway. Nat. Immunol. *2*, 835–841.

Hu, G.-Q., Song, P.-X., Chen, W., Qi, S., Yu, S.-X., Du, C.-T., Deng, X.-M., Ouyang, H.-S., and Yang, Y.-J. (2017). Cirtical role for Salmonella effector SopB in regulating inflammasome activation. Mol. Immunol. *90*, 280–286.

Hung, C.-C., Garner, C.D., Slauch, J.M., Dwyer, Z.W., Lawhon, S.D., Frye, J.G., McClelland, M., Ahmer, B.M.M., and Altier, C. (2013). The intestinal fatty acid propionate inhibits Salmonella invasion through the post-translational control of HilD. Mol. Microbiol. *87*, 1045–1060.

Jacobson, A., Lam, L., Rajendram, M., Tamburini, F., Honeycutt, J., Pham, T., Van Treuren, W., Pruss, K., Stabler, S.R., Lugo, K., et al. (2018). A Gut Commensal-Produced Metabolite Mediates Colonization Resistance to Salmonella Infection. Cell Host Microbe *24*, 296-307.e7.

Jin, M.S., and Lee, J.-O. (2008). Structures of the toll-like receptor family and its ligand complexes. Immunity *29*, 182–191.

Joeris, T., Müller-Luda, K., Agace, W.W., and Mowat, A.M. (2017). Diversity and functions of intestinal mononuclear phagocytes. Mucosal Immunol. *10*, 845–864.

Johansson, M.E.V., and Hansson, G.C. (2016). Immunological aspects of intestinal mucus and mucins. Nat. Rev. Immunol. *16*, 639–649.

Johansson, M.E.V., Phillipson, M., Petersson, J., Velcich, A., Holm, L., and Hansson, G.C. (2008). The inner of the two Muc2 mucin-dependent mucus layers in colon is devoid of bacteria. Proc. Natl. Acad. Sci. U. S. A. *105*, 15064–15069.

Johansson, M.E.V., Ambort, D., Pelaseyed, T., Schütte, A., Gustafsson, J.K., Ermund, A., Subramani, D.B., Holmén-Larsson, J.M., Thomsson, K.A., Bergström, J.H., et al. (2011). Composition and functional role of the mucus layers in the intestine. Cell. Mol. Life Sci. CMLS *68*, 3635–3641.

Jorgensen, I., Lopez, J.P., Laufer, S.A., and Miao, E.A. (2016a). IL-1β, IL-18, and eicosanoids promote neutrophil recruitment to pore-induced intracellular traps following pyroptosis. Eur. J. Immunol. *46*, 2761–2766.

Jorgensen, I., Zhang, Y., Krantz, B.A., and Miao, E.A. (2016b). Pyroptosis triggers pore-induced intracellular traps (PITs) that capture bacteria and lead to their clearance by efferocytosis. J. Exp. Med. *213*, 2113–2128.

Kagan, J.C., and Medzhitov, R. (2006). Phosphoinositide-mediated adaptor recruitment controls Toll-like receptor signaling. Cell *125*, 943–955.

Kaiser, P., Diard, M., Stecher, B., and Hardt, W.-D. (2012). The streptomycin mouse model for Salmonella diarrhea: functional analysis of the microbiota, the pathogen's virulence factors, and the host's mucosal immune response. Immunol. Rev. *245*, 56–83.

Kaiser, P., Slack, E., Grant, A.J., Hardt, W.-D., and Regoes, R.R. (2013). Lymph node colonization dynamics after oral Salmonella Typhimurium infection in mice. PLoS Pathog. *9*, e1003532.

Kamanova, J., Sun, H., Lara-Tejero, M., and Galán, J.E. (2016). The Salmonella Effector Protein SopA Modulates Innate Immune Responses by Targeting TRIM E3 Ligase Family Members. PLoS Pathog. *12*, e1005552.

Kang, J.Y., Nan, X., Jin, M.S., Youn, S.-J., Ryu, Y.H., Mah, S., Han, S.H., Lee, H., Paik, S.-G., and Lee, J.-O. (2009). Recognition of lipopeptide patterns by Toll-like receptor 2-Toll-like receptor 6 heterodimer. Immunity *31*, 873–884.

Kayagaki, N., Warming, S., Lamkanfi, M., Vande Walle, L., Louie, S., Dong, J., Newton, K., Qu, Y., Liu, J., Heldens, S., et al. (2011). Non-canonical inflammasome activation targets caspase-11. Nature *479*, 117–121.

Kayama, H., and Takeda, K. (2016). Functions of innate immune cells and commensal bacteria in gut homeostasis. J. Biochem. (Tokyo) *159*, 141–149.

Kayisoglu, O., Weiss, F., Niklas, C., Pierotti, I., Pompaiah, M., Wallaschek, N., Germer, C.-T., Wiegering, A., and Bartfeld, S. (2020). Location-specific cell identity rather than exposure to GI microbiota defines many innate immune signalling cascades in the gut epithelium. Gut gutjnl-2019-319919.

Keszei, A.F.A., Tang, X., McCormick, C., Zeqiraj, E., Rohde, J.R., Tyers, M., and Sicheri, F. (2014). Structure of an SspH1-PKN1 complex reveals the basis for host substrate recognition and mechanism of activation for a bacterial E3 ubiquitin ligase. Mol. Cell. Biol. *34*, 362–373.

Kinnebrew, M.A., Buffie, C.G., Diehl, G.E., Zenewicz, L.A., Leiner, I., Hohl, T.M., Flavell, R.A., Littman, D.R., and Pamer, E.G. (2012). Interleukin 23 production by intestinal CD103(+)CD11b(+) dendritic cells in response to bacterial flagellin enhances mucosal innate immune defense. Immunity *36*, 276–287.

Kirk, M.D., Pires, S.M., Black, R.E., Caipo, M., Crump, J.A., Devleesschauwer, B., Döpfer, D., Fazil, A., Fischer-Walker, C.L., Hald, T., et al. (2015). World Health Organization Estimates of the Global and Regional Disease Burden of 22 Foodborne Bacterial, Protozoal, and Viral Diseases, 2010: A Data Synthesis. PLoS Med. *12*, e1001921.

Klose, C.S.N., Kiss, E.A., Schwierzeck, V., Ebert, K., Hoyler, T., d'Hargues, Y., Göppert, N., Croxford, A.L., Waisman, A., Tanriver, Y., et al. (2013). A T-bet gradient controls the fate and function of CCR6-RORγt+ innate lymphoid cells. Nature *494*, 261–265.

Knodler, L.A., and Steele-Mortimer, O. (2005). The Salmonella effector PipB2 affects late endosome/lysosome distribution to mediate Sif extension. Mol. Biol. Cell *16*, 4108–4123.

Knodler, L.A., Vallance, B.A., Hensel, M., Jäckel, D., Finlay, B.B., and Steele-Mortimer, O. (2003). Salmonella type III effectors PipB and PipB2 are targeted to detergent-resistant microdomains on internal host cell membranes. Mol. Microbiol. *49*, 685–704.

Knodler, L.A., Vallance, B.A., Celli, J., Winfree, S., Hansen, B., Montero, M., and Steele-Mortimer, O. (2010). Dissemination of invasive Salmonella via bacterial-induced extrusion of mucosal epithelia. Proc. Natl. Acad. Sci. U. S. A. *107*, 17733–17738.

Knodler, L.A., Crowley, S.M., Sham, H.P., Yang, H., Wrande, M., Ma, C., Ernst, R.K., Steele-Mortimer, O., Celli, J., and Vallance, B.A. (2014). Noncanonical inflammasome activation of caspase-4/caspase-11 mediates epithelial defenses against enteric bacterial pathogens. Cell Host Microbe *16*, 249–256.

Kobayashi, T., Ogawa, M., Sanada, T., Mimuro, H., Kim, M., Ashida, H., Akakura, R., Yoshida, M., Kawalec, M., Reichhart, J.-M., et al. (2013). The Shigella OspC3 Effector Inhibits Caspase-4, Antagonizes Inflammatory Cell Death, and Promotes Epithelial Infection. Cell Host Microbe *13*, 570–583.

Kofoed, E.M., and Vance, R.E. (2011). Innate immune recognition of bacterial ligands by NAIPs determines inflammasome specificity. Nature *477*, 592–595.

Koscsó, B., Kurapati, S., Rodrigues, R.R., Nedjic, J., Gowda, K., Shin, C., Soni, C., Ashraf, A.Z., Purushothaman, I., Palisoc, M., et al. (2020). Gut-resident CX3CR1hi macrophages induce tertiary lymphoid structures and IgA response in situ. Sci. Immunol. *5*.

Kreibich, S., and Hardt, W.-D. (2015). Experimental approaches to phenotypic diversity in infection. Curr. Opin. Microbiol. *27*, 25–36.

Kreibich, S., Emmenlauer, M., Fredlund, J., Rämö, P., Münz, C., Dehio, C., Enninga, J., and Hardt, W.-D. (2015). Autophagy Proteins Promote Repair of Endosomal Membranes Damaged by the Salmonella Type Three Secretion System 1. Cell Host Microbe *18*, 527–537.

Kreuz, S., Siegmund, D., Scheurich, P., and Wajant, H. (2001). NF-κB Inducers Upregulate cFLIP, a Cycloheximide-Sensitive Inhibitor of Death Receptor Signaling. Mol. Cell. Biol. *21*, 3964–3973.

Kreuzer, M., and Hardt, W.-D. (2020). How Food Affects Colonization Resistance Against Enteropathogenic Bacteria. Annu. Rev. Microbiol. *74*, null.

Kröger, C., Colgan, A., Srikumar, S., Händler, K., Sivasankaran, S.K., Hammarlöf, D.L., Canals, R., Grissom, J.E., Conway, T., Hokamp, K., et al. (2013). An infection-relevant transcriptomic compendium for Salmonella enterica Serovar Typhimurium. Cell Host Microbe *14*, 683–695.

Kurtz, J.R., Goggins, J.A., and McLachlan, J.B. (2017). Salmonella infection: interplay between the bacteria and host immune system. Immunol. Lett. *190*, 42–50.

Latz, E., Verma, A., Visintin, A., Gong, M., Sirois, C.M., Klein, D.C.G., Monks, B.G., McKnight, C.J., Lamphier, M.S., Duprex, W.P., et al. (2007). Ligand-induced conformational changes allosterically activate Toll-like receptor 9. Nat. Immunol. *8*, 772–779.

Laughlin, R.C., Knodler, L.A., Barhoumi, R., Payne, H.R., Wu, J., Gomez, G., Pugh, R., Lawhon, S.D., Bäumler, A.J., Steele-Mortimer, O., et al. (2014). Spatial segregation of virulence gene expression during acute enteric infection with Salmonella enterica serovar Typhimurium. MBio *5*, e00946-00913.

Le Negrate, G., Faustin, B., Welsh, K., Loeffler, M., Krajewska, M., Hasegawa, P., Mukherjee, S., Orth, K., Krajewski, S., Godzik, A., et al. (2008). Salmonella secreted factor L deubiquitinase of Salmonella typhimurium inhibits NF-kappaB, suppresses IkappaBalpha ubiquitination and modulates innate immune responses. J. Immunol. Baltim. Md 1950 *180*, 5045–5056.

Lee, A.-Y., Chang, S.-Y., Kim, J.-I., Cha, H.-R., Jang, M.H., Yamamoto, M., and Kweon, M.-N. (2008). Dendritic cells in colonic patches and iliac lymph nodes are essential in mucosal IgA induction following intrarectal administration via CCR7 interaction. Eur. J. Immunol. *38*, 1127–1137.

Lee, J., Mo, J.-H., Katakura, K., Alkalay, I., Rucker, A.N., Liu, Y.-T., Lee, H.-K., Shen, C., Cojocaru, G., Shenouda, S., et al. (2006). Maintenance of colonic homeostasis by distinctive apical TLR9 signalling in intestinal epithelial cells. Nat. Cell Biol. *8*, 1327–1336.

Lee, J.D., Kravchenko, V., Kirkland, T.N., Han, J., Mackman, N., Moriarty, A., Leturcq, D., Tobias, P.S., and Ulevitch, R.J. (1993). Glycosyl-phosphatidylinositol-anchored or integral membrane forms of CD14 mediate identical cellular responses to endotoxin. Proc. Natl. Acad. Sci. U. S. A. *90*, 9930–9934.

Li, H., Xu, H., Zhou, Y., Zhang, J., Long, C., Li, S., Chen, S., Zhou, J.-M., and Shao, F. (2007). The phosphothreonine lyase activity of a bacterial type III effector family. Science *315*, 1000–1003.

Li, S., Zhang, L., Yao, Q., Li, L., Dong, N., Rong, J., Gao, W., Ding, X., Sun, L., Chen, X., et al. (2013). Pathogen blocks host death receptor signalling by arginine GlcNAcylation of death domains. Nature *501*, 242–246.

Lin, S.-C., Lo, Y.-C., and Wu, H. (2010). Helical assembly in the MyD88-IRAK4-IRAK2 complex in TLR/IL-1R signalling. Nature *465*, 885–890.

Liu, T., Zhang, L., Joo, D., and Sun, S.-C. (2017). NF-κB signaling in inflammation. Signal Transduct. Target. Ther. *2*, 1–9.

Loonen, L.M.P., Stolte, E.H., Jaklofsky, M.T.J., Meijerink, M., Dekker, J., van Baarlen, P., and Wells, J.M. (2014). REG3γ-deficient mice have altered mucus distribution and increased mucosal inflammatory responses to the microbiota and enteric pathogens in the ileum. Mucosal Immunol. *7*, 939–947.

Lotz, M., Gütle, D., Walther, S., Ménard, S., Bogdan, C., and Hornef, M.W. (2006). Postnatal acquisition of endotoxin tolerance in intestinal epithelial cells. J. Exp. Med. *203*, 973–984.

Mabbott, N.A., Donaldson, D.S., Ohno, H., Williams, I.R., and Mahajan, A. (2013). Microfold (M) cells: important immunosurveillance posts in the intestinal epithelium. Mucosal Immunol. *6*, 666–677.

Macpherson, A.J., and Uhr, T. (2004). Induction of Protective IgA by Intestinal Dendritic Cells Carrying Commensal Bacteria. Science *303*, 1662–1665.

Maier, L., Vyas, R., Cordova, C.D., Lindsay, H., Schmidt, T.S.B., Brugiroux, S., Periaswamy, B., Bauer, R., Sturm, A., Schreiber, F., et al. (2013). Microbiota-derived hydrogen fuels Salmonella typhimurium invasion of the gut ecosystem. Cell Host Microbe *14*, 641–651.

Maier, L., Diard, M., Sellin, M.E., Chouffane, E.-S., Trautwein-Weidner, K., Periaswamy, B., Slack, E., Dolowschiak, T., Stecher, B., Loverdo, C., et al. (2014). Granulocytes impose a tight bottleneck upon the gut luminal pathogen population during Salmonella typhimurium colitis. PLoS Pathog. *10*, e1004557.

Maloy, K.J., and Powrie, F. (2011). Intestinal homeostasis and its breakdown in inflammatory bowel disease. Nature *474*, 298–306.

Maltby, R., Leatham-Jensen, M.P., Gibson, T., Cohen, P.S., and Conway, T. (2013). Nutritional basis for colonization resistance by human commensal Escherichia coli strains HS and Nissle 1917 against E. coli O157:H7 in the mouse intestine. PloS One *8*, e53957.

Mamantopoulos, M., Ronchi, F., Van Hauwermeiren, F., Vieira-Silva, S., Yilmaz, B., Martens, L., Saeys, Y., Drexler, S.K., Yazdi, A.S., Raes, J., et al. (2017). Nlrp6- and ASC-Dependent Inflammasomes Do Not Shape the Commensal Gut Microbiota Composition. Immunity *47*, 339-348.e4.

Mamantopoulos, M., Ronchi, F., McCoy, K.D., and Wullaert, A. (2018). Inflammasomes make the case for littermate-controlled experimental design in studying host-microbiota interactions. Gut Microbes *9*, 374–381.

Marshman, E., Booth, C., and Potten, C.S. (2002). The intestinal epithelial stem cell. BioEssays *24*, 91–98.

Masahata, K., Umemoto, E., Kayama, H., Kotani, M., Nakamura, S., Kurakawa, T., Kikuta, J., Gotoh, K., Motooka, D., Sato, S., et al. (2014). Generation of colonic IgA-secreting cells in the caecal patch. Nat. Commun. *5*, 3704.

Mazurkiewicz, P., Thomas, J., Thompson, J.A., Liu, M., Arbibe, L., Sansonetti, P., and Holden, D.W. (2008). SpvC is a Salmonella effector with phosphothreonine lyase activity on host mitogen-activated protein kinases. Mol. Microbiol. *67*, 1371–1383.

McDonald, B., Zucoloto, A.Z., Yu, I.-L., Burkhard, R., Brown, K., Geuking, M.B., and McCoy, K.D. (2020). Programing of an Intravascular Immune Firewall by the Gut Microbiota Protects against Pathogen Dissemination during Infection. Cell Host Microbe S1931312820304108.

Medzhitov, R., and Janeway, C. (2000). The Toll receptor family and microbial recognition. Trends Microbiol. *8*, 452–456.

Mesquita, F.S., Thomas, M., Sachse, M., Santos, A.J.M., Figueira, R., and Holden, D.W. (2012). The Salmonella deubiquitinase SseL inhibits selective autophagy of cytosolic aggregates. PLoS Pathog. *8*, e1002743.

Mesquita, F.S., Holden, D.W., and Rolhion, N. (2013). Lack of effect of the Salmonella deubiquitinase SseL on the NF-κB pathway. PloS One *8*, e53064.

Miao, E.A., Alpuche-Aranda, C.M., Dors, M., Clark, A.E., Bader, M.W., Miller, S.I., and Aderem, A. (2006). Cytoplasmic flagellin activates caspase-1 and secretion of interleukin 1β via Ipaf. Nat. Immunol. *7*, 569–575.

Micheau, O., Lens, S., Gaide, O., Alevizopoulos, K., and Tschopp, J. (2001). NF-κB Signals Induce the Expression of c-FLIP. Mol. Cell. Biol. *21*, 5299–5305.

Miki, T., and Hardt, W.-D. (2013). Outer membrane permeabilization is an essential step in the killing of gram-negative bacteria by the lectin RegIIIβ. PloS One *8*, e69901.

Miki, T., Okada, N., and Hardt, W.-D. (2017a). Inflammatory bactericidal lectin RegIIIβ: Friend or foe for the host? Gut Microbes 1–9.

Miki, T., Goto, R., Fujimoto, M., Okada, N., and Hardt, W.-D. (2017b). The Bactericidal Lectin RegIIIβ Prolongs Gut Colonization and Enteropathy in the Streptomycin Mouse Model for Salmonella Diarrhea. Cell Host Microbe *21*, 195–207.

Mitchell, P.S., Roncaioli, J.L., Turcotte, E.A., Goers, L., Chavez, R.A., Lee, A.Y., Lesser, C.F., Rauch, I., and Vance, R.E. (2020). NAIP–NLRC4-deficient mice are susceptible to shigellosis. BioRxiv 2020.05.16.099929.

von Moltke, J., Trinidad, N.J., Moayeri, M., Kintzer, A.F., Wang, S.B., van Rooijen, N., Brown, C.R., Krantz, B.A., Leppla, S.H., Gronert, K., et al. (2012). Rapid induction of inflammatory lipid mediators by the inflammasome in vivo. Nature *490*, 107–111.

von Moltke, J., Ji, M., Liang, H.-E., and Locksley, R.M. (2016). Tuft-cell-derived IL-25 regulates an intestinal ILC2-epithelial response circuit. Nature *529*, 221–225.

Momose, Y., Hirayama, K., and Itoh, K. (2008). Competition for proline between indigenous Escherichia coli and E. coli O157:H7 in gnotobiotic mice associated with infant intestinal microbiota and its contribution to the colonization resistance against E. coli O157:H7. Antonie Van Leeuwenhoek *94*, 165–171.

Monteleone, I., Platt, A.M., Jaensson, E., Agace, W.W., and Mowat, A.M. (2008). IL-10-dependent partial refractoriness to Toll-like receptor stimulation modulates gut mucosal dendritic cell function. Eur. J. Immunol. *38*, 1533–1547.

Morita, N., Umemoto, E., Fujita, S., Hayashi, A., Kikuta, J., Kimura, I., Haneda, T., Imai, T., Inoue, A., Mimuro, H., et al. (2019). GPR31-dependent dendrite protrusion of intestinal CX3CR1 + cells by bacterial metabolites. Nature *566*, 110–114.

Motshwene, P.G., Moncrieffe, M.C., Grossmann, J.G., Kao, C., Ayaluru, M., Sandercock, A.M., Robinson, C.V., Latz, E., and Gay, N.J. (2009). An oligomeric signaling platform formed by the Toll-like receptor signal transducers MyD88 and IRAK-4. J. Biol. Chem. *284*, 25404–25411.

Mowat, A.M., and Agace, W.W. (2014). Regional specialization within the intestinal immune system. Nat. Rev. Immunol. *14*, 667–685.

Mowat, A.M., Scott, C.L., and Bain, C.C. (2017). Barrier-tissue macrophages: functional adaptation to environmental challenges. Nat. Med. *23*, 1258–1270.

Müller, A.A., Dolowschiak, T., Sellin, M.E., Felmy, B., Verbree, C., Gadient, S., Westermann, A.J., Vogel, J., LeibundGut-Landmann, S., and Hardt, W.-D. (2016). An NK Cell Perforin Response Elicited via IL-18 Controls Mucosal Inflammation Kinetics during Salmonella Gut Infection. PLoS Pathog. *12*, e1005723.

Müller, A.J., Kaiser, P., Dittmar, K.E.J., Weber, T.C., Haueter, S., Endt, K., Songhet, P., Zellweger, C., Kremer, M., Fehling, H.-J., et al. (2012). Salmonella gut invasion involves TTSS-2-dependent epithelial traversal, basolateral exit, and uptake by epithelium-sampling lamina propria phagocytes. Cell Host Microbe *11*, 19–32.

Muñoz-Planillo, R., Kuffa, P., Martínez-Colón, G., Smith, B.L., Rajendiran, T.M., and Núñez, G. (2013). K^+ efflux is the common trigger of NLRP3 inflammasome activation by bacterial toxins and particulate matter. Immunity *38*, 1142–1153.

Murai, M., Turovskaya, O., Kim, G., Madan, R., Karp, C.L., Cheroutre, H., and Kronenberg, M. (2009). Interleukin 10 acts on regulatory T cells to maintain expression of the transcription factor Foxp3 and suppressive function in mice with colitis. Nat. Immunol. *10*, 1178–1184.

Muzaki, A.R.B.M., Tetlak, P., Sheng, J., Loh, S.C., Setiagani, Y.A., Poidinger, M., Zolezzi, F., Karjalainen, K., and Ruedl, C. (2015). Intestinal CD103+CD11b- dendritic cells restrain colitis via IFN-γ-induced anti-inflammatory response in epithelial cells. Mucosal Immunol.

Muzio, M., Ni, J., Feng, P., and Dixit, V.M. (1997). IRAK (Pelle) family member IRAK-2 and MyD88 as proximal mediators of IL-1 signaling. Science *278*, 1612–1615.

Nadjsombati, M.S., McGinty, J.W., Lyons-Cohen, M.R., Jaffe, J.B., DiPeso, L., Schneider, C., Miller, C.N., Pollack, J.L., Gowda, G.A.N., Fontana, M.F., et al. (2018). Detection of succinate by intestinal tuft cells triggers a type 2 innate immune circuit. Immunity *49*, 33-41.e7.

Niess, J.H., Brand, S., Gu, X., Landsman, L., Jung, S., McCormick, B.A., Vyas, J.M., Boes, M., Ploegh, H.L., Fox, J.G., et al. (2005). CX3CR1-mediated dendritic cell access to the intestinal lumen and bacterial clearance. Science *307*, 254–258.

Nordlander, S., Pott, J., and Maloy, K.J. (2014). NLRC4 expression in intestinal epithelial cells mediates protection against an enteric pathogen. Mucosal Immunol. *7*, 775–785.

Owen, R.L., Piazza, A.J., and Ermak, T.H. (1991). Ultrastructural and cytoarchitectural features of lymphoreticular organs in the colon and rectum of adult BALB/c mice. Am. J. Anat. *190*, 10–18.

Pabst, O., Herbrand, H., Worbs, T., Friedrichsen, M., Yan, S., Hoffmann, M.W., Körner, H., Bernhardt, G., Pabst, R., and Förster, R. (2005). Cryptopatches and isolated lymphoid follicles: dynamic lymphoid tissues dispensable for the generation of intraepithelial lymphocytes. Eur. J. Immunol. *35*, 98–107.

Park, B.S., Song, D.H., Kim, H.M., Choi, B.-S., Lee, H., and Lee, J.-O. (2009). The structural basis of lipopolysaccharide recognition by the TLR4–MD-2 complex. Nature *458*, 1191–1195.

Pearson, J.S., Giogha, C., Ong, S.Y., Kennedy, C.L., Kelly, M., Robinson, K.S., Lung, T.W.F., Mansell, A., Riedmaier, P., Oates, C.V.L., et al. (2013). A type III effector antagonizes death receptor signalling during bacterial gut infection. Nature *501*, 247–251.

Perry, G.A., and Sharp, J.G. (1988). Characterization of proximal colonic lymphoid tissue in the mouse. Anat. Rec. *220*, 305–312.

Peterson, L.W., and Artis, D. (2014). Intestinal epithelial cells: regulators of barrier function and immune homeostasis. Nat. Rev. Immunol. *14*, 141–153.

Picard, C., von Bernuth, H., Ghandil, P., Chrabieh, M., Levy, O., Arkwright, P.D., McDonald, D., Geha, R.S., Takada, H., Krause, J.C., et al. (2010). Clinical Features and Outcome of Patients With IRAK-4 and MyD88 Deficiency. Medicine (Baltimore) *89*, 403–425.

Pilar, A.V.C., Reid-Yu, S.A., Cooper, C.A., Mulder, D.T., and Coombes, B.K. (2012). GogB is an anti-inflammatory effector that limits tissue damage during Salmonella infection through interaction with human FBXO22 and Skp1. PLoS Pathog. *8*, e1002773.

Pinaud, L., Sansonetti, P.J., and Phalipon, A. (2018). Host Cell Targeting by Enteropathogenic Bacteria T3SS Effectors. Trends Microbiol.

Poltorak, A., He, X., Smirnova, I., Liu, M.-Y., Huffel, C.V., Du, X., Birdwell, D., Alejos, E., Silva, M., Galanos, C., et al. (1998). Defective LPS Signaling in C3H/HeJ and C57BL/10ScCr Mice: Mutations in Tlr4 Gene. Science *282*, 2085–2088.

Price, A.E., Shamardani, K., Lugo, K.A., Deguine, J., Roberts, A.W., Lee, B.L., and Barton, G.M. (2018). A Map of Toll-like Receptor Expression in the Intestinal Epithelium Reveals Distinct Spatial, Cell Type-Specific, and Temporal Patterns. Immunity *49*, 560-575.e6.

Raffatellu, M., George, M.D., Akiyama, Y., Hornsby, M.J., Nuccio, S.-P., Paixao, T.A., Butler, B.P., Chu, H., Santos, R.L., Berger, T., et al. (2009). Lipocalin-2 resistance confers an advantage to Salmonella enterica serotype Typhimurium for growth and survival in the inflamed intestine. Cell Host Microbe *5*, 476–486.

Rakoff-Nahoum, S., Paglino, J., Eslami-Varzaneh, F., Edberg, S., and Medzhitov, R. (2004). Recognition of commensal microflora by toll-like receptors is required for intestinal homeostasis. Cell *118*, 229–241.

Rathinam, V.A.K., Jiang, Z., Waggoner, S.N., Sharma, S., Cole, L.E., Waggoner, L., Vanaja, S.K., Monks, B.G., Ganesan, S., Latz, E., et al. (2010). The AIM2 inflammasome is essential for host defense against cytosolic bacteria and DNA viruses. Nat. Immunol. *11*, 395–402.

Ratner, D., Orning, M.P.A., Proulx, M.K., Wang, D., Gavrilin, M.A., Wewers, M.D., Alnemri, E.S., Johnson, P.F., Lee, B., Mecsas, J., et al. (2016). The Yersinia pestis Effector YopM Inhibits Pyrin Inflammasome Activation. PLoS Pathog. *12*, e1006035.

Rauch, I., Deets, K.A., Ji, D.X., von Moltke, J., Tenthorey, J.L., Lee, A.Y., Philip, N.H., Ayres, J.S., Brodsky, I.E., Gronert, K., et al. (2017). NAIP-NLRC4 Inflammasomes Coordinate Intestinal Epithelial Cell Expulsion with Eicosanoid and IL-18 Release via Activation of Caspase-1 and -8. Immunity *46*, 649–659.

Robertson, S.J., Lemire, P., Maughan, H., Goethel, A., Turpin, W., Bedrani, L., Guttman, D.S., Croitoru, K., Girardin, S.E., and Philpott, D.J. (2019). Comparison of Co-housing and Littermate Methods for Microbiota Standardization in Mouse Models. Cell Rep. *27*, 1910-1919.e2.

Rogler, G., Brand, K., Vogl, D., Page, S., Hofmeister, R., Andus, T., Knuechel, R., Baeuerle, P.A., Schölmerich, J., and Gross, V. (1998). Nuclear factor κB is activated in macrophages and epithelial cells of inflamed intestinal mucosa. Gastroenterology *115*, 357–369.

Rolhion, N., Furniss, R.C.D., Grabe, G., Ryan, A., Liu, M., Matthews, S.A., and Holden, D.W. (2016). Inhibition of Nuclear Transport of NF-κB p65 by the Salmonella Type III Secretion System Effector SpvD. PLoS Pathog. *12*, e1005653.

Ross, B.D., Verster, A.J., Radey, M.C., Schmidtke, D.T., Pope, C.E., Hoffman, L.R., Hajjar, A.M., Peterson, S.B., Borenstein, E., and Mougous, J.D. (2019). Human gut bacteria contain acquired interbacterial defence systems. Nature *575*, 224–228.

Ryu, J.-K., Kim, S.J., Rah, S.-H., Kang, J.I., Jung, H.E., Lee, D., Lee, H.K., Lee, J.-O., Park, B.S., Yoon, T.-Y., et al. (2017). Reconstruction of LPS Transfer Cascade Reveals Structural Determinants within LBP, CD14, and TLR4-MD2 for Efficient LPS Recognition and Transfer. Immunity *46*, 38–50.

Saini, S., Ellermeier, J.R., Slauch, J.M., and Rao, C.V. (2010). The role of coupled positive feedback in the expression of the SPI1 type three secretion system in Salmonella. PLoS Pathog. *6*, e1001025.

Sallusto, F., and Lanzavecchia, A. (1994). Efficient presentation of soluble antigen by cultured human dendritic cells is maintained by granulocyte/macrophage colony-stimulating factor plus interleukin 4 and downregulated by tumor necrosis factor alpha. J. Exp. Med. *179*, 1109–1118.

Samuel, B.S., and Gordon, J.I. (2006). A humanized gnotobiotic mouse model of host-archaeal-bacterial mutualism. Proc. Natl. Acad. Sci. U. S. A. *103*, 10011–10016.

Santos, A.J.M., Lo, Y.-H., Mah, A.T., and Kuo, C.J. (2018). The Intestinal Stem Cell Niche: Homeostasis and Adaptations. Trends Cell Biol. *28*, 1062–1078.

Sassone-Corsi, M., Nuccio, S.-P., Liu, H., Hernandez, D., Vu, C.T., Takahashi, A.A., Edwards, R.A., and Raffatellu, M. (2016). Microcins mediate competition among Enterobacteriaceae in the inflamed gut. Nature *540*, 280–283.

Sato, T., Vries, R.G., Snippert, H.J., van de Wetering, M., Barker, N., Stange, D.E., van Es, J.H., Abo, A., Kujala, P., Peters, P.J., et al. (2009). Single Lgr5 stem cells build crypt-villus structures in vitro without a mesenchymal niche. Nature *459*, 262–265.

Scherer, W.F., Syverton, J.T., and Gey, G.O. (1953). Studies on the propagation in vitro of poliomyelitis viruses. IV. Viral multiplication in a stable strain of human malignant epithelial cells (strain HeLa) derived from an epidermoid carcinoma of the cervix. J. Exp. Med. *97*, 695–710.

Schlickum, S., Sennefelder, H., Friedrich, M., Harms, G., Lohse, M.J., Kilshaw, P., and Schön, M.P. (2008). Integrin αE(CD103)β7 influences cellular shape and motility in a ligand-dependent fashion. Blood *112*, 619–625.

Schlumberger, M.C., Müller, A.J., Ehrbar, K., Winnen, B., Duss, I., Stecher, B., and Hardt, W.-D. (2005). Real-time imaging of type III secretion: Salmonella SipA injection into host cells. Proc. Natl. Acad. Sci. U. S. A. *102*, 12548–12553.

Schridde, A., Bain, C.C., Mayer, J.U., Montgomery, J., Pollet, E., Denecke, B., Milling, S.W.F., Jenkins, S.J., Dalod, M., Henri, S., et al. (2017). Tissue-specific differentiation of colonic macrophages requires TGFβ receptor-mediated signaling. Mucosal Immunol. *10*, 1387–1399.

Scott, C.L., Bain, C.C., Wright, P.B., Sichien, D., Kotarsky, K., Persson, E.K., Luda, K., Guilliams, M., Lambrecht, B.N., Agace, W.W., et al. (2015). CCR2(+)CD103(-) intestinal dendritic cells develop from DC-committed precursors and induce interleukin-17 production by T cells. Mucosal Immunol. *8*, 327–339.

Scott, N.E., Giogha, C., Pollock, G.L., Kennedy, C.L., Webb, A.I., Williamson, N.A., Pearson, J.S., and Hartland, E.L. (2017). The bacterial arginine glycosyltransferase effector NleB preferentially modifies Fas-associated death domain protein (FADD). J. Biol. Chem. *292*, 17337–17350.

Sellin, M.E., Müller, A.A., Felmy, B., Dolowschiak, T., Diard, M., Tardivel, A., Maslowski, K.M., and Hardt, W.-D. (2014). Epithelium-intrinsic NAIP/NLRC4 inflammasome drives infected enterocyte expulsion to restrict Salmonella replication in the intestinal mucosa. Cell Host Microbe *16*, 237–248.

Sellin, M.E., Müller, A.A., and Hardt, W.-D. (2018). Consequences of Epithelial Inflammasome Activation by Bacterial Pathogens. J. Mol. Biol. *430*, 193–206.

Sender, R., Fuchs, S., and Milo, R. (2016). Revised Estimates for the Number of Human and Bacteria Cells in the Body. PLOS Biol. *14*, e1002533.

Shaw, T.N., Houston, S.A., Wemyss, K., Bridgeman, H.M., Barbera, T.A., Zangerle-Murray, T., Strangward, P., Ridley, A.J.L., Wang, P., Tamoutounour, S., et al. (2018). Tissue-resident macrophages in the intestine are long lived and defined by Tim-4 and CD4 expression. J. Exp. Med. *215*, 1507–1518.

Shea, J.E., Hensel, M., Gleeson, C., and Holden, D.W. (1996). Identification of a virulence locus encoding a second type III secretion system in Salmonella typhimurium. Proc. Natl. Acad. Sci. U. S. A. *93*, 2593–2597.

Sheridan, B.S., and Lefrançois, L. (2010). Intraepithelial Lymphocytes: To Serve and Protect. Curr. Gastroenterol. Rep. *12*, 513–521.

Sivick, K.E., Arpaia, N., Reiner, G.L., Lee, B.L., Russell, B.R., and Barton, G.M. (2014). Toll-like Receptor-Deficient Mice Reveal How Innate Immune Signaling Influences Salmonella Virulence Strategies. Cell Host Microbe *15*, 203–213.

Smythies, L.E., Sellers, M., Clements, R.H., Mosteller-Barnum, M., Meng, G., Benjamin, W.H., Orenstein, J.M., and Smith, P.D. (2005). Human intestinal macrophages display profound inflammatory anergy despite avid phagocytic and bacteriocidal activity. J. Clin. Invest. *115*, 66–75.

Songhet, P., Barthel, M., Stecher, B., Müller, A.J., Kremer, M., Hansson, G.C., and Hardt, W.-D. (2011). Stromal IFN-γR-signaling modulates goblet cell function during Salmonella Typhimurium infection. PloS One *6*, e22459.

Srikanth, C.V., Mercado-Lubo, R., Hallstrom, K., and McCormick, B.A. (2011). Salmonella effector proteins and host-cell responses. Cell. Mol. Life Sci. CMLS *68*, 3687–3697.

Stappenbeck, T.S., and Virgin, H.W. (2016). Accounting for reciprocal host-microbiome interactions in experimental science. Nature *534*, 191–199.

Stecher, B., and Hardt, W.-D. (2008). The role of microbiota in infectious disease. Trends Microbiol. *16*, 107–114.

Stecher, B., Hapfelmeier, S., Müller, C., Kremer, M., Stallmach, T., and Hardt, W.-D. (2004). Flagella and chemotaxis are required for efficient induction of Salmonella enterica serovar Typhimurium colitis in streptomycin-pretreated mice. Infect. Immun. *72*, 4138–4150.

Stecher, B., Robbiani, R., Walker, A.W., Westendorf, A.M., Barthel, M., Kremer, M., Chaffron, S., Macpherson, A.J., Buer, J., Parkhill, J., et al. (2007). Salmonella enterica serovar typhimurium exploits inflammation to compete with the intestinal microbiota. PLoS Biol. *5*, 2177–2189.

Stecher, B., Barthel, M., Schlumberger, M.C., Haberli, L., Rabsch, W., Kremer, M., and Hardt, W.-D. (2008). Motility allows S. Typhimurium to benefit from the mucosal defence. Cell. Microbiol. *10*, 1166–1180.

Steele-Mortimer, O. (2008). The Salmonella-containing vacuole: moving with the times. Curr. Opin. Microbiol. *11*, 38–45.

Steele-Mortimer, O., Brumell, J.H., Knodler, L.A., Méresse, S., Lopez, A., and Finlay, B.B. (2002). The invasion-associated type III secretion system of Salmonella enterica serovar Typhimurium is necessary for intracellular proliferation and vacuole biogenesis in epithelial cells. Cell. Microbiol. *4*, 43–54.

Stelter, C., Käppeli, R., König, C., Krah, A., Hardt, W.-D., Stecher, B., and Bumann, D. (2011). Salmonella-induced mucosal lectin RegIIIβ kills competing gut microbiota. PloS One *6*, e20749.

Stone, L.B., and Takemoto, K.K. (1970). Transformation of Mouse Macrophages by Simian Virus 40. J. Virol. *6*, 621–627.

Sturm, A., Heinemann, M., Arnoldini, M., Benecke, A., Ackermann, M., Benz, M., Dormann, J., and Hardt, W.-D. (2011). The cost of virulence: retarded growth of Salmonella Typhimurium cells expressing type III secretion system 1. PLoS Pathog. *7*, e1002143.

Sun, J. (2017). Intestinal organoid as an in vitro model in studying host-microbial interactions. Front. Biol. *12*, 94–102.

Sun, C.-M., Hall, J.A., Blank, R.B., Bouladoux, N., Oukka, M., Mora, J.R., and Belkaid, Y. (2007). Small intestine lamina propria dendritic cells promote de novo generation of Foxp3 T reg cells via retinoic acid. J. Exp. Med. *204*, 1775–1785.

Sun, H., Kamanova, J., Lara-Tejero, M., and Galán, J.E. (2016). A Family of Salmonella Type III Secretion Effector Proteins Selectively Targets the NF-κB Signaling Pathway to Preserve Host Homeostasis. PLoS Pathog. *12*, e1005484.

Sung, M.-H., Li, N., Lao, Q., Gottschalk, R.A., Hager, G.L., and Fraser, I.D.C. (2014). Switching of the relative dominance between feedback mechanisms in lipopolysaccharide-induced NF-κB signaling. Sci. Signal. *7*, ra6.

Takeuchi, A. (1967). Electron microscope studies of experimental Salmonella infection. I. Penetration into the intestinal epithelium by Salmonella typhimurium. Am. J. Pathol. *50*, 109–136.

Takeuchi, O., Hoshino, K., Kawai, T., Sanjo, H., Takada, H., Ogawa, T., Takeda, K., and Akira, S. (1999). Differential roles of TLR2 and TLR4 in recognition of gram-negative and gram-positive bacterial cell wall components. Immunity *11*, 443–451.

Takeuchi, O., Kawai, T., Mühlradt, P.F., Morr, M., Radolf, J.D., Zychlinsky, A., Takeda, K., and Akira, S. (2001). Discrimination of bacterial lipoproteins by Toll-like receptor 6. Int. Immunol. *13*, 933–940.

Takeuchi, O., Sato, S., Horiuchi, T., Hoshino, K., Takeda, K., Dong, Z., Modlin, R.L., and Akira, S. (2002). Cutting edge: role of Toll-like receptor 1 in mediating immune response to microbial lipoproteins. J. Immunol. Baltim. Md 1950 *169*, 10–14.

Talbot, S., Tötemeyer, S., Yamamoto, M., Akira, S., Hughes, K., Gray, D., Barr, T., Mastroeni, P., Maskell, D.J., and Bryant, C.E. (2009). Toll-like receptor 4 signalling through MyD88 is essential to control Salmonella enterica serovar Typhimurium infection, but not for the initiation of bacterial clearance. Immunology *128*, 472–483.

Tamoutounour, S., Henri, S., Lelouard, H., de Bovis, B., de Haar, C., van der Woude, C.J., Woltman, A.M., Reyal, Y., Bonnet, D., Sichien, D., et al. (2012). CD64 distinguishes macrophages from dendritic cells in the

gut and reveals the Th1-inducing role of mesenteric lymph node macrophages during colitis: HIGHLIGHTS. Eur. J. Immunol. *42*, 3150–3166.

Thanissery, R., Winston, J.A., and Theriot, C.M. (2017). Inhibition of spore germination, growth, and toxin activity of clinically relevant C. difficile strains by gut microbiota derived secondary bile acids. Anaerobe *45*, 86–100.

Theret, M., Mounier, R., and Rossi, F. (2019). The origins and non-canonical functions of macrophages in development and regeneration. Development *146*, dev156000.

Thinwa, J., Segovia, J.A., Bose, S., and Dube, P.H. (2014). Integrin-mediated first signal for inflammasome activation in intestinal epithelial cells. J. Immunol. Baltim. Md 1950 *193*, 1373–1382.

Thurston, T.L.M., Matthews, S.A., Jennings, E., Alix, E., Shao, F., Shenoy, A.R., Birrell, M.A., and Holden, D.W. (2016). Growth inhibition of cytosolic Salmonella by caspase-1 and caspase-11 precedes host cell death. Nat. Commun. *7*, 13292.

Trompette, A., Gollwitzer, E.S., Yadava, K., Sichelstiel, A.K., Sprenger, N., Ngom-Bru, C., Blanchard, C., Junt, T., Nicod, L.P., Harris, N.L., et al. (2014). Gut microbiota metabolism of dietary fiber influences allergic airway disease and hematopoiesis. Nat. Med. *20*, 159–166.

Trompette, A., Gollwitzer, E.S., Pattaroni, C., Lopez-Mejia, I.C., Riva, E., Pernot, J., Ubags, N., Fajas, L., Nicod, L.P., and Marsland, B.J. (2018). Dietary Fiber Confers Protection against Flu by Shaping Ly6c– Patrolling Monocyte Hematopoiesis and CD8+ T Cell Metabolism. Immunity *48*, 992-1005.e8.

Tsolis, R.M., Xavier, M.N., Santos, R.L., and Bäumler, A.J. (2011). How to become a top model: impact of animal experimentation on human Salmonella disease research. Infect. Immun. *79*, 1806–1814.

Veiga-Fernandes, H., and Mucida, D. (2016). Neuro-Immune Interactions at Barrier Surfaces. Cell *165*, 801–811.

Vereecke, L., Sze, M., Guire, C.M., Rogiers, B., Chu, Y., Schmidt-Supprian, M., Pasparakis, M., Beyaert, R., and van Loo, G. (2010). Enterocyte-specific A20 deficiency sensitizes to tumor necrosis factor–induced toxicity and experimental colitis. J. Exp. Med. *207*, 1513–1523.

Vereecke, L., Vieira-Silva, S., Billiet, T., van Es, J.H., Mc Guire, C., Slowicka, K., Sze, M., van den Born, M., De Hertogh, G., Clevers, H., et al. (2014). A20 controls intestinal homeostasis through cell-specific activities. Nat. Commun. *5*, 5103.

Vlantis, K., Wullaert, A., Sasaki, Y., Schmidt-Supprian, M., Rajewsky, K., Roskams, T., and Pasparakis, M. (2011). Constitutive IKK2 activation in intestinal epithelial cells induces intestinal tumors in mice. J. Clin. Invest. *121*, 2781–2793.

Vlantis, K., Wullaert, A., Polykratis, A., Kondylis, V., Dannappel, M., Schwarzer, R., Welz, P., Corona, T., Walczak, H., Weih, F., et al. (2016). NEMO Prevents RIP Kinase 1-Mediated Epithelial Cell Death and Chronic Intestinal Inflammation by NF-κB-Dependent and -Independent Functions. Immunity *44*, 553–567.

Wang, C., Deng, L., Hong, M., Akkaraju, G.R., Inoue, J., and Chen, Z.J. (2001). TAK1 is a ubiquitin-dependent kinase of MKK and IKK. Nature *412*, 346–351.

Wang, C.Y., Mayo, M.W., Korneluk, R.G., Goeddel, D.V., and Baldwin, A.S. (1998). NF-kappaB antiapoptosis: induction of TRAF1 and TRAF2 and c-IAP1 and c-IAP2 to suppress caspase-8 activation. Science *281*, 1680–1683.

Wangdi, T., Lee, C.-Y., Spees, A.M., Yu, C., Kingsbury, D.D., Winter, S.E., Hastey, C.J., Wilson, R.P., Heinrich, V., and Bäumler, A.J. (2014). The Vi capsular polysaccharide enables Salmonella enterica serovar typhi to evade microbe-guided neutrophil chemotaxis. PLoS Pathog. *10*, e1004306.

Watanabe, M., Fukiya, S., and Yokota, A. (2017). Comprehensive evaluation of the bactericidal activities of free bile acids in the large intestine of humans and rodents. J. Lipid Res. *58*, 1143–1152.

Waterman, S.R., and Holden, D.W. (2003). Functions and effectors of the Salmonella pathogenicity island 2 type III secretion system. Cell. Microbiol. *5*, 501–511.

Westermann, A.J., Förstner, K.U., Amman, F., Barquist, L., Chao, Y., Schulte, L.N., Müller, L., Reinhardt, R., Stadler, P.F., and Vogel, J. (2016). Dual RNA-seq unveils noncoding RNA functions in host-pathogen interactions. Nature *529*, 496–501.

Winnen, B., Schlumberger, M.C., Sturm, A., Schüpbach, K., Siebenmann, S., Jenny, P., and Hardt, W.-D. (2008). Hierarchical effector protein transport by the Salmonella Typhimurium SPI-1 type III secretion system. PloS One *3*, e2178.

Winsor, N., Krustev, C., Bruce, J., Philpott, D.J., and Girardin, S.E. (2019). Canonical and noncanonical inflammasomes in intestinal epithelial cells. Cell. Microbiol. e13079.

Wlodarska, M., Thaiss, C.A., Nowarski, R., Henao-Mejia, J., Zhang, J.-P., Brown, E.M., Frankel, G., Levy, M., Katz, M.N., Philbrick, W.M., et al. (2014). NLRP6 inflammasome orchestrates the colonic host-microbial interface by regulating goblet cell mucus secretion. Cell *156*, 1045–1059.

Wotzka, S.Y., Nguyen, B.D., and Hardt, W.-D. (2017). Salmonella Typhimurium Diarrhea Reveals Basic Principles of Enteropathogen Infection and Disease-Promoted DNA Exchange. Cell Host Microbe *21*, 443–454.

Wotzka, S.Y., Kreuzer, M., Maier, L., Arnoldini, M., Nguyen, B.D., Brachmann, A.O., Berthold, D.L., Zünd, M., Hausmann, A., Bakkeren, E., et al. (2019). Escherichia coli limits Salmonella Typhimurium infections after diet shifts and fat-mediated microbiota perturbation in mice. Nat. Microbiol. *4*, 2164–2174.

Wright, S.D., Ramos, R.A., Tobias, P.S., Ulevitch, R.J., and Mathison, J.C. (1990). CD14, a receptor for complexes of lipopolysaccharide (LPS) and LPS binding protein. Science *249*, 1431–1433.

Wullaert, A., Bonnet, M.C., and Pasparakis, M. (2011). NF-κB in the regulation of epithelial homeostasis and inflammation. Cell Res. *21*, 146–158.

Xu, H., Yang, J., Gao, W., Li, L., Li, P., Zhang, L., Gong, Y.-N., Peng, X., Xi, J.J., Chen, S., et al. (2014). Innate immune sensing of bacterial modifications of Rho GTPases by the Pyrin inflammasome. Nature *513*, 237–241.

Yamamoto, M., Sato, S., Hemmi, H., Hoshino, K., Kaisho, T., Sanjo, H., Takeuchi, O., Sugiyama, M., Okabe, M., Takeda, K., et al. (2003). Role of adaptor TRIF in the MyD88-independent toll-like receptor signaling pathway. Science *301*, 640–643.

Yang, W.H., Heithoff, D.M., Aziz, P.V., Sperandio, M., Nizet, V., Mahan, M.J., and Marth, J.D. (2017). Recurrent infection progressively disables host protection against intestinal inflammation. Science *358*.

Ye, Z., Petrof, E.O., Boone, D., Claud, E.C., and Sun, J. (2007). Salmonella effector AvrA regulation of colonic epithelial cell inflammation by deubiquitination. Am. J. Pathol. *171*, 882–892.

Yen, M., Cairns, L.S., and Camilli, A. (2017). A cocktail of three virulent bacteriophages prevents Vibrio cholerae infection in animal models. Nat. Commun. *8*, 14187.

Yin, Y., and Zhou, D. (2018). Organoid and Enteroid Modeling of Salmonella Infection. Front. Cell. Infect. Microbiol. *8*.

Zhang, J., Stirling, B., Temmerman, S.T., Ma, C.A., Fuss, I.J., Derry, J.M.J., and Jain, A. (2006a). Impaired regulation of NF-kappaB and increased susceptibility to colitis-associated tumorigenesis in CYLD-deficient mice. J. Clin. Invest. *116*, 3042–3049.

Zhang, K., Riba, A., Nietschke, M., Torow, N., Repnik, U., Pütz, A., Fulde, M., Dupont, A., Hensel, M., and Hornef, M. (2018). Minimal SPI1-T3SS effector requirement for Salmonella enterocyte invasion and intracellular proliferation in vivo. PLoS Pathog. *14*, e1006925.

Zhang, Y., Higashide, W.M., McCormick, B.A., Chen, J., and Zhou, D. (2006b). The inflammation-associated Salmonella SopA is a HECT-like E3 ubiquitin ligase. Mol. Microbiol. *62*, 786–793.

Zhang, Y.-G., Wu, S., Xia, Y., and Sun, J. (2014). Salmonella-infected crypt-derived intestinal organoid culture system for host-bacterial interactions. Physiol. Rep. *2*.

Zhao, Y., Yang, J., Shi, J., Gong, Y.-N., Lu, Q., Xu, H., Liu, L., and Shao, F. (2011). The NLRC4 inflammasome receptors for bacterial flagellin and type III secretion apparatus. Nature *477*, 596–600.

Zheng, Y., Valdez, P.A., Danilenko, D.M., Hu, Y., Sa, S.M., Gong, Q., Abbas, A.R., Modrusan, Z., Ghilardi, N., de Sauvage, F.J., et al. (2008). Interleukin-22 mediates early host defense against attaching and effacing bacterial pathogens. Nat. Med. *14*, 282–289.

Zhou, D., Mooseker, M.S., and Galán, J.E. (1999a). An invasion-associated Salmonella protein modulates the actin-bundling activity of plastin. Proc. Natl. Acad. Sci. *96*, 10176–10181.

Zhou, D., Mooseker, M.S., and Galán, J.E. (1999b). Role of the S. typhimurium actin-binding protein SipA in bacterial internalization. Science *283*, 2092–2095.

Zhu, Y., Li, H., Long, C., Hu, L., Xu, H., Liu, L., Chen, S., Wang, D.-C., and Shao, F. (2007). Structural insights into the enzymatic mechanism of the pathogenic MAPK phosphothreonine lyase. Mol. Cell *28*, 899–913.

Zigmond, E., Bernshtein, B., Friedlander, G., Walker, C.R., Yona, S., Kim, K.-W., Brenner, O., Krauthgamer, R., Varol, C., Müller, W., et al. (2014). Macrophage-restricted interleukin-10 receptor deficiency, but not IL-10 deficiency, causes severe spontaneous colitis. Immunity *40*, 720–733.

CHAPTER 2 - ELUCIDATING HOST-MICROBE INTERACTIONS *IN VIVO* BY STUDYING POPULATION DYNAMICS USING NEUTRAL GENETIC TAGS

The content of this chapter was partially adapted from the following manuscript:

Elucidating Host-Microbe Interactions *in vivo* by Studying Population Dynamics Using Neutral Genetic Tags

Annika Hausmann[1] and Wolf-Dietrich Hardt[1]

Author Affiliations:

[1]Institute of Microbiology, D-BIOL, ETH Zurich, Zurich, Switzerland

Author Contributions:

AH designed the scope of the review with input by WDH. AH wrote the manuscript with corrections and suggestions by WDH.

Published in Immunology on 15.09.2020. Doi: 10.1111/imm.13266

Host-microbe interactions are highly dynamic in space and time, in particular in the case of infections. Pathogen population sizes, microbial phenotypes and the nature of the host responses often change dramatically over time. These features pose particular challenges when deciphering the underlying mechanisms of these interactions experimentally, as traditional microbiological and immunological methods mostly provide snapshots of population sizes or sparse time series. Recent approaches - combining experiments using neutral genetic tags with stochastic population dynamic models - allow a more precise quantification of biologically relevant parameters that govern the interaction between microbe and host cell populations. This is accomplished by exploiting the patterns of change of tag composition in the microbe or host cell population under study. These models can be used to predict effects of immunodeficiencies or therapies (e.g. antibiotic treatment) on populations, and thereby generate hypotheses and refine experimental designs.

This chapter contains part of the indicated manuscript.

SPATIOTEMPORAL DYNAMICS OF HOST-MICROBE INTERACTIONS

Our bodies are exposed to billions of microbes every day. Most of them are harmless and some even beneficial. A few pathogenic microbes however can invade multicellular organisms and cause life-threatening infections. To block systemic proliferation of harmless, commensal microbes after accidental entry (and thereby enable a long-lasting symbiotic relationship with commensals), and to fend off pathogenic microbes, multicellular organisms have evolved sophisticated systems of immune defenses (Murphy and Weaver, 2016).

The interaction of the immune system with microbes is highly complex. Innate immune responses are triggered by tissue damage and the recognition of conserved molecular patterns associated with beneficial and pathogenic microbes (Medzhitov and Janeway, 2000). Host responses to microbe exposure must therefore be highly context-dependent and have evolved to minimize immune reactions to commensals while providing efficient defense against invading pathogens. Localization, duration and intensity of the microbial stimulus influence the outcome of the host response (Chen et al., 2015; Pradeu et al., 2013; Tateda et al., 1996). Adaptive immune responses can further modify pathogen-host interactions at later phases of infections or after a second encounter with pathogens. The immune response affects the microbial population, which, in turn, feeds back onto the immune response. The final state of this dynamic system, in which the microbial population and immune responses mutually affect each other, is difficult to predict and can range from microbial clearance to persistent infection (Figure 1A).

Deciphering these complex interactions is one of the major challenges in the field of host-microbe studies (Germain, 2001). In systems with two or more interacting populations, the spatiotemporal dynamics make it challenging to dissect the underlying reciprocal interactions and to identify and quantify contributions of different components (Table 1).

Table 1 ***Examples for experimental systems in the context of host-microbe interaction****. Please note that the listed options are examples. This is not a complete list.*

system	components (examples)	environments (examples)	interactions (examples)	parameters (examples)
in vitro bacterial growth assay	strain A, strain B	culture medium	competition, inhibition, cooperation	replication rate, death rate (strain A, B); as control "without" host modulation
in vitro T cell proliferation assay	T cells, Dendritic cells (DCs)	culture medium	activation, inhibition	replication rate, death rate, activation (T cells, DCs)
mouse associated with SPF microbiota	microbiota, various immune cells	intestinal lumen, mucosa, distant body sites	tolerance, killing, symbiosis, activation, silencing	replication rate, death rate, activation, migration (microbiota, immune cells)
oral *S.* Tm infection	microbiota, *S.* Tm, various immune cells	intestinal lumen, mucosa, distant body sites	competition, inhibition, cooperation, tolerance, killing, activation, silencing	replication rate, death rate, activation, migration (microbiota, *S.* Tm, immune cells)

The traditional approach of knocking out single host genes to assess their contribution to microbial defense often neglects the complexity of host-microbial interactions. Many powerful immune effectors show surprisingly small effects when knocked out in models of pathogenic infection of a host (Abeler-Dörner et al., 2020). We hypothesize that the redundancy of response pathways, their time-dependent functions during pathogen defense and the pathogen's ability to adapt its phenotype (i.e. in case of surviving pathogen subpopulations) in response to the environment (i.e. the type of immune defense mechanism faced by a particular pathogen cell at a particular time point) contribute to the difficulty to connect phenotypes to single immune effectors. Additional challenges arise from pathogens expressing inhibitors of or resistance against particular immune effectors. Given the importance of constant immune surveillance, backup mechanisms that maintain functions even in the absence of a particular immune effector are crucial. Therefore, if the absence of a single immune effector in an infection setup does not produce a phenotype, it does not necessarily mean that this effector is irrelevant. Instead, it could also point to a specific relevance of the context of this effector for the analyzed system, which favored the evolution of redundant mechanisms. Nevertheless, the lack of single immune effector mechanisms can shift the dynamics of the microbe-host interaction. These can be detected by advanced methods as discussed below.

We thus postulate that, while traditional tools can help to dissect fundamental relations in defined conditions, more holistic approaches are needed to decipher the complex dynamics underlying host-microbe interactions and other complex disease scenarios. Omics- and single cell analysis methods are certainly important tools to achieve this task, and, together with increasing integration of different omics-approaches, will continue to play a central role (Gardy et al., 2009; Gottschalk et al., 2013; Jansen et al., 2019; Pulendran et al., 2010; Zak et al., 2014). In this context, phenomenological mathematical models are used extensively to dissect patterns from big datasets. These models however do not explicitly account for molecular and cellular mechanisms (Handel et al., 2020).

Complementary to this, mechanistic mathematical models (MMMs) are powerful tools to dissect the functions of essential components within complex systems. These models capture the changing population sizes of microbes and host cells during an infection. Despite being often highly simplified, in a given system, MMMs can identify and quantify the relative contributions of its components to the dynamics of the system (Table 1). This facilitates mechanistic insights, reveals interaction networks, challenges assumptions, or identifies gaps in our understanding (Abel et al., 2015a; Gunawardena, 2014; Handel et al., 2020; Jansen et al., 2019). For a detailed, easy-to-read overview on mathematical modeling of immune responses, we direct the reader to Handel et al., 2020 (Handel et al., 2020). MMM approaches have been successfully applied to quantify the dynamics of viral infections (Davenport et al., 2007; Perelson, 2002), the population dynamics of T-cells (Borghans and Boer, 2007; Perelson, 2002) and to understand the generation and maintenance of immune memory (Buchholz et al., 2013; Gerlach et al., 2013).

More recently, MMMs have been extended to describe experiments in which pathogens or host cells have been tagged genetically (Abel et al., 2015a; Grant et al., 2008; Höfer et al., 2016). By accounting for the stochastic dynamics of tagged subpopulations, such mathematical models allow dissection of the intricate relations underlying host-microbe interactions, and therefore represent a promising extension of traditional methods (further described below). A major obstacle is the requirement of detailed knowledge of the analyzed system to set up MMMs. Especially in complex systems, it can be challenging to identify relevant processes and parameters to include into the MMM. To verify hypotheses based on

mathematical models, experimentation is required (Abel et al., 2015a; Gunawardena, 2014; Handel et al., 2020; Jansen et al., 2019). The crosstalk between modelers and wet lab scientists is therefore of critical importance.

COMPARTMENTAL MODELS TO DESCRIBE HOST-MICROBE INTERACTIONS

A large fraction of models applied to the field of host-microbe interaction are compartmental models. In these models, a group of individuals is classified into compartments that subdivide the population according to traits of interest, such as spatial location or differentiation state (Handel et al., 2020). This can be as simple as one bacterial strain growing in a liquid culture (Figure 1B). The replication rate *r* of this population and its death rate *d* define the population size at any given time, as described by the differential equation in Figure 1B. Figure 1C displays a compartmental model of a more complex situation, describing bacterial growth (*r*) in the cecal lumen (P_C), migration (*m*) from that compartment to the mesenteric lymph nodes (mLN), and microbial growth (*r*) at that site (P_{LN}).

MMMs are based on *a priori* information on the biological system. For example, the model in Figure 1C is built on knowing that the bacteria first colonize the intestine and from there spread to the mLN. The model parameters quantitatively characterize processes that shape the dynamics of the respective compartment (here: a population within a specific anatomic site), e.g. replication, death and migration. Computer simulations can be run with different values for these parameters. Comparing the output of simulations to empirical data then allows estimation of parameter values that are most consistent with observations. In simulations, the validity of different experimental or mechanistic scenarios can be tested against experimental data. Once set up, MMMs enable the prediction of the behavior of a system under altered conditions, e.g. the effect of an antibiotic treatment on a bacterial population during infection. Thus, besides the quantification of biologically relevant parameters, modeling can provide a formal, quantitative, cost-efficient and fast way of hypothesis generation and the design of optimal follow-up experiments. Iterative improvement is achieved by feedback between wet lab experimentation and modelers to fully exploit the potential of MMMs (Handel et al., 2020).

POPULATION DYNAMICS OF NEUTRAL GENETIC TAGS AS A TOOL TO DECIPHER SPATIOTEMPORAL KINETICS OF HOST-MICROBE INTERACTION

Population dynamics describe the kinetics of changes in the structure of a population, e.g. regarding age, developmental stage, disease state, phenotypic manifestation or localization. In the following, we will focus on approaches analyzing the distribution of neutral genetic tags within a population ("population structure"). When using the term "population dynamics", we refer to the dynamics of the distribution of a set of neutral genetic tags within a population. This serves as a readout for changes within that population.

To characterize a host-microbe interaction, compartmental MMMs allow quantification of parameters describing a population, e.g. its replication rate, death rate and pheno- or genotypic subpopulations of the microbe and/or the affected host cells (Abel et al., 2015a; Höfer et al., 2016). This approach is especially fruitful for well-characterized experimental models. Here, analysis of population structures by genetic tagging enables precise descriptions of the underlying population dynamics by MMMs. These approaches

can be applied to host cell and microbial populations. Below, we review the tools available in the different fields, and give examples for their application.

STUDYING BACTERIAL POPULATION DYNAMICS *IN VIVO*

In studies of host-bacterial interactions, the success of microbial colonization is traditionally assessed by selective plating of homogenized organs on agars which are permissive for the growth of the bacterium of interest. In some cases, qPCR or 16S-sequencing have also been employed. However, all these methods share an important shortcoming: they only provide a snapshot of the current size of the microbial population, but lack information about its past changes.

A widely applied approach in population dynamics of host-bacterial interactions is the analysis of bottlenecks. A bottleneck describes internal and external factors (constraints, e.g. intraspecies competition, effects of immune responses) which restrict the capacity (e.g. population size) of a component (e.g. a pathogen population in a host organ) (Abel et al., 2015a) (Figure 1D). The total population size can "easily" be measured. For bacterial infections, enumeration of CFU provides information about the size of a population at a given time in a certain organ. For immune cells, e.g. flow cytometric methods yield cell numbers. These measures integrate events of migration, replication and cell death. Disentangling those parameters can help to identify immune defenses or intervention strategies, even if these fail to completely control the infection. This is however highly challenging, especially in complex *in vivo* settings where pathogen populations can shrink and grow and host defenses respond in a dynamic fashion (Figure 1A, bottom panel). Here, continuous sampling is often not possible, which renders the experimental analysis of population sizes a snapshot analysis integrating all events that affected the population until then. In multistep processes like infections, it becomes especially difficult to assign bottlenecks to certain events. By contrast, analyzing changes in the diversity of neutral genetic tags in a population provides information about the population structure at earlier time points. Thereby, bottleneck-inflicted changes in a population can be traced with the help of genetic tags.

Approaches employing neutral genetic tags for the studies of population dynamics assume that the manifestation of genetic diversity (i.e. the genetic tags) is fitness neutral in the studied condition. Given this, changes in diversity of a population are typically a direct consequence of a reduction in population size (Abel et al., 2015a). This altered diversity will remain imprinted on the pathogen population, no matter how much it expands after passing a particular bottleneck (Figure 1E). In principle, this approach employs the evolutionary concept of genetic drift, which is particularly pronounced in events of dramatic population reduction or the founding of a new, spatially separated population by a low number of founder organisms (Arnold, 2001). Importantly, these changes reflect stochastic sampling events and are fitness independent (as the analyzed organisms are isogenic and equally fit, see above). By contrast, an expansion of population size in this context usually stably maintains diversity (Abel et al., 2015a). Figure 1E illustrates a scenario in which the same starting population of cells with equal fitness in a given system undergoes one contraction and two expansion events in different order, and how this affects population structure. Notably, the number of cells at the start as well as at the end of the experiment are equal in both scenarios. This example illustrates how two scenarios, indistinguishable by conventional methods of cell counting, derive from two different population dynamics and result in a very different population (genetic tag) structure. This principle can also be employed as a quality control for experiments analyzing the competitive index (CI) of bacterial mutants, in which the number of mutant bacteria in an organ of interest is divided by the number of wild type bacteria to assess fitness differences. Using a batch of

tagged isogenic mutant strains, and a batch of tagged wild type strains allows the detection of stochastic loss in the infection model and thereby enables the differentiation between fitness-related and stochastic effects (Figure 1F) (Hensel et al., 1995; Nguyen et al., 2020).

POPULATION DYNAMICS APPROACHES TO STUDY HOST-PATHOGEN INTERACTIONS

Population dynamics approaches successfully defined and quantified parameters of bacterial infection in *in vivo* experimental setups. Illustrative published examples using genetic tagging approaches are summarized in Table 2. As described above, changes in genetic diversity help to deduce changes in population dynamics retrospectively. In an experimental setup, diversity - as a readout for population structure - should ideally be traceable. Traditional tools for tracing of genetic diversity are different antibiotic resistances (MEYNELL, 1957; Moxon and Murphy, 1978), serotypes (MEYNELL and STOCKER, 1957) or the tagging with fluorescent proteins (Moor et al., 2017). As these markers potentially interfere with infection kinetics and might skew population dynamics by introducing different fitness costs, new approaches were developed to label bacteria genetically with phenotypically neutral sequence tags ("barcodes") (Abel et al., 2015a; Grant et al., 2008). Strains resulting from this approach are often referred to as wild type isogenic tagged strains (WITS) (Grant et al., 2008) (Figure 2A) and are phenotypically identical. Besides being fitness neutral, a large variety of these barcodes can be introduced into the population. This results in a higher number of distinguishable markers (i.e. genetic variation), and thereby increases the sensitivity for detecting large bottlenecks in the history of a given pathogen population (see (Abel et al., 2015b) and (Zhang et al., 2017) for a detailed analysis of the relation between number of barcodes and bottleneck sensitivity). qPCR or sequence counting techniques by next-generation sequencing allow precise and fast quantification of the relative distribution of these barcodes within the population. Absolute numbers of each barcoded bacterium are deduced by combining the relative barcode distributions with bacterial numbers obtained by conventional methods. These data serve as input for the MMMs. More recently, the usage of hundreds of barcodes in combination with high-throughput DNA sequencing methods has helped to further increase the sensitivity of this approach (Abel et al., 2015a; Nguyen et al., 2020). The here-described approach will be applied in the presented thesis (Chapter 4).

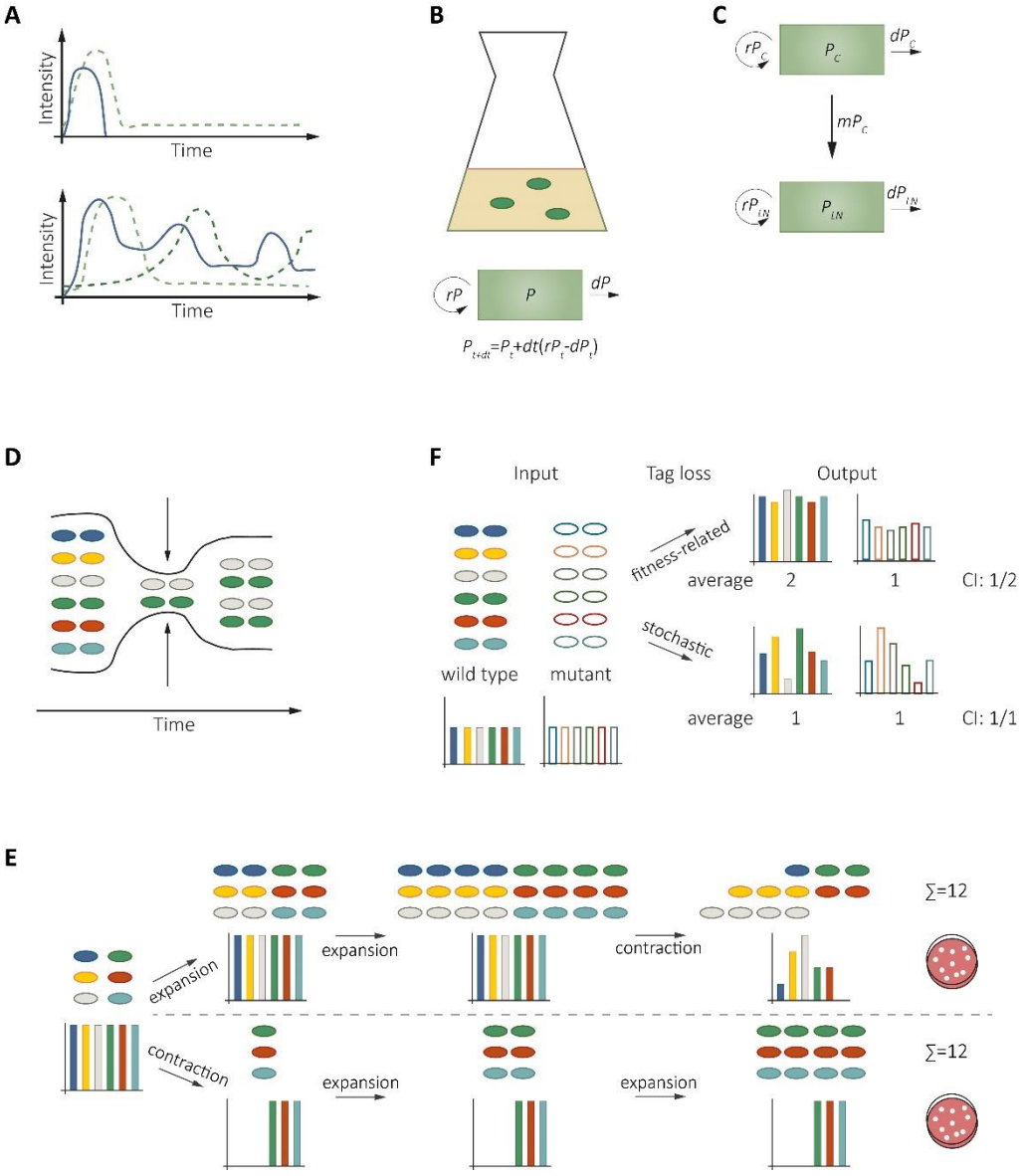

Figure 1 ***A*** *Intensity of a microbial trigger (blue line) and the induced host response(s) (dashed green line(s)) vary over time. Examples for accidental spillover of a commensal into the host body (upper panel) and for prolonged colonization of a host by a pathogenic bacterium (lower panel).* ***B*** *Compartmental model describing a bacterial population* P *growing in an Erlenmeyer flask, defined by the parameters replication rate* (r) *and death rate* (d). ***C*** *Compartmental model describing the migration (m) of a bacterium from the cecum* (P_C) *to the mLN* (P_{LN}) *(similar to (Kaiser et al., 2013)).* ***D*** *Bottlenecks represent constraints (arrows) on a population leading to a reduction in population size. Loss of genetic diversity during bottleneck passage remains imprinted on the population even after re-expansion.* ***E*** *Schematic drawing of two hypothetical population dynamic trajectories of one starting population. In both panels (upper and lower), the population undergoes two expansion events (doubling population size) and one contraction event (reducing population size by 50%). The final population size is equal while the population structure (genetic diversity, different colors) differs.* ***F*** *Tracing of genetic diversity by neutral genetic tags can be used to differentiate stochastic from fitness-related effects on populations. CI experiments allow the fitness assessment of bacterial mutants in comparison to wild type bacteria during a co-infection. The CI of a mutant is calculated by dividing the number of mutant bacteria by the number of wild type bacteria (CI > 1: mutant has a fitness advantage; CI < 1: mutant has a fitness disadvantage; CI = 1: no fitness difference). Using a pool of genetically tagged wild type and mutant bacteria allows the assessment of the nature of genetic tag loss: if the genetic tag loss is fitness related, the genetic diversity within one bacterial population (wild type or mutant, respectively) should remain similar (high evenness). Stochastic genetic tag loss, by contrast, leads to substantial variation in genetic diversity within one bacterial population (wild type or mutant, respectively; low evenness).*

Table 2 Studies analyzing pathogen population dynamics in vivo. bp = base pairs.

Bacterium	Method	Number of unique identifiers	Analyzed parameters	Main finding	Reference
Vibrio cholerae (*V. cholerae*)	STAMP - 30 bp barcodes, DNA sequencing	~500	bottleneck size, genetic distance between subpopulations	upstream migration of *V. cholerae* within the intestine	(Abel et al., 2015b)
L. monocytogenes	STAMP - 30 bp barcodes, DNA sequencing	200	bottleneck size, genetic distance between subpopulations	identification of gall bladder as critical reservoir for host-to-host transmission; role for $Gr1^+$ immune cells and microbiota in pathogen restriction	(Zhang et al., 2017)
L. monocytogenes	40 bp barcodes, qPCR/sequencing	20	migration and replication rate of *L. monocytogenes* to/in various organs	identification of small intestinal villi as reservoir for bacterial replication; identification of direct and indirect pathways of dissemination	(Melton-Witt et al., 2012)
Yersinia pseudotuberculosis (*Y. pseudotuberculosis*)	40 bp barcodes, qPCR	33	bottleneck size, genetic distance between subpopulations	intestinal *Y. pseudotuberculosis* critical for dissemination; establishment of independent subpopulations	(Barnes et al., 2006)
Hemophilus influenzae (*H. influenzae*)	antibiotic resistances, differential plating	2	bottleneck size	*H. influenzae* dissemination is independent of bacterial cooperation	(Moxon and Murphy, 1978)
H. influenzae	antibiotic resistances, differential plating	2	bottleneck size	bacteremia is caused by single dissemination events of *H. influenzae*	(Margolis and Levin, 2007)
Streptococcus pnemoniae (*S. pneumoniae*)	OVA/AVO surface tags, qPCR	2	migration, replication and death rate of nasal *S. pneumoniae* population	small founding population required for stable nasal colonization by *S. pneumoniae*	(Li et al., 2013)
S. Tm	antibiotic resistances, differential plating	2	bottleneck size	*S.* Tm dissemination from the intestine is a rare event and independent of bacterial cooperation	(MEYNELL, 1957)
S. Tm	serotypes, metabolic functions	3, 2	bottleneck size	independent host invasion by few *Salmonella* cells	(MEYNELL and STOCKER, 1957)
S. Tm	fluorescent proteins	2	clumping dynamics of *S.* Tm in intestinal content	protection by vaccination-induced IgA is mediated via enchainment of dividing bacteria, resulting in clonal elimination of *S.* Tm from intestinal lumen	(Moor et al., 2017)
S. Tm	WITS - 40 bp barcodes, qPCR	8	migration, replication and death rate of *S.* Tm to/in various organs	independent organ subpopulations during early infection, mixing via hematogenous spread at later stages	(Grant et al., 2008)
S. Tm	WITS - 40 bp barcodes, qPCR	7	bottleneck size during intestinal colonization, "evenness" score	identification of a $Gr1^+$-cell, inflammation dependent contraction of the intestinal *S.* Tm population at 2 dpi	(Maier et al., 2014)

S. Tm	WITS - 40 bp barcodes, qPCR	8	genetic distance between organ subpopulations,	intraspecies competition for intestinal colonization impacts host-to-host transmission	(Lam and Monack, 2014)
S. Tm	WITS - 40 bp barcodes, qPCR	8	genetic distance between organ subpopulations	antibiotic treatment efficiently targets fast-dividing *S.* Tm cells	(Rossi et al., 2017)
S. Tm	WITS - 40 bp barcodes, qPCR	7	migration to and replication in mLN	mLN colonization during oral *S.* Tm infection depends on immune cell migration from the intestinal mucosa to mLN. Restriction of replication of *S.* Tm in the mLN depends on NADPH oxidase	(Kaiser et al., 2013)
S. Tm	WITS - 40 bp barcodes, qPCR	7	migration to and replication in mLN	intestinal epithelial NAIP/NLRC4 restricts *S.* Tm migration to the mLN and thereby protects from systemic dissemination	Chapter 4
S. Tm	WITS - 40 bp barcodes, qPCR	7	migration to and replication in mLN	slow growing intracellular *S.* Tm persist after antibiotic treatment and can cause relapse	(Kaiser et al., 2014)
S. Tm	40 bp barcodeson plasmids, qPCR	5	plasmid transfer rates, intestinal luminal replication	systemic *S.* Tm persisters can reseed to the gut lumen and promote spread of antibiotic resistance by plasmid transfer	(Bakkeren et al., 2019)
S. Tm	WITS - 40 bp barcodes, qPCR	7	bottleneck size in intestinal lumen as quality control for STM screen	*S.* Tm uses microbiota-derived hydrogen as energy source in the intestinal lumen	(Nguyen et al., 2020)

STUDYING HOST RESPONSE DYNAMICS *IN VIVO*

During infection, both pathogen and host cell numbers vary over time, in parallel with changes in the infection environment that the respective components are exposed to. This, in turn, affects phenotypes of the interaction partners, which again affects the infection environment. Given the complexity of these systems, studying host response dynamics to pathogen infection *in vivo* is a challenging task. As outlined above, mathematical modeling can help to decipher these complex interactions. A set of well-established tools exists to study host cell population dynamics in this context.

It should be pointed out that tagging and tag-based population dynamics are not limited to bacteria. In the field of immunology and developmental biology, population dynamics approaches based on genetic tags have been applied especially to lineage tracing. Lineage tracing is used to study cell proliferation and differentiation during development (Gerlach et al., 2013; Guiu et al., 2019; Lu et al., 2011; Snippert et al., 2010; Spanjaard et al., 2018) and in the adult (Livet et al., 2007), under homeostatic and disease conditions (Buchholz et al., 2013; Cabeza-Cabrerizo et al., 2019; Tay et al., 2017). Lineage tracing tools include microscopy-based techniques such as the Brainbow/Confetti construct, in which stochastic Cre-mediated recombination results in cells tagged with different fluorescent markers (Livet et al., 2007; Snippert et al., 2010). This tool is well suited to study clonality, proliferation and migration dynamics within a specific tissue (Cabeza-Cabrerizo et al., 2019; Livet et al., 2007; Snippert et al., 2010; Tay et al., 2017) (Figure 3A). A higher variety in possible unique markers to increase sensitivity was a rationale for the development of neutral genetic barcoding strategies similarly to the WITS approach in bacteria. These barcodes are classically introduced via retroviral vectors *ex vivo* (Lu et al., 2011; Naik et al., 2013; Schepers et al., 2008), and the manipulated cells are subsequently transferred into hosts (Figure 3B). This approach is well suited for studies of circulating immune cells such as T-cells (Gossel et al., 2017; Schepers et al., 2008). To allow instead tracing of tissue resident cells in their native environment, *in vivo* barcoding tools have been developed recently. These approaches use the CRISPR/Cas9 system for the labelling of embryos (Spanjaard et al., 2018), or inducible CRISPR (Bowling et al., 2020), transposase (Sun et al., 2014) and Cre recombinase (Weber et al., 2016) systems for barcoding of cells in the adult organism *in vivo*. The latter approaches allow time-, site-, and/or cell-specific inducible introduction of barcodes, which makes them exceptionally powerful tools to resolve complex dynamic processes in particular target tissues of the adult host. Illustrative studies applying different genetic tag-based population dynamic approaches are summarized in Table 3.

The recently developed CARLIN mouse line (Bowling et al., 2020) allows CRISPR-mediated, large-scale, cell-type independent, inducible barcoding. Importantly, transcription of the CARLIN barcodes allows for a combined read-out of barcodes and gene expression at the single cell level. This enables an unbiased analysis of cell populations, as well as correlation of clonality with gene expression. Specifically, the application of the CARLIN system revealed skewed proliferative responses of hematopoietic stem cells (HSCs) under stress conditions. Surprisingly, only a small fraction of HSCs contributed to hematopoiesis upon exposure to e.g. irradiation or chemotherapy. Differential gene expression analysis of inactive versus active HSCs revealed a potential regulator of HSC stress responses.

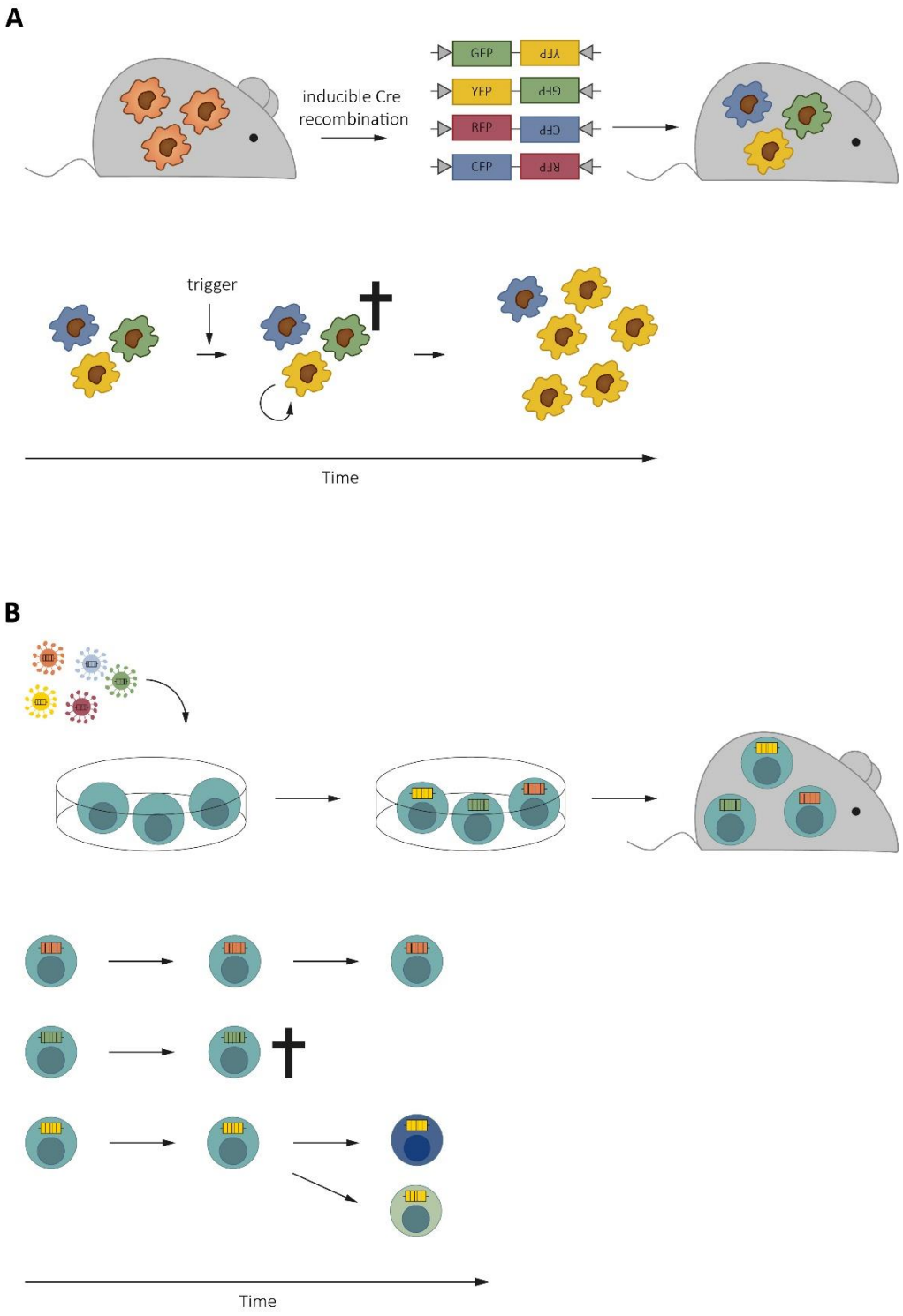

Figure 2 ***A*** *Schematic of the Confetti approach for fluorescent labeling of immune cells (Snippert et al., 2010). Inducible Cre-mediated recombination of the Confetti locus leads to differential labeling of cells with GFP, YFP, RFP or CFP (upper panel). This experimental approach can e.g. be used for analysis of local replication, death and migration rates of immune cells as observed upon exposure to a microbial trigger (lower panel).* ***B*** *Schematic of a neutral genetic barcoding approach of T cells. Genetic barcodes are introduced ex vivo by retroviruses. The barcoded cells can be transplanted into recipient hosts (upper panel) and employed to study cell survival, death, replication, differentiation and migration (lower panel) (Schepers et al., 2008).*

Table 3 Studies analyzing host cell population dynamics in vivo.

Cell population	Method	Number of unique identifiers	Analyzed parameters	Main finding	Reference
Neurons	Cre/LoxP-mediated tagging by fluorescent proteins *in vivo*, "Brainbow" reporter	~90	cellular interactions in the brain	visualization of neurons and cellular interactions in the mouse brain	(Livet et al., 2007)
Intestinal epithelial stem cells	Cre/LoxP-mediated tagging by fluorescent proteins *in vivo*, "Confetti" reporter	4	cell differentiation, replication rate	intestinal epithelial stem cells divide symmetrically	(Snippert et al., 2010)
Microglia	Cre/LoxP-mediated tagging by fluorescent proteins *in vivo*, "Confetti" reporter	4	replication and death rate, longevity	stochastic, high self-renewal capacity of microglia in steady-state; selected clonal expansion *in situ* during disease conditions	(Tay et al., 2017)
DCs	Cre/LoxP-mediated tagging by fluorescent proteins *in vivo*, "Confetti" reporter	4	replication rate, longevity, migration	mucosal DCs highly depend on homeostatic replenishment from HSC-derived precursors; clonal expansion *in situ* during disease conditions	(Cabeza-Cabrerizo et al., 2019)
HSCs	Cre/LoxP-mediated tagging by fluorescent protein *in vivo*	1	cell differentiation, replication rate	HSC-derived progenitors self-renew and mainly contribute to steady-state hematopoiesis	(Busch et al., 2015)
$CD4^+$ T cells	congenic surface markers markers, flow cytometry	2	replication rate, longevity	naïve $CD4^+$ T cell pool impacts $CD4^+$ T memory cell lifetime and replication rate	(Gossel et al., 2017)
$CD8^+$ T cells	congenic surface markers markers, flow cytometry	8	cell differentiation, replication rate	multiple precursors are required for induction of a robust effector and memory $CD8^+$ T cell response	(Buchholz et al., 2013)
$CD8^+$ T cells	lentiviral barcoding *ex vivo*, microarray	~10^2	differentiation and migration of antigen-specific $CD8^+$ T cells	antigen-specific $CD8^+$ T cells in different organs derive from a common precursor pool	(Schepers et al., 2008)
$CD8^+$ T cells	lentiviral barcoding *ex vivo*, DNA sequencing	~10^3	cell differentiation, replication rate	T cells with identical T cell receptors display heterogenous expansion and differentiation patterns	(Gerlach et al., 2013)
$CD8^+$ T cells	lentiviral barcoding *ex vivo*, microarray	~10^2	genetic distance between organ subpopulations	both low and high avidity T cells can differentiate into T effector and memory cells	(Gerlach et al., 2010)
HSCs	33 bp tags, lentiviral barcoding *ex vivo*, DNA sequencing	~10^2-10^3	cell differentiation	distinct HSC differentiation patterns	(Lu et al., 2011)
HSCs	lentiviral bracoding *ex vivo*, DNA sequencing	~10^2	cell differentiation	graded commitment model of hematopoiesis	(Naik et al., 2013)

$CD8^+$ T cells	Potentially ~600 bp Cre/LoxP-mediated random barcodes *in vivo*, DNA sequencing; here analyzed *in situ*	theoretically ~10^12	not applicable	*in situ* simulation of barcode generation by optimized Cre/loxP construct	(Weber et al., 2016)
HSCs	Doxycycline-inducible transposon barcoding *in vivo*, DNA sequencing	theoretically unlimited	cell differentiation	long-lived progenitors rather than HSCs mainly contribute to steady-state hematopoiesis	(Sun et al., 2014)
Germ cells (embryogenesis of zebrafish)	LINNAEUS - CRISPR/Cas9-induced genetic scars *in vivo*, scRNAseq	theoretically unlimited	cell differentiation	detailed cell differentiation map during zebrafish embryogenesis	(Spanjaard et al., 2018)
HSCs	CARLIN - CRISPR/Cas9-induced barcoding *in vivo* (sequential induction possible), DNA sequencing (transcriptomics)	~10^4; barcodes are transcribed	cell differentiation and single cell gene expression	unbiased lineage tracing and transcriptional profiling of HSCs *in vivo*, expansion potential of fetal liver HSCs is imprinted by the cellular niche	(Bowling et al., 2020)

REFERENCES

Abel, S., Wiesch, P.A. zur, Davis, B.M., and Waldor, M.K. (2015a). Analysis of Bottlenecks in Experimental Models of Infection. PLOS Pathogens *11*, e1004823.

Abel, S., zur Wiesch, P.A., Chang, H.-H., Davis, B.M., Lipsitch, M., and Waldor, M.K. (2015b). STAMP: Sequence tag-based analysis of microbial population dynamics. Nat Methods *12*, 223–226.

Abeler-Dörner, L., Laing, A.G., Lorenc, A., Ushakov, D.S., Clare, S., Speak, A.O., Duque-Correa, M.A., White, J.K., Ramirez-Solis, R., Saran, N., et al. (2020). High-throughput phenotyping reveals expansive genetic and structural underpinnings of immune variation. Nat. Immunol. *21*, 86–100.

Arnold, J. (2001). Genetic Drift. In Encyclopedia of Genetics, S. Brenner, and J.H. Miller, eds. (New York: Academic Press), pp. 832–834.

Bakkeren, E., Huisman, J.S., Fattinger, S.A., Hausmann, A., Furter, M., Egli, A., Slack, E., Sellin, M.E., Bonhoeffer, S., Regoes, R.R., et al. (2019). Salmonella persisters promote the spread of antibiotic resistance plasmids in the gut. Nature *573*, 276–280.

Barnes, P.D., Bergman, M.A., Mecsas, J., and Isberg, R.R. (2006). Yersinia pseudotuberculosis disseminates directly from a replicating bacterial pool in the intestine. J Exp Med *203*, 1591–1601.

Borghans, J.A.M., and Boer, R.J.D. (2007). Quantification of T-cell dynamics: from telomeres to DNA labeling. Immunological Reviews *216*, 35–47.

Bowling, S., Sritharan, D., Osorio, F.G., Nguyen, M., Cheung, P., Rodriguez-Fraticelli, A., Patel, S., Yuan, W.-C., Fujiwara, Y., Li, B.E., et al. (2020). An Engineered CRISPR-Cas9 Mouse Line for Simultaneous Readout of Lineage Histories and Gene Expression Profiles in Single Cells. Cell.

Buchholz, V.R., Flossdorf, M., Hensel, I., Kretschmer, L., Weissbrich, B., Gräf, P., Verschoor, A., Schiemann, M., Höfer, T., and Busch, D.H. (2013). Disparate Individual Fates Compose Robust CD8+ T Cell Immunity. Science *340*, 630–635.

Busch, K., Klapproth, K., Barile, M., Flossdorf, M., Holland-Letz, T., Schlenner, S.M., Reth, M., Höfer, T., and Rodewald, H.-R. (2015). Fundamental properties of unperturbed haematopoiesis from stem cells in vivo. Nature *518*, 542–546.

Cabeza-Cabrerizo, M., van Blijswijk, J., Wienert, S., Heim, D., Jenkins, R.P., Chakravarty, P., Rogers, N., Frederico, B., Acton, S., Beerling, E., et al. (2019). Tissue clonality of dendritic cell subsets and emergency DCpoiesis revealed by multicolor fate mapping of DC progenitors. Sci Immunol *4*.

Chen, K., Geng, S., Yuan, R., Diao, N., Upchurch, Z., and Li, L. (2015). Super-low Dose Endotoxin Pre-conditioning Exacerbates Sepsis Mortality. EBioMedicine *2*, 324–333.

Davenport, M.P., Ribeiro, R.M., Zhang, L., Wilson, D.P., and Perelson, A.S. (2007). Understanding the mechanisms and limitations of immune control of HIV. Immunol. Rev. *216*, 164–175.

Gardy, J.L., Lynn, D.J., Brinkman, F.S.L., and Hancock, R.E.W. (2009). Enabling a systems biology approach to immunology: focus on innate immunity. Trends in Immunology *30*, 249–262.

Gerlach, C., van Heijst, J.W.J., Swart, E., Sie, D., Armstrong, N., Kerkhoven, R.M., Zehn, D., Bevan, M.J., Schepers, K., and Schumacher, T.N.M. (2010). One naive T cell, multiple fates in CD8+ T cell differentiation. J Exp Med *207*, 1235–1246.

Gerlach, C., Rohr, J.C., Perié, L., Rooij, N. van, Heijst, J.W.J. van, Velds, A., Urbanus, J., Naik, S.H., Jacobs, H., Beltman, J.B., et al. (2013). Heterogeneous Differentiation Patterns of Individual CD8+ T Cells. Science *340*, 635–639.

Germain, R.N. (2001). The Art of the Probable: System Control in the Adaptive Immune System. Science *293*, 240–245.

Gossel, G., Hogan, T., Cownden, D., Seddon, B., and Yates, A.J. (2017). Memory CD4 T cell subsets are kinetically heterogeneous and replenished from naive T cells at high levels. Elife *6*.

Gottschalk, R.A., Martins, A.J., Sjoelund, V.H., Angermann, B.R., Lin, B., and Germain, R.N. (2013). Recent progress using systems biology approaches to better understand molecular mechanisms of immunity. Seminars in Immunology *25*, 201–208.

Grant, A.J., Restif, O., McKinley, T.J., Sheppard, M., Maskell, D.J., and Mastroeni, P. (2008). Modelling within-host spatiotemporal dynamics of invasive bacterial disease. PLoS Biol. *6*, e74.

Guiu, J., Hannezo, E., Yui, S., Demharter, S., Ulyanchenko, S., Maimets, M., Jørgensen, A., Perlman, S., Lundvall, L., Mamsen, L.S., et al. (2019). Tracing the origin of adult intestinal stem cells. Nature *570*, 107–111.

Gunawardena, J. (2014). Models in biology: 'accurate descriptions of our pathetic thinking.' BMC Biology *12*, 29.

Handel, A., La Gruta, N.L., and Thomas, P.G. (2020). Simulation modelling for immunologists. Nature Reviews Immunology *20*, 186–195.

Hausmann, A., Böck, D., Geiser, P., Berthold, D.L., Fattinger, S.A., Furter, M., Bouman, J.A., Barthel-Scherrer, M., Lang, C.M., Bakkeren, E., et al. (2020). Intestinal epithelial NAIP/NLRC4 restricts systemic dissemination of the adapted pathogen Salmonella Typhimurium due to site-specific bacterial PAMP expression. Mucosal Immunol *13*, 530–544.

Hensel, M., Shea, J.E., Gleeson, C., Jones, M.D., Dalton, E., and Holden, D.W. (1995). Simultaneous identification of bacterial virulence genes by negative selection. Science *269*, 400–403.

Höfer, T., Barile, M., and Flossdorf, M. (2016). Stem-cell dynamics and lineage topology from in vivo fate mapping in the hematopoietic system. Current Opinion in Biotechnology *39*, 150–156.

Jansen, J.E., Gaffney, E.A., Wagg, J., and Coles, M.C. (2019). Combining Mathematical Models With Experimentation to Drive Novel Mechanistic Insights Into Macrophage Function. Front Immunol *10*, 1283.

Kaiser, P., Slack, E., Grant, A.J., Hardt, W.-D., and Regoes, R.R. (2013). Lymph node colonization dynamics after oral Salmonella Typhimurium infection in mice. PLoS Pathog. *9*, e1003532.

Kaiser, P., Regoes, R.R., Dolowschiak, T., Wotzka, S.Y., Lengefeld, J., Slack, E., Grant, A.J., Ackermann, M., and Hardt, W.-D. (2014). Cecum Lymph Node Dendritic Cells Harbor Slow-Growing Bacteria Phenotypically Tolerant to Antibiotic Treatment. PLOS Biology *12*, e1001793.

Lam, L.H., and Monack, D.M. (2014). Intraspecies Competition for Niches in the Distal Gut Dictate Transmission during Persistent Salmonella Infection. PLOS Pathogens *10*, e1004527.

Li, Y., Thompson, C.M., Trzciński, K., and Lipsitch, M. (2013). Within-host selection is limited by an effective population of Streptococcus pneumoniae during nasopharyngeal colonization. Infect. Immun. *81*, 4534–4543.

Livet, J., Weissman, T.A., Kang, H., Draft, R.W., Lu, J., Bennis, R.A., Sanes, J.R., and Lichtman, J.W. (2007). Transgenic strategies for combinatorial expression of fluorescent proteins in the nervous system. Nature *450*, 56–62.

Lu, R., Neff, N.F., Quake, S.R., and Weissman, I.L. (2011). Tracking single hematopoietic stem cells in vivo using high-throughput sequencing in conjunction with viral genetic barcoding. Nature Biotechnology *29*, 928–933.

Maier, L., Diard, M., Sellin, M.E., Chouffane, E.-S., Trautwein-Weidner, K., Periaswamy, B., Slack, E., Dolowschiak, T., Stecher, B., Loverdo, C., et al. (2014). Granulocytes impose a tight bottleneck upon the gut luminal pathogen population during Salmonella typhimurium colitis. PLoS Pathog. *10*, e1004557.

Margolis, E., and Levin, B.R. (2007). Within-host evolution for the invasiveness of commensal bacteria: an experimental study of bacteremias resulting from Haemophilus influenzae nasal carriage. J. Infect. Dis. *196*, 1068–1075.

Medzhitov, R., and Janeway, CharleS.J. (2000). Innate immune recognition: mechanisms and pathways. Immunol Rev *173*, 89–97.

Melton-Witt, J.A., Rafelski, S.M., Portnoy, D.A., and Bakardjiev, A.I. (2012). Oral infection with signature-tagged Listeria monocytogenes reveals organ-specific growth and dissemination routes in guinea pigs. Infect. Immun. *80*, 720–732.

MEYNELL, G.G. (1957). The Applicability of the Hypothesis of Independent Action to Fatal Infections in Mice given Salmonella typhimurium by Mouth. Microbiology, *16*, 396–404.

MEYNELL, G.G., and STOCKER, B.A.D. (1957). Some Hypotheses on the Aetiology of Fatal Infections in Partially Resistant Hosts and their Application to Mice Challenged with Salmonella paratyphi-B or Salmonella typhimurium by Intraperitoneal Injection. Microbiology, *16*, 38–58.

Moor, K., Diard, M., Sellin, M.E., Felmy, B., Wotzka, S.Y., Toska, A., Bakkeren, E., Arnoldini, M., Bansept, F., Co, A.D., et al. (2017). High-avidity IgA protects the intestine by enchaining growing bacteria. Nature *544*, 498–502.

Moxon, E.R., and Murphy, P.A. (1978). Haemophilus influenzae bacteremia and meningitis resulting from survival of a single organism. Proc. Natl. Acad. Sci. U.S.A. *75*, 1534–1536.

Murphy, K., and Weaver, C. (2016). Janeway's Immunobiology (Garland Science).

Naik, S.H., Perié, L., Swart, E., Gerlach, C., van Rooij, N., de Boer, R.J., and Schumacher, T.N. (2013). Diverse and heritable lineage imprinting of early haematopoietic progenitors. Nature *496*, 229–232.

Nguyen, B.D., Cuenca V, M., Hartl, J., Gül, E., Bauer, R., Meile, S., Rüthi, J., Margot, C., Heeb, L., Besser, F., et al. (2020). Import of Aspartate and Malate by DcuABC Drives H2/Fumarate Respiration to Promote Initial Salmonella Gut-Lumen Colonization in Mice. Cell Host Microbe.

Perelson, A.S. (2002). Modelling viral and immune system dynamics. Nat. Rev. Immunol. *2*, 28–36.

Pradeu, T., Jaeger, S., and Vivier, E. (2013). The speed of change: towards a discontinuity theory of immunity? Nat Rev Immunol *13*, 764–769.

Pulendran, B., Li, S., and Nakaya, H.I. (2010). Systems vaccinology. Immunity *33*, 516–529.

Rossi, O., Dybowski, R., Maskell, D.J., Grant, A.J., Restif, O., and Mastroeni, P. (2017). Within-host spatiotemporal dynamics of systemic Salmonella infection during and after antimicrobial treatment. J Antimicrob Chemother *72*, 3390–3397.

Schepers, K., Swart, E., van Heijst, J.W.J., Gerlach, C., Castrucci, M., Sie, D., Heimerikx, M., Velds, A., Kerkhoven, R.M., Arens, R., et al. (2008). Dissecting T cell lineage relationships by cellular barcoding. J. Exp. Med. *205*, 2309–2318.

Snippert, H.J., Flier, L.G. van der, Sato, T., Es, J.H. van, Born, M. van den, Kroon-Veenboer, C., Barker, N., Klein, A.M., Rheenen, J. van, Simons, B.D., et al. (2010). Intestinal Crypt Homeostasis Results from Neutral Competition between Symmetrically Dividing Lgr5 Stem Cells. Cell *143*, 134–144.

Spanjaard, B., Hu, B., Mitic, N., Olivares-Chauvet, P., Janjuha, S., Ninov, N., and Junker, J.P. (2018). Simultaneous lineage tracing and cell-type identification using CRISPR-Cas9-induced genetic scars. Nat. Biotechnol. *36*, 469–473.

Sun, J., Ramos, A., Chapman, B., Johnnidis, J.B., Le, L., Ho, Y.-J., Klein, A., Hofmann, O., and Camargo, F.D. (2014). Clonal dynamics of native haematopoiesis. Nature *514*, 322–327.

Tateda, K., Matsumoto, T., Miyazaki, S., and Yamaguchi, K. (1996). Lipopolysaccharide-induced lethality and cytokine production in aged mice. Infect. Immun. *64*, 769–774.

Tay, T.L., Mai, D., Dautzenberg, J., Fernández-Klett, F., Lin, G., Sagar, Datta, M., Drougard, A., Stempfl, T., Ardura-Fabregat, A., et al. (2017). A new fate mapping system reveals context-dependent random or clonal expansion of microglia. Nature Neuroscience *20*, 793–803.

Weber, T.S., Dukes, M., Miles, D.C., Glaser, S.P., Naik, S.H., and Duffy, K.R. (2016). Site-specific recombinatorics: in situ cellular barcoding with the Cre Lox system. BMC Systems Biology *10*, 43.

Zak, D.E., Tam, V.C., and Aderem, A. (2014). Systems-Level Analysis of Innate Immunity. Annual Review of Immunology *32*, 547–577.

Zhang, T., Abel, S., Abel Zur Wiesch, P., Sasabe, J., Davis, B.M., Higgins, D.E., and Waldor, M.K. (2017). Deciphering the landscape of host barriers to Listeria monocytogenes infection. Proc. Natl. Acad. Sci. U.S.A. *114*, 6334–6339.

CHAPTER 3 - CD11B$^+$ CD103$^-$ SENTINEL MPS RELAY A TUNABLE ANTIBACTERIAL NFKB RESPONSE IN INTESTINAL EPITHELIAL CELLS VIA TNF

Annika Hausmann[1, 7], Boas Felmy[1, 7], Leo Kunz[2], Giverny Ganz[1], Dorothée L. Berthold[1], Toshihiro Nakamura[1], Tamas Dolowschiak[1], Stefan A. Fattinger[1, 3], Markus Furter[1], Anna A. Müller-Hauser[1], Manja Barthel-Scherrer[1], Katerina Vlantis[4], Laurens Wachsmuth[4], Luigi Tortola[5], Jan Kisielow[5], Danjiela Heide[6], Mathias Heikenwälder[6], Manfred Kopf[5], Timm Schroeder[2], Manolis Pasparakis[4], Mikael E. Sellin[1,3], Wolf-Dietrich Hardt[1]

Author affiliations:

[1]Institute of Microbiology, Department of Biology, ETH Zurich, Zurich, Switzerland
[2]Department of Biosystems Science and Engineering, ETH Zurich, Basel, Switzerland
[3]Science for Life Laboratory, Department of Medical Biochemistry and Microbiology, Uppsala University, Uppsala, Sweden
[4]Institute for Genetics, Cologne Excellence Cluster on Cellular Stress Responses in Aging-Associated Diseases (CECAD), University of Cologne, Cologne, Germany.
[5]Institute of Molecular Health Sciences, Department of Biology, ETH Zurich, Zurich, Switzerland
[6]Division of Chronic Inflammation and Cancer, German Cancer Research Center (DKFZ), Heidelberg, German
[7]these authors contributed equally

Author contributions:

AH, BF, LK, GG, DLB, TN, TD, SAF, MES performed experiments and AH, BF, LK, GG, DLB, TN, TD analyzed the data. LK, KV, LW, LT, DH, MH, MK, TS, MP contributed reagents/materials/mice/analysis tools. MF, AAMH and MBS provided technical assistance. AH, BF, LK, TD, TS, MES, WDH conceived and designed the experiments. AH wrote the manuscript with corrections and comments by MES and WDH. All authors read, amended and approved the manuscript.

Intestinal epithelial cell (IEC) NFκB signaling regulates the fine balance between mucosal homeostasis and inflammation. It is not fully understood which signals tune this balance, and how bacterial exposure elicits the process. Pure LPS induces epithelial NFκB activation *in vivo*. We found that in mice, IECs do not respond directly to LPS. Instead, CD11b$^+$ CD103$^-$ intercrypt mononuclear phagocytes (MPs) sense LPS via TLR4 and secrete TNF to elicit epithelial NFκB signaling in their immediate neighborhood. This response is relevant also during oral enteropathogen infection. The MP-TNF-IEC axis avoids responses to luminal microbiota LPS, but enables localized or tissue-wide epithelial NFκB responses in proportion to the microbial threat. Thereby, the CD11b$^+$ CD103$^-$ intercrypt MPs serve as important sentinels for Gram-negative microbes breaching the epithelial barrier. The tunability of this crypt response allows induction of defense mechanisms at an appropriate scale according to localization and intensity of microbial triggers.

INTRODUCTION

The mucosal immune system maintains host-microbiota homeostasis and defends against pathogen infections. This is a challenging task, as symbionts and pathogens share many common patterns (microbe-associated molecular patterns; MAMPs), which are recognized by innate immune receptors (pattern recognition receptors; PRRs) (Chapter 1). These features make it difficult to distinguish commensals from pathogenic bacteria. Different cell types in the intestinal mucosa act in synergy to achieve this demanding task. Intestinal epithelial cells (IECs) form a critical physical barrier between the intestinal lumen containing dense microbial communities, and the sterile host compartment (Johansson and Hansson, 2016) (Chapter 1). Besides shielding immune cells in the lamina propria from the microbes in the lumen, IECs possess sensor and defense-effector functions contributing actively to host defense (Birchenough et al., 2016; Cunliffe and Mahida, 2004; Knodler et al., 2010; Kreibich et al., 2015; Rauch et al., 2017; Sellin et al., 2014) (Chapter 4). IEC - immune cell crosstalk plays an important role in integrating tissue level signals and inducing appropriate host responses. Intestinal dendritic cells (DCs) have a high antigen sampling capacity and express an arsenal of PRRs (Diebold, 2009; Rescigno et al., 2001), thereby placing them at the nexus of this crosstalk. The surface markers CD11b and CD103 define DC subsets in the intestine (Bogunovic et al., 2009; Muzaki et al., 2015; Scott et al., 2015). A role of $CD11b^{-}$ $CD103^{+}$ (Muzaki et al., 2015) and $CD11b^{+}$ $CD103^{+}$ (Kinnebrew et al., 2012) DCs in eliciting IL12/IL15/IFNγ or IL23/IL22 signaling to trigger IEC production of IL18bp or Reg3γ has been described. It remains unknown whether intestinal $CD11b^{+}$ $CD103^{-}$ DCs and macrophages trigger innate immune tissue responses and interact with IECs upon microbial sensing.

PRRs are critical for the detection of microbes. The PRRs Toll-like receptor (TLR) 4 and 5 sense bacterial MAMPs and are widely expressed in mammals (Fitzgerald and Kagan, 2020; Nie et al., 2018). Both immune cells and IECs express TLR5, which detects flagella (Fulde et al., 2018; Hayashi et al., 2001; Yang and Yan, 2017). Similarly, immune cell expression of TLR4, which recognizes the bacterial membrane component Lipopolysaccharide (LPS) (Poltorak et al., 1998), is well described (Medzhitov and Janeway, 2000a). By contrast, its expression by IECs remains controversial. Several studies report TLR4 expression by IECs (Cario et al., 2000; Hornef et al., 2002, 2003; Price et al., 2018; Wang et al., 2010). These studies are, however, potentially obscured by the difficulty to efficiently isolate and culture IECs, the use of epithelial cell lines that incompletely recapitulate primary IEC expression patterns (Chapter 5), and the lack of reliable antibodies against TLR4 (Price et al., 2018). Therefore, the expression and, more importantly, the functional relevance of epithelial TLR4 is still debated.

NFκB transcription factors integrate numerous signals and drive immune defense. TLR signaling via MyD88 and Ticam1 (Trif) (Akira and Hoshino, 2003; Fitzgerald et al., 2003), but also TNF and IL1β cytokine receptor engagement (Adachi et al., 1998; Hayden and Ghosh, 2014; Muzio et al., 1997), activate the NFκB pathway. The exact contributions of these stimuli and how they mediate NFκB signaling across the variety of cell types found in the gut mucosa remain incompletely understood.

NFκB transcription factor expression is ubiquitous. Inhibitory regulators sequester them in the cytosol of resting cells (Hayden and Ghosh, 2008). Upon activation, these transcription factors shuttle to the nucleus to induce gene transcription (Adachi et al., 1998; Wang et al., 2001). Epithelial NFκB signaling maintains intestinal homeostasis by regulating proliferation, survival and apoptosis of IECs (Guma et al., 2011; Liu et al., 2017; Vlantis et al., 2016; Wullaert et al., 2011). In line with these complex functions, a delicate balance in epithelial NFκB signaling is crucial. Both inactivation and hyperactivation of this pathway predispose to intestinal inflammation (Dheer et al., 2016; Guma et al., 2011; Vereecke et al., 2010, 2014; Vlantis et al., 2011, 2016). Alterations in the NFκB signaling pathway and its regulators can consequently spark chronic inflammatory conditions in the gut, e.g. inflammatory bowel disease (IBD) (Rogler et al., 1998; Zhang et al., 2006). Hence, epithelial NFκB acts as an integrator of signals, able to tip the mucosal tissue balance between homeostasis and

inflammation in a fine-tuned manner. To date, it remains unclear what combination of signals and cell types ensure an appropriately balanced NFκB response in the mucosa upon microbial insult.

We here deciphered how epithelial NFκB signaling is elicited upon exposure to bacterial LPS. In the murine gut, IECs do not directly respond to extracellular LPS. Instead, TNF-producing $CD11b^{+}$ $CD103^{-}$ intestinal MPs in intercrypt regions specifically trigger epithelial NFκB signaling, inducing a multifaceted, tunable antibacterial response.

RESULTS

$TLR4^{+}$ RADIOSENSITIVE CELLS INDUCE GUT EPITHELIUM NFKB ACTIVATION UPON LPS EXPOSURE

To analyze NFκB signaling dynamics in the intestinal mucosa, we made use of $p65^{GFP\text{-}FL}$ mice (De Lorenzi et al., 2009). In these mice, the wild type p65 gene is replaced by a gene encoding a fusion protein of the NFκB transcription factor p65 and GFP. This fusion protein allows real time assessment of the NFκB activation status within a cell, by monitoring the subcellular localization of the tagged p65 protein. Under homeostatic conditions, p65 resides in the cytosol, while nuclear translocation (and subsequent recycling) occurs upon activation of NFκB signaling (Adachi et al., 1998).

We injected the reporter mice intravenously (iv) with 5 µg ultrapure *Salmonella* Typhimurium (*S*. Tm) LPS, which activates TLR4, but no other relevant PRRs (see below). We chose this LPS concentration to model bacterial exposure during infection. This is considered a low dose, ≥100-fold below the LD_{50} (Chen et al., 2015; Tateda et al., 1996). 2-photon microscopy imaging of cecal explants from LPS-injected mice allowed us to monitor epithelial NFκB activation in the intestinal mucosa. Analysis of the cecal tissue at 1h post injection (h.p.inj.) revealed NFκB activation in ~100% of the IECs (Figure 1A, S1A), which coincided with the upregulation of the NFκB target genes *A20* (*Tnfaip3*), *Cxcl2* and *Tnf* (Figure S1B) (Burke et al., 2014; Collart et al., 1990; Shakhov et al., 1990; Vereecke et al., 2010). Due to the small nucleus size, the complex tissue architecture, as well as the relatively weak fluorescence of the $p65^{GFP\text{-}FL}$ reporter, this experiment could not resolve potential NFκB activation in lamina propria cells. In line with previous reports (Fitzgerald et al., 2003; Poltorak et al., 1998), NFκB activation in our model depended on TLR4, and was absent in LPS-injected $p65^{GFP\text{-}FL}$x$Tlr4^{-/-}$ mice (Figure 1A). This also held true for the small intestine (ileum) and colon (Figure S1C, D). To probe whether IECs are able to directly sense LPS via TLR4, we generated bone marrow chimeras (BMCs). Specifically, we reconstituted irradiated $p65^{GFP\text{-}FL}$ or $p65^{GFP\text{-}FL}$x$Tlr4^{-/-}$ mice with $p65^{GFP\text{-}FL}$ or $p65^{GFP\text{-}FL}$x$Tlr4^{-/-}$ bone marrow (BM), resulting in $p65^{GFP\text{-}FL}$ > $p65^{GFP\text{-}FL}$, $p65^{GFP\text{-}FL}$x$Tlr4^{-/-}$ > $p65^{GFP\text{-}FL}$, $p65^{GFP\text{-}FL}$x$Tlr4^{-/-}$ > $p65^{GFP\text{-}FL}$x$Tlr4^{-/-}$ and $p65^{GFP\text{-}FL}$ > $p65^{GFP\text{-}FL}$x$Tlr4^{-/-}$ BMCs. While $p65^{GFP\text{-}FL}$ > $p65^{GFP\text{-}FL}$x$Tlr4^{-/-}$ mice still showed ~100% epithelial NFκB activation, $p65^{GFP\text{-}FL}$x$Tlr4^{-/-}$ > $p65^{GFP\text{-}FL}$ BMCs displayed NFκB activation in only a fraction of IECs (Figure 1B). In line with that, we detected stronger upregulation of NFκB target genes in the BMCs reconstituted with TLR4-proficient BM (Figure S2A). Again, analysis of the small intestine and the colon revealed similar kinetics (Figure S2B, C). Remaining radioresistant immune cells in tissues after radiation represent a well described confounding factor in studies using BMCs (Bogunovic et al., 2006; Shaw et al., 2018). To directly assess the responsiveness of IECs to LPS, we therefore generated small intestinal epithelial organoids from $p65^{GFP\text{-}FL}$ mice and treated them with LPS. The organoids did not respond with NFκB activation to LPS stimulation (Figure S3), in line with previous reports (Günther et al., 2015; Price et al., 2018). We thus concluded that the residual epithelial NFκB activation observed in the $p65^{GFP\text{-}FL}$x$Tlr4^{-/-}$ > $p65^{GFP\text{-}FL}$ BMCs likely stemmed from residual radioresistant TLR4-proficient immune cells remaining in the recipients (this was later confirmed; see below, Figure S6D). To rigorously assess the role of TLR4 signaling by particular mucosal cell types, we therefore used $p65^{GFP\text{-}FL}$x$Tlr4^{-/-}$ mice as recipients for the remaining BMC experiments in this study. LPS injections into $MyD88^{-/-}$ > $p65^{GFP\text{-}FL}$x$Tlr4^{-/-}$, $Ticam1^{-/-}$ > $p65^{GFP\text{-}FL}$x$Tlr4^{-/-}$and $MyD88^{-/-}$x$Ticam1^{-/-}$ > $p65^{GFP\text{-}FL}$x$Tlr4^{-/-}$ BMCs

revealed MyD88 as the main downstream signal transducer in LPS sensing immune cells. Ticam1 induced only scattered foci of epithelial NFκB activation in the absence of MyD88 (Figure 1C). Recent work has shown that MyD88 mediated signaling induces an early, reliable and transient NFκB response, whereas Ticam1 signaling is more sensitive to cell-to-cell variation and leads to a late, prolonged response in some cells (Cheng et al., 2015). This higher sensitivity of Ticam1 mediated signaling to stochastic effects might explain the observed variability in epithelial NFκB activation in *MyD88*$^{-/-}$ > p65$^{GFP\text{-}FL}$x*Tlr4*$^{-/-}$ BMCs. By contrast, dependency of LPS mediated NFκB activation on robust, but transient MyD88 signal transduction might contribute to restriction of signaling propagation (Cheng et al., 2015). Taken together, these data conclusively show that, in contrast to previous reports from tissue culture models, primary IECs in the intact murine gut do not directly respond to LPS via TLR4, but that NFκB signaling rather is induced by a secondary signal produced by radiosensitive immune cells upon LPS stimulation.

CD11C^{+} CELLS IN THE INTESTINAL MUCOSA MEDIATE LOCALLY RESTRICTED EPITHELIAL NFKB ACTIVATION VIA SECRETION OF TNF

Myeloid cells are involved in induction of tissue responses after exposure to microbial stimuli (Diebold, 2009; Kinnebrew et al., 2012; Muzaki et al., 2015). While previous reports suggest that also IECs directly sense and respond to LPS (Cario et al., 2000; Hornef et al., 2002, 2003), our data described above point towards an indirect activation of epithelial NFκB signaling via immune cells in the lamina propria *in vivo*. To further examine this secondary NFκB activation in IECs via TLR4-proficient immune cells, we reconstituted irradiated p65$^{GFP\text{-}FL}$x*Tlr4*$^{-/-}$ mice with a 1:10 mix of *ActRFP* (10%, *Tlr4*$^{+/+}$) and p65$^{GFP\text{-}FL}$x*Tlr4*$^{-/-}$ (90%) BM. We reasoned that this technique would allow us to observe signals emanating from individual RFP^{+} (*Tlr4*$^{+/+}$) lamina propria cells. Strikingly, LPS injection into these mixed BMCs resulted in epithelial NFκB activation only in the vicinity of RFP^{+}, TLR4-proficient cells (Figure 2A, Figure S4A). By contrast, mice reconstituted with 100% *ActRFP* BM showed NFκB activation across the entire epithelium (Figure S4B).

Interestingly, the activation zone around an RFP^{+} (*Tlr4*$^{+/+}$) lamina propria cell was rather small with a median diameter of ~50 µm (Figure 2A). This corresponds roughly to the diameter of a crypt and indicates that any signal driving epithelial NFκB activation must be locally restricted. Importantly, local accumulation of RFP^{+} cells resulted in a larger activation zone (Figure 2A; rightmost panel), pointing to a soluble signal. The shape of the RFP^{+} cells at the center of such activation zones suggested that these cells might be MPs. To test this hypothesis, we reconstituted p65$^{GFP\text{-}FL}$x*Tlr4*$^{-/-}$ mice with a 1:20 mix of *CD11c-DTR* (5%) and p65$^{GFP\text{-}FL}$x*Tlr4*$^{-/-}$ (95%) BM. LPS injection into those BMCs resulted in ~20% epithelial NFκB activation. Importantly, this activation was abolished by specific depletion of CD11c^{+} cells from the TLR4-proficient immune cell pool via Diphtheria toxin (DTX) pretreatment (Figure 2B).

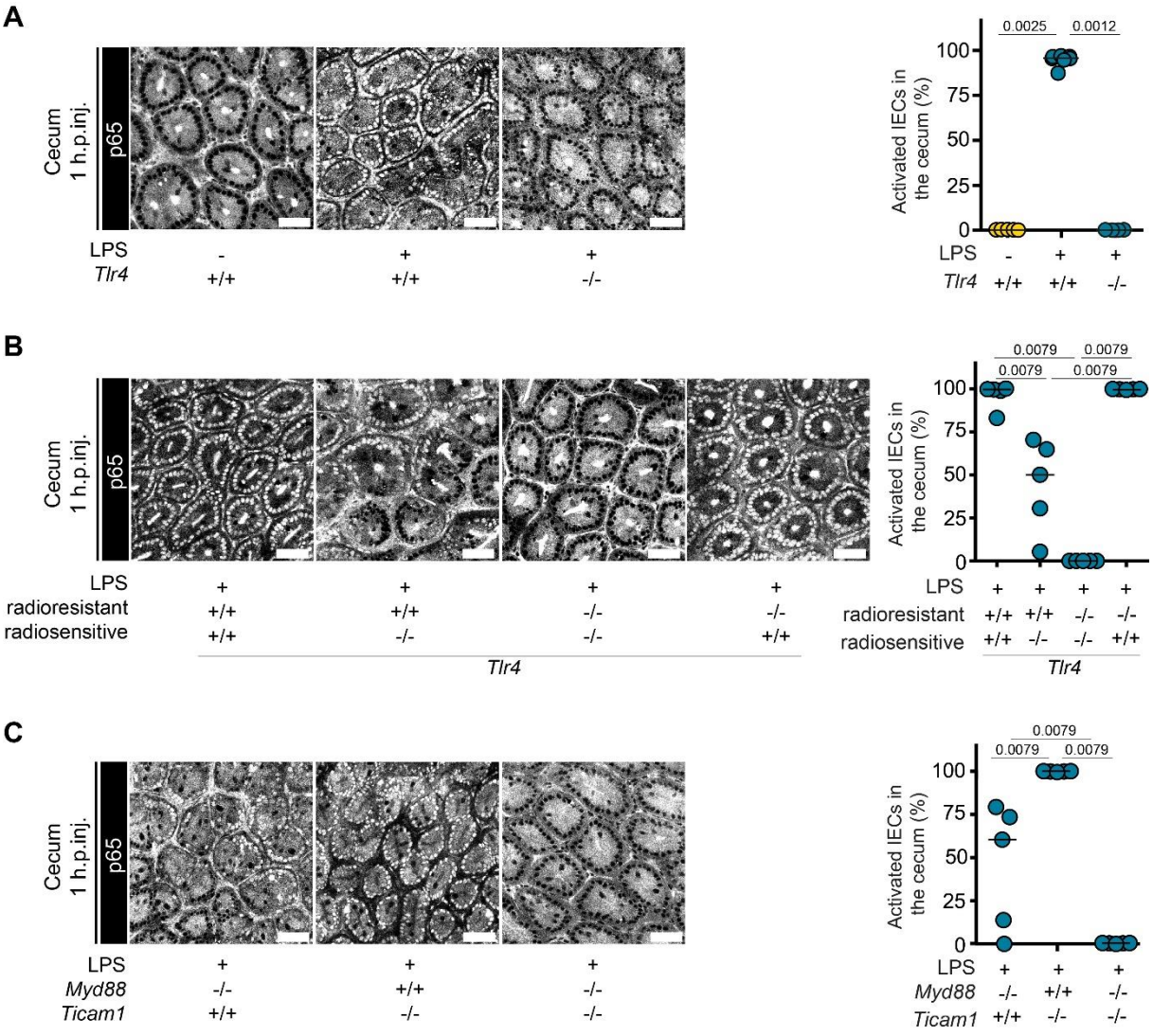

Figure 1 **Tlr4$^{+/+}$ *immune cells induce epithelial NFκB signaling in the cecal mucosa upon LPS exposure.*** *Mice were iv injected with S. Tm LPS. Cecal explants were imaged at 1 h.p.inj. by 2-photon microscopy. Representative images of the cecal mucosa and quantification of epithelial NFκB activation of* ***A*** *Tlr4$^{+/+}$ and Tlr4$^{-/-}$ mice,* ***B*** *p65^{GFP-FL} > p65^{GFP-FL}, p65^{GFP-FL}xTlr4$^{-/-}$ > p65^{GFP-FL}, p65^{GFP-FL}xTlr4$^{-/-}$ > p65^{GFP-FL}xTlr4$^{-/-}$, p65^{GFP-FL} > p65^{GFP-FL}xTlr4$^{-/-}$, and* ***C*** Myd88$^{-/-}$ > p65^{GFP-FL}xTlr4$^{-/-}$, Ticam1$^{-/-}$ > p65^{GFP-FL}xTlr4$^{-/-}$, MyD88$^{-/-}$xTicam1$^{-/-}$ > p65^{GFP-FL}xTlr4$^{-/-}$ *BMCs. Black line: Median. Statistical analysis: Mann-Whitney-U Test, p-values indicated. Each circle represents one mouse. Combined data of one (C), three (A) or four (B) independent experiments. Scale bars: 50 µm.*

To identify the signal released by the CD11c^{+} cells to induce epithelial NFκB activation, we next examined the impact of the NFκB activating cytokines IL1α, IL1β, IL18 and TNF (Collart et al., 1990; Hiscott et al., 1993; Kojima et al., 1999; Mori and Prager, 1996; Shakhov et al., 1990). To this end, we used BMCs generated by reconstituting irradiated p65^{GFP-FL}x*Tlr4$^{-/-}$* mice with BM from the respective knock-out mice. While mice reconstituted with *Il18$^{-/-}$*, *Il18r$^{-/-}$* and *Il1ab$^{-/-}$* BM still showed full epithelial NFκB activation after LPS injection (Figure S4C), reconstitution with *TNFa$^{-/-}$* BM abolished epithelial NFκB activation in LPS-injected mice (Figure 2C). The TNF requirement for epithelial NFκB activation upon LPS injection was confirmed in p65^{GFP-FL} mice pretreated with TNF-neutralizing antibodies, which phenocopied the *TNFa$^{-/-}$* > p65^{GFP-FL} BMCs (Figure 2C). This indicated that TNF induces epithelial NFκB signaling, which was further supported by time course data. While epithelial NFκB activation after LPS injection took ~1h, we observed full-blown epithelial activation as early as 15 min in TNF-injected mice (Figure 2D). TNF treatment of organoids confirmed that TNF was sufficient for swift NFκB activation

within 15 min (Figure S4D, 50 ng/ml TNF). Furthermore, TNF injection into the DTX-pretreated BMCs described in Figure 2B induced complete epithelial NFκB activation (Figure S4E).

Finally, we sought to establish if the TNF was produced directly by the LPS-sensing CD11c^{+} cells, or alternatively involved secondary TNF production by some other cell type. For this purpose, we generated BMCs by reconstituting irradiated p65^{GFP-FL}x*Tlr4*$^{-/-}$ mice with a 1:20 mix of *CD11c-DTR* (5%) and *TNFa*$^{-/-}$ (95%) BM. While LPS injection into those BMCs resulted in ~5% epithelial NFκB activation, the depletion of CD11c^{+} cells from the pool of TNF-proficient cells (by DTX-pretreatment) completely abrogated epithelial NFκB activation (Figure 2E). This established CD11c^{+} cells in the lamina propria as the TNF producing subset fueling epithelial NFκB activation after LPS injection. Taken together, CD11c^{+} cell-derived TNF is both required and sufficient to drive NFκB activation in the intestinal epithelium upon LPS exposure. This hints to a CD11c^{+} cell type as the missing link between the sentinel function of the gut associated immune system and the epithelium.

LPS EXPOSURE INDUCES A RAPID RESPONSE IN LAMINA PROPRIA CELLS, FOLLOWED BY SECONDARY EPITHELIAL NFKB ACTIVATION

To confirm the link to LPS-sensing lamina propria cells and establish their localization within the mucosa, we performed a novel large-volume multi-color high-resolution fluorescence microscopy technique (Coutu et al., 2018; Kunz and Schroeder, 2019) on fixed sections of naïve and LPS-injected p65^{GFP-FL} mice. In line with the observations from 2-photon microscopy, we did not detect NFκB activation in the bulk of IECs in naïve mice (Figure 3A). Solely IECs close to the top of crypts displayed a low degree of NFκB activation. At 40 min.p.inj. of LPS, NFκB activation was detectable in MHCII^{+} cells, which stretched out and filled the lamina propria between crypts. The CD11c^{+} TNF-producing lamina propria cells identified above likely belong to this cell population. By contrast, epithelial NFκB signaling was still largely inactive (Figure 3B). At 1 h.p.inj., we observed full blown epithelial NFκB activation, in line with the explant experiments above (compare Figure 3C with Figure 1A, 2D). Interestingly, our high-resolution imaging approach revealed that dome-epithelium, which shields lymphoid follicles from the intestinal lumen, specifically lacked NFκB activation at 1 h.p.inj.. This phenotype pertained to the cecal patch (Figure S5A), as well as to smaller lymphoid follicles in the lamina propria (Figure S5B). In conclusion, these data support a temporally and physically spaced response to LPS, including early activation of CD11c^{+} MHCII^{+} lamina propria cells and subsequent epithelial NFκB activation. Notably, certain regionally differentiated IEC subpopulations displayed desynchronized NFκB signaling kinetics.

The shifted activation kinetics were confirmed using a flow cytometric approach. In detail, we employed Kappable mice, which express destabilized GFP under a synthetic NFκB promotor (see Methods section). Active NFκB signaling in these mice elicits GFP expression by the affected cells. We iv injected Kappable mice with LPS and performed flow cytometric analysis on the cecal mucosa (Figure S6A). As observed before, the CD45^{+} compartment reacted quickly to the LPS stimulus. In comparison, the CD45^{-} compartment (~96% Villin^{+} IECs, Figure S6B) started to produce GFP only 30-60 min later. Importantly, and in line with our microscopy observations, TNF injection evoked a faster NFκB response compared to LPS specifically in IECs (Figure S6A). Hence, the results from multiple experimental approaches all point to an indirect activation of epithelial NFκB signaling by immune cell-derived TNF upon LPS exposure.

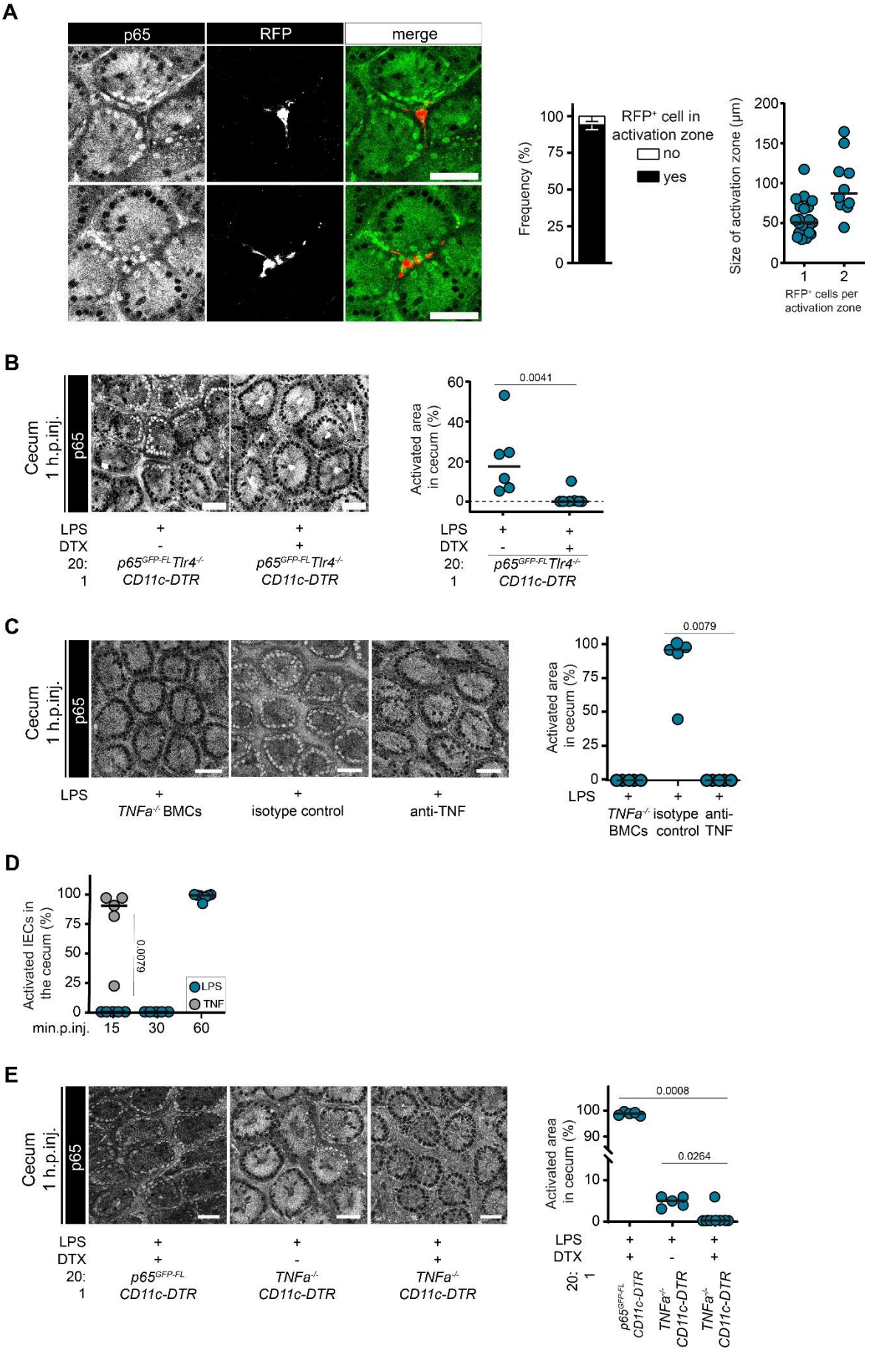
A
p65
RFP
merge
Frequency (%)
RFP+ cell in activation zone
no
yes
Size of activation zone (µm)
RFP+ cells per activation zone
B
Cecum 1 h.p.inj.
p65
Activated area in cecum (%)
0.0041
LPS
DTX
20:1
p65GFP-FLTlr4-/- CD11c-DTR
C
Cecum 1 h.p.inj.
p65
LPS
TNFa-/- BMCs
isotype control
anti-TNF
Activated area in cecum (%)
0.0079
D
Activated IECs in the cecum (%)
0.0079
LPS
TNF
min.p.inj.
15
30
60
E
Cecum 1 h.p.inj.
p65
LPS
DTX
20:1
p65GFP-FL CD11c-DTR
TNFa-/- CD11c-DTR
Activated area in cecum (%)
0.0008
0.0264

Figure 2 ***CD11c^{+} cells induce local epithelial NFκB activation via TNF.*** *Mice were iv injected with LPS and cecal explants were imaged at 1 h.p.inj. by 2-photon microscopy if not indicated differently.* ***A*** *Representative images of the cecal mucosa of p65^{GFP-FL}xTlr4$^{-/-}$ mice reconstituted with a 1:10 mix of* ActRFP *(10%, Tlr4$^{+/+}$) and p65^{GFP-FL}xTlr4$^{-/-}$ (90%) BM (left panel), quantification of the frequency of RFP^{+} cells within an epithelial NFκB activation zone (see Figure S4) (middle panel) and quantification of the size of epithelial NFκB activation zones (right panel).* ***B-E*** *Representative images of the cecal epithelium and quantification of epithelial NFκB activation of* ***B*** *p65^{GFP-FL}xTlr4$^{-/-}$ mice reconstituted with a 1:20 mix of CD11c-DTR and p65^{GFP-FL}xTlr4$^{-/-}$ BM and pretreated with DTX,* ***C*** TNFa$^{-/-}$ *> p65^{GFP-FL}xTlr4$^{-/-}$ BMCs or p65^{GFP-FL} mice pretreated with isotype control/anti-TNF antibody,* ***D*** *p65^{GFP-FL} mice iv injected with LPS or TNF and analyzed at the indicated time points, and* ***E*** *p65^{GFP-FL}xTlr4$^{-/-}$ mice reconstituted with a 1:20 mix of CD11c-DTR and* TNFa$^{-/-}$ *BM, pretreated with DTX. Black line: Median. Statistical analysis: Mann-Whitney-U Test, p-values indicated. Each circle represents one mouse. Combined data of two (A, B), three (C, D) or four (E) independent experiments. Scale bars: 50 µm.*

A likely explanation for the lack of a direct epithelial response to LPS is the lack of expression of the LPS receptor TLR4. To test for TLR4 expression, we applied our high-resolution microscopy approach to the cecal mucosa and stained for TLR4. In line with our hypothesis, TLR4 was highly expressed on lamina propria cells (Figure 3D). By contrast, much weaker TLR4 expression was detected in the epithelium (Figure 3D). In a previous study, we identified differential regulation of PRRs in an epithelial cell line compared to primary epithelial cells as a potential confounding factor for host-pathogen interaction studies (Chapter 5). Reevaluation of this transcriptome data set revealed a similar expression pattern for *Tlr4*. In contrast to other TLRs, this PRR was highly expressed in m-IC$_{C12}$ cells, an immortalized small intestinal epithelial cell line previously used as a model for murine IECs (Bens et al., 1996; Hornef et al., 2002). However, *Tlr4* expression was virtually undetectable in primary small intestinal epithelial organoids (Figure S6C). This discrepancy might explain some of the seemingly contradictory observations in previous studies (Cario et al., 2000; Hornef et al., 2002, 2003). In notable contrast to TLR4, we detected expression of TNFR1 in IECs *in vivo*, as described before (Feng and Teitelbaum, 2013; Hauwermeiren et al., 2015; Storey et al., 2002) (Figure S5C) and in line with our transcriptome data (*Tnfrsf1a*, Figure S6C). In summary, our data show an at maximum low-level, expression of TLR4 in murine IECs, and no functional implication of epithelial TLR4 with regard to NFκB-mediated signaling in our model.

TNF PRODUCTION UPON LPS EXPOSURE IN THE INTESTINAL MUCOSA IS A LOCAL RESPONSE DRIVEN BY CD11B^{+} CD103^{-} INTESTINAL MPS

Our data suggested that locally produced TNF within the intestinal mucosa is the key driver of epithelial NFκB activation. However, as LPS was iv injected, we could not formally exclude a role of TNF released at systemic sites. To test this, we measured TNF concentrations in spleen, serum and cecal tissue of LPS-injected mice. At 30 min.p.inj., splenic TNF levels increased ~50-fold, and reached a peak at 1 h.p.inj. of ~1 µg TNF/g spleen (Figure S7A). Serum TNF levels followed similar kinetics, increasing at 30 min.p.inj. and reaching a plateau at 1 h.p.inj of ~20 ng/ml. Overall TNF levels in the serum were markedly lower (~50-fold) compared to the spleen (Figure S7A). In contrast to this, the levels in the cecal mucosa appeared to rise slightly later (i.e. by 1 h.p.inj., ~ 20 ng/g tissue), peaking at ~100 ng/g tissue by 4 h.p.inj (Figure 4A). Equivalent mucosal TNF concentrations were achieved in TNF-injected controls (Figure 2D; Figure S7B). Taken together, the differences in the timing of TNF production and concentrations in the analyzed compartments suggest that TNF levels in the cecal mucosa are largely independent of spleen- (and serum-) derived TNF and that the mucosal TNF is therefore likely locally produced. Importantly, the kinetics of cecal TNF production correspond closely to the induction of epithelial NFκB activation (compare Figures 2, 3, S6).

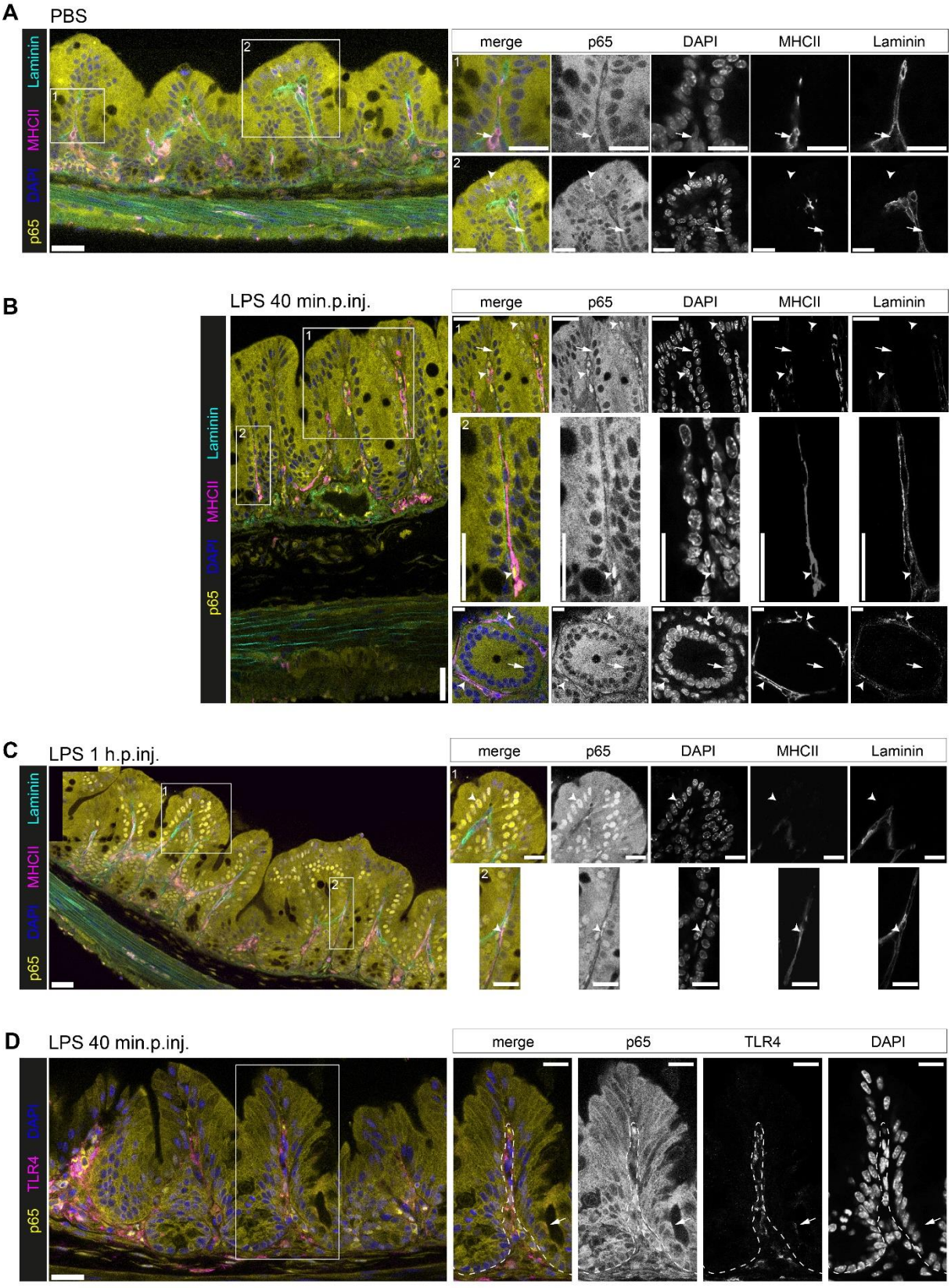

Figure 3 ***LPS exposure induces a rapid response in lamina propria cells, followed by secondary epithelial NFκB activation.*** *Confocal microscopy images of fixed ceca of $p65^{GFP-FL}$ mice iv injected with* ***A*** *PBS; or* ***B-D*** *LPS and analyzed at 40 min.p.inj. (B, D) or 1 h.p.inj. (C). Boxes in overview images indicate cut-outs. Arrow heads indicate $p65^{+}$ nuclei. Arrows indicate $p65^{-}$ nuclei (A-C), or epithelial TLR4/MD2 signal (D). Dashed line indicates epithelium/lamina propria border. Scale bars: 30 µm (overview images) or 10 µm (cut-outs). Representative images of mice from three independent experiments.*

We next aimed to further define the CD11c^{+} cell type which induces epithelial NFκB activation via TNF secretion (Figure 2E). To this end, we analyzed lamina propria immune cell populations by flow cytometry. Both CD11b^{+} CD103^{-} and CD11b^{-} CD103^{+} intestinal MP subsets activated NFκB signaling upon LPS injection into Kappable mice (Figure 4B, Figure S7C). Importantly, intracellular staining for TNF in LPS-injected wild type mice identified specifically the CD11b^{+} CD103^{-} MP subset as the local TNF producing cell population (Figure 4C). In line with the kinetics identified by microscopy and ELISA, the peak of TNF production occurred at ~40 min.p.inj., while the fraction of TNF producing CD11b^{+} CD103^{-} MPs declined by 3 h.p.inj. (Figure 4C). It should be noted that the CD11b^{-} CD103^{+} intestinal MP subset began producing TNF to a lesser extent at 3 h.p.inj.. This is likely attributable to secondary activation of this cell type and occurred much later than the observed epithelial NFκB activation. We therefore conclude that CD11b^{+} CD103^{-} intestinal MPs constitute a first local source of TNF upon LPS exposure, thereby inducing epithelial NFκB activation in their immediate vicinity. To assess the frequency of remaining recipient-derived MPs in BMCs, we analyzed MP subsets in the cecal mucosa after reconstitution. We observed ~9% recipient-derived CD11b^{+} CD103^{-} MPs at 6 weeks of reconstitution (Figure S6D). This remaining cell population is likely sufficient to explain the residual epithelial NFκB activation noted in Figure 1B.

To visualize MP-epithelium crosstalk in the mucosa, we applied high-resolution microscopy and the recently published 3D Tissue-wide Digital Imaging Pipeline for Quantitation of Secreted Molecules (Kunz and Schroeder, 2019) to mixed BMCs. Similar to in Figure 2A, we reconstituted irradiated p65$^{GFP\text{-}FL}$x*Tlr4*$^{-/-}$ mice with a 1:40 mix of *ActRFP* (2.5%, *Tlr4*$^{+/+}$) and p65$^{GFP\text{-}FL}$x*Tlr4*$^{-/-}$ (97.5%) BM and performed a proximity ligation assay (PLA) for TNF on fixed cecal tissue after LPS injection. This setup allowed us to use crypts without RFP^{+} cells in the lamina propria (i.e. in which epithelial NFκB activation was not triggered, Figure S7D, dashed line) as internal, *on-slide* controls. The analysis revealed a stronger expression of TNF specifically within and in immediate vicinity of MHCII^{+} lamina propria cells localized in crypts with epithelial NFκB activation (Figure 4D). In summary, our combined data demonstrate that CD11b^{+} CD103^{-} intestinal MPs secrete TNF to trigger locally restricted epithelial NFκB activation in the intestinal mucosa upon LPS exposure.

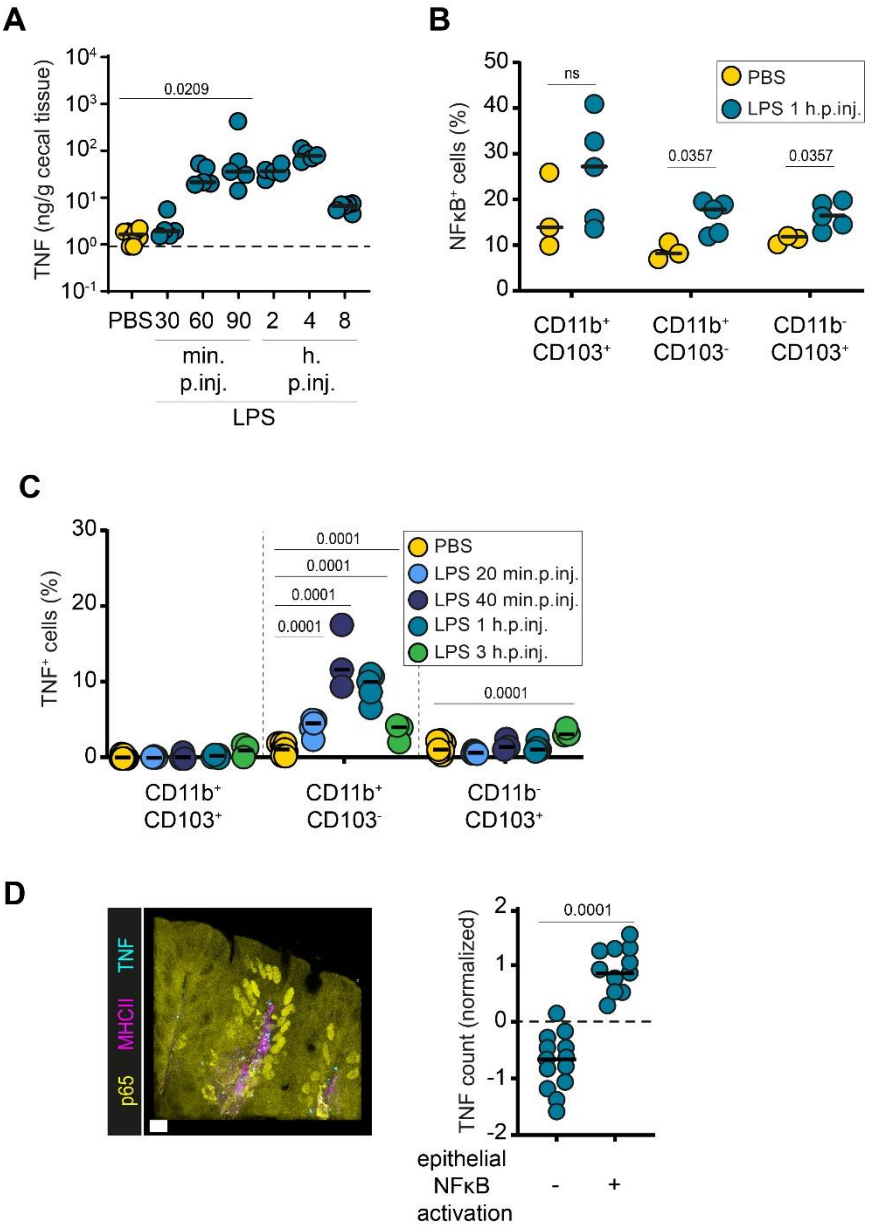

Figure 4 ***CD11b⁺ CD103⁻ intestinal MPs secrete TNF to induce local epithelial NFκB activation. A*** *ELISA measurements of TNF concentrations in the cecal mucosa of LPS-injected wild type mice. Dashed line: detection limit. y-axis in log_{10} scale. Flow cytometry analysis of cecal MPs from PBS- or LPS-injected* ***B*** *Kappable mice for assessment of NFκB activation (gating: Figure S7C) or* ***C*** *wild type mice for identification of TNF-producing MP subsets (gating as described in Figure S7C).* ***D*** *TNF-PLA analysis of ceca from p65^{GFP-FL}xTlr4$^{-/-}$ mice reconstituted with a 1:40 mix of* ActRFP *(2.5%,* Tlr4$^{+/+}$*) and p65^{GFP-FL}xTlr4$^{-/-}$ (97.5%) BM. Representative confocal microscopy image of fixed cecal tissue at 40 min.p.inj. (left panel) and quantification of PLA for TNF in crypts without (-) or with (+) epithelial NFκB activation (Figure S7D) at 1 h.p.inj.. Scale bar: 10 µm. Black line: Median. Statistical analysis: One-way ANOVA with Dunett`s correction (A, B), two-way ANOVA with Tukey`s correction (C) or Mann-Whitney-U Test (D), p-values indicated. Each circle represents one mouse (A-C), or one crypt (D; 5 mice analyzed). Combined data of one (D), three (B), six (A) or nine (C) independent experiments.*

TNF-MEDIATED NFKB ACTIVATION IN THE GUT EPITHELIUM OCCURS UPON BACTERIAL EXPOSURE

So far, we had used LPS injection as a model for bacterial exposure. To probe whether bacterial infection would trigger epithelial NFκB activation to a similar degree, we infected streptomycin-pretreated p65^{GFP-FL} mice with *S*. Tm. In this model, *S*. Tm invades the cecum epithelium and thereby elicits a pronounced, acute inflammatory response by ~8-12h post infection (h.p.inf.) (Barthel et al., 2003). We sacrificed the mice at 8-13.5 h.p.inf., and analyzed their ceca with 2-photon microscopy.

Epithelial NFκB activation was detectable in those mice. However, the degree of activation varied considerably between the animals, with no clear correlation to the time of infection (Figure 5A, S8A). We reasoned that this might be attributable to inter-individual differences in the disease kinetics, to which noise sensitive Ticam1 signaling might contribute (compare Figure 1C) (Cheng et al., 2015). To stratify the samples, we thus assigned them to stages of epithelial NFκB signaling from "no activation" (green), via "onset of activation" (blue) and "activation" (orange), to "inflammation" (red; tissue distortion evident) (Figure 5A, S8A). In a subgroup of samples, we did not detect $p65^{+}$ epithelial nuclei, but they clearly differed from the samples categorized as "no activation". This sample group ("unspecified", grey) most likely represents a state of active epithelial transcription (enlarged nuclei), and onset of inflammation in the tissue (space between crypts enlarged, a sign of edema). We have however not analyzed this in detail and therefore excluded this sample group from further analysis.

Interestingly, we observed areas with epithelial NFκB activation independently of the presence of intraepithelial *S*. Tm (Figure S9A-B), as well as *S*. Tm in tissue featuring epithelial NFκB activation (Figure S9C). This indicates that epithelial NFκB activation in this model is largely independent of single *S*. Tm invasion events into the epithelium and rather represents a crypt-scale response, i.e. in full agreement with the observations from LPS-injected mice.

NFκB target genes were upregulated in correlation to the NFκB activation status of the cecal tissue (Figure S8C, compare to S8B). This indicates that the scoring scheme based on epithelial NFκB activation describes the progression of the infection in an individual mouse more realistically than the actual time point post-infection. Calculating the ratio of samples with NFκB activation out of all analyzed samples, we found that at 8-13.5 h.p.inf., ~50% of the mice showed either onset or full blown epithelial NFκB signaling (Figure 5B, yellow). Importantly, the epithelial NFκB activation status significantly correlated with *Tnf* expression levels in the cecal tissue, hinting towards a role of TNF in this phenotype (Figure 5C).

To test whether specifically TNF induces epithelial NFκB signaling also during bacterial infection, we generated BMCs by reconstituting $p65^{GFP\text{-}FL\ L}$x*Tlr4*$^{-/-}$ mice with either *TNFa*$^{+/-}$ or *TNFa*$^{-/-}$ BM. In *TNFa*$^{+/-}$ > $p65^{GFP\text{-}FL\ L}$x*Tlr4*$^{-/-}$ BMCs analyzed at 8-13 h.p.inf., a similar fraction of samples featured epithelial NFκB signaling as in our previous experiment (Figure 5D, compare Figure 5B). By contrast, *TNFa*$^{-/-}$ > $p65^{GFP\text{-}FL\ L}$x*Tlr4*$^{-/-}$ BMCs featured significantly fewer animals with active epithelial NFκB signaling (Figure 5D). Taken together, these data show that also during early *S*. Tm infection, epithelial NFκB activation is induced via TNF production in radiosensitive immune cells.

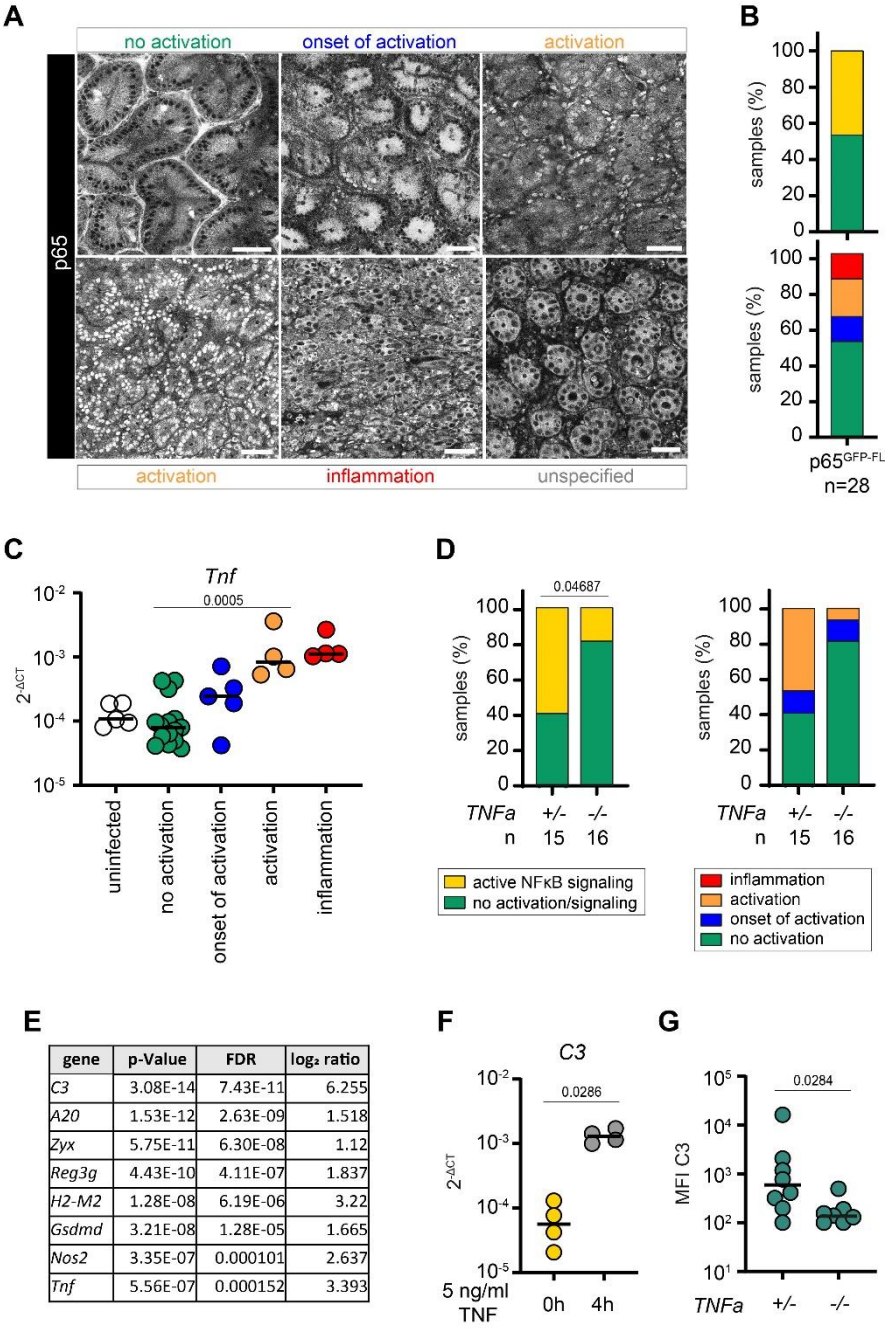

gene	p-Value	FDR	log₂ ratio
C3	3.08E-14	7.43E-11	6.255
A20	1.53E-12	2.63E-09	1.518
Zyx	5.75E-11	6.30E-08	1.12
Reg3g	4.43E-10	4.11E-07	1.837
H2-M2	1.28E-08	6.19E-06	3.22
Gsdmd	3.21E-08	1.28E-05	1.665
Nos2	3.35E-07	0.000101	2.637
Tnf	5.56E-07	0.000152	3.393

Figure 5 ***TNF-mediated epithelial NFκB activation occurs upon bacterial infection and induces an antibacterial response. A*** *Representative 2-photon microscopy images of cecal explants of streptomycin-pretreated p65^{GFP-FL} mice infected with S. Tm for 8-13.5h. Categories for scoring of epithelial NFκB activation status: "no activation" (green); "onset of activation" (blue); "activation" (orange); "inflammation" (red; tissue distortion evident); "unspecified", (grey; was excluded from further analysis). Scale bars: 50 µm.* ***B*** *Distribution of the analyzed 28 samples of A among the four epithelial NFκB activation categories (lower panel). For simplification, the blue, orange and red categories were also summarized as "NFκB signaling" (yellow, upper panel).* ***C*** Tnf *transcript levels in the cecal mucosa of mice described in A and naive p65^{GFP-FL} mice, grouped according to the epithelial NFκB activation status of the respective mice and depicted as $2^{-\Delta CT}$. Expression levels were normalized to* Actb. ***D*** TNFa$^{+/-}$ *or* TNFa$^{-/-}$ *> p65^{GFP-FL}x*Tlr4$^{-/-}$ *BMCs were analyzed as described in A and B.* ***E*** *Log$_2$ ratios of selected genes in a transcriptome analysis of TNF-treated (8h, 5 ng/ml) compared to untreated small intestinal epithelial organoids (Chapter 5). FDR = false discovery rate.* ***F*** C3 *transcript levels in untreated and TNF-treated (5 ng/ml, 4h) small intestinal organoids depicted as $2^{-\Delta CT}$. Expression levels were normalized to* Actb. ***G*** *Streptomycin-pretreated* TNFa$^{-/-}$ *mice and heterozygous littermates were orally infected with S. Tm for 36h. S. Tm in the cecal lumen (gated on O5$^+$ O12$^+$ cells) were stained for surface C3 to assess coating of luminal bacteria by flow cytometry (C3$^+$ population). MFI = median fluorescence intensity. y-axis in log$_{10}$ scale (C, F, G). Statistical analysis: Mann-Whitney-U Test (C, F, G) or Chi-square Test (D), p-values indicated. Each circle represents one mouse (C, G) or one experiment (average) (F). Combined data of three (G), four (F), five (A) or six (D) independent experiments.*

PATHOGEN-ELICITED TNF INDUCES A MULTIFACETED EPITHELIAL RESPONSE

To analyze the effect of TNF induced NFκB signaling on epithelial defense functions, we employed data from organoid culture and *in vivo* experiments. First, we reanalyzed a previously published transcriptome data set of TNF treated intestinal organoids (Chapter 5). In the organoids, TNF exposure led to upregulation of well characterized NFκB target genes, some of which are involved in host defense (Figure 5E; Chapter 5 (Leppkes et al., 2014)). A separate organoid experiment confirmed NFκB-dependent upregulation of the analyzed target genes upon TNF exposure (Figure S10A).

Next, we assessed the induction of antibacterial responses in our *in vivo* model, specifically focusing on the chemokine CXCL1 (Blackwell et al., 2012; Chintakuntlawar and Chodosh, 2009) and the IL22-Reg3γ axis (Kinnebrew et al., 2012; Miki et al., 2017). LPS injection triggered production of CXCL1 (Figure S11A), *Il22* (Figure S11D) and *Reg3g* (Figure S11E) in the cecal mucosa. The comparison between *TNFa*$^{-/-}$ and *TNFa*$^{+/-}$ mice revealed a partially TNF-dependent signature. TNF treatment elicited CXCL1 production in the cecal mucosa (Figure S11A) and in organoids (Figure S11B), alike. Moreover, mucosal *Cxcl1* and *Reg3g* expression levels correlated with the epithelial NFκB activation status of *S*. Tm-infected mice as described in Figure 5A (Figure S11C, F). All factors analyzed here were still produced, albeit at lower levels, in *TNFa*$^{-/-}$ mice, hinting towards parallel processes that induce the expression of key cytokines and antibacterial effector proteins. Specifically MP-epithelium crosstalk seems redundantly wired, as e.g. induction of epithelial Reg3γ production is also mediated via CD11b^{-} CD103^{+} DC (Kinnebrew et al., 2012).

Interestingly, the complement component *C3* was strongly induced in TNF-treated organoids (~40-50-fold upregulation; Figure 5E, 5F), in an NFκB-dependent manner (Figure S10B). C3 production by IECs is supported by previous reports (Matsumoto et al., 2017; Sina et al., 2018; Sünderhauf et al., 2017). To probe this C3 induction at the protein level, we analyzed C3 concentrations in the cecum at different time points post LPS injection. C3 levels increased to around 100 ng/g tissue at 4-8 h.p.inj. (Figure S10C). Upon TNF injection, similar levels were detected as early as 1 h.p.inj.. This is in line with our results above and indicates that TNF shortcuts the LPS-mediated induction of C3 via direct stimulation of IECs. C3 was also detectable in the cecal content, though at lower levels of around 10 ng/g content by 4 h.p.inj. (Figure S10D). Again, this response was promptly triggered by injection of TNF (Figure S10D).

To test how the absence of TNF would affect C3 production during *S*. Tm infection, we infected *TNFa*$^{-/-}$ mice and heterozygous littermate controls with *S*. Tm. At 36 h.p.inf., we stained the gut luminal *S*. Tm for C3 surface-coating and measured the levels by flow cytometry. Strikingly, C3-coating of gut luminal *S*. Tm was significantly reduced in *TNFa*$^{-/-}$ mice (Figure 5G), although still detectable. This indicates that TNF is important, but not absolutely required, for eliciting C3 production in the mucosa.

Taken together, TNF promotes epithelial NFκB signaling not only upon LPS injection, but also during oral *S*. Tm infection. Importantly, the extent of epithelial NFκB activation in the mucosa correlates with the induction of several prominent antibacterial defense mechanisms. An array of those IEC-produced factors (here exemplified by C3, CXCL1 and the IL22-Reg3γ axis) is induced by TNF, but appears to not solely depend on this cytokine. This highlights how a redundantly wired network drives antibacterial responses in the gut, and partially explains why it has been challenging to pinpoint the contribution of individual genes and cells in the defense against bacterial infection (Abeler-Dörner et al., 2020). Despite these challenges, we have here identified a linear multi-component circuit, whereby TLR4-MyD88(/Ticam1) in CD11b^{+} CD103^{-} intestinal sentinel MPs senses bacterial LPS, resulting in release of TNF that drives local epithelial NFκB signaling.

DISCUSSION

TLR4 is well established as the receptor for non-cytosolic LPS (Poltorak et al., 1998). TLR4 on myeloid cells induces pro-inflammatory responses upon LPS binding (Beutler and Rietschel, 2003; Medzhitov and Janeway, 2000b; Shakhov et al., 1990). Previous work, largely based on the epithelial cell line m-IC_{c12}, indicated a role also for epithelial TLR4 in sensing LPS (Cario et al., 2000; Hornef et al., 2002, 2003). A recent study using fluorescent reporter mouse lines described TLR4 expression in the colon and, at low levels, in the small intestine (Price et al., 2018). Technical obstacles (Price et al., 2018) (Chapter 5), the complex regulation of TLR4 reactivity (Chassin et al., 2010; Negishi et al., 2006; Zhang et al., 2006) and the dynamic expression of TLR4 during development and disease (Cario and Podolsky, 2000; Dheer et al., 2016; Lotz et al., 2006) however made it difficult to pinpoint a functional relevance of epithelial TLR4 in the intestine. Our analysis conclusively shows that, in contrast to earlier reports (Cario et al., 2000; Hornef et al., 2002, 2003), IECs do not directly sense LPS *in vivo*, at least when LPS is applied parenterally. This is partially in line with previous reports (Günther et al., 2015; Kayisoglu et al., 2020; Price et al., 2018). Instead, $TLR4^+$ immune cells sense LPS and trigger secondary epithelial NFκB activation. Although previous studies described regional differences in epithelial TLR4 expression (Price et al., 2018; Wang et al., 2010), we found consistent dependence of epithelial NFκB activation on immune cell TLR4 in small intestine, cecum and colon upon LPS exposure. Of note, this applies to unperturbed, adult mice with a relatively controlled microbiota. We cannot refute a role of epithelial TLR4 in settings of e.g. chronic inflammation, or during development (Cario and Podolsky, 2000; Lotz et al., 2006). Whether the non-responsiveness of IECs to LPS is due to a lack of TLR4 or co-receptor expression (Kayisoglu et al., 2020), or rather due to inhibition of epithelial TLR signaling remains to be fully resolved. We can however conclude that epithelial TLR4 has no functional relevance as an LPS sensor *in vivo* in the mature, unperturbed mouse gut.

Instead, we identified $CD11b^+$ $CD103^-$ intestinal MPs located in intercrypt regions to specifically elicit epithelial NFκB activation by secreting TNF upon LPS exposure. This activation is strikingly spatially restricted. The dependency of signal transduction on MyD88 might contribute to this restriction by limiting the duration of the MP NFκB response (Cheng et al., 2015). One intercrypt MP activates an epithelial zone of ~50 µm in the adjacent crypts. In line with their role as tissue sentinels, intercrypt MPs stretch out through the entire length of the lamina propria between crypts, located in close proximity to the epithelial basal lamina. Upon LPS exposure, these intercrypt MPs react swiftly within 40 min with NFκB activation and production of TNF, which in a next step elicits NFκB signaling in IECs. Interestingly, this local response circuit appears largely independent from systemically produced TNF, despite the high vascularization of the intestinal tissue. Likely, the swift clearance of serum TNF contributes to the apparent independence of TNF levels in different organs. This could represent a protective mechanism to preserve tissue homeostasis during inflammation at distant sites and prevent exacerbation of immune responses. In summary, the epithelium forms an LPS-non-responsive physical barrier that prevents bacterial invasion into the lamina propria. $CD11b^+$ $CD103^-$ intercrypt MPs, in turn, act as sentinels for invasion of gram-negative bacteria, and secrete TNF to induce a locally restricted antibacterial response in IECs upon LPS sensing. DC – epithelium crosstalk in the integration of microbial signals was reported previously for $CD11b^+$ $CD103^+$ (Kinnebrew et al., 2012) and $CD11b^-$ $CD103^+$ DC subsets (Muzaki et al., 2015), making it likely that the $CD11b^+$ $CD103^-$ sentinel MP subset belongs to the DC family. Based on the markers used for characterization here, we can however not fully exclude a macrophage identity of these cells. Further experimentation is therefore required to categorize the here-identified sentinel MP subset as a DC or macrophage subpopulation.

Notably, TNF-mediated induction of IEC NFκB activation also occurs during bacterial infection. In line with the observations from the LPS injection model, this activation appears independent of single IEC-intrinsic bacterial invasion events, but rather represents a crypt-scale response. TNF induced epithelial

NFκB activation triggers a highly parallelized antibacterial program in IECs. Importantly, TNF exposure triggers the expression of several central IEC cytokines and antibacterial effectors (CXCL1, Reg3γ, C3). Still, also TNF-independent means of inducing above-baseline levels of these proteins exist. This highlights the redundant wiring of tissue responses to pathogen threats to ensure proficient defense even in the absence of single effectors. This redundancy may in part explain the difficulty to pinpoint individual contributions of single genes and/or cell types to pathogen defense, and likely also in the context of IBD (Abeler-Dörner et al., 2020).

Taken together, we have identified $CD11b^{+}$ $CD103^{-}$ MPs as intercrypt sentinels in the lamina propria, which detect bacterial LPS via TLR4 and secrete TNF to induce a local epithelial NFκB-mediated antibacterial program. Notably, the spatially restricted nature of this communication ensures triggering of an antibacterial response only in close vicinity of the microbial insult. The signaling circuit identified here therefore represents a tunable defense mechanism to induce appropriate responses according to the localization and intensity of a microbial trigger. We suggest that this is a mechanism of preventing overshooting immune activation at tissue scale and thereby exacerbation of tissue inflammation. As the breakdown of appropriate responses to microbial stimuli is a hallmark of IBD, the signaling circuit presented here might help to decipher the derailment of intestinal immune responses during chronic intestinal inflammation.

ACKNOWLEDGEMENTS

I am grateful to the members of the Hardt lab, especially Ersin Gül, for helpful scientific discussions and technical support. The RCHCI staff (especially Katharina Holzinger, Dennis Mollenhauer & Dominik Bacovcin) for excellent support of our animal work is acknowledged. I thank ScopeM, especially Justine Kusch, for technical support. I am grateful to Otto Holst for providing ultrapure LPS and input on the manuscript. The authors have no conflicting financial interests. TS acknowledges funding be the Swiss National Science Foundation (SNF 179490). Work in MPs laboratory has been supported by the European Research Council (ERC grant agreement number 323040). MES has been supported by the Swedish Research Council (2012-262, 2015-00635, 2018-02223) and the Swedish Foundation for Strategic Research (ICA16-0031), and WDH by the Swiss National Science Foundation (310030_53074, 310030B_173338/1, 310030_192567, NCCR Microbiomes).

METHODS

Mouse experiments

All animal experiments were performed in accordance to legal and ethical regulations. Experiments were approved by Kantonales Veterinäramt Zürich (licenses 222/2013, 193/2016 and 158/2019). The mice were housed in individually ventilated cages under specific pathogen-free conditions at ETH Phenomics Center (EPIC) or Rodent Center HCI (RCHCI) at ETH Zürich. All transgenic animals presented here have C57BL/6 background. With exception for the BMCs, mice were 8-12 weeks old at the time of experimentation. Cohoused heterozygous littermates were used as controls where applicable. The following mouse lines were used: C57BL/6J (wild type; *Ly5.2*), *Ly5.1* (B6.SJL-*Ptprc*^{a} *Pepc*^{b}/BoyJ (Charbonneau et al., 1988)), $p65^{GFP\text{-}FL}$ (De Lorenzi et al., 2009), $p65^{GFP\text{-}FL}$x*Tlr4*$^{-/-}$ (this study, generated by crossing $p65^{GFP\text{-}FL}$ mice with B6.129-*Tlr4*$^{tm1Aki/Aki}$ mice (Hoshino et al., 1999)), *ActRFP* (B6.Cg-Tg(CAG-DsRed*MST)1Nagy/J (Vintersten et al., 2004)), *VillinRFP* (Müller et al., 2012), Kappable (Tortola, Kopf et al., unpublished, manuscript in preparation), *Il1ab*$^{-/-}$ (B6.D-*Il1a*^{tm1Yiw}/*Il1b*^{tm1Yiw} (Horai et al., 1998)), *TNFa*$^{-/-}$ (B6.129-*Tnf*^{tm1Ljo} (Marino et al., 1997)), *MyD88*$^{-/-}$x*Ticam1*$^{-/-}$ (this study, generated by crossing B6.129-*Myd88*^{tm1Aki} (Adachi et al., 1998) with B6.B6-*Ticam1*^{LPS2}/J (Hoebe et al., 2003) mice), $NFκB^{ΔIEC}$

(Vlantis et al., 2016), *CD11c-DTR* (B6.FVB-*1700016L21Rik*$^{Tg(Itgax\text{-}DTR/EGFP)57Lan}$/J (Jung et al., 2002). For LPS/TNF treatment, mice were iv injected with 5 µg ultrapure *S*. Tm LPS (kind gift of Otto Holst, Borstel, Germany) or 3 µg TNF (Preprotech) in 100 µl PBS and euthanized at the indicated time points post injection. For DTX treatment, mice were intraperitoneally (ip) injected with 120 ng DTX (Sigma Aldrich) at 24h prior to LPS injection. For anti-TNF treatment, mice were ip injected with 200 µg anti-TNF antibody (InVivoMAb, BE0058) or the respective isotype control (InVivoMAb, BE0088) in 100 µl PBS 24h prior to LPS injection. For *S*. Tm infection, mice were pretreated with 25 mg streptomycin by intragastrical gavage 24h prior to infection as described previously (Barthel et al., 2003). *S*. Tm SB300 (Hoiseth and Stocker, 1981) (carrying no plasmid or pZ400 (SPI2^{mCherry})) was grown for 12h at 37°C shaking in LB/0.3M NaCl supplemented with 50 µg/ml streptomycin, diluted 1:20 and sub-cultured for 4h prior to infection. Mice were infected with $5x10^7$ bacteria by gavage and euthanized at the indicated time points.

Generation of BMCs

For BMC experiments, recipient mice were irradiated (950 rad) at 6-12 weeks of age. Donor BM was isolated, washed in 20 ml ice-cold PBS (BioConcept) and resuspended at a concentration of 10^7 cells/ml. Recipients were iv injected with $5x10^6$ donor BM cells. For mixed BMCs, donor cells were counted after isolation and mixed in the respective ratios prior to injection. Mice were given Borgal (Veterinaria AG) in the drinking water for 3 weeks, and used for experiments after 6-20 weeks of reconstitution.

Organoid culture and treatment

Small intestinal epithelial organoids were established, cultured, TNF-treated and sampled as described previously (Chapter 5). The following organoid cultures were used: wild type – Z908, Z911, AG120; NFκB$^{\Delta IEC}$ – AE118; p65$^{GFP\text{-}FL}$ – W35.

Two-photon microscopy

For explant microscopy, mice were iv injected with LPS or TNF, or infected with *S*. Tm as described above. At indicated time points, mice were euthanized, the cecum was excised, cut open longitudinally and the cecal content was carefully removed. The cecal mucosa was mounted onto a slide (Thermo Fisher Scientific), submerged in DMEM F12 medium (Life Technologies) and subsequently imaged. For organoid imaging, organoids were seeded in 10 µl Matrigel domes into 8-well chambers on a microscopy slide (Thermo Fisher Scientific). Imaging was performed on a Leica SP8 DMI 6000B microscope equipped with an HC PL IRAPO CORR 40x/1.10 water immersion objective, using filters for GFP (525/50) and RFP (585/40) and Leica HyD SP GaAsP detectors, located at ScopeM, ETH Zürich. Excitation was performed with a Mai Tai XF Laser (Spectra-Physics) tuned to 920 nm, and an InSight DeepSee Laser (Spectra-Physics) tuned to 1110 nm. Image acquisition and data extraction was performed with the Leica application suite 3. Image analysis was performed with Fiji 1.51n.

Confocal microscopy

For fluorescence microscopy images shown in Figure S9, cecal tissue that was previously imaged by 2-photon microscopy was fixed (4% PFA, 4h at 4°C), dehydrated (PBS/20% sucrose, 4h at 4°C),

embedded in optimum cutting temperature medium (Tissue-Tek) and snap-frozen in liquid nitrogen. Samples were stored at -80°C until further analysis. 5 µm thick Cryosections were cut with a Microtome, air-dried, rehydrated (PBS, 1 min), permeabilized (PBS/0.5% TritonX-100, 5 min) and blocked (PBS/10% Normal Goat Serum, 30 min). Samples were subsequently incubated for 40 min in 1:100 anti-GFP antibody (Novus Biologicals, NB600-308SS) in PBS/10% Normal Goat Serum. After washing with PBS, samples were incubated in 1:200 goat anti-rabbit-AF488 antibody (ab150077, abcam) and 1:1000 DAPI (Sigma Aldrich) in PBS/10% Normal Goat Serum for 40 min at room temperature, washed with PBS and mounted in ~15 µl Mowiol. Imaging was performed on a Zeiss Axiovert 200 m microscope with a spinning disc laser unit (Visitron), and two Evolve 512 EMCCD camers (Photometrics), using an 40x oil objective. Image analysis was performed using Fiji 1.51n.

For high resolution fluorescence microscopy, samples were fixed in 4% PFA for 4h at 4°C. Subsequently, the cecal content was flushed out manually, samples were washed in ice-cold PBS for 3 x 2 min and stored in PBS at 4°C until further processing. Staining was conducted using primary and secondary antibodies as described (Coutu et al., 2018). Briefly, cecum samples were embedded in low-gelling temperature agarose and cut into 150 µm thick cross-section using a vibratome. The tissue sections were permeabilized using TBS (plus 0.05% Tween and 1% Triton X) and blocked with 10% Donkey Serum. Subsequently, primary and secondary antibodies were applied overnight and for 3 hours respectively. Tissue sections were mounted in homemade mounting medium (80% Glycerol, 20% TBS containing 0.1 M N-Propyl Gallate, pH 8.5) in silicon molds, to avoid sample compression, on 1.5 coverslips. Image acquisition was carried out on a Leica SP8 microscope, using the Leica 63x Glycerol Objective with Leica Glycerol immersion medium. The following antibodies were used for the stainings:

Primary Antibodies:

MHC II:	Biolegend	110002
TLR4:	BioRad	MCA2154T
GFP	Novus Biologicals	NB600-308
CD31:	R&D Systems	AF3628
TNFR1:	R&D Systems	AF-425
TNF:	R&D Systems	AF-410
LamininAF647:	Novus Biologicals	NB300-144AF647

Secondary antibodies, dyes and visualization kits:

Donkey anti-rat Cy3	Jackson ImmunoResearch	712-165-153
Donkey anti-rabbit AF488	Thermo Fisher Scientific	A-21206
Donkey anti-goat AF488	Thermo Fisher Scientific	A-11055
Donkey anti-rat biotin	Jackson ImmunoResearch	712-065-153
Donkey anti-goat biotin	Jackson ImmunoResearch	705-065-147
Streptavidin 555	Thermo Fisher Scientific	S21381
Streptavidin 633	Thermo Fisher Scientific	S21375

Donkey anti-goat MINUS	Merck	DUO92006
Donkey anti-goat PLUS	Merck	DUO92003
PLA Detection Kit Far Red	Merck	DUO92013-100RXN
DAPI	Thermo Fisher Scientific	D1306

Proximity Ligation Assay

The Proximity Ligation Assay was carried out as described before (Kunz and Schroeder, 2019). Briefly, cecum samples were cut and permeabilized as described above. Primary antibodies were added overnight. Instead of fluorescently-labeled secondary antibodies, for TNF, PLA-secondary antibodies, recognizing the FC part of the goat-IgG of the anti-TNF antibody were added. Further fluorescently-labeled secondary antibodies were added for 3 hours. After overnight incubation of the PLA-secondary antibodies, the ligation and rolling circle amplification were carried out on the slide at 37°C. After the PLA, the tissue sections were mounted and imaged as described above.

For the quantification of the TNF PLA signal per crypt (epithelial NFκB activation vs. no activation), we segmented the $MCHII^+$ signal coarsely and separated it in distinct crypts based on the tissue morphology. We then counted the TNF signals within each *MHCII isosurface (corresponding to a single activated or non-activated crypt)*, yielding TNF counts per volume. To normalize for differences in staining efficiency between different slides, we performed z-transformation on the TNF counts per sample (slide).

ELISA measurements

For ELISA measurements in the cecal tissue and content, small pieces of tissue/content were snap frozen and kept at -80°C until further analysis. For organoid samples, two wells were pooled to obtain one sample. Serum was obtained by heart puncture and the use of serum separator tubes tubes (BD), and stored at -20°C. Cecal tissue and content were weighed before analysis, homogenized in 300 µl washing buffer of the respective ELISA kit and spun down for 5 min at 4°C. The supernatant was used directly or diluted for the ELISA, which was performed according to the manufacturer`s instructions (TNF-ELISA: Invitrogen, BMS607HS; C3-ELISA: Abcam, 157711; CXCL1: CBA assay for murine KC, BD Biosciences).

Lamina propria cell isolation and flow cytometric analysis

Lamina propria cell preparation and staining was performed as described previously (Chapter 4). For intracellular TNF staining, cell isolation and staining was performed in the presence of 5 µg/ml Brefeldin A (Biologend). After surface staining, cells were fixed and permeabilized in 100 µl PermMix solution (BD red blood cell lysis buffer, diluted 1:5 in ddH2O, 1:1000 Tween20) for 10 min at room temperature. After washing, the cells were incubated with anti-TNF antibody for 30 min at room temperature, washed in PermMix and resuspended in FACS buffer (1% heat-inactivated FCS, 5mM EDTA in PBS) for subsequent flow cytometric analysis. The following antibodies/reagents were used for the staining: CD45-PerCP (Biolegend, 30-F11, 1:100), MHCII-APC (Biolegend, M5/114.15.2, 1:400), CD103-PE (Biolegend, 2E7, 1:100), CD11b-BV605 (Biolegend, M1/70, 1:200), CD11c-PE/Cy7 (Biolegend, N418, 1:200), Sytox-blue (Invitrogen, 1:1000), fixable viability dye (Zombie NIR Fixable

Viability Kit, Biolegend, 1:1000), TNF-FITC (Biolegend, MP6-XT22, 1:100). Samples were measured on a LSRII (BD Biosciences) and data were analyzed with FlowJo V10 (TreeStar).

Bacterial flow cytometric analysis

For the assessment of C3 coating of *S*. Tm in the cecal lumen, cecal content was homogenized. The bacteria were fixed in 2% PFA/PBS for 20 min at room temperature, washed in PBS and incubated with rat anti-C3 (Abcam, 11H9, 1:200), rabbit anti-O5 (Difco, Antiserum, 1:200) and human anti-O12 (kind gift from Antonio Lanzavecchia, STA5, 1:500) antibody in 1% BSA/PBS for 30 min at room temperature. After washing with 1%BSA/PBS, bacteria were incubated in anti-rat-FITC (1:200), anti-rabbit-BV421 (1:200) and anti-human-Alexa647 (1:200) antibody in 1%BSA/PBS for 40 min at 4°C. Subsequently, bacteria were washed, resuspended in PBS and analyzed on a CytoflexS cytometer (Beckmann Coulter).

Gene expression analysis

Tissue RNA extraction (Chapter 4), organoid RNA extraction (Chapter 5) and qPCR analysis of the respective genes were performed as previously described (Chapter 4).

Transcriptome analysis

The transcriptome data set described previously (Chapter 5) was partially reanalyzed with R Studio (version 3.6.0).

Statistical analysis

Statistical analysis was performed with GraphPad Prism 8 or R Studio (version 3.6.0).

REFERENCES

Abeler-Dörner, L., Laing, A.G., Lorenc, A., Ushakov, D.S., Clare, S., Speak, A.O., Duque-Correa, M.A., White, J.K., Ramirez-Solis, R., Saran, N., et al. (2020). High-throughput phenotyping reveals expansive genetic and structural underpinnings of immune variation. Nat. Immunol. *21*, 86–100.

Adachi, O., Kawai, T., Takeda, K., Matsumoto, M., Tsutsui, H., Sakagami, M., Nakanishi, K., and Akira, S. (1998). Targeted disruption of the MyD88 gene results in loss of IL-1- and IL-18-mediated function. Immunity *9*, 143–150.

Akira, S., and Hoshino, K. (2003). Myeloid Differentiation Factor 88—Dependent and —Independent Pathways in Toll-Like Receptor Signaling. J Infect Dis *187*, S356-63.

Barthel, M., Hapfelmeier, S., Quintanilla-Martínez, L., Kremer, M., Rohde, M., Hogardt, M., Pfeffer, K., Rüssmann, H., and Hardt, W.-D. (2003). Pretreatment of Mice with Streptomycin Provides a Salmonella enterica Serovar Typhimurium Colitis Model That Allows Analysis of Both Pathogen and Host. Infect Immun *71*, 2839–2858.

Bens, M., Bogdanova, A., Cluzeaud, F., Miquerol, L., Kerneis, S., Kraehenbuhl, J.P., Kahn, A., Pringault, E., and Vandewalle, A. (1996). Transimmortalized mouse intestinal cells (m-ICc12) that maintain a crypt phenotype. Am. J. Physiol. *270*, C1666-1674.

Beutler, B., and Rietschel, E.Th. (2003). Innate immune sensing and its roots: the story of endotoxin. Nat Rev Immunol *3*, 169–176.

Birchenough, G.M.H., Nyström, E.E.L., Johansson, M.E.V., and Hansson, G.C. (2016). A sentinel goblet cell guards the colonic crypt by triggering Nlrp6-dependent Muc2 secretion. Science *352*, 1535–1542.

Blackwell, T.S., Holden, E.P., Blackwell, T.R., DeLarco, J.E., and Christman, J.W. (2012). Cytokine-induced neutrophil chemoattractant mediates neutrophilic alveolitis in rats: association with nuclear factor kappa B activation. American Journal of Respiratory Cell and Molecular Biology.

Bogunovic, M., Ginhoux, F., Wagers, A., Loubeau, M., Isola, L.M., Lubrano, L., Najfeld, V., Phelps, R.G., Grosskreutz, C., Scigliano, E., et al. (2006). Identification of a radio-resistant and cycling dermal dendritic cell population in mice and men. J. Exp. Med. *203*, 2627–2638.

Bogunovic, M., Ginhoux, F., Helft, J., Shang, L., Hashimoto, D., Greter, M., Liu, K., Jakubzick, C., Ingersoll, M.A., Leboeuf, M., et al. (2009). Origin of the Lamina Propria Dendritic Cell Network. Immunity *31*, 513–525.

Burke, S.J., Lu, D., Sparer, T.E., Masi, T., Goff, M.R., Karlstad, M.D., and Collier, J.J. (2014). NF-κB and STAT1 control CXCL1 and CXCL2 gene transcription. Am. J. Physiol. Endocrinol. Metab. *306*, E131-149.

Cario, E., and Podolsky, D.K. (2000). Differential alteration in intestinal epithelial cell expression of toll-like receptor 3 (TLR3) and TLR4 in inflammatory bowel disease. Infect. Immun. *68*, 7010–7017.

Cario, E., Rosenberg, I.M., Brandwein, S.L., Beck, P.L., Reinecker, H.C., and Podolsky, D.K. (2000). Lipopolysaccharide activates distinct signaling pathways in intestinal epithelial cell lines expressing Toll-like receptors. J. Immunol. *164*, 966–972.

Charbonneau, H., Tonks, N.K., Walsh, K.A., and Fischer, E.H. (1988). The leukocyte common antigen (CD45): a putative receptor-linked protein tyrosine phosphatase. Proc. Natl. Acad. Sci. U.S.A. *85*, 7182–7186.

Chassin, C., Kocur, M., Pott, J., Duerr, C.U., Gütle, D., Lotz, M., and Hornef, M.W. (2010). miR-146a mediates protective innate immune tolerance in the neonate intestine. Cell Host Microbe *8*, 358–368.

Chen, K., Geng, S., Yuan, R., Diao, N., Upchurch, Z., and Li, L. (2015). Super-low Dose Endotoxin Pre-conditioning Exacerbates Sepsis Mortality. EBioMedicine *2*, 324–333.

Cheng, Z., Taylor, B., Ourthiague, D.R., and Hoffmann, A. (2015). Distinct single-cell signaling characteristics are conferred by the MyD88 and TRIF pathways during TLR4 activation. Sci Signal *8*, ra69.

Chintakuntlawar, A.V., and Chodosh, J. (2009). Chemokine CXCL1/KC and its Receptor CXCR2 Are Responsible for Neutrophil Chemotaxis in Adenoviral Keratitis. J Interferon Cytokine Res *29*, 657–666.

Collart, M.A., Baeuerle, P., and Vassalli, P. (1990). Regulation of tumor necrosis factor alpha transcription in macrophages: involvement of four kappa B-like motifs and of constitutive and inducible forms of NF-kappa B. Mol. Cell. Biol. *10*, 1498–1506.

Coutu, D.L., Kokkaliaris, K.D., Kunz, L., and Schroeder, T. (2018). Multicolor quantitative confocal imaging cytometry. Nat. Methods *15*, 39–46.

Cunliffe, R.N., and Mahida, Y.R. (2004). Expression and regulation of antimicrobial peptides in the gastrointestinal tract. J. Leukoc. Biol. *75*, 49–58.

De Lorenzi, R., Gareus, R., Fengler, S., and Pasparakis, M. (2009). GFP-p65 knock-in mice as a tool to study NF-κB dynamics in vivo. Genesis *47*, 323–329.

Dheer, R., Santaolalla, R., Davies, J.M., Lang, J.K., Phillips, M.C., Pastorini, C., Vazquez-Pertejo, M.T., and Abreu, M.T. (2016). Intestinal Epithelial Toll-Like Receptor 4 Signaling Affects Epithelial Function and Colonic Microbiota and Promotes a Risk for Transmissible Colitis. Infect. Immun. *84*, 798–810.

Diebold, S.S. (2009). Activation of Dendritic Cells by Toll-Like Receptors and C-Type Lectins. In Dendritic Cells, G. Lombardi, and Y. Riffo-Vasquez, eds. (Berlin, Heidelberg: Springer), pp. 3–30.

Feng, Y., and Teitelbaum, D.H. (2013). Tumour necrosis factor--induced loss of intestinal barrier function requires TNFR1 and TNFR2 signalling in a mouse model of total parenteral nutrition. J. Physiol. (Lond.) *591*, 3709–3723.

Fitzgerald, K.A., and Kagan, J.C. (2020). Toll-like Receptors and the Control of Immunity. Cell *180*, 1044–1066.

Fitzgerald, K.A., Rowe, D.C., Barnes, B.J., Caffrey, D.R., Visintin, A., Latz, E., Monks, B., Pitha, P.M., and Golenbock, D.T. (2003). LPS-TLR4 signaling to IRF-3/7 and NF-kappaB involves the toll adapters TRAM and TRIF. J. Exp. Med. *198*, 1043–1055.

Fulde, M., Sommer, F., Chassaing, B., van Vorst, K., Dupont, A., Hensel, M., Basic, M., Klopfleisch, R., Rosenstiel, P., Bleich, A., et al. (2018). Neonatal selection by Toll-like receptor 5 influences long-term gut microbiota composition. Nature *560*, 489–493.

Guma, M., Stepniak, D., Shaked, H., Spehlmann, M.E., Shenouda, S., Cheroutre, H., Vicente-Suarez, I., Eckmann, L., Kagnoff, M.F., and Karin, M. (2011). Constitutive intestinal NF-κB does not trigger destructive inflammation unless accompanied by MAPK activation. J. Exp. Med. *208*, 1889–1900.

Günther, C., Buchen, B., He, G.-W., Hornef, M., Torow, N., Neumann, H., Wittkopf, N., Martini, E., Basic, M., Bleich, A., et al. (2015). Caspase-8 controls the gut response to microbial challenges by Tnf-α-dependent and independent pathways. Gut *64*, 601–610.

Hausmann, A., Russo, G., Grossmann, J., Zünd, M., Schwank, G., Aebersold, R., Liu, Y., Sellin, M.E., and Hardt, W.-D. (2020). Germ-free and microbiota-associated mice yield small intestinal epithelial organoids with equivalent and robust transcriptome/proteome expression phenotypes. Cell. Microbiol. e13191.

Hauwermeiren, F.V., Vandenbroucke, R.E., Grine, L., Lodens, S., Wonterghem, E.V., Rycke, R.D., Geest, N.D., Hassan, B., and Libert, C. (2015). TNFR1-induced lethal inflammation is mediated by goblet and Paneth cell dysfunction. Mucosal Immunol *8*, 828–840.

Hayashi, F., Smith, K.D., Ozinsky, A., Hawn, T.R., Yi, E.C., Goodlett, D.R., Eng, J.K., Akira, S., Underhill, D.M., and Aderem, A. (2001). The innate immune response to bacterial flagellin is mediated by Toll-like receptor 5. Nature *410*, 1099–1103.

Hayden, M.S., and Ghosh, S. (2008). Shared principles in NF-kappaB signaling. Cell *132*, 344–362.

Hayden, M.S., and Ghosh, S. (2014). Regulation of NF-κB by TNF family cytokines. Semin. Immunol. *26*, 253–266.

Hiscott, J., Marois, J., Garoufalis, J., D'Addario, M., Roulston, A., Kwan, I., Pepin, N., Lacoste, J., Nguyen, H., and Bensi, G. (1993). Characterization of a functional NF-kappa B site in the human interleukin 1 beta promoter: evidence for a positive autoregulatory loop. Mol. Cell. Biol. *13*, 6231–6240.

Hoebe, K., Du, X., Georgel, P., Janssen, E., Tabeta, K., Kim, S.O., Goode, J., Lin, P., Mann, N., Mudd, S., et al. (2003). Identification of Lps2 as a key transducer of MyD88-independent TIR signalling. Nature *424*, 743–748.

Hoiseth, S.K., and Stocker, B.A. (1981). Aromatic-dependent Salmonella typhimurium are non-virulent and effective as live vaccines. Nature *291*, 238–239.

Horai, R., Asano, M., Sudo, K., Kanuka, H., Suzuki, M., Nishihara, M., Takahashi, M., and Iwakura, Y. (1998). Production of mice deficient in genes for interleukin (IL)-1alpha, IL-1beta, IL-1alpha/beta, and IL-1 receptor antagonist shows that IL-1beta is crucial in turpentine-induced fever development and glucocorticoid secretion. J. Exp. Med. *187*, 1463–1475.

Hornef, M.W., Frisan, T., Vandewalle, A., Normark, S., and Richter-Dahlfors, A. (2002). Toll-like receptor 4 resides in the Golgi apparatus and colocalizes with internalized lipopolysaccharide in intestinal epithelial cells. J. Exp. Med. *195*, 559–570.

Hornef, M.W., Normark, B.H., Vandewalle, A., and Normark, S. (2003). Intracellular recognition of lipopolysaccharide by toll-like receptor 4 in intestinal epithelial cells. J. Exp. Med. *198*, 1225–1235.

Hoshino, K., Takeuchi, O., Kawai, T., Sanjo, H., Ogawa, T., Takeda, Y., Takeda, K., and Akira, S. (1999). Cutting edge: Toll-like receptor 4 (TLR4)-deficient mice are hyporesponsive to lipopolysaccharide evidence for TLR4 as the Lps gene product. Journal of Immunology *162*, 3749–3752.

Johansson, M.E.V., and Hansson, G.C. (2016). Immunological aspects of intestinal mucus and mucins. Nat. Rev. Immunol. *16*, 639–649.

Jung, S., Unutmaz, D., Wong, P., Sano, G.-I., De los Santos, K., Sparwasser, T., Wu, S., Vuthoori, S., Ko, K., Zavala, F., et al. (2002). In Vivo Depletion of CD11c+ Dendritic Cells Abrogates Priming of CD8+ T Cells by Exogenous Cell-Associated Antigens. Immunity *17*, 211–220.

Kayisoglu, O., Weiss, F., Niklas, C., Pierotti, I., Pompaiah, M., Wallaschek, N., Germer, C.-T., Wiegering, A., and Bartfeld, S. (2020). Location-specific cell identity rather than exposure to GI microbiota defines many innate immune signalling cascades in the gut epithelium. Gut gutjnl-2019-319919.

Kinnebrew, M.A., Buffie, C.G., Diehl, G.E., Zenewicz, L.A., Leiner, I., Hohl, T.M., Flavell, R.A., Littman, D.R., and Pamer, E.G. (2012). Interleukin 23 production by intestinal CD103(+)CD11b(+) dendritic cells in response to bacterial flagellin enhances mucosal innate immune defense. Immunity *36*, 276–287.

Knodler, L.A., Vallance, B.A., Celli, J., Winfree, S., Hansen, B., Montero, M., and Steele-Mortimer, O. (2010). Dissemination of invasive Salmonella via bacterial-induced extrusion of mucosal epithelia. Proc. Natl. Acad. Sci. U.S.A. *107*, 17733–17738.

Kojima, H., Aizawa, Y., Yanai, Y., Nagaoka, K., Takeuchi, M., Ohta, T., Ikegami, H., Ikeda, M., and Kurimoto, M. (1999). An essential role for NF-kappa B in IL-18-induced IFN-gamma expression in KG-1 cells. J. Immunol. *162*, 5063–5069.

Kreibich, S., Emmenlauer, M., Fredlund, J., Rämö, P., Münz, C., Dehio, C., Enninga, J., and Hardt, W.-D. (2015). Autophagy Proteins Promote Repair of Endosomal Membranes Damaged by the Salmonella Type Three Secretion System 1. Cell Host Microbe *18*, 527–537.

Kunz, L., and Schroeder, T. (2019). A 3D Tissue-wide Digital Imaging Pipeline for Quantitation of Secreted Molecules Shows Absence of CXCL12 Gradients in Bone Marrow. Cell Stem Cell *25*, 846-854.e4.

Leppkes, M., Roulis, M., Neurath, M.F., Kollias, G., and Becker, C. (2014). Pleiotropic functions of TNF-α in the regulation of the intestinal epithelial response to inflammation. Int Immunol *26*, 509–515.

Liu, T., Zhang, L., Joo, D., and Sun, S.-C. (2017). NF-κB signaling in inflammation. Sig Transduct Target Ther *2*, 1–9.

Lotz, M., Gütle, D., Walther, S., Ménard, S., Bogdan, C., and Hornef, M.W. (2006). Postnatal acquisition of endotoxin tolerance in intestinal epithelial cells. J. Exp. Med. *203*, 973–984.

Marino, M.W., Dunn, A., Grail, D., Inglese, M., Noguchi, Y., Richards, E., Jungbluth, A., Wada, H., Moore, M., Williamson, B., et al. (1997). Characterization of tumor necrosis factor-deficient mice. Proc. Natl. Acad. Sci. U.S.A. *94*, 8093–8098.

Matsumoto, N., Satyam, A., Geha, M., Lapchak, P.H., Dalle Lucca, J.J., Tsokos, M.G., and Tsokos, G.C. (2017). C3a Enhances the Formation of Intestinal Organoids through C3aR1. Front Immunol *8*, 1046.

Medzhitov, R., and Janeway, C. (2000a). The Toll receptor family and microbial recognition. Trends Microbiol. *8*, 452–456.

Medzhitov, R., and Janeway, CharleS.J. (2000b). Innate immune recognition: mechanisms and pathways. Immunol Rev *173*, 89–97.

Miki, T., Okada, N., and Hardt, W.-D. (2017). Inflammatory bactericidal lectin RegIIIβ: Friend or foe for the host? Gut Microbes 1–9.

Mori, N., and Prager, D. (1996). Transactivation of the interleukin-1alpha promoter by human T-cell leukemia virus type I and type II Tax proteins. Blood *87*, 3410–3417.

Müller, A.J., Kaiser, P., Dittmar, K.E.J., Weber, T.C., Haueter, S., Endt, K., Songhet, P., Zellweger, C., Kremer, M., Fehling, H.-J., et al. (2012). Salmonella gut invasion involves TTSS-2-dependent epithelial traversal, basolateral exit, and uptake by epithelium-sampling lamina propria phagocytes. Cell Host Microbe *11*, 19–32.

Muzaki, A.R.B.M., Tetlak, P., Sheng, J., Loh, S.C., Setiagani, Y.A., Poidinger, M., Zolezzi, F., Karjalainen, K., and Ruedl, C. (2015). Intestinal CD103+CD11b- dendritic cells restrain colitis via IFN-γ-induced anti-inflammatory response in epithelial cells. Mucosal Immunol.

Muzio, M., Ni, J., Feng, P., and Dixit, V.M. (1997). IRAK (Pelle) family member IRAK-2 and MyD88 as proximal mediators of IL-1 signaling. Science *278*, 1612–1615.

Negishi, H., Fujita, Y., Yanai, H., Sakaguchi, S., Ouyang, X., Shinohara, M., Takayanagi, H., Ohba, Y., Taniguchi, T., and Honda, K. (2006). Evidence for licensing of IFN-gamma-induced IFN regulatory factor 1 transcription factor by MyD88 in Toll-like receptor-dependent gene induction program. Proc. Natl. Acad. Sci. U.S.A. *103*, 15136–15141.

Nie, L., Cai, S.-Y., Shao, J.-Z., and Chen, J. (2018). Toll-Like Receptors, Associated Biological Roles, and Signaling Networks in Non-Mammals. Front Immunol *9*.

Poltorak, A., He, X., Smirnova, I., Liu, M.-Y., Huffel, C.V., Du, X., Birdwell, D., Alejos, E., Silva, M., Galanos, C., et al. (1998). Defective LPS Signaling in C3H/HeJ and C57BL/10ScCr Mice: Mutations in Tlr4 Gene. Science *282*, 2085–2088.

Price, A.E., Shamardani, K., Lugo, K.A., Deguine, J., Roberts, A.W., Lee, B.L., and Barton, G.M. (2018). A Map of Toll-like Receptor Expression in the Intestinal Epithelium Reveals Distinct Spatial, Cell Type-Specific, and Temporal Patterns. Immunity *49*, 560-575.e6.

Rauch, I., Deets, K.A., Ji, D.X., von Moltke, J., Tenthorey, J.L., Lee, A.Y., Philip, N.H., Ayres, J.S., Brodsky, I.E., Gronert, K., et al. (2017). NAIP-NLRC4 Inflammasomes Coordinate Intestinal Epithelial Cell Expulsion with Eicosanoid and IL-18 Release via Activation of Caspase-1 and -8. Immunity *46*, 649–659.

Rescigno, M., Urbano, M., Valzasina, B., Francolini, M., Rotta, G., Bonasio, R., Granucci, F., Kraehenbuhl, J.P., and Ricciardi-Castagnoli, P. (2001). Dendritic cells express tight junction proteins and penetrate gut epithelial monolayers to sample bacteria. Nat. Immunol. *2*, 361–367.

Rogler, G., Brand, K., Vogl, D., Page, S., Hofmeister, R., Andus, T., Knuechel, R., Baeuerle, P.A., Schölmerich, J., and Gross, V. (1998). Nuclear factor κB is activated in macrophages and epithelial cells of inflamed intestinal mucosa. Gastroenterology *115*, 357–369.

Scott, C.L., Bain, C.C., Wright, P.B., Sichien, D., Kotarsky, K., Persson, E.K., Luda, K., Guilliams, M., Lambrecht, B.N., Agace, W.W., et al. (2015). CCR2(+)CD103(-) intestinal dendritic cells develop from DC-committed precursors and induce interleukin-17 production by T cells. Mucosal Immunol *8*, 327–339.

Sellin, M.E., Müller, A.A., Felmy, B., Dolowschiak, T., Diard, M., Tardivel, A., Maslowski, K.M., and Hardt, W.-D. (2014). Epithelium-intrinsic NAIP/NLRC4 inflammasome drives infected enterocyte expulsion to restrict Salmonella replication in the intestinal mucosa. Cell Host Microbe *16*, 237–248.

Shakhov, A.N., Collart, M.A., Vassalli, P., Nedospasov, S.A., and Jongeneel, C.V. (1990). Kappa B-type enhancers are involved in lipopolysaccharide-mediated transcriptional activation of the tumor necrosis factor alpha gene in primary macrophages. J. Exp. Med. *171*, 35–47.

Shaw, T.N., Houston, S.A., Wemyss, K., Bridgeman, H.M., Barbera, T.A., Zangerle-Murray, T., Strangward, P., Ridley, A.J.L., Wang, P., Tamoutounour, S., et al. (2018). Tissue-resident macrophages in the intestine are long lived and defined by Tim-4 and CD4 expression. J. Exp. Med. *215*, 1507–1518.

Sina, C., Kemper, C., and Derer, S. (2018). The intestinal complement system in inflammatory bowel disease: Shaping intestinal barrier function. Semin. Immunol. *37*, 66–73.

Storey, H., Stewart, A., Vandenabeele, P., and Luzio, J.P. (2002). The p55 tumour necrosis factor receptor TNFR1 contains a trans-Golgi network localization signal in the C-terminal region of its cytoplasmic tail. Biochem. J. *366*, 15–22.

Sünderhauf, A., Skibbe, K., Preisker, S., Ebbert, K., Verschoor, A., Karsten, C.M., Kemper, C., Huber-Lang, M., Basic, M., Bleich, A., et al. (2017). Regulation of epithelial cell expressed C3 in the intestine - Relevance for the pathophysiology of inflammatory bowel disease? Mol. Immunol. *90*, 227–238.

Tateda, K., Matsumoto, T., Miyazaki, S., and Yamaguchi, K. (1996). Lipopolysaccharide-induced lethality and cytokine production in aged mice. Infect. Immun. *64*, 769–774.

Vereecke, L., Sze, M., Guire, C.M., Rogiers, B., Chu, Y., Schmidt-Supprian, M., Pasparakis, M., Beyaert, R., and van Loo, G. (2010). Enterocyte-specific A20 deficiency sensitizes to tumor necrosis factor–induced toxicity and experimental colitis. J Exp Med *207*, 1513–1523.

Vereecke, L., Vieira-Silva, S., Billiet, T., van Es, J.H., Mc Guire, C., Slowicka, K., Sze, M., van den Born, M., De Hertogh, G., Clevers, H., et al. (2014). A20 controls intestinal homeostasis through cell-specific activities. Nat Commun *5*, 5103.

Vintersten, K., Monetti, C., Gertsenstein, M., Zhang, P., Laszlo, L., Biechele, S., and Nagy, A. (2004). Mouse in red: red fluorescent protein expression in mouse ES cells, embryos, and adult animals. Genesis *40*, 241–246.

Vlantis, K., Wullaert, A., Sasaki, Y., Schmidt-Supprian, M., Rajewsky, K., Roskams, T., and Pasparakis, M. (2011). Constitutive IKK2 activation in intestinal epithelial cells induces intestinal tumors in mice. J. Clin. Invest. *121*, 2781–2793.

Vlantis, K., Wullaert, A., Polykratis, A., Kondylis, V., Dannappel, M., Schwarzer, R., Welz, P., Corona, T., Walczak, H., Weih, F., et al. (2016). NEMO Prevents RIP Kinase 1-Mediated Epithelial Cell Death and Chronic Intestinal Inflammation by NF-κB-Dependent and -Independent Functions. Immunity *44*, 553–567.

Wang, C., Deng, L., Hong, M., Akkaraju, G.R., Inoue, J., and Chen, Z.J. (2001). TAK1 is a ubiquitin-dependent kinase of MKK and IKK. Nature *412*, 346–351.

Wang, Y., Devkota, S., Musch, M.W., Jabri, B., Nagler, C., Antonopoulos, D.A., Chervonsky, A., and Chang, E.B. (2010). Regional Mucosa-Associated Microbiota Determine Physiological Expression of TLR2 and TLR4 in Murine Colon. PLoS ONE *5*, e13607.

Wullaert, A., Bonnet, M.C., and Pasparakis, M. (2011). NF-κB in the regulation of epithelial homeostasis and inflammation. Cell Res. *21*, 146–158.

Yang, J., and Yan, H. (2017). TLR5: beyond the recognition of flagellin. Cell. Mol. Immunol. *14*, 1017–1019.

Zhang, J., Stirling, B., Temmerman, S.T., Ma, C.A., Fuss, I.J., Derry, J.M.J., and Jain, A. (2006). Impaired regulation of NF-kappaB and increased susceptibility to colitis-associated tumorigenesis in CYLD-deficient mice. J. Clin. Invest. *116*, 3042–3049.

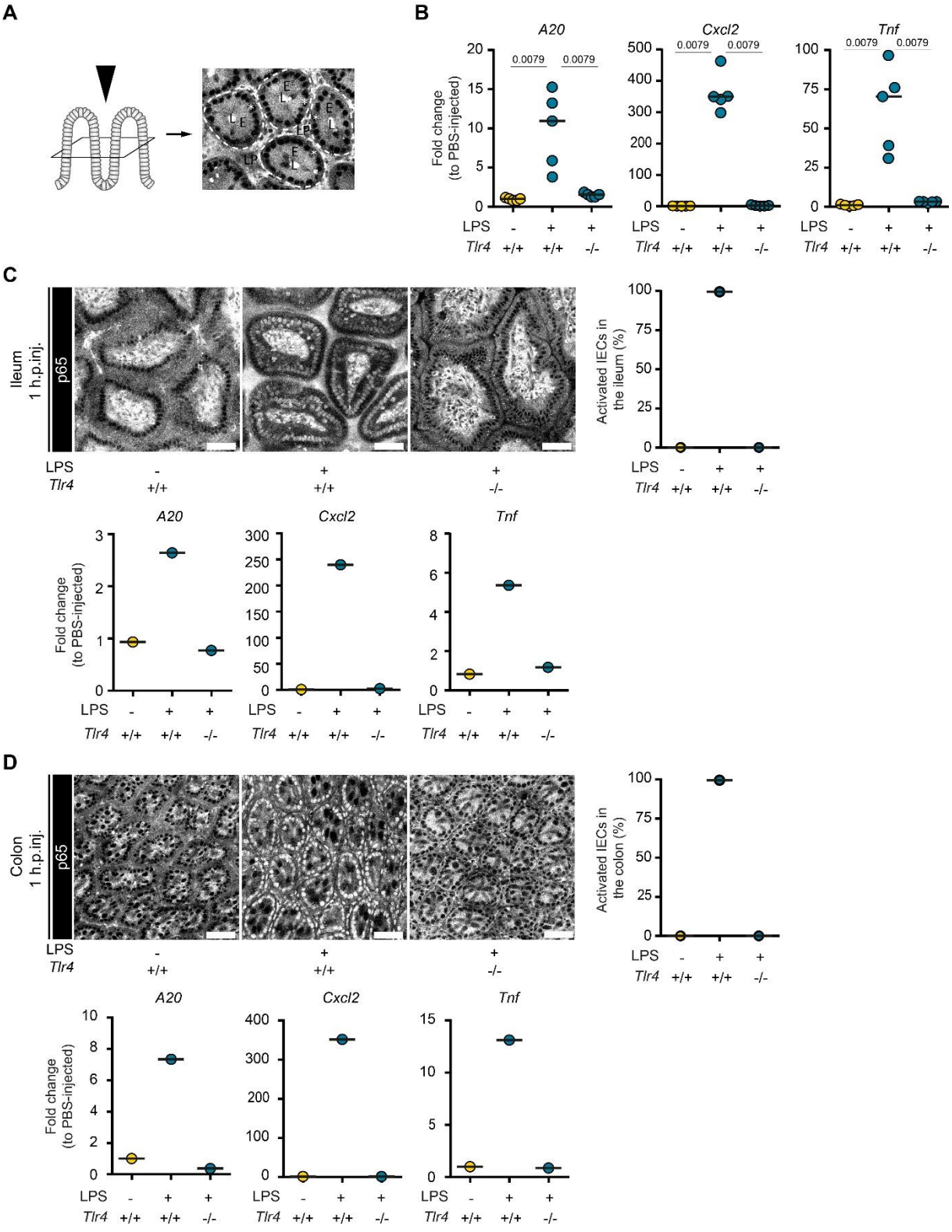

Figure S1 ***TLR4 mediates epithelial NFκB activation in the small intestine and colon. A*** *Schematic drawing of the 2-photon imaging (left panel). The intestinal mucosa is imaged from the luminal side (black arrow head), resulting in images of the horizontal plane of the mucosa (right panel). White dashed line/E: epithelium, L: lumen, LP: lamina propria, white asterisks: epithelial nuclei.* ***B*** *Fold changes in expression of* A20, Cxcl2 *and* Tnf *in the cecal mucosa of mice depicted in Figure 1A.* ***C-D*** *2-photon microscopy images, quantification of epithelial*

NFκB activation and expression of A20*,* Cxcl2 *and* Tnf *in the (**C**) small intestine and (**D**) colon of LPS-injected* $p65^{GFP\text{-}FL}$ *mice at 1 h.p.inj.. Each circle represents one mouse. Black line: Median. Statistical analysis in A: Mann-Whitney-U Test,* p*-values indicated. Scale bars: 50 µm.*

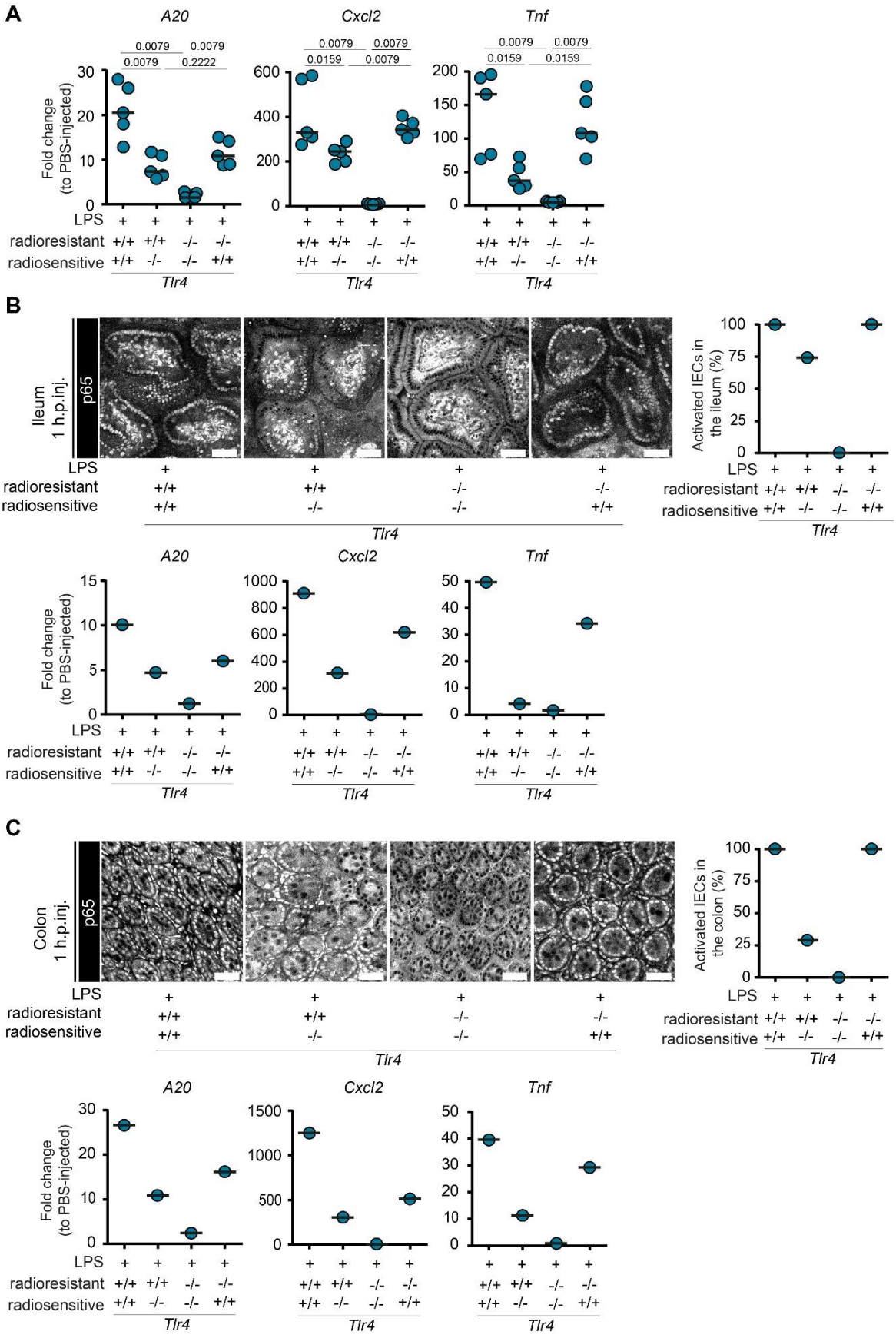

Figure S2 ***TLR4⁺ immune cells induce epithelial NFκB activation in the small intestine and colon. A*** *Fold changes in expression of* A20, Cxcl2 *and* Tnf *in the cecal mucosa of mice depicted in Figure 1B in comparison to PBS-injected mice in Figure 1A.* ***B-C*** *2-photon microscopy images, quantification of epithelial NFκB activation and expression of* A20, Cxcl2 *and* Tnf *in the (**B**) small intestine and (**C**) colon of LPS-injected p65^{GFP-FL} > p65^{GFP-FL},*

$p65^{GFP\text{-}FL}xTlr4^{-/-}$ > $p65^{GFP\text{-}FL}$, $p65^{GFP\text{-}FL}xTlr4^{-/-}$ > $p65^{GFP\text{-}FL}xTlr4^{-/-}$ and $p65^{GFP\text{-}F-}$ > $p65^{GFP\text{-}FL}xTlr4^{-/-}$ BMCs. Each circle represents one mouse. Black line: Median. Statistical analysis: Mann-Whitney-U Test, p*-values indicated. Scale bars: 50 µm.*

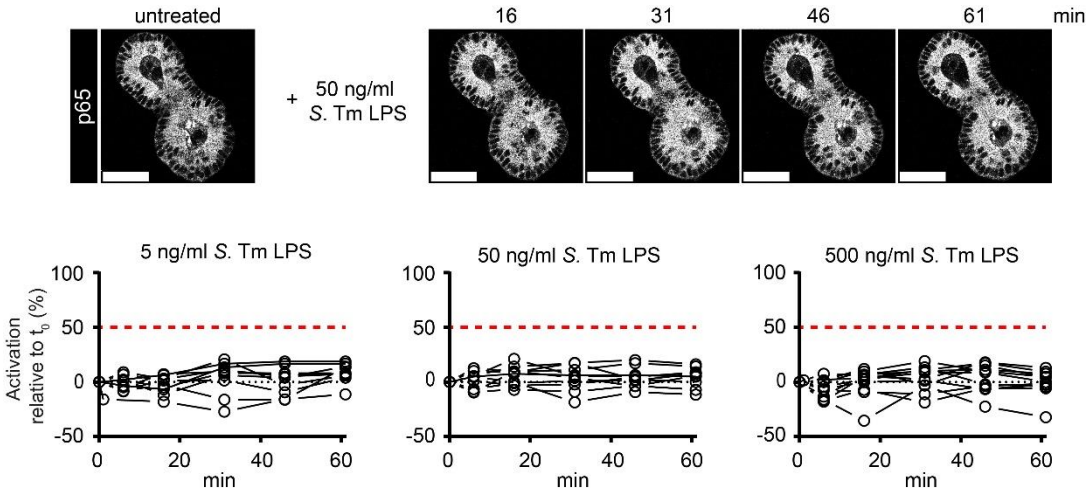

Figure S3 ***LPS exposure does not trigger NFκB activation in small intestinal epithelial organoids.*** *Small intestinal epithelial organoids were treated with 5, 50 or 500 ng/ml LPS and imaged for 1h. Representative images of one organoid over time (upper panel) and quantification of NFκB activation in all analyzed organoids (lower panel) indicated as relative change in comparison to the start of the treatment. Each circle represents one organoid at the given time (min after start of the treatment). Lines connect data points from the same organoid. Red dashed line: 50% activation threshold. Black dotted line: no change. Scale bars: 50 µm.*

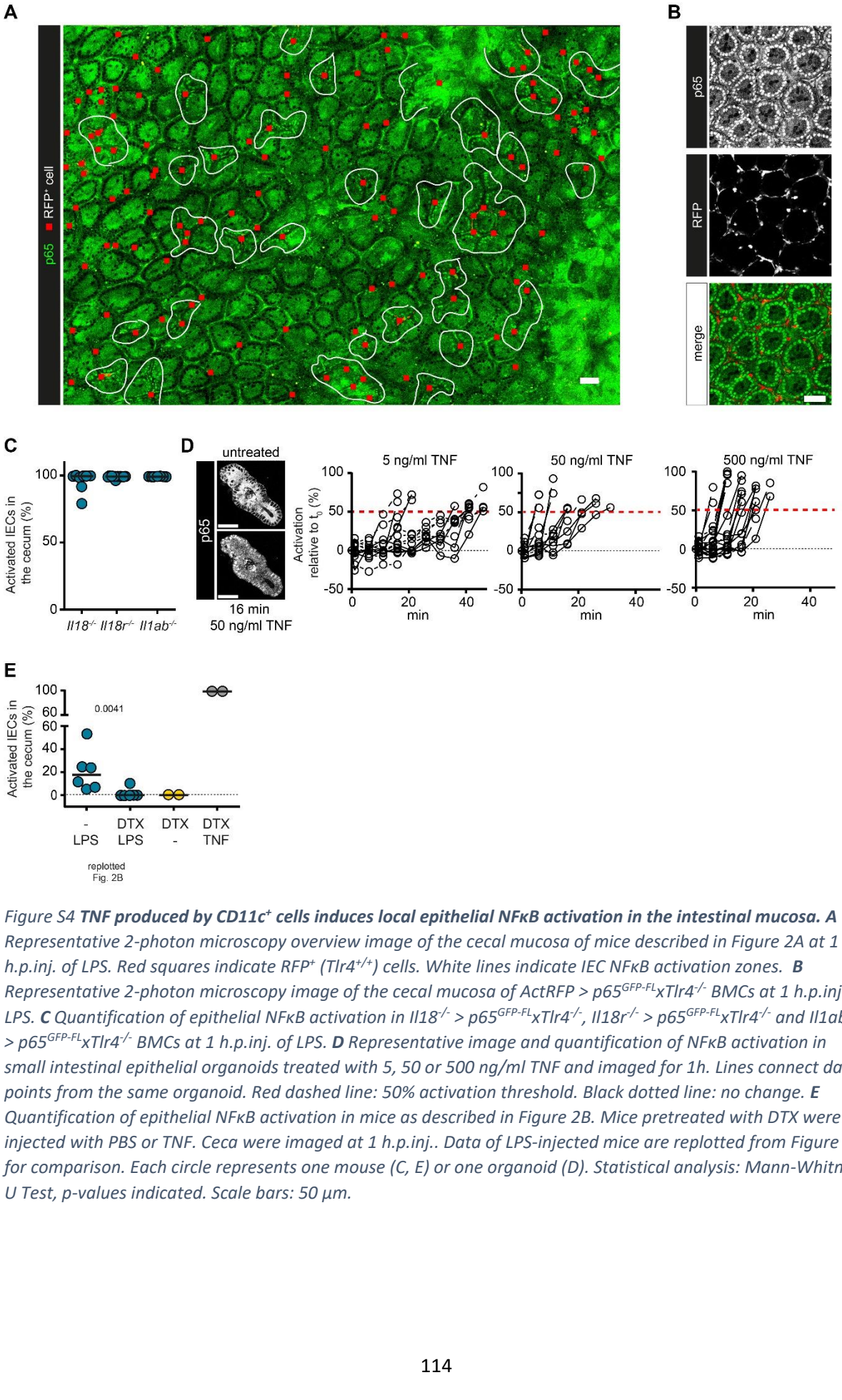

Figure S4 ***TNF produced by CD11c⁺ cells induces local epithelial NFκB activation in the intestinal mucosa. A*** *Representative 2-photon microscopy overview image of the cecal mucosa of mice described in Figure 2A at 1 h.p.inj. of LPS. Red squares indicate RFP⁺ (Tlr4$^{+/+}$) cells. White lines indicate IEC NFκB activation zones.* ***B*** *Representative 2-photon microscopy image of the cecal mucosa of ActRFP > p65^{GFP-FL}xTlr4$^{-/-}$ BMCs at 1 h.p.inj. of LPS.* ***C*** *Quantification of epithelial NFκB activation in Il18$^{-/-}$ > p65^{GFP-FL}xTlr4$^{-/-}$, Il18r$^{-/-}$ > p65^{GFP-FL}xTlr4$^{-/-}$ and Il1ab$^{-/-}$ > p65^{GFP-FL}xTlr4$^{-/-}$ BMCs at 1 h.p.inj. of LPS.* ***D*** *Representative image and quantification of NFκB activation in small intestinal epithelial organoids treated with 5, 50 or 500 ng/ml TNF and imaged for 1h. Lines connect data points from the same organoid. Red dashed line: 50% activation threshold. Black dotted line: no change.* ***E*** *Quantification of epithelial NFκB activation in mice as described in Figure 2B. Mice pretreated with DTX were injected with PBS or TNF. Ceca were imaged at 1 h.p.inj.. Data of LPS-injected mice are replotted from Figure 2B for comparison. Each circle represents one mouse (C, E) or one organoid (D). Statistical analysis: Mann-Whitney-U Test, p-values indicated. Scale bars: 50 µm.*

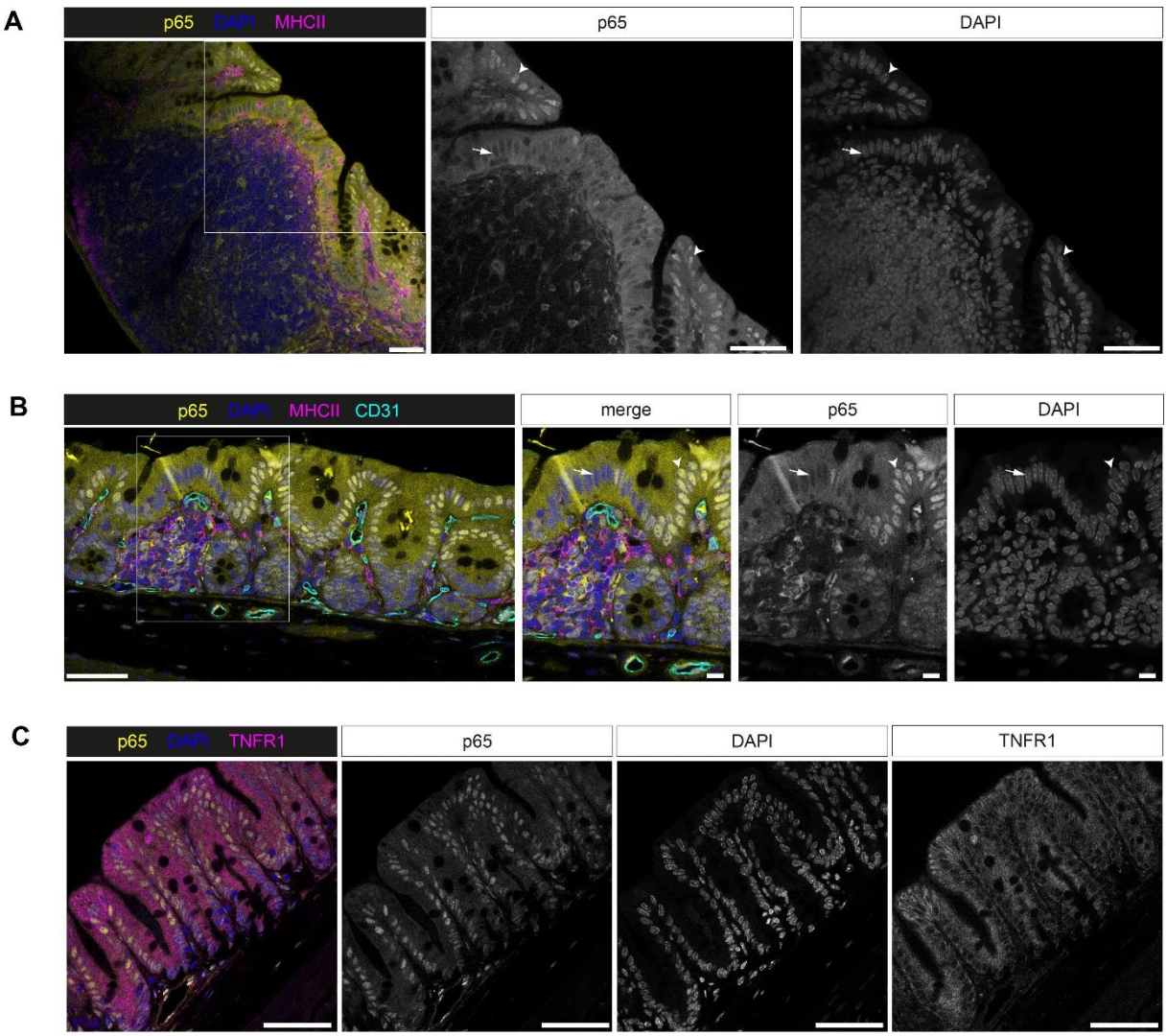

Figure S5 ***Dome epithelium displays desynchronized NFκB activation kinetics upon LPS exposure.*** *Confocal microscopy images of* ***A*** *the cecal patch,* ***B*** *a mucosa-associated lymphoid follicle in fixed ceca of p65^{GFP-FL} mice iv injected with LPS at 1 h.p.inj., and* ***C*** *the cecal mucosa stained for TNFR1 at 1 h.p.inj. of LPS. Boxes in overview images indicate cut-outs. Arrow heads indicate p65^{+} nuclei. Arrows indicate p65^{-} nuclei. Scale bars: 50 µm (overview images) or 10 µm (cut-outs).*

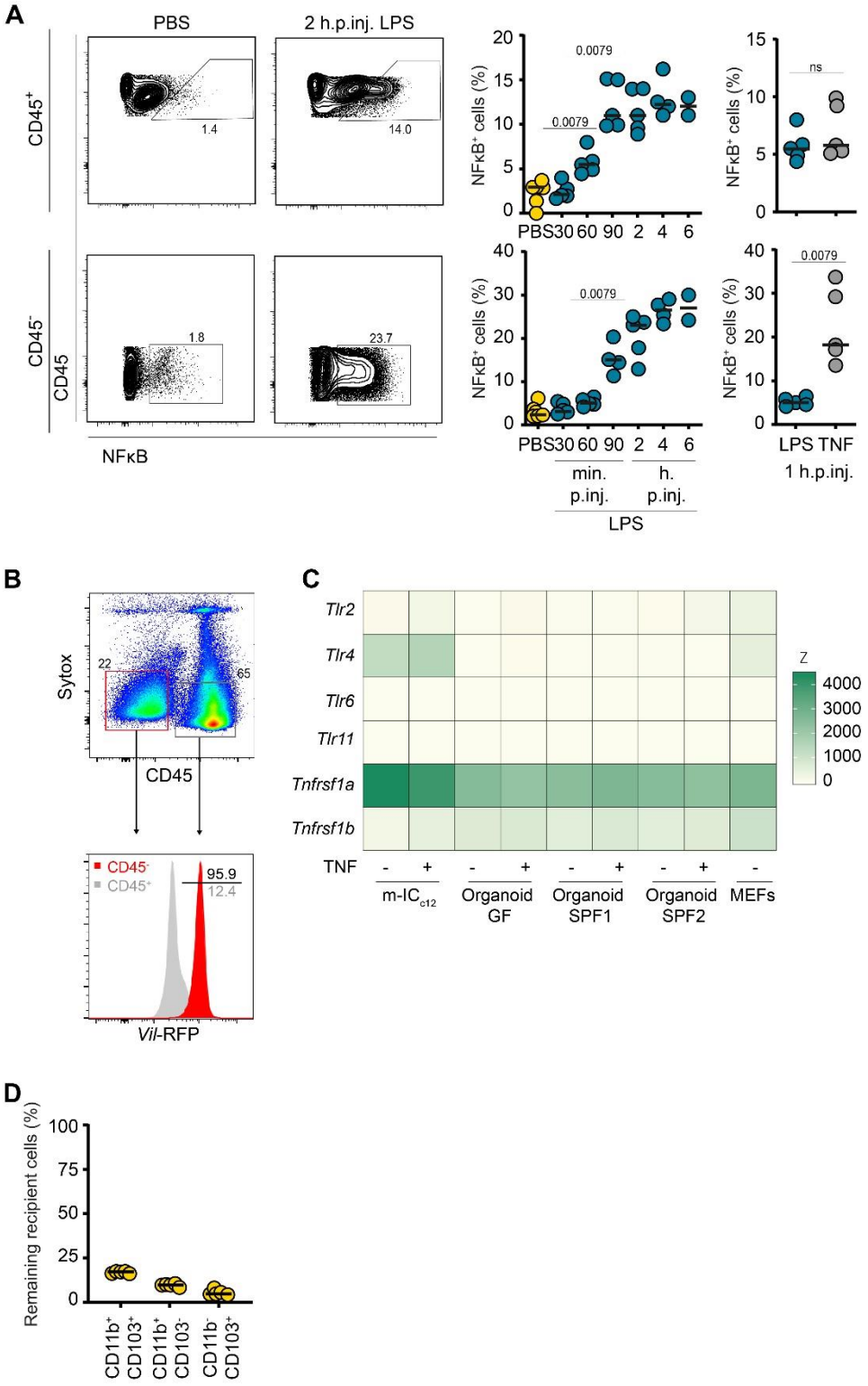

Figure S6 ***Immune cells respond swiftly to LPS, while the epithelium is indirectly activated via TNF. A*** *Flow cytometric analysis of cecal mucosal cell subsets of Kappable mice iv injected with LPS or TNF. Cells were pre-gated as follows: CD45⁺ cells: CD45⁺ Sytox^{dim}, CD45⁻ cells: CD45⁻ Sytox⁻. Statistical analysis: Mann-Whitney-U test, p-values indicated.* ***B*** *Gating strategy to differentiate CD45⁺ and CD45⁻ cells of a VilRFP mouse to enumerate* Villin*-expressing IEC fractions within the CD45⁻ gate.* ***C*** *Heat map depicting expression levels of* Tlr2, Tlr4, Tlr6, Tlr11, Tnfrsf1a *(TNFR1) and* Tnfrsf1b *(TNFR2) in untreated or TNF-treated (5 ng/ml, 8h) small intestinal epithelial organoids derived from SPF (SPF1, SPF2) or germfree (GF) mice, m-IC$_{c12}$ cells and mouse embryonic fibroblasts (MEFs) (reanalysis of a previously published transcriptome data set, all detectable Tlrs depicted (Chapter 5)).* ***D*** *Frequency of remaining recipient MP subsets in the cecal mucosa of BMCs at 6 weeks*

of reconstitution. Each circle represents one mouse. Black line: Median. Combined data of one (D) or 14 (A) independent experiments.

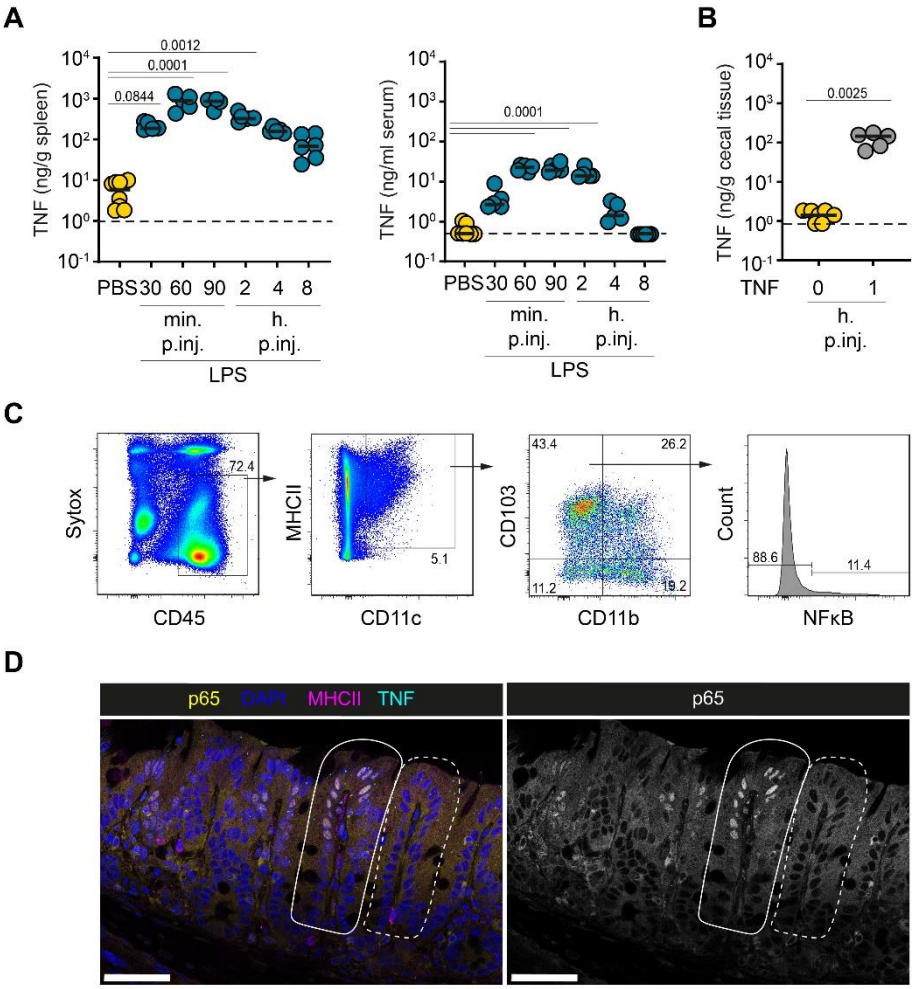

Figure S7 ***LPS-induced mucosal TNF concentrations are independent of systemically produced TNF.*** *ELISA measurements of TNF concentrations in* ***A*** *the spleen (left panel) and serum (right panel) of LPS-injected wild type mice and* ***B*** *the cecal mucosa of wild type mice iv injected with TNF. Combined data of three independent experiments. Dashed line: detection limit. y-axis in* log_{10} *scale. Statistical analysis: One-way ANOVA with Dunett`s correction (A) or Mann-Whitney-U Test (B), p-values indicated.* ***C*** *Gating strategy for intestinal MP subsets in the cecal mucosa of mice depicted in Figure 4B.* ***D*** *Representative image of TNF-PLA in the cecal mucosa of LPS-injected mice as described in Figure 4D. Dashed line indicates a crypt without epithelial NFκB activation. Solid line indicates a crypt with epithelial NFκB activation. Scale bars: 50 µm.*

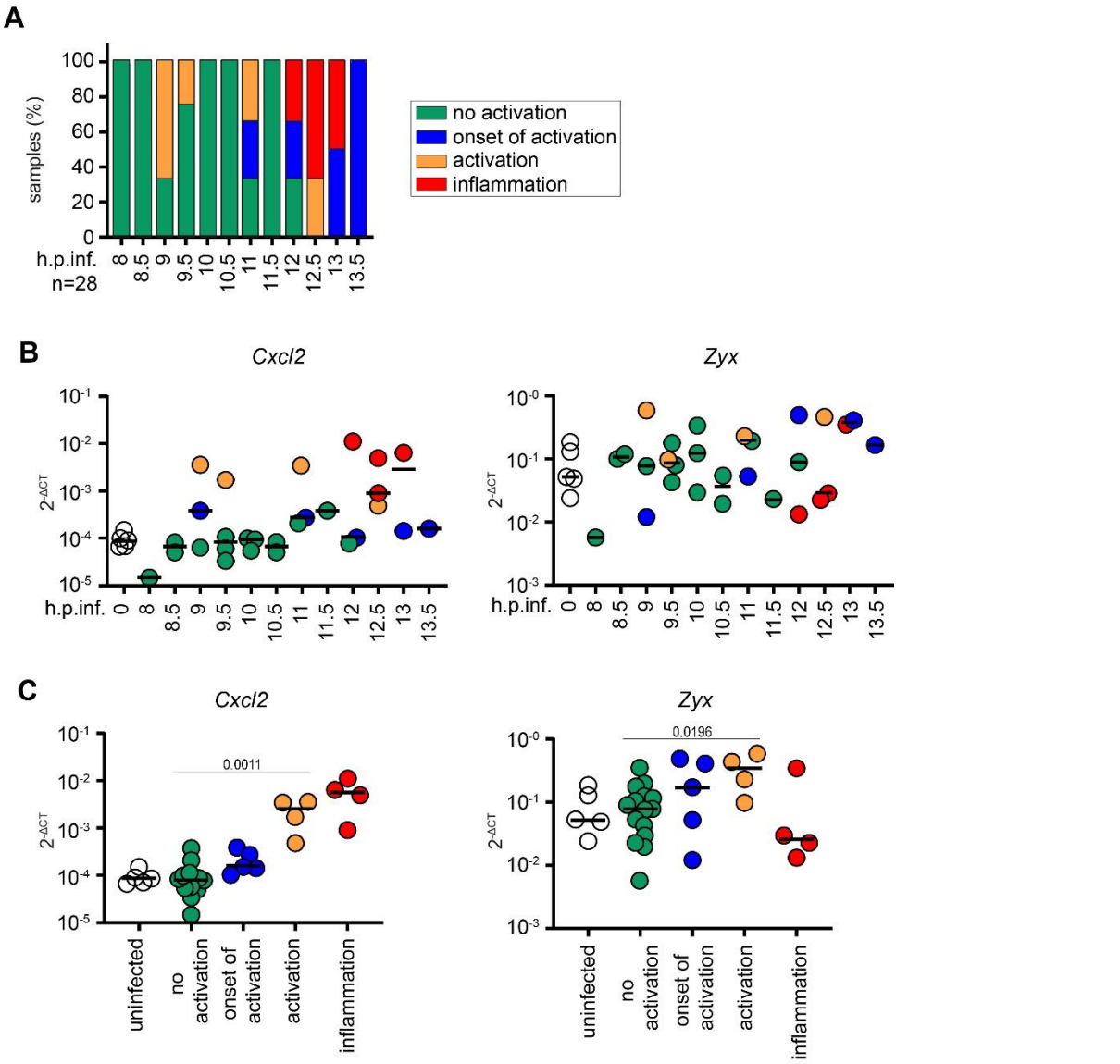

Figure S8 ***Intestinal epithelial NFκB activation status of S. Tm-infected mice correlates with mucosal expression of NFκB target genes. A*** *Relative distribution of intestinal epithelial NFκB activation status of* S. *Tm infected mice described in Figure 5A, sorted by time of infection.* ***B****-****C*** *Transcript levels of* Cxcl2 *and* Zyx *in the cecal mucosa of mice described in A and naive p65^{GFP-FL} mice, grouped according to* ***B*** *the time point of infection (color-code as in A) or* ***C*** *the epithelial NFκB activation status of the respective mice. Expression levels were normalized to* Actb *and depicted in 2$^{-\Delta CT}$. Statistical analysis: Mann-Whitney-U Test,* p*-values indicated.*

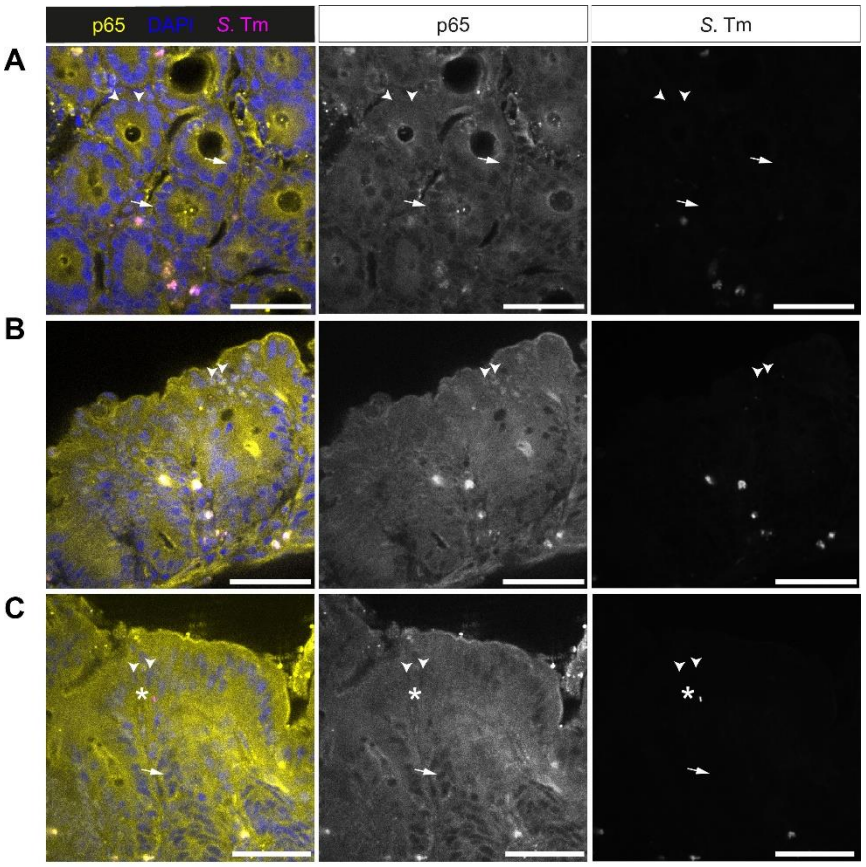

Figure S9 ***Epithelial NFκB signaling during S. Tm infection is independent of single bacterial invasion events****.* ***A-C*** *Confocal microscopy image examples of fixed cecal tissue of mice analyzed in Figure 5A. Arrow heads indicate p65⁺ nuclei. Arrows indicate p65⁻ nuclei. Asterisk indicates SPI2⁺ S. Tm. A SPI2$^{m\text{-}Cherry}$ plasmid (pZ400) was used for detection of S. Tm. Scale bars: 50 µm.*

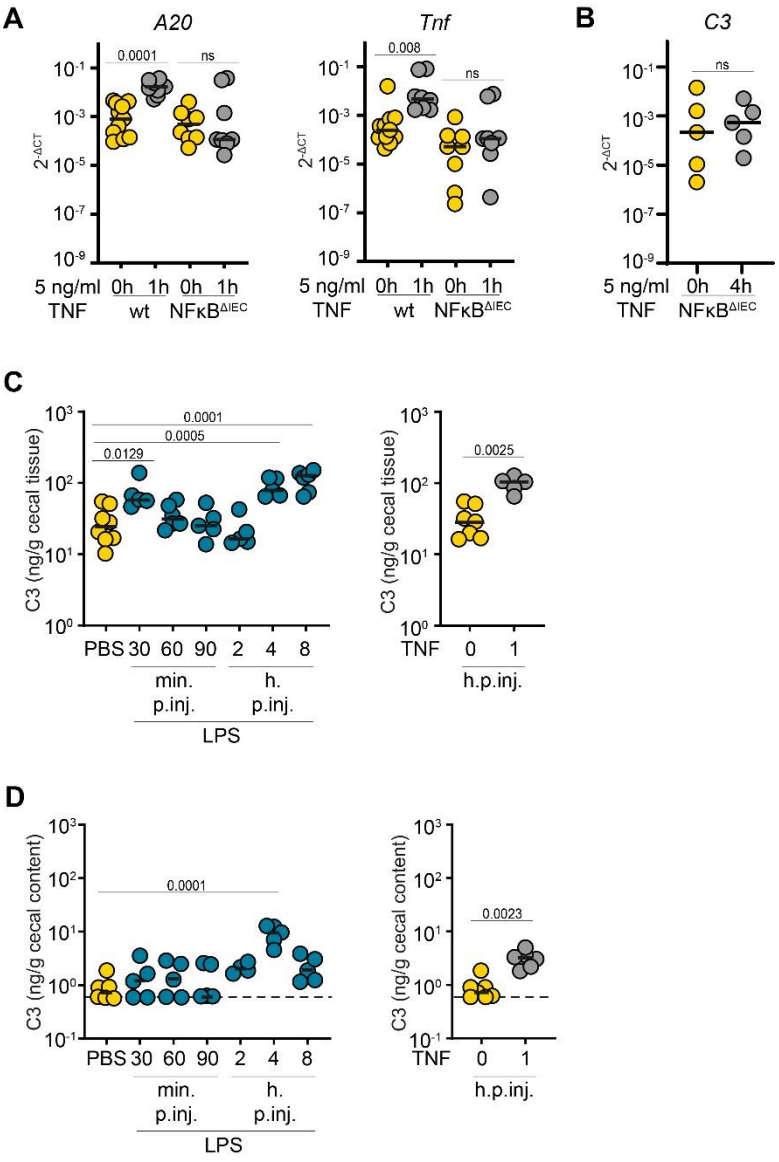

Figure S10 ***Epithelial NFκB signaling mediates C3 production in the cecal mucosa. A*** A20 *and* Tnf *transcript levels in untreated and TNF-treated (5 ng/ml, 1h) wild type and NFκB$^{\Delta IEC}$ small intestinal epithelial organoids, depicted as $2^{-\Delta CT}$. Expression levels were normalized to* Actb*. Combined data of four (wt) or five (NFκB$^{\Delta IEC}$) independent experiments.* ***B*** C3 *transcription levels in untreated and TNF-treated (5 ng/ml, 4h) NFκB$^{\Delta IEC}$ small intestinal epithelial organoids depicted as $2^{-\Delta CT}$. Expression levels were normalized to* Actb*. Combined data of five experiments.* ***C-D*** *ELISA measurements of C3 concentrations in the (**C**) cecal tissue and (**D**) cecal content of LPS- (left panel) and TNF- (right panel) injected wild type mice as in Figure 4A. Each dot represents one organoid sample (A), one experiment (average) (B) or one mouse (C, D). Black line: Median. Dashed line: detection limit. y-axes in log_{10} scale. Statistical analysis: One-way ANOVA with Dunett`s correction (left panels of C, D) or Mann-Whitney-U Test (A, B; right panels of C, D),* p*-values indicated.*

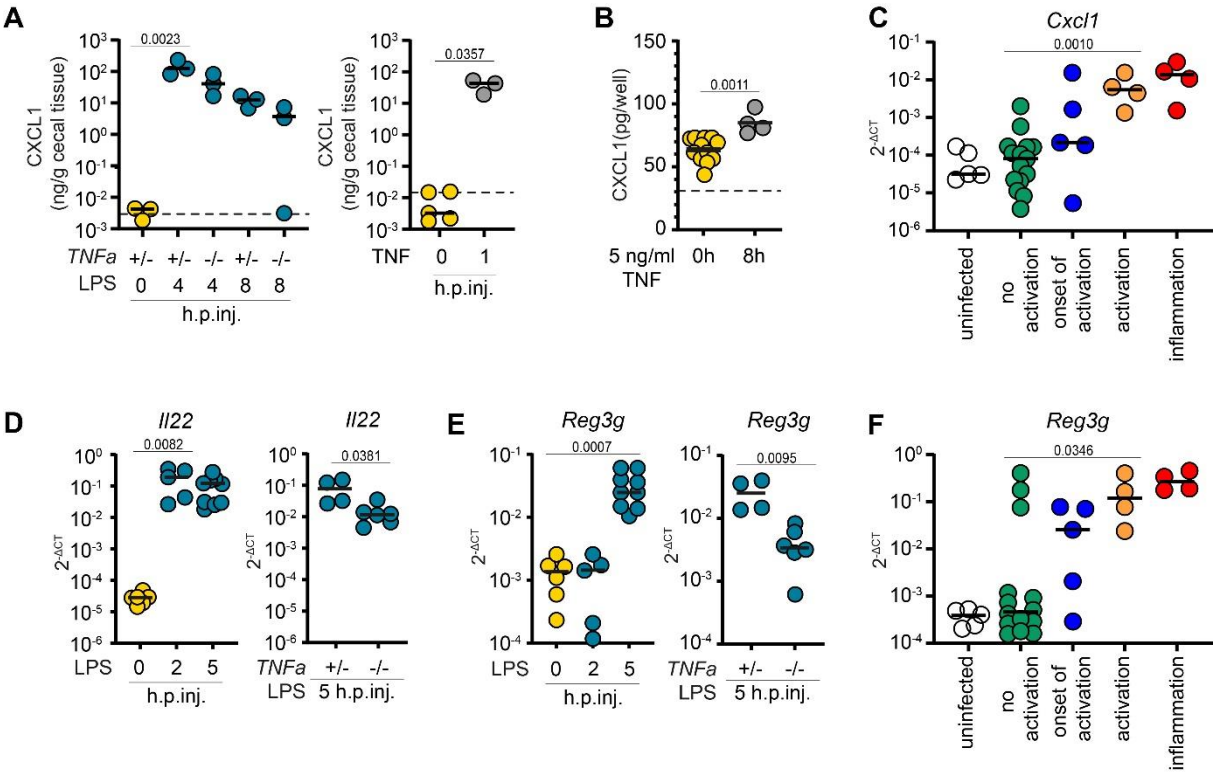

Figure S11 ***TNF-mediated epithelial NFκB activation induces a multifaceted antibacterial response.*** ***A*** *ELISA measurements of CXCL1 in the cecal mucosa of LPS-injected* TNFa$^{+/-}$ *and* TNFa$^{-/-}$ *(left panel) and TNF-injected wild type mice (right panel).* ***B*** *ELISA measurement of untreated and TNF-treated (5 ng/ml, 8h) small intestinal epithelial organoids.* ***C*** Cxcl1 *transcript levels in the cecal mucosa of mice described in Figure 5A and naive p65^{GFP-FL} mice, grouped according to the epithelial NFκB activation status of the respective mice.* ***D*** *Transcript levels of* Il22 *in LPS-injected wild type (left panel) and* TNFa$^{+/-}$ *and* TNFa$^{-/-}$ *mice (right panel).* ***E*** *Transcript levels of* Reg3g *in LPS-injected wild type (left panel) and* TNFa$^{+/-}$ *and* TNFa$^{-/-}$ *mice (right panel).* ***F*** Reg3g *transcript levels in the cecal mucosa of mice described in Figure 5A and naive p65^{GFP-FL} mice, grouped according to the epithelial NFκB activation status of the respective mice. Gene expression levels were normalized to* Actb *and depicted in 2$^{-ΔCT}$. Black line: Median. Dashed line: detection limit. Statistical analysis: One-way ANOVA with Dunett`s correction (left panel of A, D and E) or Mann-Whitney-U Test (B, C, F; right panel of A, D and E),* p-*values indicated. Each circle represents one mouse (A, C-F), or one organoid sample (B). Combined data of three (A) or four (D, E) independent experiments.*

CHAPTER 4 - INTESTINAL EPITHELIAL NAIP/NLRC4 RESTRICTS SYSTEMIC DISSEMINATION OF THE ADAPTED PATHOGEN *SALMONELLA* TYPHIMURIUM DUE TO SITE-SPECIFIC BACTERIAL PAMP EXPRESSION

Annika Hausmann[1], Desirée Böck[2], Petra Geiser[1#], Dorothée L. Berthold[1], Stefan A. Fattinger[1,3], Markus Furter[1], Judith Bouman[4], Manja Barthel-Scherrer[1], Crispin M. Lang[1], Erik Bakkeren[1], Isabel Kolinko[1], Médéric Diard[1], Dirk Bumann[5], Emma Slack[1], Roland R. Regoes[4], Martin Pilhofer[2], Mikael E. Sellin[1,3], Wolf-Dietrich Hardt[1]

Author affiliations:

[1]Institute of Microbiology, Department of Biology, ETH Zurich, Zurich, Switzerland
[2]Institute of Molecular Biology and Biophysics, Department of Biology, ETH Zurich, Zurich, Switzerland
[3]Science for Life Laboratory, Department of Medical Biochemistry and Microbiology, Uppsala University, Uppsala, Sweden
[4]Institute for Integrative Biology, Department of Environmental Science, ETH Zurich, Zurich, Switzerland
[5]Biozentrum Basel, University of Basel, Basel, Switzerland
[#]Present address: Science for Life Laboratory, Department of Medical Biochemistry and Microbiology, Uppsala University, Uppsala, Sweden

Author contributions:

AH, DBö, PG, DLB, SAF and MF performed experiments and analyzed data. DBö established and performed cryo-FIBmilling/cryoET. JB and RRR performed mathematical modeling. MBS, CML, IK provided technical assistance. MF, EB, DB, MD provided bacterial strains. AH, DBö, ES, MP, MES and WDH designed experiments. AH, MES and WDH devised the project and wrote the manuscript. All authors read, amended and approved the manuscript.

Inflammasomes can prevent systemic dissemination of enteropathogenic bacteria. As adapted pathogens including *Salmonella* Typhimurium (*S*. Tm) have evolved evasion strategies, it has remained unclear when and where inflammasomes restrict their dissemination. Bacterial population dynamics establish that the NAIP/NLRC4 inflammasome specifically restricts *S*. Tm migration from the gut to draining lymph nodes. This is solely attributable to NAIP/NLRC4 within intestinal epithelial cells (IECs), while *S*. Tm evades restriction by phagocyte NAIP/NLRC4. NLRP3 and Caspase-11 also fail to restrict *S*. Tm mucosa traversal, migration to lymph nodes, and systemic pathogen growth. The ability of IECs (not phagocytes) to mount a NAIP/NLRC4 defense *in vivo* is explained by particularly high NAIP/NLRC4 expression in IECs and the necessity for epithelium-invading *S*. Tm to express the NAIP1-6 ligands – flagella and type-III-secretion-system-1. Imaging reveals both ligands to be promptly downregulated following IEC-traversal. These results highlight the importance of intestinal epithelial NAIP/NLRC4 in blocking bacterial dissemination *in vivo*, and explain why this constitutes a uniquely evasion-proof defense against the adapted enteropathogen *S*. Tm.

Published in Mucosal Immunology, 17.01.2020

INTRODUCTION

Oral bacterial infection causes localized gastrointestinal disease, but pathogen dissemination (from here on termed migration) to systemic sites can lead to life-threatening complications. Multiple host defenses therefore cooperate to limit mucosal infection and pathogen spread (Chapter 1). The intestinal mucus lining and antimicrobial peptide secretion restrict mucosal invasion (Birchenough et al., 2016; Brandl et al., 2007; Furter et al., 2019; Johansson and Hansson, 2016; Miki and Hardt, 2013; Ostaff et al., 2013). Intestinal epithelial cells (IECs) and lamina propria phagocytes mount cell-intrinsic programs and release pro-inflammatory signals to counter pathogens that breach this first barrier (Birchenough et al., 2016; Franchi et al., 2012; Kinnebrew et al., 2012; Rauch et al., 2017; Sellin et al., 2014). Diverse immune cell types also patrol systemic organs and prevent excessive pathogen replication (Conlan, 1997; Felmy et al., 2013; Jorgensen et al., 2016; Nathan and Shiloh, 2000). This multilayered host defense is triggered by pattern recognition receptors (PRRs) that detect pathogen-associated molecular patterns (PAMPs), exposed by invading microbes. However, it is not fully understood which innate defense mechanisms act at which stage of the infection *in vivo* and what quantitative impact can be assigned to each layer of the defense.

The prototypic enteropathogen *Salmonella enterica* Typhimurium (*S*. Tm) colonizes the gut lumen, invades the mucosa, and can migrate to mesenteric lymph nodes (mLN), spleen, and liver, causing life-threatening infection e.g. in immunocompromised hosts (Chapter 1). Luminal *S*. Tm expresses flagella to target gaps in the mucus layer (Furter et al., 2019; Stecher et al., 2008), a type-III-secretion system (TTSS-1) to actively invade IECs (Galán and Curtiss, 1989), and, upon cell invasion, a second TTSS (TTSS-2) to promote IEC traversal (Müller et al., 2012). Mononuclear phagocytes (e.g. dendritic cells (DCs), macrophages) are involved in multiple steps of the *S*. Tm infection cycle. They facilitate *S*. Tm uptake across the epithelial barrier (Hapfelmeier et al., 2008; Niess et al., 2005; Rescigno et al., 2001), lodge *S*. Tm within the lamina propria and at systemic sites (Diehl et al., 2013; Müller et al., 2012), and act as vessels for *S*. Tm migration between organs (Bravo-Blas et al., 2019). Consequently, restriction of systemic *S*. Tm infection may depend on the capacity of both IECs and phagocytes to recognize the pathogen through PRR(s) and mount appropriate counter measures. For an adapted pathogen like *S*. Tm, this task is complicated by the bacterium's evolved ability to evade PRR recognition, through e.g. context-dependent regulation of its gene expression or inhibition of host-cell signaling (Chapter 1) (Bastedo et al., 2019; Brewer et al., 2019).

Inflammasomes are multimeric signaling complexes that assemble in the host cell cytosol upon sensing of PAMPs or cellular damage by PRRs of the Nod-like receptor family (NLRs; NLRP1, NLRP3, NLRC4), Aim2, or Pyrin (Broz, 2019). Inflammasome assembly causes cleavage of pro-inflammatory Caspase-1 (Martinon et al., 2002), secretion of interleukin-1 family cytokines and lipid mediators (von Moltke et al., 2012; Rauch et al., 2017), and prompt cell death (Shi et al., 2015). During bacterial infection, these effects promote clearance of intracellular pathogens, elicit local inflammation, and foster recruitment of effector cells, e.g. neutrophils, to sites of infection (Jorgensen et al., 2016; Miao and Warren, 2010; Müller et al., 2016). Work in cultured macrophages or DCs established several inflammasomes capable of responding to *S*. Tm infection. NAIP receptors (NAIP1, 2, 5, 6 in mice) recognize the TTSS-1 rod and needle proteins (NAIP1, 2) or flagellin (NAIP 5, 6) in the cytoplasm (Kofoed and Vance, 2011; Rauch et al., 2016; Rayamajhi et al., 2013; Yang et al., 2013; Zhao et al., 2011), and drive assembly of a NAIP/NLRC4 inflammasome. NLRP3 can also sense *S*. Tm infection (Broz et al., 2010; Diamond et al., 2017; Man et al., 2014), although the specific ligand(s) detected remains unknown. In addition, a non-canonical Caspase-4/11 inflammasome directly senses lipopolysaccharide (LPS) upon cytosolic escape of *S*. Tm from the endosomal compartment (Aachoui et al., 2013; Kayagaki et al., 2011a; Thurston et al., 2016). Inflammasome activation upon *S*. Tm infection is not confined to

phagocytes, but has also been shown to occur in epithelial cells, in IECs particularly involving NAIP/NLRC4 (Rauch et al., 2017; Sellin et al., 2014) or Caspase-4/11 (Knodler et al., 2014).

The capacity of inflammasomes to restrict *S*. Tm migration and growth at systemic sites *in vivo* has been subject to much debate. Caspase-1/11-deficient mice showed either reduced or enhanced susceptibility to systemic *S*. Tm infection (Lara-Tejero et al., 2006; Monack et al., 2000; Raupach et al., 2006). NLRC4-deficiency enhanced susceptibility to systemic infection (Carvalho et al., 2012; Franchi et al., 2006; Lara-Tejero et al., 2006), but not in all mouse backgrounds (Franchi et al., 2012). Moreover, *Nlrp3*$^{-/-}$ mice exhibited identical disease kinetics as controls (Broz et al., 2010; De Jong et al., 2014; Lara-Tejero et al., 2006), but a functional redundancy between NLRP3 and NLRC4 during oral *S*. Tm infection has been proposed (Broz et al., 2010; Man et al., 2014). Finally, Caspase-11 deletion had no impact on systemic *S*. Tm loads (Broz et al., 2012; Knodler et al., 2014), but one study found higher *S*. Tm loads in the gut mucosa during late stage infection (Knodler et al., 2014). It has become evident that separately held control animals develop a unique gut microbiota that can deviate considerably from the experimental group (Mamantopoulos et al., 2017, 2018; Robertson et al., 2019; Wullaert et al., 2018). This confounding factor may explain some of the discrepancies between early *in vivo S*. Tm infection studies.

In a littermate-controlled study of early *S*. Tm gut infection we identified IEC NAIP/NLRC4 as a key mucosal defense, which drives expulsion of infected IECs to limit mucosal tissue *S*. Tm loads (Sellin et al., 2014). Protection by epithelial NLRC4 was confirmed in a subsequent study (Rauch et al., 2017), and also pertains to *Citrobacter rodentium* infection (Nordlander et al., 2014). Importantly, mice globally lacking NAIP proteins also featured elevated systemic *S*. Tm loads upon oral challenge (Sellin et al., 2014). Due to the central involvement of phagocytes in pathogen migration and growth at systemic sites, this raised the question if NAIP/NLRC4 within IECs, phagocytes, or both, restrict disseminated *S*. Tm infection. Moreover, it remained unclear if pathogen restriction also involved NLRP3 and/or Caspase-11 and whether redundancies between the inflammasomes exist *in vivo*.

Here, we applied a bacterial population dynamics approach and littermate-controlled infections of inflammasome-deficient mice to address which inflammasome(s) in which cell types restrict disseminated oral *S*. Tm infection. We find that *S*. Tm successfully escapes restriction by phagocyte inflammasomes that in principle can recognize the bacterium. By contrast, the necessity for *S*. Tm to express the NAIP ligands – flagella and TTSS-1 – during the epithelial cell invasion step explains why intestinal epithelial NAIP/NLRC4 constitutes a unique restriction system that even this highly adapted pathogen cannot fully evade.

RESULTS

NAIP/NLRC4 POTENTLY RESTRICTS *S*. TM MIGRATION FROM THE GUT LUMEN TO SYSTEMIC SITES

Our *in vivo* analysis of the NAIP/NLRC4-mediated defense focused on the *S*. Tm infection dynamics during the first 24h after orogastric inoculation in the Streptomycin pretreated mouse model (Barthel et al., 2003). Due to its highly reproducible, fast and robust kinetics, this infection setup is ideally suited to study innate immune restriction of enteropathogen dissemination to systemic sites. Within 24h, the pathogen colonizes the gut lumen of Streptomycin pretreated mice, invades the gut mucosa, and disseminates systemically via gut-draining mLN (Kaiser and Hardt, 2011). The size of a pathogen population inside the mLN is the product of several parameters, i.e. bacterial immigration to this site, replication on the way to and within the organ, emigration to other sites and elimination of the

pathogen by the host. In contrast to classical selective plating of infected organs, which merely provides a snapshot of the bacterial population size, infections with mixtures of wild-type isogenic tagged strains (WITS), combined with mathematical modelling can reveal the dynamic parameters and thereby provide essential information on pathogen restrictive mechanisms (Figure S1) (Grant et al., 2008; Kaiser et al., 2013, 2016; Maier et al., 2014; Mastroeni and Grant, 2013; Moor et al., 2017).

To establish the quantitative infection parameters, we infected Streptomycin pretreated mice with a mixed inoculum ($5x10^7$ total CFU per gavage), comprised of non-tagged *S*. Tm and seven WITS each spiked in at a 1:140 dilution (i.e. the WITS strains together made up 5% of the inoculum). By conventional plating, we detected ~10-fold increased total *S*. Tm loads in the mLN of *Nlrc4*$^{-/-}$ (Mariathasan et al., 2004) mice compared to their heterozygous littermate controls at 24h post-infection (hpi) (Figure 1A, "all *S*. Tm"). This phenotype was confirmed by selective plating of the WITS population (Figure 1A, "WITS"). In line with earlier work establishing that gut luminal *S*. Tm loads are independent of gut inflammation during the first 24h (Stecher et al., 2007), we did not detect any changes in luminal colonization (Figure S2A). To determine the cause of the elevated mLN pathogen loads, we analyzed the number of distinct WITS recovered from this organ. In the mLN of infected *Nlrc4*$^{-/-}$ mice all, or close to all, of the seven WITS were recovered at 24 hpi. By striking contrast, *Nlrc4*$^{+/-}$ littermate control mLN harbored on average only two WITS (Figure 1B).

The higher diversity of WITS in the mLN of *Nlrc4*$^{-/-}$ mice suggested that more bacteria seed the organ to give rise to the mLN-lodged pathogen population. To test this hypothesis, we applied a mathematical model for analysis of population dynamics, considering pathogen migration (μ) and net growth (r (Kaiser et al., 2013); see materials and methods for details). This established that the *S*. Tm migration rate (μ) from the cecal lumen to the mLN was elevated by 8.7-fold in *Nlrc4*$^{-/-}$ mice compared to controls (Figure 1C). Notably however, the presence or absence of NLRC4 did not affect the pathogen's net replication rate (r) within the mLN (Figure 1D). We repeated these experiments in *Naip1-6*$^{\Delta/\Delta}$ (Allam et al., 2015) mice, which lack the receptors activating the NLRC4 inflammasome (Allam et al., 2015). These mice phenocopied *Nlrc4*$^{-/-}$ animals, showing a 6.7-fold increase in *S*. Tm migration to the mLN, but a similar within-mLN pathogen replication rate as control animals (Figure 1E-H, S2B).

Taken together, these findings show that the NAIP/NLRC4 inflammasome is of key importance for restricting *S*. Tm migration from the gut lumen to the mLN, but does not affect the pathogen's replication within this target organ. By inference, this indicates that phagocyte NAIP/NLRC4 is dispensable for controlling pathogen growth in the mLN. It remained to be established if IEC or phagocyte NAIP/NLRC4 could explain restriction of pathogen migration from the gut, and if additional inflammasomes also impact this process.

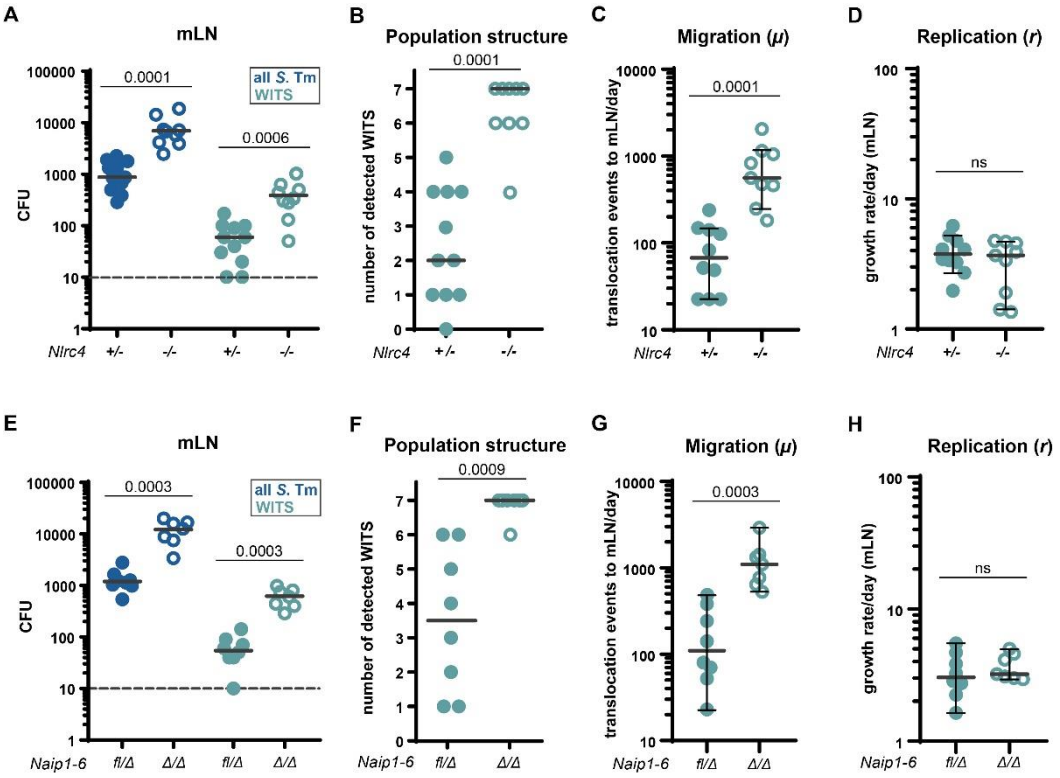

Figure 1 ***The NAIP/NLRC4 inflammasome restricts pathogen migration to the mLN during oral S. Tm infection.*** *Streptomycin pretreated mice were orally infected with 5x10^7 CFU S. Tm.* ***A*** *S. Tm counts (colony forming units, CFU) in the mLN at 24 hpi in* Nlrc4$^{-/-}$ *mice (open circles) are ~10-fold increased compared to* Nlrc4$^{+/-}$ *(circles) littermates.* ***B*** *The populations recovered from the mLN of Nlrc4$^{-/-}$ mice (open circles) display higher variety in WITS than those isolated from* Nlrc4$^{+/-}$ *(circles) littermates. Analysis of mice depicted in A. Only mice with detectable WITS (plating) in the mLN were included in the analysis, remaining samples were set to 0.* ***C*** *The migration rate* μ *from the cecal lumen (of mice shown in B with ≥ 1 WITS-CFU per mLN, translocation events/day) to the mLN of* Nlrc4$^{-/-}$ *mice (open circles) is 8.7-fold increased compared to* Nlrc4$^{+/-}$ *(circles) littermates.* ***D*** *S. Tm growth rate* r *within the mLN (of mice shown in B with ≥ 1 WITS-CFU per mLN, depicted as growth rate per day) is independent of NLRC4.* ***E*** *S. Tm counts in the mLN of* Naip1-6$^{Δ/Δ}$ *mice (open circles) are ~10-fold increased at 24 hpi compared to* Naip1-6$^{fl/Δ}$ *(circles) littermates.* ***F*** *The populations recovered from the mLN of* Naip1-6$^{Δ/Δ}$ *mice (open circles) display higher variety in WITS than that of* Naip1-6$^{fl/Δ}$ *(circles) littermates. Analysis of mice depicted in E. Only mice with detectable WITS (plating) in the mLN were included in the analysis, remaining samples were set to 0.* ***G*** *The migration rate* μ *from the cecal lumen (of mice shown in F with ≥ 1 WITS-CFU per mLN, translocation events/day) to the mLN of* Naip1-6$^{Δ/Δ}$ *mice (open circles) is 6.7-fold increased compared to* Naip1-6$^{fl/Δ}$ *(circles) littermates.* ***H*** *S. Tm growth rate* r *within the mLN (of mice shown in F with ≥ 1 WITS-CFU per mLN, depicted as growth rate per day) is independent of NAIP1-6. Depicted are counts of all S. Tm (dark blue, selected for with Streptomycin) and specifically of the WITS (light blue, selected for with Kanamycin, 5 % of inoculum). Each circle represents one mouse. Combined data of three (E-H) or four (A-D) independent experiments. Dotted line: detection limit. Grey line: Median, in C, D, G and H 95%-Confidence Intervals are indicated. Statistical analysis: Mann-Whitney-U Test,* p*-values indicated, ns:* p ≥ 0.05.

NLRP3 AND CASPASE-11 ARE DISPENSABLE FOR CONTROL OF *S.* TM DISSEMINATION FROM THE GUT, EVEN IN THE ABSENCE OF NLRC4

The significance of the NLRP3 inflammasome and the non-canonical Caspase-11 inflammasome during oral *S.* Tm infection and their role in limiting pathogen levels at systemic sites are ambiguous (Broz et al., 2010, 2012; De Jong et al., 2014; Knodler et al., 2014; Man et al., 2014; Sellin et al., 2014). To quantitatively assess the involvement of these inflammasomes, we infected *Nlrp3$^{-/-}$* (Martinon et al., 2006) and *Casp11$^{-/-}$* (Kayagaki et al., 2011b) mice using the experimental setup described in Figure 1.

We did not observe any difference between the total bacterial loads in the cecal lumen and mLN, the WITS loads, or the numbers of WITS recovered from the mLN of either knockout line, when compared to their respective littermate controls (Figure S2C-D, S3A-B). Moreover, mathematical inference confirmed equivalent values for migration (μ) and net replication (r) in knockouts and controls (Figure 2A-B; values for *Nlrc4*$^{-/-}$ mice replotted from Figure 1C-D for comparison). Hence, neither NLRP3, nor Caspase-11, impact the dynamic parameters of oral *S*. Tm dissemination. *Casp1/11*$^{-/-}$ (Li et al., 1995) mice featured an intermediate phenotype with regards to total mLN pathogen loads, which were increased ~3-fold (Figure S3C), while luminal colonization (Figure S2E), migration and replication of the bacterium were not altered (Figure 2A-B). These data agree with a previously reported partial, but non-absolute, dependence of NAIP/NLRC4 on Caspase-1 (Mascarenhas et al., 2017; Rauch et al., 2017; Sellin et al., 2014; Van Opdenbosch et al., 2017).

As NAIP/NLRC4 potently limits pathogen migration (Figure 1), we reasoned that the lack of involvement of NLRP3 and Caspase-11 might be attributable to redundancies with this inflammasome. We thus crossed *Nlrc4*$^{-/-}$ mice with *Nlrp3*- or *Casp11*-knockout animals to obtain *Nlrc4*$^{-/-}$*Nlrp3*$^{+/-}$ and *Nlrc4*$^{-/-}$*Nlrp3*$^{-/-}$ littermates, as well as *Nlrc4*$^{-/-}$*Casp11*$^{+/-}$ and *Nlrc4*$^{-/-}$*Casp11*$^{-/-}$ littermates, for infections. However, also in an *Nlrc4*$^{-/-}$ background, neither *Nlrp3*- nor *Casp11*-ablation affected pathogen migration (μ) to the mLN, pathogen replication (r), total *S*. Tm loads in this organ by 24 hpi (Figure 2C-D, Figure S3D-E), or cecal luminal growth (Figure S2F-G). In line with these data, we did not detect significant differences in mucosal inflammation between the mice (Figure S4). Thus, we conclude that in our oral infection model, NLRP3 and Caspase-11 are not involved in the control of *S*. Tm dissemination from the gut lumen during the first day of infection. As our approach monitors all infection steps from the gut lumen to the mLN, these data should exclude an impact of IEC and phagocyte NLRP3 and Caspase-11, alike.

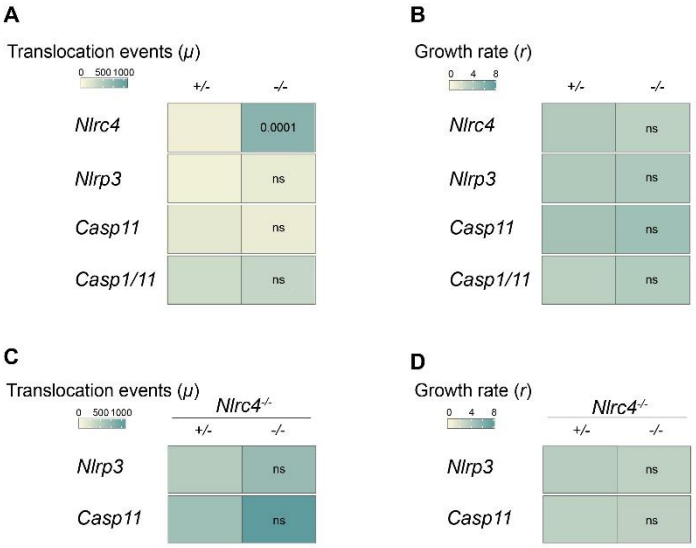

Figure 2 ***NLRP3 and Caspase-11 inflammasomes do not contribute to restriction of early S. Tm migration to the mLN. A*** *S. Tm migration rate μ (of mice shown in Figure S3A-C with ≥ 1 WITS-CFU per mLN, translocation events per day) is independent of NLRP3, Caspase-11 and Caspase-1. Data for* Nlrc4$^{+/-}$ *and* Nlrc4$^{-/-}$ *mice replotted from Figure 1C for reference.* ***B*** *S. Tm growth rate per day r within the mLN (mice shown in Figure S3A-C with ≥ 1 WITS-CFU per mLN) is independent of NLRP3, Caspase-11 and Caspase-1. Data for* Nlrc4$^{+/-}$ *and* Nlrc4$^{-/-}$ *replotted from Figure 1D for reference. Even in the absence of NLRC4, S. Tm migration rate μ (mice shown in Figure S3D-E with ≥ 1 WITS-CFU per mLN, translocation events per day,* ***C****) and S. Tm growth rate per day r within the mLN (mice shown in Figure S3D-E with ≥ 1 WITS-CFU per mLN,* ***D****) are independent of NLRP3 and Caspase-11. Combined data of three (*Nlrp3$^{-/-}$, Casp11$^{-/-}$, Casp11xNlrc4$^{-/-}$*) or four (*Nlrc4$^{-/-}$, Casp1/11$^{-/-}$,

Nalp3xNlrc4$^{-/-}$*) independent experiments. Statistical analysis: Mann-Whitney-U Test,* p*-values indicated, ns:* p ≥ *0.05.*

NAIP/NLRC4 IN IECS, NOT IN PHAGOCYTES, RESTRICTS SYSTEMIC SPREAD OF *S*. TM FROM THE GUT LUMEN

The population dynamics analysis revealed that NAIP/NLRC4 restricts migration (μ) of *S*. Tm from the intestinal lumen to the mLN, but appears dispensable for containment of pathogen replication (*r*) within the mLN. The parameter μ in the model summarizes two main steps of the infection process: i) the invasion/translocation of *S*. Tm across the cecal mucosa and ii) the subsequent transport of the pathogen from the mucosa into the mLN. To specify which of the two components is impacted by NAIP/NLRC4, and in which cell type the restriction takes place, we infected mice lacking the NAIP receptors specifically in IECs (*Naip1-6*$^{\Delta/\Delta IEC}$). Surprisingly, we found that IEC-specific ablation of NAIPs was sufficient to reproduce the pathogen migration phenotype observed in full body *Naip1-6* knockouts (Figure 3A, compare with Figure 1), while luminal colonization was unaffected (Figure S2H). The replication parameter (*r*) remained unaffected in *Naip1-6*$^{\Delta/\Delta IEC}$ animals (Figure 3A), further supporting a role for IEC NAIP/NLRC4 specifically in preventing pathogen migration from the gut lumen.

Notably, the restriction of systemic bacterial loads by epithelial NAIP/NLRC4 was equally relevant in an infection with a different *S*. Tm strain (*S*. Tm^{14028}; Figure S5A, S2I). This suggests that the epithelial inflammasome is of general relevance for protection against *S*. Tm strains.

Active epithelial invasion, most prominently in the cecum (Furter et al., 2019), is the main pathway by which *S*. Tm traverses the intestinal epithelium to reach the mLN in the Streptomycin mouse model. By contrast, passive pathogen transport via lymphoid follicles and/or gut lumen-sampling DCs accounts for only ~10% of the total transport (Hapfelmeier et al., 2008; Kaiser and Hardt, 2011). Due to the pronounced effect of the IEC NAIP/NLRC4 inflammasome, it remained unclear if this "alternative" sampling route for traversal might also be restricted by the NAIP/NLRC4 inflammasome. The *S*. Tm mutant *S*. Tm$^{\Delta 4}$ (SL1344 *sipAsopBsopEsopE2*) lacks the TTSS-1-delivered effector proteins necessary for active invasion into IECs, but retains the TTSS-1 structural components sensed by NAIP/NLRC4 (Ehrbar et al., 2003). While being severely attenuated for IEC invasion, non-invasive mutants like *S*. Tm$^{\Delta 4}$ can still traverse the epithelial barrier by the passive sampling route (Hapfelmeier et al., 2008). Hence, this strain only rarely passes through IECs on the way from the gut lumen to the mLN, but instead promptly enters the lamina propria phagocyte compartment. This feature allowed us to specifically analyze the impact of phagocyte NAIP/NLRC4 on the pathogen migration rate. Towards this aim, we applied the same procedure as described in Figure 1. We infected *Nlrc4*$^{-/-}$ mice for 24h with a mixture of non-tagged *S*. Tm$^{\Delta 4}$ and spiked in the seven barcoded WITS$^{\Delta 4}$ strains at a 1:21 dilution (i.e. the WITS$^{\Delta 4}$ strains together made up 33.3% of the inoculum). In line with this strain only migrating through the passive sampling pathway, the absolute mLN loads of *S*. Tm$^{\Delta 4}$ were ~10-fold lower than in an infection with wild type *S*. Tm (compare Figure 3B with Figure 1A) and no detectable mucosal pathology was induced at 24 hpi (Figure S4C). This is in line with earlier work indicating that *sipAsopBsopEsopE2*-mediated epithelium invasion is the key trigger of acute mucosal inflammation (Hapfelmeier et al., 2005; Müller et al., 2009). Importantly, when infecting with *S*. Tm$^{\Delta 4}$, we did not observe any effect of the ablation of NLRC4 on the mLN infection dynamics and cecal lumen colonization (Figure 3B, S2K). This was also the case for *Naip1-6*$^{\Delta/\Delta IEC}$ mice (Figure 3C, S2L). It is interesting to note that we observed a slight, but non-significant trend towards higher mLN counts in *Naip1-6*$^{\Delta/\Delta IEC}$ mice. We suspect that this is attributable to some residual epithelial invasion capacity of *S*. Tm$^{\Delta 4}$ (Hapfelmeier et al., 2008; Misselwitz et al., 2011)and/or uptake by M-cells.

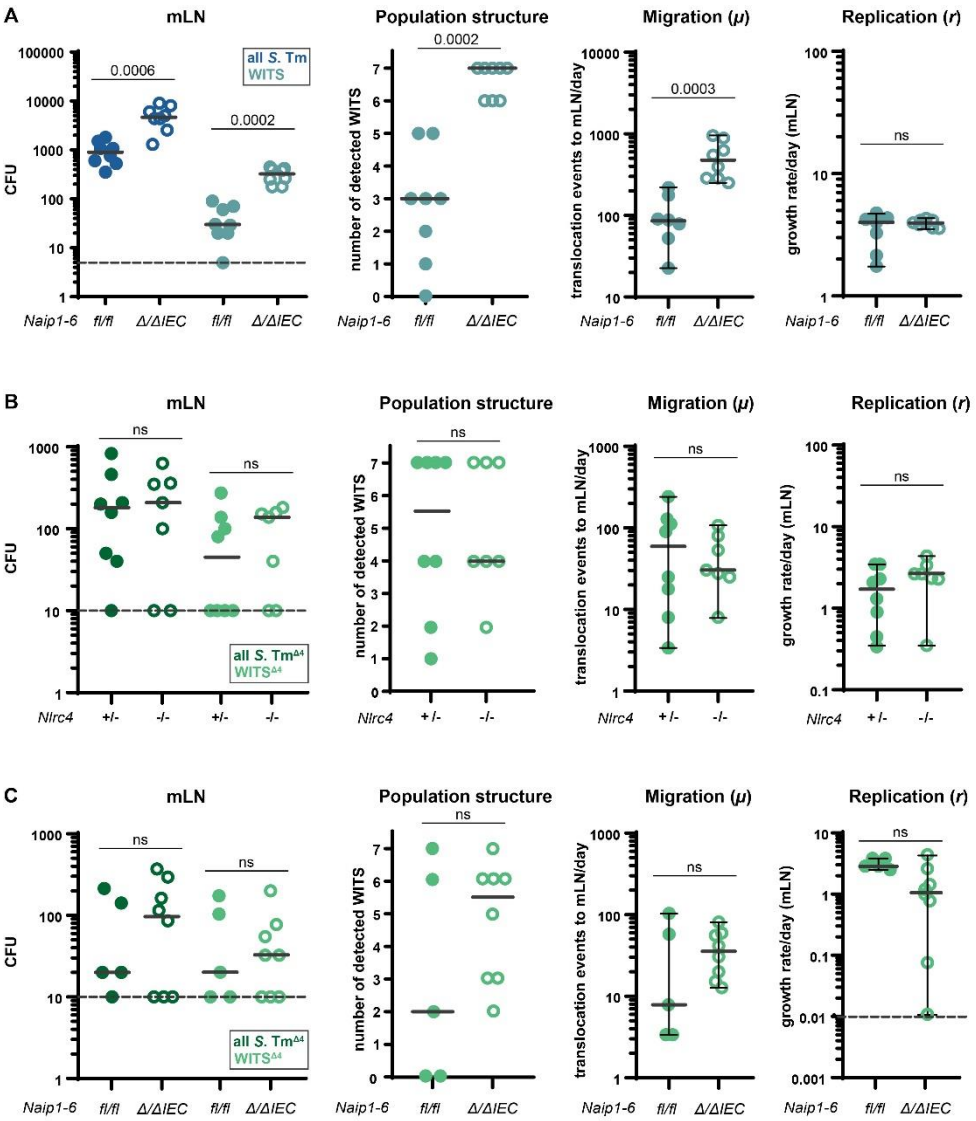

Figure 3 ***Intestinal epithelial NAIP/NLRC4 restricts pathogen migration to the mLN. A*** *Streptomycin pretreated mice were orally infected with 5x10^7 CFU* S. Tm. *S. Tm counts in the mLN at 24 hpi, number of WITS tags in the mLN and S. Tm migration rate μ to the mLN were significantly increased in* Naip1-6$^{Δ/ΔIEC}$ *mice (open circles) compared to* Naip1-6$^{fl/fl}$ *littermates (circles) and phenocopied* Naip1-6$^{Δ/Δ}$ *mice (compare Figure 1E-H). Growth rate r within the mLN was independent of NAIP1-6 within IECs.* ***B*** *Streptomycin pretreated mice were orally infected with 5x10^7 CFU S. Tm^{Δ4}. S. Tm^{Δ4}, which bypasses IECs, is unaffected by NLRC4-mediated restriction during migration to and colonization of the mLN. This extends to epithelial NAIP1-6 (**C**). Depicted are counts of all S. Tm (dark blue, selected for with Streptomycin) and specifically of the WITS (light blue, selected for with Kanamycin, 5% of the inoculum) or S. Tm^{Δ4} (dark green, selected for with Streptomycin) and specifically of the WITS^{Δ4} (light green, selected for with Kanamycin, 33.3% of the inoculum). Each circle represents one mouse. Combined data of two (B, C) or three (A) independent experiments. Dotted line: detection limit. Grey line: Median, for μ and r, 95%-Confidence Intervals are indicated. Statistical analysis: Mann-Whitney-U Test,* p*-values indicated, ns:* p ≥ 0.05.

Finally, to formally exclude the involvement of DC NAIP/NLRC4 in *S*. Tm restriction, we infected mice lacking the NAIP receptors specifically in CD11c$^+$ cells (*Naip1-6$^{Δ/ΔCD11c}$*) with wild type *S*. Tm as described above. In line with our previous observations, the ablation of *Naip1-6* in CD11c$^+$ cells did not affect luminal colonization (Figure S2M), mLN pathogen loads, migration of *S*. Tm to the mLN and replication of the bacterium at this site (Figure S5B). Altogether, these data demonstrate that i) NAIP/NLRC4 specifically in IECs acts as a firewall against pathogen dissemination from the gut lumen, whereas ii) this inflammasome has minimal impact in phagocyte populations that take up *S.* Tm in the

mucosa, transport the pathogen to the mLN, or lodge the bacteria within this site (Bravo-Blas et al., 2019; Hapfelmeier et al., 2008; Müller et al., 2012).

NLRC4, NLRP3 AND CASPASE-11 INFLAMMASOMES ARE ALL DISPENSABLE DURING EARLY SYSTEMIC *S*. TM INFECTION

As a more direct test for a possible involvement of phagocytes in inflammasome-mediated containment of *S*. Tm, we employed a systemic infection model. Here, *S*. Tm (10^4 CFU) were applied intravenously (iv), resulting in a rapid uptake by phagocytes, and subsequent pathogen growth in the spleen and other systemic organs within 6-10 hpi (Grant et al., 2008; Sheppard et al., 2003). In this model, the main lymphoid organ infected during the first 2 days is the spleen, which was analyzed here (Figure 4) at 24 hpi, analogously to the mLN in the oral infection model (Figure 1-3). For estimation of μ and r, the inoculum was spiked with the seven barcoded WITS in a dilution of 1:700 (i.e. the WITS strains together made up 1% of the inoculum).

Strikingly, when analyzing spleen *S*. Tm loads in *Nlrc4*$^{-/-}$ mice and littermate controls, we found NLRC4 to be completely dispensable for pathogen control. In line with this, we did not detect any differences in the number of WITS recovered from the spleen of these mice. Furthermore, the migration rate μ and the replication rate r within the spleen were not altered upon ablation of NLRC4 (Figure 4A). We also observed no effect of NLRP3, or Caspase-11, on the containment of systemic *S*. Tm infection, even when analyzed in an *Nlrc4*$^{-/-}$ background (Figure 4B-C). *Casp1/11*$^{-/-}$ mice again featured an intermediate phenotype, similar to our observations in the oral infection model, i.e. ~3-fold increased bacterial loads in the spleen by 24 hpi (Figure 4D, compare to Figure S3C). Mathematical modeling suggests that this effect is due to a Caspase-1 mediated restriction of initial *S*. Tm migration to the spleen, rather than involvement in suppression of pathogen replication within this organ (Figure 4D, population structure, μ and r). Hence, our data refute a significant impact of NLRC4, NLRP3 and Caspase-11 during early systemic *S*. Tm infection, while Caspase-1 contributes modestly to the control of pathogen loads. This resolves long-standing controversies in the literature about the involvement of different inflammasomes in host responses to wild type *S*. Tm infection (Broz et al., 2010, 2012; Carvalho et al., 2012; De Jong et al., 2014; Knodler et al., 2014; Man et al., 2014, 2017). It should be noted that differences in the studied infection time points or distinct virulence factor expression patterns of the employed *S*. Tm strains may also account for disparate phenotypes. Nevertheless, in our iv infections, Caspase-1 mediated defense appears independent of NLRC4, NLRP3 or Caspase-11. It remains to be established which other activation pathway might be involved.

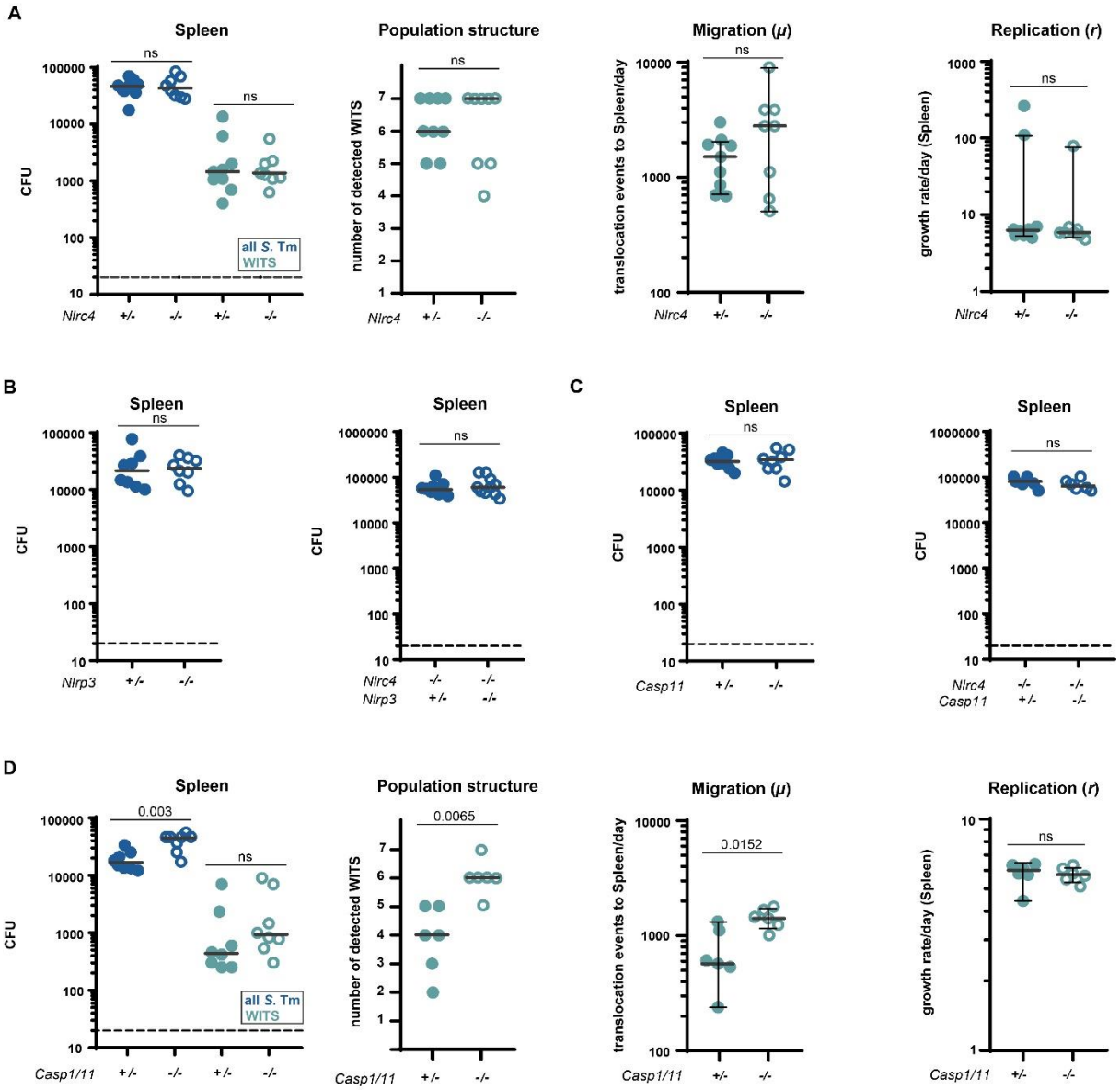

Figure 4 ***NLRC4, NLRP3 and Caspase-11 are dispensable for pathogen defense in a systemic infection model.*** *Mice were infected iv with 10^4 CFU S. Tm for 24 h.* ***A*** *S. Tm counts in the spleen at 24 hpi, number of WITS tags, S. Tm migration rate μ to and replication rate r within the spleen were not altered by ablation of NLRC4 (*Nlrc4$^{+/-}$ *(circles) and* Nlrc4$^{-/-}$ *(open circles)).* ***B*** *S. Tm counts in the spleen at 24 hpi were not altered in* Nlrp3$^{-/-}$ *(open circles) compared to* Nlrp3$^{+/-}$ *(circles) mice (left panel). This was also the case in an* Nlrc4$^{-/-}$ *background (*Nlrc4$^{-/-}$ Nlrp3$^{+/-}$ *(circles) and* Nlrc4$^{-/-}$ Nlrp3$^{-/-}$ *(open circles), right panel) mice.* ***C*** *S. Tm counts in the spleen at 24 hpi were not altered in* Casp11$^{-/-}$ *(open circles) compared to* Casp11$^{+/-}$ *(circles) mice (left panel), even in an* Nlrc4$^{-/-}$ *background (*Nlrc4$^{-/-}$Casp11$^{+/-}$ *(circles) and* Nlrc4$^{-/-}$ Casp11$^{-/-}$ *(open circles), right panel).* ***D*** *S. Tm counts in the spleen, number of WITS tags and S. Tm migration rate μ in* Casp1/11$^{-/-}$ *mice (open circles) are slightly increased at 24 hpi compared to* Casp1/11$^{+/-}$ *littermates (circles), whereas the replication rate is not affected. Each circle represents one mouse. In A and D counts of all S. Tm (dark blue, selected for with Streptomycin) and specifically of the WITS (light blue, selected for with Kanamycin, 1% of the inoculum) are shown. Combined data of three (A, B* Nlrp3$^{-/-}$*, C) or four (B* Nlrp3xNlrc4$^{-/-}$*,* Casp1/11$^{-/-}$*) independent experiments. Dotted line: detection limit. Grey line: Median, for μ and r, 95%-Confidence Intervals are indicated. Statistical analysis: Mann-Whitney-U Test,* p*-values indicated, ns:* $p \geq 0.05$.

IECS EXPRESS MORE *NAIP* AND *NLRC4* TRANSCRIPTS THAN THE REMAINING MUCOSAL TISSUE CELL TYPES

To assess the NAIP/NLRC4 sensing potential of the specific cell types that interact with *S.* Tm during oral infection in mucosal and systemic tissues, we analyzed *Naip/Nlrc4* expression by quantitative PCR (qPCR). For assessment of *Naip* transcript levels in IECs vs. other cells of the mucosa (including phagocytes), and to set the baseline of the assay, we initially compared tissues from uninfected wild type mice (*Naip1-6*$^{fl/fl}$), to those of *Naip1-6*$^{\Delta/\Delta\ IEC}$ and *Naip1-6*$^{\Delta/\Delta}$ animals. Mice carrying just one intact allele of the *Naip1-6* locus (*Naip1-6*$^{fl/\Delta}$) served as an additional control for the sensitivity of the assay.

Nlrc4 and *Naip1, 2, 5* and *6* expression levels were markedly higher in the cecum tissue, as compared to both mLN and spleen (Figure 5A-E, data from *Naip1-6*$^{fl/fl}$ mice). *Nlrc4* was expressed at ~10-fold higher levels in the cecal mucosa than in the mLN and around 100-fold higher than in the spleen (Figure 5A). Similar differences could be observed for the *Naip* transcripts. Especially *Naip1* was strongly expressed in the cecum, but ~100-fold reduced in the spleen (Figure 5B). The bulk of the cecal *Naip1, 2, 5,* and *6* expression was attributable to IECs, in agreement with earlier work by us and others (Sellin et al., 2014; Winsor et al., 2019) (Figure 5B-E, compare *Naip1-6*$^{fl/fl}$ with *Naip1-6*$^{\Delta/\Delta IEC}$). Interestingly, when we analyzed the liver as a non-barrier, non-lymphoid organ, we found that the expression levels of *Nlrc4* and *Naip1-6* were generally ~100-fold lower than in the cecal mucosa (Figure S6A-B, compare to Figure 5A-E). Hence, the cecal epithelium appears to be particularly loaded with NAIP/NLRC4 for detection of invading pathogens. This charging of non-immune cells with inflammasome receptors might be particularly pronounced in barrier tissues that are in close contact with microbes and engage actively in defense (Knodler et al., 2014; Nordlander et al., 2014; Rauch et al., 2017; Sellin et al., 2014; Tomalka et al., 2011).

In addition to the major epithelial *Naip* transcript pool, we noted a significant contribution from other cell types to the expression of the *Naip* genes in the cecal mucosa (Figure 5B-F, compare *Naip1-6*$^{\Delta/\Delta\ IEC}$ and *Naip1-6*$^{\Delta/\Delta}$ animals). From the available dataset we could not infer to what percentage various immune cells, fibroblasts, endothelium and/or other cell types contribute to this non-IEC expression. To specifically analyze the expression of *Naip/Nlrc4* in intestinal DCs – the cell type that has been reported to take up *S*. Tm in the cecal mucosa and transport it to the mLN (Bravo-Blas et al., 2019; Hapfelmeier et al., 2008) – we sorted intestinal DC subsets from wild type LPS-injected mice and PBS vehicle controls. Whereas *Nlrc4* was expressed equally in all intestinal DC subsets, CD103^{+} DCs expressed *Naip1* and *Naip2* at increased levels compared to other subsets (Figure S6C). The expression of these receptors was not boosted by exposure to the pro-inflammatory stimulus LPS. In fact, LPS-priming rather led to a downregulation of expression in some of the DC subsets, which might be explained by the immuno-tolerant phenotype of mucosal myeloid cells (Stagg, 2018). Additionally, this downregulation might represent a protective mechanism by which self-destruction of infected DCs is prevented to ensure antigen presentation.

Taken together, our data highlight that IECs express particularly high levels of *Naip* and *Nlrc4* transcripts, whereas DCs encountered by *S*. Tm subsequent to epithelial traversal and/or upon passive sampling appear to express more modest levels. Importantly though, the failure of DCs to restrict *S*. Tm dissemination through NAIP/NLRC4 *in vivo* cannot be explained by a complete lack of this inflammasome. However, the reduced expression levels (compared to IECs) might explain why *S*. Tm$^{\Delta 4}$ dissemination is not efficiently restricted by NAIP/NLRC4 (Figure 3).

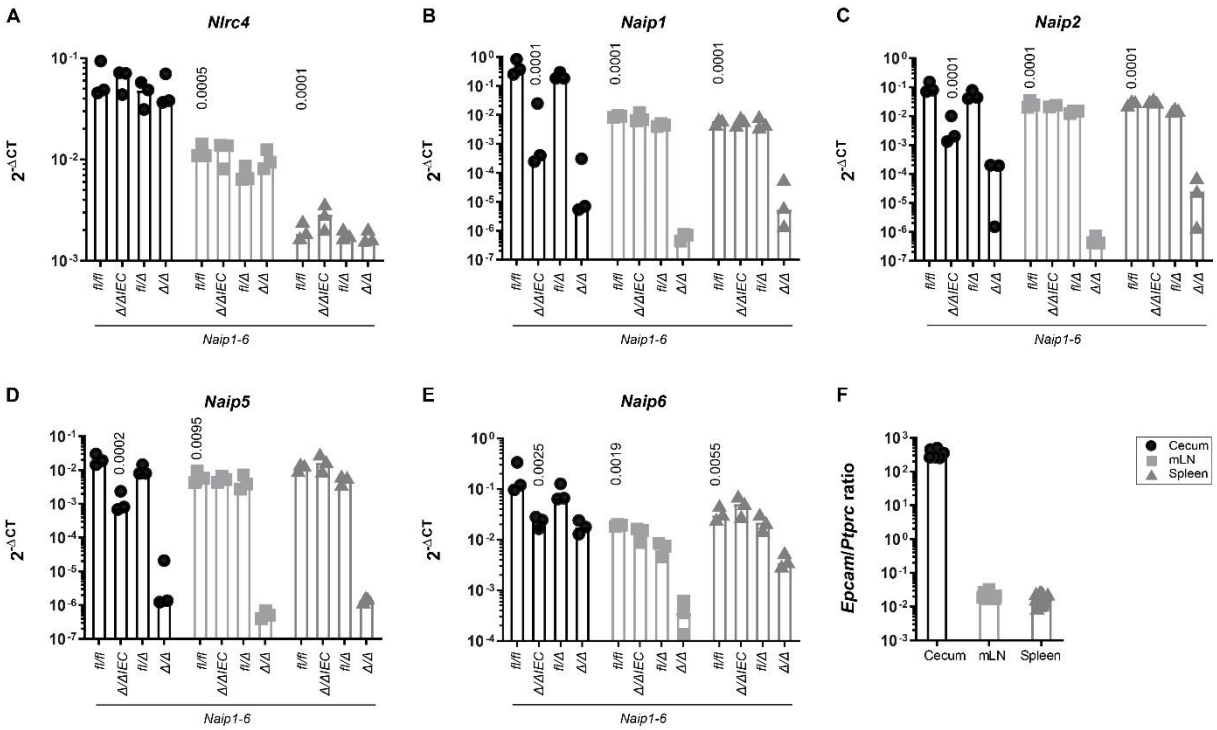

Figure 5 ***NAIP/NLRC4 inflammasome components are expressed in the cecal mucosa and in secondary lymphoid tissues. A*** Nlrc4*,* ***B*** Naip1*,* ***C*** Naip2*,* ***D*** Naip5 *and* ***E*** Naip6 *are expressed in the cecal mucosa, mLN and spleen. The cecal mucosa, and specifically IECs express high levels of Naip transcripts. Transcript levels of* Naip1-6$^{fl/fl}$, Naip1-6$^{\Delta/\Delta IEC}$, Naip1-6$^{\Delta/fl}$ *and* Naip1-6$^{\Delta/\Delta}$ *mice depicted as* $2^{-\Delta CT}$ *values. Expression levels were normalized to* Actb*.* ***F*** *For the samples depicted in A-E, expression levels of* Epcam *as an epithelial cell marker, and* Ptprc*, as a marker for immune cells, were compared to estimate the relative contribution of both cell types to the transcripts within the respective tissue. n=3, each symbol represents one mouse. Median plotted. Statistical analysis: two-way ANOVA with Tukey`s correction. Selected* p*-values indicated in comparison to levels in cecal tissue of* Naip1-6$^{fl/fl}$ *animals.*

S. TM EXPRESSES THE NAIP LIGAND STRUCTURES TTSS-1 AND FLAGELLA DURING IEC INVASION, BUT PROMPTLY DOWNREGULATES THEM UPON TRANSIT TO THE LAMINA PROPRIA AND SYSTEMIC TISSUES

S. Tm migration to systemic sites is potently restricted by IEC NAIP/NLRC4, but apparently not by phagocyte NAIP/NLRC4, even though both cell types express detectable levels of the required receptors (Figure 3-5; Figure S6C). One reason for this discrepancy might reside in the pathogen's gene expression program, which may prevent PAMP expression at certain sites. Such compartment-specific down regulation has been observed previously in various infection models (Brewer et al., 2019; Hong et al., 2018; Laughlin et al., 2014; Maldonado et al., 2016). *S*. Tm requires TTSS-1 and flagella (composed of flagellin subunits) for the initial colonization and establishment of gut infection (Hapfelmeier et al., 2005; Stecher et al., 2008). Especially for invasion of IECs, which strongly express *Naip1*, *2*, *5*, *6* and *Nlrc4* (Figure 5A-E), the NAIP ligand structures TTSS-1 (for the delivery of the effector proteins SipA, SopB, SopE, and SopE2) (Hapfelmeier et al., 2005; Müller et al., 2009) and flagella (to subvert gaps in the mucus layer and reach the epithelium by directed motility) (Furter et al., 2019; Stecher et al., 2008) are both crucial. This could explain why infection events are efficiently sensed and restricted specifically by IEC NAIP/NLRC4. However, it remained unclear to which extent *S*. Tm regulates TTSS-1 and flagella expression during and after epithelium traversal.

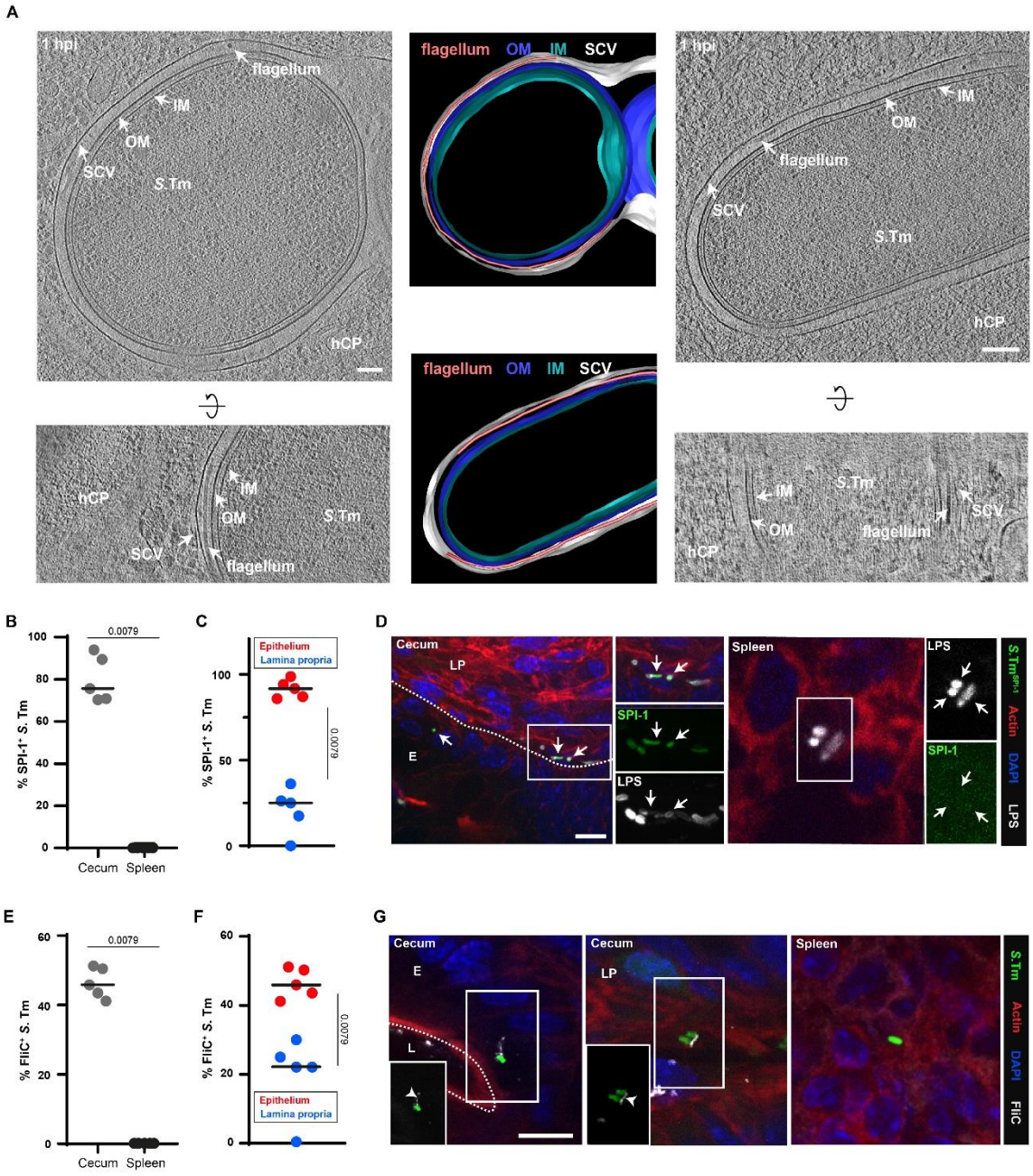

Figure 6 ***S. Tm expresses PAMPs recognized by NAIP/NLRC4 in the cecal epithelium, but downregulates them upon traversal****. **A** S. Tm with potentially detached (left/upper panel) and attached (right/lower panel) flagella can be found inside SCVs. Shown are 15 nm slices of cryotomograms of cryo-FIB milled HeLa cells and the respective segmentations (representative for six tomograms; frozen at 1 hpi and MOI 300). OM: outer membrane. IM: inner membrane. SCV:* Salmonella *containing vacuole. hCP: host cell cytoplasm. Scale bar, 100 nm. **B** S. Tm as a rule expresses SPI-1 in the cecum (12 hpi, $n^{total\ S.\ Tm}$=322) and downregulates the expression in the spleen (3 dpi, $n^{total\ S.\ Tm}$=35) of $JH^{-/-}$ mice. **C** The fraction of SPI-1^{+} S. Tm within the cecal mucosa decreases upon traversal to the lamina propria ($n^{total\ S.\ Tm\ epithelium}$=253; $n^{total\ S.\ Tm\ lamina\ propria}$=69). Quantifications shown in B and C are based on fluorescence microscopy of S. $Tm^{SPI\text{-}1\text{-}GFP}$ expressing cytoplasmic GFP under the prgH-promotor and an LPS immunostaining. **D** Representative images of tissue sections (cecum, spleen), which were used for the quantifications in B and C. **E** Flagella are prominent in the cecal mucosa (12 hpi, $n^{total\ S.\ Tm}$=341), while they are completely absent in the spleen (3 dpi, $n^{total\ S.\ Tm}$=50) of $JH^{-/-}$ mice. Quantifications were performed by fluorescence immunostaining of FliC. **F** Similar to SPI-1 (C) expression, flagella are less evident in the lamina propria ($n^{total\ S.\ Tm\ lamina\ propria}$=39) than within IECs ($n^{total\ S.\ Tm\ epithelium}$=302). **G** Representative images of tissue sections (cecum, spleen), which were used for the quantifications in E and F. White arrowheads: flagella; white*

arrows: SPI-1-GFP$^+$ S. Tm (epithelium and lamina propria); E: epithelium; L: lumen; LP: lamina propria. Black bar: Median. Statistical analysis: Mann-Whitney-U Test, p-values indicated. Scale bars, 10 µm.

To clarify this aspect, we assessed the expression of NAIP-activating *S*. Tm PAMPs during the infection process. Initially, we optimized staining procedures in *S*. Tm infections of cultured HeLa epithelial cells, a process that relies on TTSS-1 (TTSS-1-deficient mutants ~500-1000-fold attenuated) (Misselwitz et al., 2011) and flagella-driven motility (Stecher et al., 2008). While HeLa cells are clearly a simplistic test system riddled by genetic drift (Liu et al., 2019) they nevertheless provide an efficient test system for establishing microscopy analysis pipelines. Notably, when infected HeLa cells were immunostained for the flagella subunit FliC, we could detect a significant fraction of FliC$^+$ *S*. Tm also within the epithelial cells (Figure S7A). Notably, ~30 % of the bacteria still stained positive for FliC at 7 hpi (Figure S7B). This is in line with previous work (Knodler et al., 2010). These findings were supported by parallel analyses of infected HeLa cells using cryo-focused ion beam (cryo-FIB) milling and cryo-electron tomography (cryoET). Cryotomograms showed fully assembled flagella located between the bacterial surface and the membrane of the *Salmonella* containing vacuole (SCV) (Figure 6A).

Previous work has shown that a subfraction of *S*. Tm may escape the SCV over time and become cytosolic (Kreibich et al., 2015; Laughlin et al., 2014). When we analyzed the cytosolic subpopulation with the help of *S*. Tm^{localizer}, carrying a reporter for cytosolic escape (pCK100, glucose-6-phosphate (Glc6P)-driven expression of mCherry) (Cooper et al., 2017; Finn et al., 2017; Lau et al., 2019; Spinnenhirn et al., 2014), we found that at 7 hpi, around one quarter of all the cytosolic bacteria was FliC$^+$ (Figure S7B). Strikingly, we frequently detected bacteria with protruding flagella (Figure S7A, S7C). Cryotomograms, however, indicated a tight enclosure of both bacterium and flagellum within the SCV (Figure 6A). Indeed, cytosolic localization correlated with a protruding flagellum conformation (Figure S7C). These data suggest that in addition to the mandatory expression of TTSS-1, a significant fraction of *S*. Tm carry flagella within cultured epithelial cells, and maintain or re-express these during egress into the cytosol, which is in line with observations by Knodler et al. (Knodler et al., 2010). These cytosolic *S*. Tm carrying the flagellum might be a potent trigger of epithelial inflammasome activation.

Results from immortalized cell lines exhibit limited reproducibility to *in vivo* settings due to altered cell physiology and lack of tissue environment (Ben-David et al., 2018; Liu et al., 2019; Niepel et al., 2019). We therefor assessed if our observations also apply *in vivo* during IEC infection in the mouse model. We infected mice orally with *S*. Tm carrying a transcriptional reporter (*prgH-GFP*) for TTSS-1 expression (*S*. Tm$^{SPI\text{-}1\text{-}GFP}$) and analyzed the pathogen populations in the cecum tissue (12 hpi) and at systemic sites (spleen, 3 dpi to obtain sufficient bacterial loads). Fluorescence microscopy was used to assess TTSS-1 expression (i.e. *prgH-GFP*) and flagella expression (staining with anti-FliC antibodies). Around 80 % of the *S*. Tm lodged in IECs were SPI-1$^+$ (Figure 6B-D). This sharply contrasted to SPI-1 expression in the lamina propria (~20 % SPI-1$^+$ *S*. Tm) and the spleen (no detectable SPI-1 expression) (Figure 6B-D). In line with the tissue culture data above, ~50 % of the *S*. Tm lodged in the cecal epithelium also stained positive for FliC (Figure 6E-G). This population was increased two-fold in the absence of epithelial NAIP receptors (Figure S8A), which correlated with a significantly increased fraction of cytosolic bacteria, especially with regard to microcolonies consisting ≥4 bacterial cells, in *Nlrc4*$^{-/-}$ mice compared to *Nlrc4*$^{+/-}$ or wild type mice (Figure S8B). These observations are consistent with NLRC4/NAIP-dependent expulsion of IECs containing flagellated *S*. Tm. By contrast, we detected significantly less FliC$^+$ *S*. Tm in the lamina propria (Figure 6F-G) and no FliC$^+$ bacteria in the spleen (Figure 6E, 6G). It is currently not entirely clear if fully assembled flagella structures can activate the NAIP/NLRC4 inflammasome. Nevertheless, one can take the flagella as a proxy for the presence of flagellar subunits. Assuming that 90% of the lamina propria-lodged pathogens have reached this site by traversing the IECs (which necessitates the expression of PAMPs recognized by NAIP/NLRC4), our

data indicate that the pathogen promptly down regulates expression of both structures during transit, thereby evading recognition by phagocyte NAIP/NLRC4.

To formally test if PAMP down regulation explains *S*. Tm evasion of phagocyte NAIP/NLRC4-restriction, we analyzed the effect of forced PAMP expression. This strategy has been used in the past to assess the PAMP-specificity of individual inflammasomes (Miao et al., 2010). To this end, we infected *Nlrc4*$^{+/-}$ and *Nlrc4*$^{-/-}$ littermate mice iv with a 1:1 mix of *S*. Tm^{ECV} (*S*. Tm$^{\Delta flgB\ TAG13}$ (pZ2500); empty control vector) and *S*. Tm$^{fliC\text{ind}}$ (*S*. Tm$^{\Delta flgB\ TAG1}$ (pEM087); expression of FliC under a Doxycycline-inducible promoter (Jorgensen et al., 2016)). We induced FliC expression by iv Doxycycline administration at 17 hpi, a time point when most of the bacteria should be lodged within splenic phagocytes. In NLRC4 proficient hosts, splenic *S*. Tm$^{fliC\text{ind}}$ loads were ~10-fold lower than those of *S*. Tm^{ECV} by 24 hpi (Figure S9). Notably, this phenotype was not observed in *Nlrc4*$^{-/-}$ mice (Figure S9). Thus, splenic phagocytes are able to sense *S*. Tm via the NAIP/NLRC4 inflammasome, but *S*. Tm as a rule avoids recognition. This further supports that downregulation of PAMP expression upon traversal of the gut epithelium contributes to *S*. Tm evasion.

DISCUSSION

Earlier work has implicated NAIP/NLRC4 in host defense against *S*. Tm and related enteropathogens (Carvalho et al., 2012; Franchi et al., 2012; Lara-Tejero et al., 2006; Miao and Warren, 2010; Nordlander et al., 2014; Rauch et al., 2017; Sellin et al., 2014). Mice globally lacking key components of this inflammasome suffer from exacerbated systemic infection and higher pathogen loads in lymph nodes, spleen and liver upon oral inoculation (Broz et al., 2010; Carvalho et al., 2012; Franchi et al., 2012; Lara-Tejero et al., 2006; Rauch et al., 2017; Sellin et al., 2014). As mechanistic work on NAIP/NLRC4 signaling has focused on phagocytic cell types (Broz, 2019), and as *S*. Tm frequently lodge within such cells at extraintestinal locations (Grant et al., 2008), it has been assumed that phagocytes mediate protection of systemic organs via NAIP/NLRC4. In sharp contrast, our analysis proves phagocyte NAIP/NLRC4 to be dispensable for restriction of *S*. Tm migration to, and replication at, systemic sites (Figure 1, 3, 4, S5A) during early infection. This pertains also to an *S*. Tm strain that enters promptly into lamina propria phagocytes upon passive uptake of luminal bacteria (*S*. Tm$^{\Delta 4}$; Figure 3B-C). Instead, our data show that inflammasome defense against dissemination of different *S*. Tm strains from the gut relies specifically on intestinal epithelial NAIP/NLRC4 (Figure 3, S5), previously shown to drive the expulsion of infected IECs and restrict mucosal pathogen loads by >>50-fold during oral *S*. Tm or *Citrobacter rodentium* infection (Nordlander et al., 2014; Sellin et al., 2014). These results establish IEC NAIP/NLRC4 as the warden of not only the gut mucosa, but also of the systemic compartment, upon infection with a host-adapted pathogen.

The expression levels of *Naip* and *Nlrc4* transcripts are notably high in IECs, but also clearly detectable across systemic organs and mucosal tissue DCs (Figure 5, Figure S6). On top of this, the downregulation of NAIP-activating PAMPs within host tissues provides an explanation to the failure of phagocytes, but ability of IECs, to utilize NAIP/NLRC4 for combatting *S*. Tm *in vivo* (Figure 6, Figure S7-S8).

Following flagella- and TTSS-1-driven invasion of IECs, which by necessity exposes these PAMPs to epithelial NAIP receptors, *S*. Tm promptly downregulates expression of both structures, thereby preventing NAIP/NLRC4 activation beyond the epithelial barrier (Figure 6, Figure S8-S9) (Cummings et al., 2006). Other evasion mechanisms, e.g. SCV membrane shielding of PAMPs from the cytosolic NAIPs, and active interference by secreted virulence factors, might further dampen residual inflammasome activation in a cell-type specific manner (Chapter 1) (Bastedo et al., 2019). Also, it remains to be fully shown how polymerization into the flagellum affects the NAIP/NLRC4 triggering intensity of flagellin. Anyhow, the evasion of recognition is possibly already employed during IEC-

invasion, but may be hampered by high bacterial invasion rates and relatively long lifetimes of the bacterial proteins. Nevertheless, even when administered systemically, *S*. Tm is not recognized by phagocyte NAIP/NLRC4, except if expression of the flagella component FliC, a NAIP5-6 ligand, is artificially forced (Figure 4, Figure S9) (Miao et al., 2010). Therefore, while phagocytes at systemic sites would indeed be capable of pathogen restriction via NAIP/NLRC4 (Figure 5, Figure S9), our population dynamics data conclusively show that different *S*. Tm strains evade this defense. This is in stark contrast to less-well adapted bacteria, like *Chromobacterium violaceum*, which are vigorously restricted (>>1.000-fold in liver) by the NAIP/NLRC4 inflammasome in systemic organs (Maltez et al., 2015). Based on these observations, it is tempting to speculate that mechanisms for avoiding the NAIP/NLRC4 defense have contributed to the evolution of gene-regulatory circuits in host-adapted bacterial pathogens.

Other inflammasomes have previously been deemed protective during *S*. Tm infection in mice (Broz et al., 2010; Knodler et al., 2014; Man et al., 2014). However, under stringent littermate-controlled conditions, we here find that neither NLRP3, nor Caspase-11, impact *S*. Tm transmucosal migration or early systemic replication *in vivo*, at least in the Streptomycin pretreated mouse model (Figure 2). Caspase-11 can protect against systemic infection by bacteria colonizing the host cell's cytosol, e.g. *Burkholderia* spp. (Aachoui et al., 2013). Other intracellular pathogens, including *S*. Tm and *Legionella pneumophila* (*L. pn*), express virulence factors that stabilize the intracellular vacuole (Beuzón et al., 2000; Lau et al., 2019). Mutant *S*. Tm and *L. pn* strains lacking those factors breach the vacuolar membrane with higher frequency and are efficiently detected by Caspase-11 (Aachoui et al., 2013; Thurston et al., 2016). Our finding that Caspase-11 is dispensable for restriction of *S*. Tm dissemination/replication (Figure 2, Figure S3) agrees with these reports, supporting that wild type *S*. Tm evades Caspase-11 recognition after oral infection *in vivo*. Importantly, deletion of *Casp11* in *Nlrc4*$^{-/-}$ mice does not increase pathogen migration or systemic colonization (Figure 2, S3, 4). This refutes the possibility that a potent epithelial NAIP/NLRC4 response masks any effect of Caspase-11. Furthermore, *Casp1/11*$^{-/-}$ animals only partially recapitulate the elevated *S*. Tm dissemination of NAIP1-6 or NLRC4-deficient animals (Figure 2, S3, 4). This points to the potential involvement of also other Caspases, e.g. Caspase-8 (Rauch et al., 2017), in the execution of the IEC NAIP/NLRC4 response. The molecular wiring of this defense system will be an important topic for future work.

During acute infection, NLRP3 does not contribute to restriction of *S*. Tm infection neither in the gut mucosa (Figure 2, Figure S3), nor at systemic sites (Figure 4), not even in the absence of NLRC4 (Figure 2, S3, 4). This contrasts to previous reports in the literature (Broz et al., 2010; Man et al., 2014). We can only speculate about the origins of this discrepancy. Our results apply to different, widely used *S*. Tm strains (SL1344 and 14028), rendering the use of different strains an unlikely cause. It might be attributable to the huge impact of the intestinal microbiota on non-typhoidal *Salmonella* infection models, as well as to small differences in genetic backgrounds that have recently been revealed (Mamantopoulos et al., 2017, 2018; Robertson et al., 2019). These could have been confounding in experiments using separately bred wild type mice as controls rather than littermates. Again, the lack of an NLRP3-linked response may also be explained by efficient *S*. Tm evasion of this inflammasome (Wynosky-Dolfi et al., 2014). Furthermore, NLRP3 and/or Caspase-11 may serve some more specific function(s) during late-stages of a persistent infection or in hosts other than mice.

Taken together, our data extend previous work (Broz et al., 2010, 2012; Carvalho et al., 2012; De Jong et al., 2014; Lara-Tejero et al., 2006; Man et al., 2014, 2017; Monack et al., 2000; Rauch et al., 2017; Sellin et al., 2014; Thurston et al., 2016), highlight that *in vivo* studies of host–pathogen interactions are highly sensitive to the experimental conditions, and may be subject to confounding effects that limit reproducibility. The general approach presented here – a combination of littermate controlled infections, host cell type-specific gene knockouts, genetically tagged bacterial consortia, mathematical modelling and high-resolution imaging of the infected cells/organs– allowed us to decipher the impact of specific host responses *in vivo*. Here, this led us to refute a protective function for phagocyte

inflammasome defense and to uncover intestinal epithelial NAIP/NLRC4 as a firewall preventing systemic dissemination of the orally acquired adapted pathogen *S*. Tm. We expect the same approach to be powerful for (re-) assessing also the impact of other barriers during the step-wise progression of infectious disease, with extension to other pathogens.

ACKNOWLEDGEMENTS

We are thankful to the members of the Hardt, Sellin, Slack and Pilhofer labs for discussions and input, and to the staff of the RCHCI and EPIC animal facilities for their support. We would like to thank Edward Miao at the Department of Microbiology and Immunology, University of Carolina, USA for providing the pEM087 plasmid and Otto Holst at the Division of Structural Biochemistry at the Research Center Borstel, Germany for providing ultrapure LPS. WDH was supported by the Swiss National Science Foundation (SNF) (310030_53074 and 310030B_173338/1; Sinergia CRSII_154414/1), and the Promedica Foundation, Chur. MES was supported by the Swedish Research Council (2015-00635, 2018-02223) and the Swedish Foundation for Strategical Research (ICA16-0031). MP was supported by the SNF (164092), and the European Research Council (679209). RRR acknowledges financial support from SNF (31003A_179170). ES acknowledges funding from Gebert Rüf Microbials GRS17_93, and the SNF (310030_185128 and 20B2-1_180953). IK was funded by a postdoctoral Research Fellowship of the Deutsche Forschungsgemeinschaft.

METHODS

Salmonella strains and growth conditions

Strains used in this study are *S*. Tm SL1344 (SB300, Streptomycin resistant), or derivatives thereof, except for *S*. Tm^{14028} (Diard et al., 2017) and $WITS^{14028}$. *S*. $Tm^{\Delta 4}$ lacks four TTSS-1 effector proteins (*sipA*, *sopB*, *sopE*, *sopE2*), but still expresses the TTSS-1 secretion apparatus, and was described previously (Ehrbar et al., 2003). The tags for the WITS strains as described in (Grant et al., 2008), were introduced by P22 phage transduction. We used *S*. Tm carrying pM975 (*S*. $Tm^{SPI\text{-}2\text{-}GFP}$) (Hapfelmeier et al., 2005) as a reporter for SPI-2 expression (*S*. $Tm^{SPI\text{-}2}$, within the SCV), *S*. Tm expressing GFP under a *prgH*-promotor (JH3010, *S*. $Tm^{SPI\text{-}1\text{-}GFP}$) to mark SPI-1 expressing bacteria (*S*. $Tm^{SPI\text{-}1}$), *S*. Tm carrying pCK100 (Glc6P-driven mCherry expression, *S*. $Tm^{Glc6P\text{-}mCherry}$)) as a reporter for cytosolic bacteria (*S*. Tm^{Glc6P}) and *S*. $Tm^{localizer}$ expressing GFP under the *ssaG* promotor (JH3009) and carrying pCK100 to track SCV/cytosolic localization of *S*. Tm. pCK100 was constructed as follows: A 137 bp genomic fragment immediately upstream of the *uhpT* gene in *Shigella flexneri* 2a 2457T (GenBank: AE014073.1, 3869168...3869032) was cloned upstream of the ribosomal binding site of phage T7 gene 10 and mCherry on a pSC101 backbone. *S.* Tm carrying this plasmid showed induced red fluorescence when cultured in presence of Glc6P but not in presence of glucose. As Glc6P is specifically present in the host cell cytosol, this is a reporter plasmid for cytosolic localization, as described previously for *Shigella flexneri* (Runyen-Janecky and Payne, 2002). *S*. $Tm^{\Delta fliGHI}$ carrying pM975 (*pssa*G-GFPmut2) was used as a control for specificity of the FliC staining. *S*. $Tm^{fliCind}$ was generated by electroporation of the plasmid pEM087 (Jorgensen et al., 2016) into *S*. $Tm^{\Delta flgB}$. *S*. $Tm^{\Delta flgB}$ carrying an empty control plasmid was used as "wild type" control in the respective experiment (*S*. Tm^{ECV}, Figure S7). Genetic barcodes were introduced by P22 phage transduction into *S*. $Tm^{fliCind}$ and *S*. Tm^{ECV} for relative quantification of the abundance of the two strains during competitive infection. See Table 1 for further information. For oral and HeLa cell infections, *S*. Tm was grown overnight at 37°C in LB/0.3M NaCl and sucultured for four hours at a dilution of 1:20. For iv infections, *S*. Tm was grown overnight in LB/0.3M NaCl.

Tissue culture and infections

HeLa CCL-2 cells (ATCC) were grown in DMEM (Gibco) supplemented with 10% inactivated FCS (Thermo Fischer) and 50 µg/mL streptomycin (AppliChem) at 37°C and 5% CO_2. For immunofluorescence experiments, 80.000 HeLa cells were seeded in 24-well plates (Nunc, Thermo Fisher) containing glass cover slips 24 h prior to infection. Cells were infected with *S*. Tm$^{SPI\text{-}2\text{-}GFP}$ at an estimated MOI of 300, *S*. Tm^{localizer} at an estimated MOI of 300, and *S*. Tm$^{\Delta fliGHI}$ (p*ssaG*-GFPmut2) at an estimated MOI of 1000 for 14 mpi, 1 hpi, 3 hpi, 5 hpi and 7 hpi (*S*. Tm$^{SPI\text{-}2\text{-}GFP}$, *S*. Tm^{localizer}) and 14 mpi and 1 hpi (*S*. Tm$^{\Delta fliGHI}$(p*ssaG*-GFPmut2)). After 20 min, infected HeLa cells were washed three times with DMEM/10% FCS and incubated with DMEM/10% FCS containing 400 µg/mL gentamicin to prevent further infection. For electron microscopy (EM) imaging experiments, EM finder grids (gold NH2 R2/2, Quantifoil) were sterilized under UV light and then glow discharged. Grids were placed on the bottom of the wells of a 12-well plate (Nunc, Thermo Fisher) and equilibrated with DMEM for 30 min. Subsequently, 30.000 HeLa cells were seeded into each well (containing one grid each) and incubated overnight. Cells were infected with *S*. Tm$^{SPI\text{-}2\text{-}GFP}$ at an estimated MOI of 300 for 1 h as described above. Grids were washed twice with HBSS before vitrification.

Mice and infections

All studies were performed in accordance with ethical and legal requirements and were approved by the Kantonales Veterinäramt Zürich under the licenses 222/2013 and 193/2016. Mice were kept under specific pathogen-free conditions in individually ventilated cages (EPIC and RCHCI, ETH Zürich). All knockout mouse lines presented here have a C57BL/6 background, *Naip1-6*$^{-/-}$, *Naip1-6*$^{\Delta IEC}$ and *Naip1-6*$^{\Delta CD11c}$ have a C57BL/6J background, *Nlrc4*$^{-/-}$ mice a C57BL/6NJ background. *S*. Tm infections were performed as described before (Barthel et al., 2003) on 8-12 week old mice. Cohoused, heterozygous littermates were used as controls in all infections. Control mice for Figure S8B were supplemented with unrelated wild type mice (*Nlrc4*$^{+/+}$). For oral infection, mice were pretreated orally with 25 mg Streptomycin or 10 mg Kanamycin (for *S*. Tm^{14028}) 24 h prior to infection. Infection was performed by intragastrical inoculation with $5x10^7$ bacteria in 50 µl PBS. For WITS infections, the WITS strains (Kanamycin resistant) were diluted 1:140 (for wild type *S*. Tm) or 1:21 (for *S*. Tm$^{\Delta 4}$) in the respective untagged *S*. Tm strain. For iv infection, 10^4 *S*. Tm in 100 µl PBS were injected into the tail vein. For WITS iv infections, WITS strains (Kanamycin resistant) were diluted 1:700 in untagged wild type *S*. Tm. The infection with *S*. Tm^{fliCind} was performed by iv injection of 10^4 CFU in a 1:1 mix of *S*. Tm^{fliCind} and *S*. Tm^{ECV}. Both strains showed equal growth *in vitro* (data not shown). At 17 hpi, 0.8 mg Doxycycline in 100 µl PBS was administered iv for induction of FliC expression. At 24 hpi, mice were euthanized and organs and cecal content were collected, homogenized, and plated on MacConkey Agar (Oxoid) containing the respective antibiotics for enumeration of bacterial counts in the respective tissue. For competitive infections, relative abundance of the two competitors in the tissue of interest was assessed by quantitative real-time PCR (qPCR) with the help of neutral genetic tags as described below.

LPS injections and sorting of intestinal DCs

Mice were iv injected with 5 µg ultrapure *S*. Tm LPS (Otto Holst) in 100 µl PBS, or 100 µl PBS as control. 1h post injection, mice were euthanized and cecae were excised. Cecum tissue was washed extensively with PBS, cut into small pieces and incubated twice for 20 min at 37°C shaking in 13 ml PBS supplemented with 5 mM EDTA (Life Technologies), 15 mM HEPES (Life Technologies) and 10% heat-inactivated FBS (Life Technologies). Tissue pieces were washed in 7 ml RPMI 1640 (Life Technologies)/30% FBS and subsequently incubated for 1h at 37°C shaking in 900 µl RPMI containing

0.2 mg/ml DNase I (Roche) and 1 mg/ml collagenase VIII (Sigma). Digested material was mashed through a 70 µm cell strainer and washed with 10 ml RPMI. After washing, cells were resuspended in 6 ml RPMI, carefully loaded onto 3 ml NycoPrep 1.077 and centrifuged for 30 min at 400 g (room temperature). The interphase fraction was collected (~2 ml), washed in 6 ml RPMI containing 15% FBS, and subsequently stained for fluorescent activated cell sorting (FACS). Cells from three mice were pooled per sample for sorting. The following antibodies were used for staining of intestinal DCs: CD45-PerCP (Biolegend, 30-F11, 1:100), MHCII-APC (Biolegend, M5/114.15.2, 1:400), CD103-PE (Biolegend, 2E7, 1:100), CD11b-BV605 (Biolegend, M1/70, 1:200), CD11c-PE/Cy7 (Biolegend, N418, 1:200), Sytox-blue (Invitrogen, 1:1000). Intestinal DCs were sorted for $CD45^+$ $MHCII^{hi}$ $CD11c^{hi}$ live cells and differentiated into $CD103^+$ $CD11b^-$, $CD103^-$ $CD11b^+$, $CD103^+$ $CD11b^+$ and $CD103^-$ $CD11b^-$ populations. Cells were FACS sorted with a BD FACSAria III sorter into 50 µl RNAlater (Sigma) and flash frozen in liquid nitrogen.

WITS quantification

WITS-tagged *S*. Tm from mLN (oral infection) or spleen (iv infection) homogenate were specifically enriched in 3 ml LB supplemented with 50 µg/ml Kanamycin overnight. Bacterial DNA was isolated from enrichment cultures (Qiagen QIAamp DNA Mini Kit) and subsequently analyzed on a StepOne Plus Cycler (Thermo Fisher), using FastStart Universal SYBR Green Master (Rox) reagents (Roche) and primers as described before (Grant et al., 2008). Total abundance of the WITS strains was assessed by integrating their relative distribution analyzed by qPCR with total bacterial CFU obtained through plating.

Population dynamics analysis

Population dynamics were analyzed with a previously published model (Kaiser et al., 2013), based on total WITS counts in the organ of interest of each mouse. This method was developed for the estimation of the migration rate μ from the gut lumen to the mLN and the replication rate r within the mLN during oral *S*. Tm infection, and was directly used for the estimates of the oral infection experiments (Figure 1-3, S5). We applied the same method to estimate the migration rate μ from the blood to and the replication rate r within the spleen for the iv infection experiments (Figure 4). We note that the interpretation of the migration rate estimate for this application of the model differs from the original application. The migration is assumed to be constant over time in the model, however, previous research has shown that the number of bacteria in the blood exponentially decreases for iv inoculation (Coward et al., 2014). Therefore, the migration we estimate to occur with a constant rate over one day, might have migrated only within the first few hours after inoculation. However, because we are not primarily interested in the migration rates themselves but rather the differences in migration rates between wild type and knockout mice, this interpretational subtlety does not confound our conclusions. Calculations were performed with R Studio, R version 3.6.0.

Gene expression analysis

For gene expression analysis, tissue was snap frozen in RNAlater (Sigma-Aldrich). RNA isolation was performed with the Qiagen RNeasy Mini Kit according to the manufacturer`s instructions, including DNase digestion. For sorted intestinal DCs, RNA isolation was performed with the Qiagen RNeasy Micro Kit after cell lysis with the QIAShredder Kit (Qiagen) according to the manufacturer`s instructions. 1 µg of isolated RNA was subsequently transcribed into cDNA using the Qiagen RT2 HT First Strand cDNA Kit, and stored at -20°C until analysis. qPCR was performed with FastStart Universal

SYBR Green Master (Rox) reagents (Roche) on a StepOne Plus Cycler (Thermo Fischer). mRNA levels were normalized to *Actb* and calculated with the $2^{-\Delta CT}$-method. Primers for the indicated genes were purchased from Qiagen (RT2 qPCR Primer Assay).

Histopathology

For the assessment of histopathology, cecal tissue was snap-frozen in OCT (Tissue-Tek) and stored at -80°C. 5 µm sections were cut from the tissue and stained with hematoxylin and eosin as described before (Barthel et al., 2003). Tissue pathology was scored according to the extent of submucosal edema, epithelial integrity, goblet cell loss and infiltration of polymorphonuclear neutrophils (PMNs) into the lamina propria.

Fluorescence microscopy

Infected HeLa cells were fixed with 4% Paraformaldehyde (Sigma-Aldrich) for 15 min (room temperature) and subsequently permeabilized with 0.1% Triton X-100 for 5 min (room temperature). Afterwards cells were washed twice with 4% sucrose and incubated in 20% sucrose for 20 min. Next, cells were incubated with blocking buffer for 1h (3% bovine serum albumin, BSA; 3% sucrose in DPBS) before staining with the respective primary antibodies (rabbit-αLPS, Difco™ *Salmonella* O Antiserum, 1:200; mouse-αFliC, Abcam, 1:300) for 1h. After three washes with PBS samples were incubated with secondary antibodies (goat-αmouse IgG Cy5; goat-αrabbit IgG Alexa Fluor 405; 1:600, Thermo Fischer) for 1h. Finally, samples were washed three times with PBS and mounted on microscope slides with 5 µL Mowiol. For immunofluorescence staining of infected organs, cecal tissue and spleens of infected mice were fixed in 4% Paraformaldehyde (Sigma-Aldrich) for 4h at 4°C, dehydrated in 20% sucrose for 4h at 4°C, embedded in OCT (Tissue-Tek), flash frozen and stored at -80°C. For detection of flagellated intracellular *S*. Tm, 20 µm sections of cecal mucosa and spleen were prepared. After rehydration (PBS, 1 min), sections were permeabilized with 0.5% Triton X-100 for 5 min (room temperature). Next, samples were incubated in blocking buffer (10% normal goat serum, Reactolab) for 30 min. Sections from *JH*$^{-/-}$ mice were stained for 40 min (room temperature) using a mouse-αFliC antibody (Abcam, 1:300). Sections from *Naip1-6*$^{\Delta/\Delta IEC}$ knockout mice were incubated with a FliC-Cy3-conjugated antibody (1:300; Cy3® Fast Conjugation Kit Abcam; ab188287). After three washes with PBS, samples were stained for 40 min (αmouse IgG-Cy3, 1:200; Phalloidin-A647, 1:200; DAPI, 1:1000; Thermo Fischer). Finally, samples were washed three times with PBS and a coverslip was mounted on the microscope slide with 15 µL Mowiol. Image acquisition was performed with a Nikon Eclipse T1 (inverse) microscope equipped with a Yokogawa CSU-W1-T2 spinning-disk confocal unit (Visitron), a sCMOS camera (Orca Flash 4.0 V2) and a 100x oil objective (PLAN Apochromat, NA 1.49). All data were analyzed in Fiji (Schindelin et al., 2012).

Preparation of frozen-hydrated specimens

Plunge freezing was performed as previously described (Weiss et al., 2017). Briefly, grids containing infected HeLa cells, were removed from the wells using tweezers. The forceps were then mounted in the Vitrobot chamber and the grid was blotted from the backside by installing a Teflon sheet on one of the blotting pads. Grids were plunge-frozen in liquid ethane-propane (37%/63%) using a Vitrobot (Thermo Fisher) and stored in liquid nitrogen (Medeiros et al., 2018).

Cryo-focused ion beam milling

Cryo-focused ion beam (cryoFIB) milling was used to prepare samples of plunge-frozen infected HeLa cells that could then be imaged by cryo-electron tomography (Marko and Hsieh, 2007). Frozen grids with infected HeLa cells were prepared and processed as previously described (Medeiros et al., 2018). Briefly, lamellae were milled in several steps in a Helios NanoLab600i dual beam FIB/SEM instrument (Thermo Fisher). In a first step, two rectangular regions were used to generate a lamella with ~2 µm thickness with the ion beam set to 30 kV and ~400 pA. The current of the ion beam was then gradually reduced until the lamella reached a nominal thickness of ~250 nm (ion beam set to ~25 pA). The stage temperature was maintained below -154°C during loading, milling and unloading procedures. CryoFIB-processed grids were unloaded and stored in liquid nitrogen until further use.

Cryo-electron microscopy and cryo-electron tomography

CryoFIB processed infected HeLa cells were examined by cryo-electron microscopy (cryoEM) and cryo-electron tomography (cryoET) (Medeiros et al., 2018; Weiss et al., 2017). Images were recorded on a Titan Krios TEM (Thermo Fisher) equipped with a Quantum LS imaging filter and K2 Summit (Gatan). The microscope was operated at 300kV and the imaging filter was set to a 20 eV slit width. The pixel size at the specimen level was 5.42 Å. Tilt series covered an angular range from -60° to +60° with 2° increments and -8 µm defocus. The total dose of a tilt series was 120 $e^-/Å^2$. Tilt series and 2D projection images were acquired automatically using SerialEM (Mastronarde, 2005). Three-dimensional reconstructions and segmentations were generated using the IMOD program suite (Mastronarde, 2008).

Disclosure

The authors state no conflicts of interest.

Table 1: Strains used in this study. *Sm = Streptomycin. Km = Kanamycin. Cm = Chloramphenicol. Amp = Ampicillin. Tet = Tetracycline.*

Strain name in manuscript	Strain number	Relevant genotypes	Comment	Resistances	Reference
SL1344	SB300	wild type	Referred to as *S.* Tm	Sm	(Hoiseth and Stocker, 1981)
SB300^{TAG1}	M3147	*Tag1-aphT*	Collectively referred to as WITS	Sm, Km	(Kaiser et al., 2013)
SB300^{TAG2}	M3148	*Tag2-aphT*		Sm, Km	
SB300^{TAG11}	M3149	*Tag11-aphT*		Sm, Km	
SB300^{TAG13}	M3150	*Tag13-aphT*		Sm, Km	
SB300^{TAG17}	M3151	*Tag17-aphT*		Sm, Km	
SB300^{TAG19}	M3152	*Tag19-aphT*		Sm, Km	
SB300^{TAG21}	M3153	*Tag21-aphT*		Sm, Km	
S. Tm$^{\Delta4}$	M566	*ΔsipAsopBsopEsopE2*	IEC invasion-deficient mutant	Sm	(Ehrbar et al., 2003)
S. Tm$^{\Delta4\ TAG1}$	Z2557	*ΔsipAsopBsopEsopE2, Tag1-aphT*	Collectively referred to as WITS$^{\Delta4}$	Sm, Km	This study
S. Tm$^{\Delta4\ TAG2}$	Z2558	*ΔsipAsopBsopEsopE2, Tag2-aphT*		Sm, Km	This study
S. Tm$^{\Delta4\ TAG11}$	Z2559	*ΔsipAsopBsopEsopE2, Tag11-aphT*		Sm, Km	This study
S. Tm$^{\Delta4\ TAG13}$	Z2560	*ΔsipAsopBsopEsopE2, Tag13-aphT*		Sm, Km	This study
S. Tm$^{\Delta4\ TAG17}$	Z2561	*ΔsipAsopBsopEsopE2, Tag17-aphT*		Sm, Km	This study
S. Tm$^{\Delta4\ TAG19}$	Z2562	*ΔsipAsopBsopEsopE2, Tag19-aphT*		Sm, Km	This study
S. Tm$^{\Delta4\ TAG21}$	Z2563	*ΔsipAsopBsopEsopE2, Tag21-aphT*		Sm, Km	This study
S. Tm$^{SPI\text{-}2\text{-}GFP}$	SB300	p*ssaG-GFPmut2*	p*ssaG-GFPmut2* (pM975): expression of GFPmut2 under *ssaG* (SPI-2) promotor, which is active inside the SCV (*S.* Tm$^{SPI\text{-}2}$)	Sm, Amp	(Hapfelmeier et al., 2005)
S. Tm$^{SPI\text{-}1\text{-}GFP}$	Z1404	*prgH-GFP*	SPI-1 regulated expression of GFP (*S.* Tm$^{SPI\text{-}1}$)	Sm, Cm	(Hautefort et al., 2003)
S. Tm^{localizer}	Z1440	*ssaG-GFP* p*uhpT-mCherry*	p*uhpT-mCherry* (pCK100/pZ1400): Glc6P induced mCherry expression as a reporter for cytosolic localization (*S.* Tm^{Glc6P}). Additionally, this strain contains an	Sm, Amp, Cm	This study

			ssaG-driven GFP reporter for SCV localization (*S.* Tm^{SPI-2})		
S. $Tm^{Glc6p-mCherry}$	Z1439	p*uhpT-mCherry*	p*uhpT-mCherry* (pCK100/pZ1400): Glc6P induced mCherry expression as a reporter for cytosolic localization (*S.* Tm^{Glc6P}).	Sm, Amp	This study
S. $Tm^{\Delta fliGHI}$	M913	*ΔfliGHI* p*ssaG-GFPmut2*	Flagella-deficient mutant. Also contains p*ssaG-GFPmut2* (pM975): expression of GFPmut2 under *ssaG* (SPI-2) promotor, which is active inside the SCV (*S.* Tm^{SPI-2})	Sm, Amp, Tet	(Stecher et al., 2004)
S. $Tm^{fliCind}$	Z2500	Δ*flgB, Tag1-aphT* pEM087	Flagella-deficient mutant. Also contains pEM087: Doxycycline inducible expression of FliC	Sm, Cm, Amp, Tet, Km	(Jorgensen et al., 2016)
S. Tm^{ECV}	Z2530	Δ*flgB, Tag13-aphT* pZ2500	Flagella-deficient mutant. Also contains pZ2500: Empty control vector for pEM087 carrying a Tet (Doxycycline) resistance cassette	Sm, Cm, Amp, Tet, Km	(Jorgensen et al., 2016)
14028	M3168	*lpfED::aphT*	Referred to as *S.* Tm^{14028}	Km	(Diard et al., 2017)
14028^{TAG1}	Z6708	*lpfED::aphT*, *Tag1-cat*	Collectively referred to as $WITS^{14028}$	Km, Cm	This study
14028^{TAG2}	Z6709	*lpfED::aphT*, *Tag2-cat*		Km, Cm	This study
14028^{TAG11}	Z6710	*lpfED::aphT*, *Tag11-cat*		Km, Cm	This study
14028^{TAG13}	Z6711	*lpfED::aphT*, *Tag13-cat*		Km, Cm	This study
14028^{TAG17}	Z6712	*lpfED::aphT*, *Tag17-cat*		Km, Cm	This study
14028^{TAG19}	Z6713	*lpfED::aphT*, *Tag19-cat*		Km, Cm	This study
14028^{TAG21}	Z6714	*lpfED::aphT*, *Tag21-cat*		Km, Cm	This study

REFERENCES

Aachoui, Y., Leaf, I.A., Hagar, J.A., Fontana, M.F., Campos, C.G., Zak, D.E., Tan, M.H., Cotter, P.A., Vance, R.E., Aderem, A., et al. (2013). Caspase-11 protects against bacteria that escape the vacuole. Science *339*, 975–978.

Allam, R., Maillard, M.H., Tardivel, A., Chennupati, V., Bega, H., Yu, C.W., Velin, D., Schneider, P., and Maslowski, K.M. (2015). Epithelial NAIPs protect against colonic tumorigenesis. J. Exp. Med. *212*, 369–383.

Barthel, M., Hapfelmeier, S., Quintanilla-Martínez, L., Kremer, M., Rohde, M., Hogardt, M., Pfeffer, K., Rüssmann, H., and Hardt, W.-D. (2003). Pretreatment of Mice with Streptomycin Provides a Salmonella enterica Serovar Typhimurium Colitis Model That Allows Analysis of Both Pathogen and Host. Infect Immun *71*, 2839–2858.

Bastedo, D.P., Lo, T., Laflamme, B., Desveaux, D., and Guttman, D.S. (2019). Diversity and Evolution of Type III Secreted Effectors: A Case Study of Three Families. Curr. Top. Microbiol. Immunol.

Ben-David, U., Siranosian, B., Ha, G., Tang, H., Oren, Y., Hinohara, K., Strathdee, C.A., Dempster, J., Lyons, N.J., Burns, R., et al. (2018). Genetic and transcriptional evolution alters cancer cell line drug response. Nature *560*, 325–330.

Beuzón, C.R., Méresse, S., Unsworth, K.E., Ruíz-Albert, J., Garvis, S., Waterman, S.R., Ryder, T.A., Boucrot, E., and Holden, D.W. (2000). Salmonella maintains the integrity of its intracellular vacuole through the action of SifA. EMBO J. *19*, 3235–3249.

Birchenough, G.M.H., Nyström, E.E.L., Johansson, M.E.V., and Hansson, G.C. (2016). A sentinel goblet cell guards the colonic crypt by triggering Nlrp6-dependent Muc2 secretion. Science *352*, 1535–1542.

Brandl, K., Plitas, G., Schnabl, B., DeMatteo, R.P., and Pamer, E.G. (2007). MyD88-mediated signals induce the bactericidal lectin RegIII gamma and protect mice against intestinal Listeria monocytogenes infection. J. Exp. Med. *204*, 1891–1900.

Bravo-Blas, A., Utriainen, L., Clay, S.L., Kästele, V., Cerovic, V., Cunningham, A.F., Henderson, I.R., Wall, D.M., and Milling, S.W.F. (2019). Salmonella enterica Serovar Typhimurium Travels to Mesenteric Lymph Nodes Both with Host Cells and Autonomously. J. Immunol. *202*, 260–267.

Brewer, S.M., Brubaker, S.W., and Monack, D.M. (2019). Host inflammasome defense mechanisms and bacterial pathogen evasion strategies. Current Opinion in Immunology *60*, 63–70.

Broz, P. (2019). Recognition of Intracellular Bacteria by Inflammasomes. Microbiol Spectr *7*.

Broz, P., Newton, K., Lamkanfi, M., Mariathasan, S., Dixit, V.M., and Monack, D.M. (2010). Redundant roles for inflammasome receptors NLRP3 and NLRC4 in host defense against Salmonella. J. Exp. Med. *207*, 1745–1755.

Broz, P., Ruby, T., Belhocine, K., Bouley, D.M., Kayagaki, N., Dixit, V.M., and Monack, D.M. (2012). Caspase-11 increases susceptibility to Salmonella infection in the absence of caspase-1. Nature *490*, 288–291.

Carvalho, F.A., Nalbantoglu, I., Aitken, J.D., Uchiyama, R., Su, Y., Doho, G.H., Vijay-Kumar, M., and Gewirtz, A.T. (2012). Cytosolic flagellin receptor NLRC4 protects mice against mucosal and systemic challenges. Mucosal Immunol *5*, 288–298.

Conlan, J.W. (1997). Critical roles of neutrophils in host defense against experimental systemic infections of mice by Listeria monocytogenes, Salmonella typhimurium, and Yersinia enterocolitica. Infect. Immun. *65*, 630–635.

Cooper, K.G., Chong, A., Starr, T., Finn, C.E., and Steele-Mortimer, O. (2017). Predictable, Tunable Protein Production in Salmonella for Studying Host-Pathogen Interactions. Front Cell Infect Microbiol *7*.

Coward, C., Restif, O., Dybowski, R., Grant, A.J., Maskell, D.J., and Mastroeni, P. (2014). The effects of vaccination and immunity on bacterial infection dynamics in vivo. PLoS Pathog. *10*, e1004359.

Cummings, L.A., Wilkerson, W.D., Bergsbaken, T., and Cookson, B.T. (2006). In vivo, fliC expression by Salmonella enterica serovar Typhimurium is heterogeneous, regulated by ClpX, and anatomically restricted. Mol. Microbiol. *61*, 795–809.

De Jong, H.K., Koh, G.C.K.W., van Lieshout, M.H.P., Roelofs, J.J.T.H., van Dissel, J.T., van der Poll, T., and Wiersinga, W.J. (2014). Limited role for ASC and NLRP3 during in vivo Salmonella Typhimurium infection. BMC Immunol. *15*, 30.

Diamond, C.E., Leong, K.W.K., Vacca, M., Rivers-Auty, J., Brough, D., and Mortellaro, A. (2017). Salmonella typhimurium-induced IL-1 release from primary human monocytes requires NLRP3 and can occur in the absence of pyroptosis. Sci Rep *7*, 6861.

Diard, M., Bakkeren, E., Cornuault, J.K., Moor, K., Hausmann, A., Sellin, M.E., Loverdo, C., Aertsen, A., Ackermann, M., Paepe, M.D., et al. (2017). Inflammation boosts bacteriophage transfer between Salmonella spp. Science *355*, 1211–1215.

Diehl, G.E., Longman, R.S., Zhang, J.-X., Breart, B., Galan, C., Cuesta, A., Schwab, S.R., and Littman, D.R. (2013). Microbiota restricts trafficking of bacteria to mesenteric lymph nodes by CX(3)CR1(hi) cells. Nature *494*, 116–120.

Ehrbar, K., Friebel, A., Miller, S.I., and Hardt, W.-D. (2003). Role of the Salmonella pathogenicity island 1 (SPI-1) protein InvB in type III secretion of SopE and SopE2, two Salmonella effector proteins encoded outside of SPI-1. J. Bacteriol. *185*, 6950–6967.

Felmy, B., Songhet, P., Slack, E.M.C., Müller, A.J., Kremer, M., Van Maele, L., Cayet, D., Heikenwalder, M., Sirard, J.-C., and Hardt, W.-D. (2013). NADPH oxidase deficient mice develop colitis and bacteremia upon infection with normally avirulent, TTSS-1- and TTSS-2-deficient Salmonella Typhimurium. PLoS ONE *8*, e77204.

Finn, C.E., Chong, A., Cooper, K.G., Starr, T., and Steele-Mortimer, O. (2017). A second wave of Salmonella T3SS1 activity prolongs the lifespan of infected epithelial cells. PLOS Pathogens *13*, e1006354.

Franchi, L., Amer, A., Body-Malapel, M., Kanneganti, T.-D., Özören, N., Jagirdar, R., Inohara, N., Vandenabeele, P., Bertin, J., Coyle, A., et al. (2006). Cytosolic flagellin requires Ipaf for activation of caspase-1 and interleukin 1β in salmonella-infected macrophages. Nat Immunol *7*, 576–582.

Franchi, L., Kamada, N., Nakamura, Y., Burberry, A., Kuffa, P., Suzuki, S., Shaw, M.H., Kim, Y.-G., and Núñez, G. (2012). NLRC4-driven production of IL-1β discriminates between pathogenic and commensal bacteria and promotes host intestinal defense. Nat. Immunol. *13*, 449–456.

Furter, M., Sellin, M.E., Hansson, G.C., and Hardt, W.-D. (2019). Mucus Architecture and Near-Surface Swimming Affect Distinct Salmonella Typhimurium Infection Patterns along the Murine Intestinal Tract. Cell Rep *27*, 2665-2678.e3.

Galán, J.E., and Curtiss, R. (1989). Cloning and molecular characterization of genes whose products allow Salmonella typhimurium to penetrate tissue culture cells. Proc. Natl. Acad. Sci. U.S.A. *86*, 6383–6387.

Grant, A.J., Restif, O., McKinley, T.J., Sheppard, M., Maskell, D.J., and Mastroeni, P. (2008). Modelling within-host spatiotemporal dynamics of invasive bacterial disease. PLoS Biol. *6*, e74.

Hapfelmeier, S., Stecher, B., Barthel, M., Kremer, M., Müller, A.J., Heikenwalder, M., Stallmach, T., Hensel, M., Pfeffer, K., Akira, S., et al. (2005). The Salmonella pathogenicity island (SPI)-2 and SPI-1 type III secretion systems allow Salmonella serovar typhimurium to trigger colitis via MyD88-dependent and MyD88-independent mechanisms. J. Immunol. *174*, 1675–1685.

Hapfelmeier, S., Müller, A.J., Stecher, B., Kaiser, P., Barthel, M., Endt, K., Eberhard, M., Robbiani, R., Jacobi, C.A., Heikenwalder, M., et al. (2008). Microbe sampling by mucosal dendritic cells is a discrete, MyD88-independent step in DeltainvG S. Typhimurium colitis. J. Exp. Med. *205*, 437–450.

Hautefort, I., Proença, M.J., and Hinton, J.C.D. (2003). Single-copy green fluorescent protein gene fusions allow accurate measurement of Salmonella gene expression in vitro and during infection of mammalian cells. Appl. Environ. Microbiol. *69*, 7480–7491.

Hoiseth, S.K., and Stocker, B.A. (1981). Aromatic-dependent Salmonella typhimurium are non-virulent and effective as live vaccines. Nature *291*, 238–239.

Hong, X., Chen, H.D., and Groisman, E.A. (2018). Gene expression kinetics governs stimulus-specific decoration of the Salmonella outer membrane. Sci Signal *11*.

Johansson, M.E.V., and Hansson, G.C. (2016). Immunological aspects of intestinal mucus and mucins. Nat. Rev. Immunol. *16*, 639–649.

Jorgensen, I., Zhang, Y., Krantz, B.A., and Miao, E.A. (2016). Pyroptosis triggers pore-induced intracellular traps (PITs) that capture bacteria and lead to their clearance by efferocytosis. J. Exp. Med. *213*, 2113–2128.

Kaiser, P., and Hardt, W.-D. (2011). Salmonella typhimurium diarrhea: switching the mucosal epithelium from homeostasis to defense. Curr. Opin. Immunol. *23*, 456–463.

Kaiser, P., Slack, E., Grant, A.J., Hardt, W.-D., and Regoes, R.R. (2013). Lymph node colonization dynamics after oral Salmonella Typhimurium infection in mice. PLoS Pathog. *9*, e1003532.

Kaiser, P., Regoes, R.R., and Hardt, W.-D. (2016). Population Dynamics Analysis of Ciprofloxacin-Persistent S. Typhimurium Cells in a Mouse Model for Salmonella Diarrhea. Methods Mol. Biol. *1333*, 189–203.

Kayagaki, N., Warming, S., Lamkanfi, M., Vande Walle, L., Louie, S., Dong, J., Newton, K., Qu, Y., Liu, J., Heldens, S., et al. (2011a). Non-canonical inflammasome activation targets caspase-11. Nature *479*, 117–121.

Kayagaki, N., Warming, S., Lamkanfi, M., Vande Walle, L., Louie, S., Dong, J., Newton, K., Qu, Y., Liu, J., Heldens, S., et al. (2011b). Non-canonical inflammasome activation targets caspase-11. Nature *479*, 117–121.

Kinnebrew, M.A., Buffie, C.G., Diehl, G.E., Zenewicz, L.A., Leiner, I., Hohl, T.M., Flavell, R.A., Littman, D.R., and Pamer, E.G. (2012). Interleukin 23 production by intestinal CD103(+)CD11b(+) dendritic cells in response to bacterial flagellin enhances mucosal innate immune defense. Immunity *36*, 276–287.

Knodler, L.A., Vallance, B.A., Celli, J., Winfree, S., Hansen, B., Montero, M., and Steele-Mortimer, O. (2010). Dissemination of invasive Salmonella via bacterial-induced extrusion of mucosal epithelia. Proc. Natl. Acad. Sci. U.S.A. *107*, 17733–17738.

Knodler, L.A., Crowley, S.M., Sham, H.P., Yang, H., Wrande, M., Ma, C., Ernst, R.K., Steele-Mortimer, O., Celli, J., and Vallance, B.A. (2014). Noncanonical inflammasome activation of caspase-4/caspase-11 mediates epithelial defenses against enteric bacterial pathogens. Cell Host Microbe *16*, 249–256.

Kofoed, E.M., and Vance, R.E. (2011). Innate immune recognition of bacterial ligands by NAIPs determines inflammasome specificity. Nature *477*, 592–595.

Kreibich, S., Emmenlauer, M., Fredlund, J., Rämö, P., Münz, C., Dehio, C., Enninga, J., and Hardt, W.-D. (2015). Autophagy Proteins Promote Repair of Endosomal Membranes Damaged by the Salmonella Type Three Secretion System 1. Cell Host Microbe *18*, 527–537.

Lara-Tejero, M., Sutterwala, F.S., Ogura, Y., Grant, E.P., Bertin, J., Coyle, A.J., Flavell, R.A., and Galán, J.E. (2006). Role of the caspase-1 inflammasome in Salmonella typhimurium pathogenesis. Journal of Experimental Medicine *203*, 1407–1412.

Lau, N., Haeberle, A.L., O'Keeffe, B.J., Latomanski, E.A., Celli, J., Newton, H.J., and Knodler, L.A. (2019). SopF, a phosphoinositide binding effector, promotes the stability of the nascent Salmonella-containing vacuole. PLoS Pathog. *15*, e1007959.

Laughlin, R.C., Knodler, L.A., Barhoumi, R., Payne, H.R., Wu, J., Gomez, G., Pugh, R., Lawhon, S.D., Bäumler, A.J., Steele-Mortimer, O., et al. (2014). Spatial segregation of virulence gene expression during acute enteric infection with Salmonella enterica serovar Typhimurium. MBio *5*, e00946-00913.

Li, P., Allen, H., Banerjee, S., Franklin, S., Herzog, L., Johnston, C., McDowell, J., Paskind, M., Rodman, L., and Salfeld, J. (1995). Mice deficient in IL-1 beta-converting enzyme are defective in production of mature IL-1 beta and resistant to endotoxic shock. Cell *80*, 401–411.

Liu, Y., Mi, Y., Mueller, T., Kreibich, S., Williams, E.G., Van Drogen, A., Borel, C., Frank, M., Germain, P.-L., Bludau, I., et al. (2019). Multi-omic measurements of heterogeneity in HeLa cells across laboratories. Nat. Biotechnol. *37*, 314–322.

Maier, L., Diard, M., Sellin, M.E., Chouffane, E.-S., Trautwein-Weidner, K., Periaswamy, B., Slack, E., Dolowschiak, T., Stecher, B., Loverdo, C., et al. (2014). Granulocytes impose a tight bottleneck upon the gut luminal pathogen population during Salmonella typhimurium colitis. PLoS Pathog. *10*, e1004557.

Maldonado, R.F., Sá-Correia, I., and Valvano, M.A. (2016). Lipopolysaccharide modification in Gram-negative bacteria during chronic infection. FEMS Microbiol. Rev. *40*, 480–493.

Maltez, V.I., Tubbs, A.L., Cook, K.D., Aachoui, Y., Falcone, E.L., Holland, S.M., Whitmire, J.K., and Miao, E.A. (2015). Inflammasomes Coordinate Pyroptosis and Natural Killer Cell Cytotoxicity to Clear Infection by a Ubiquitous Environmental Bacterium. Immunity *43*, 987–997.

Mamantopoulos, M., Ronchi, F., Van Hauwermeiren, F., Vieira-Silva, S., Yilmaz, B., Martens, L., Saeys, Y., Drexler, S.K., Yazdi, A.S., Raes, J., et al. (2017). Nlrp6- and ASC-Dependent Inflammasomes Do Not Shape the Commensal Gut Microbiota Composition. Immunity *47*, 339-348.e4.

Mamantopoulos, M., Ronchi, F., McCoy, K.D., and Wullaert, A. (2018). Inflammasomes make the case for littermate-controlled experimental design in studying host-microbiota interactions. Gut Microbes *9*, 374–381.

Man, S.M., Hopkins, L.J., Nugent, E., Cox, S., Glück, I.M., Tourlomousis, P., Wright, J.A., Cicuta, P., Monie, T.P., and Bryant, C.E. (2014). Inflammasome activation causes dual recruitment of NLRC4 and NLRP3 to the same macromolecular complex. Proc. Natl. Acad. Sci. U.S.A. *111*, 7403–7408.

Man, S.M., Karki, R., Briard, B., Burton, A., Gingras, S., Pelletier, S., and Kanneganti, T.-D. (2017). Differential roles of caspase-1 and caspase-11 in infection and inflammation. Sci Rep *7*, 45126.

Mariathasan, S., Newton, K., Monack, D.M., Vucic, D., French, D.M., Lee, W.P., Roose-Girma, M., Erickson, S., and Dixit, V.M. (2004). Differential activation of the inflammasome by caspase-1 adaptors ASC and Ipaf. Nature *430*, 213–218.

Marko, M., and Hsieh, C.-E. (2007). Three-dimensional cryotransmission electron microscopy of cells and organelles. Methods Mol. Biol. *369*, 407–429.

Martinon, F., Burns, K., and Tschopp, J. (2002). The inflammasome: a molecular platform triggering activation of inflammatory caspases and processing of proIL-beta. Mol. Cell *10*, 417–426.

Martinon, F., Pétrilli, V., Mayor, A., Tardivel, A., and Tschopp, J. (2006). Gout-associated uric acid crystals activate the NALP3 inflammasome. Nature *440*, 237–241.

Mascarenhas, D.P.A., Cerqueira, D.M., Pereira, M.S.F., Castanheira, F.V.S., Fernandes, T.D., Manin, G.Z., Cunha, L.D., and Zamboni, D.S. (2017). Inhibition of caspase-1 or gasdermin-D enable caspase-8 activation in the Naip5/NLRC4/ASC inflammasome. PLoS Pathog *13*.

Mastroeni, P., and Grant, A. (2013). Dynamics of spread of Salmonella enterica in the systemic compartment. Microbes and Infection *15*, 849–857.

Mastronarde, D.N. (2005). Automated electron microscope tomography using robust prediction of specimen movements. J. Struct. Biol. *152*, 36–51.

Mastronarde, D.N. (2008). Correction for non-perpendicularity of beam and tilt axis in tomographic reconstructions with the IMOD package. J Microsc *230*, 212–217.

Medeiros, J.M., Böck, D., Weiss, G.L., Kooger, R., Wepf, R.A., and Pilhofer, M. (2018). Robust workflow and instrumentation for cryo-focused ion beam milling of samples for electron cryotomography. Ultramicroscopy *190*, 1–11.

Miao, E.A., and Warren, S.E. (2010). Innate immune detection of bacterial virulence factors via the NLRC4 inflammasome. J. Clin. Immunol. *30*, 502–506.

Miao, E.A., Leaf, I.A., Treuting, P.M., Mao, D.P., Dors, M., Sarkar, A., Warren, S.E., Wewers, M.D., and Aderem, A. (2010). Caspase-1-induced pyroptosis is an innate immune effector mechanism against intracellular bacteria. Nat. Immunol. *11*, 1136–1142.

Miki, T., and Hardt, W.-D. (2013). Outer membrane permeabilization is an essential step in the killing of gram-negative bacteria by the lectin RegIIIβ. PLoS ONE *8*, e69901.

Misselwitz, B., Kreibich, S.K., Rout, S., Stecher, B., Periaswamy, B., and Hardt, W.-D. (2011). Salmonella enterica Serovar Typhimurium Binds to HeLa Cells via Fim-Mediated Reversible Adhesion and Irreversible Type Three Secretion System 1-Mediated Docking. Infection and Immunity *79*, 330–341.

von Moltke, J., Trinidad, N.J., Moayeri, M., Kintzer, A.F., Wang, S.B., van Rooijen, N., Brown, C.R., Krantz, B.A., Leppla, S.H., Gronert, K., et al. (2012). Rapid induction of inflammatory lipid mediators by the inflammasome in vivo. Nature *490*, 107–111.

Monack, D.M., Hersh, D., Ghori, N., Bouley, D., Zychlinsky, A., and Falkow, S. (2000). Salmonella exploits caspase-1 to colonize Peyer's patches in a murine typhoid model. J. Exp. Med. *192*, 249–258.

Moor, K., Diard, M., Sellin, M.E., Felmy, B., Wotzka, S.Y., Toska, A., Bakkeren, E., Arnoldini, M., Bansept, F., Co, A.D., et al. (2017). High-avidity IgA protects the intestine by enchaining growing bacteria. Nature *544*, 498–502.

Müller, A.A., Dolowschiak, T., Sellin, M.E., Felmy, B., Verbree, C., Gadient, S., Westermann, A.J., Vogel, J., LeibundGut-Landmann, S., and Hardt, W.-D. (2016). An NK Cell Perforin Response Elicited via IL-18 Controls Mucosal Inflammation Kinetics during Salmonella Gut Infection. PLoS Pathog. *12*, e1005723.

Müller, A.J., Hoffmann, C., Galle, M., Van Den Broeke, A., Heikenwalder, M., Falter, L., Misselwitz, B., Kremer, M., Beyaert, R., and Hardt, W.-D. (2009). The S. Typhimurium effector SopE induces caspase-1 activation in stromal cells to initiate gut inflammation. Cell Host Microbe *6*, 125–136.

Müller, A.J., Kaiser, P., Dittmar, K.E.J., Weber, T.C., Haueter, S., Endt, K., Songhet, P., Zellweger, C., Kremer, M., Fehling, H.-J., et al. (2012). Salmonella gut invasion involves TTSS-2-dependent epithelial traversal, basolateral exit, and uptake by epithelium-sampling lamina propria phagocytes. Cell Host Microbe *11*, 19–32.

Nathan, C., and Shiloh, M.U. (2000). Reactive oxygen and nitrogen intermediates in the relationship between mammalian hosts and microbial pathogens. Proc. Natl. Acad. Sci. U.S.A. *97*, 8841–8848.

Niepel, M., Hafner, M., Mills, C.E., Subramanian, K., Williams, E.H., Chung, M., Gaudio, B., Barrette, A.M., Stern, A.D., Hu, B., et al. (2019). A Multi-center Study on the Reproducibility of Drug-Response Assays in Mammalian Cell Lines. Cell Systems *9*, 35-48.e5.

Niess, J.H., Brand, S., Gu, X., Landsman, L., Jung, S., McCormick, B.A., Vyas, J.M., Boes, M., Ploegh, H.L., Fox, J.G., et al. (2005). CX3CR1-mediated dendritic cell access to the intestinal lumen and bacterial clearance. Science *307*, 254–258.

Nordlander, S., Pott, J., and Maloy, K.J. (2014). NLRC4 expression in intestinal epithelial cells mediates protection against an enteric pathogen. Mucosal Immunol *7*, 775–785.

Ostaff, M.J., Stange, E.F., and Wehkamp, J. (2013). Antimicrobial peptides and gut microbiota in homeostasis and pathology. EMBO Mol Med *5*, 1465–1483.

Rauch, I., Tenthorey, J.L., Nichols, R.D., Al Moussawi, K., Kang, J.J., Kang, C., Kazmierczak, B.I., and Vance, R.E. (2016). NAIP proteins are required for cytosolic detection of specific bacterial ligands in vivo. J. Exp. Med. *213*, 657–665.

Rauch, I., Deets, K.A., Ji, D.X., von Moltke, J., Tenthorey, J.L., Lee, A.Y., Philip, N.H., Ayres, J.S., Brodsky, I.E., Gronert, K., et al. (2017). NAIP-NLRC4 Inflammasomes Coordinate Intestinal Epithelial Cell Expulsion with Eicosanoid and IL-18 Release via Activation of Caspase-1 and -8. Immunity *46*, 649–659.

Raupach, B., Peuschel, S.-K., Monack, D.M., and Zychlinsky, A. (2006). Caspase-1-Mediated Activation of Interleukin-1β (IL-1β) and IL-18 Contributes to Innate Immune Defenses against Salmonella enterica Serovar Typhimurium Infection. Infect. Immun. *74*, 4922–4926.

Rayamajhi, M., Zak, D.E., Chavarria-Smith, J., Vance, R.E., and Miao, E.A. (2013). Cutting edge: Mouse NAIP1 detects the type III secretion system needle protein. J. Immunol. *191*, 3986–3989.

Rescigno, M., Urbano, M., Valzasina, B., Francolini, M., Rotta, G., Bonasio, R., Granucci, F., Kraehenbuhl, J.P., and Ricciardi-Castagnoli, P. (2001). Dendritic cells express tight junction proteins and penetrate gut epithelial monolayers to sample bacteria. Nat. Immunol. *2*, 361–367.

Robertson, S.J., Lemire, P., Maughan, H., Goethel, A., Turpin, W., Bedrani, L., Guttman, D.S., Croitoru, K., Girardin, S.E., and Philpott, D.J. (2019). Comparison of Co-housing and Littermate Methods for Microbiota Standardization in Mouse Models. Cell Rep *27*, 1910-1919.e2.

Runyen-Janecky, L.J., and Payne, S.M. (2002). Identification of chromosomal Shigella flexneri genes induced by the eukaryotic intracellular environment. Infect. Immun. *70*, 4379–4388.

Schindelin, J., Arganda-Carreras, I., Frise, E., Kaynig, V., Longair, M., Pietzsch, T., Preibisch, S., Rueden, C., Saalfeld, S., Schmid, B., et al. (2012). Fiji: an open-source platform for biological-image analysis. Nat. Methods *9*, 676–682.

Sellin, M.E., Müller, A.A., Felmy, B., Dolowschiak, T., Diard, M., Tardivel, A., Maslowski, K.M., and Hardt, W.-D. (2014). Epithelium-intrinsic NAIP/NLRC4 inflammasome drives infected enterocyte expulsion to restrict Salmonella replication in the intestinal mucosa. Cell Host Microbe *16*, 237–248.

Sheppard, M., Webb, C., Heath, F., Mallows, V., Emilianus, R., Maskell, D., and Mastroeni, P. (2003). Dynamics of bacterial growth and distribution within the liver during Salmonella infection. Cell. Microbiol. *5*, 593–600.

Shi, J., Zhao, Y., Wang, K., Shi, X., Wang, Y., Huang, H., Zhuang, Y., Cai, T., Wang, F., and Shao, F. (2015). Cleavage of GSDMD by inflammatory caspases determines pyroptotic cell death. Nature *526*, 660–665.

Spinnenhirn, V., Farhan, H., Basler, M., Aichem, A., Canaan, A., and Groettrup, M. (2014). The ubiquitin-like modifier FAT10 decorates autophagy-targeted Salmonella and contributes to Salmonella resistance in mice. J. Cell. Sci. *127*, 4883–4893.

Stagg, A.J. (2018). Intestinal Dendritic Cells in Health and Gut Inflammation. Front. Immunol. *9*.

Stecher, B., Hapfelmeier, S., Müller, C., Kremer, M., Stallmach, T., and Hardt, W.-D. (2004). Flagella and chemotaxis are required for efficient induction of Salmonella enterica serovar Typhimurium colitis in streptomycin-pretreated mice. Infect. Immun. *72*, 4138–4150.

Stecher, B., Robbiani, R., Walker, A.W., Westendorf, A.M., Barthel, M., Kremer, M., Chaffron, S., Macpherson, A.J., Buer, J., Parkhill, J., et al. (2007). Salmonella enterica serovar typhimurium exploits inflammation to compete with the intestinal microbiota. PLoS Biol. *5*, 2177–2189.

Stecher, B., Barthel, M., Schlumberger, M.C., Haberli, L., Rabsch, W., Kremer, M., and Hardt, W.-D. (2008). Motility allows S. Typhimurium to benefit from the mucosal defence. Cell. Microbiol. *10*, 1166–1180.

Thurston, T.L.M., Matthews, S.A., Jennings, E., Alix, E., Shao, F., Shenoy, A.R., Birrell, M.A., and Holden, D.W. (2016). Growth inhibition of cytosolic Salmonella by caspase-1 and caspase-11 precedes host cell death. Nat Commun *7*, 13292.

Tomalka, J., Ganesan, S., Azodi, E., Patel, K., Majmudar, P., Hall, B.A., Fitzgerald, K.A., and Hise, A.G. (2011). A novel role for the NLRC4 inflammasome in mucosal defenses against the fungal pathogen Candida albicans. PLoS Pathog. *7*, e1002379.

Van Opdenbosch, N., Van Gorp, H., Verdonckt, M., Saavedra, P.H.V., de Vasconcelos, N.M., Gonçalves, A., Vande Walle, L., Demon, D., Matusiak, M., Van Hauwermeiren, F., et al. (2017). Caspase-1 Engagement and TLR-Induced c-FLIP Expression Suppress ASC/Caspase-8-Dependent Apoptosis by Inflammasome Sensors NLRP1b and NLRC4. Cell Rep *21*, 3427–3444.

Weiss, G.L., Medeiros, J.M., and Pilhofer, M. (2017). In Situ Imaging of Bacterial Secretion Systems by Electron Cryotomography. Methods Mol. Biol. *1615*, 353–375.

Winsor, N., Krustev, C., Bruce, J., Philpott, D.J., and Girardin, S.E. (2019). Canonical and noncanonical inflammasomes in intestinal epithelial cells. Cell. Microbiol. e13079.

Wullaert, A., Lamkanfi, M., and McCoy, K.D. (2018). Defining the Impact of Host Genotypes on Microbiota Composition Requires Meticulous Control of Experimental Variables. Immunity *48*, 605–607.

Wynosky-Dolfi, M.A., Snyder, A.G., Philip, N.H., Doonan, P.J., Poffenberger, M.C., Avizonis, D., Zwack, E.E., Riblett, A.M., Hu, B., Strowig, T., et al. (2014). Oxidative metabolism enables Salmonella evasion of the NLRP3 inflammasome. J. Exp. Med. *211*, 653–668.

Yang, J., Zhao, Y., Shi, J., and Shao, F. (2013). Human NAIP and mouse NAIP1 recognize bacterial type III secretion needle protein for inflammasome activation. Proc. Natl. Acad. Sci. U.S.A. *110*, 14408–14413.

Zhao, Y., Yang, J., Shi, J., Gong, Y.-N., Lu, Q., Xu, H., Liu, L., and Shao, F. (2011). The NLRC4 inflammasome receptors for bacterial flagellin and type III secretion apparatus. Nature *477*, 596–600.

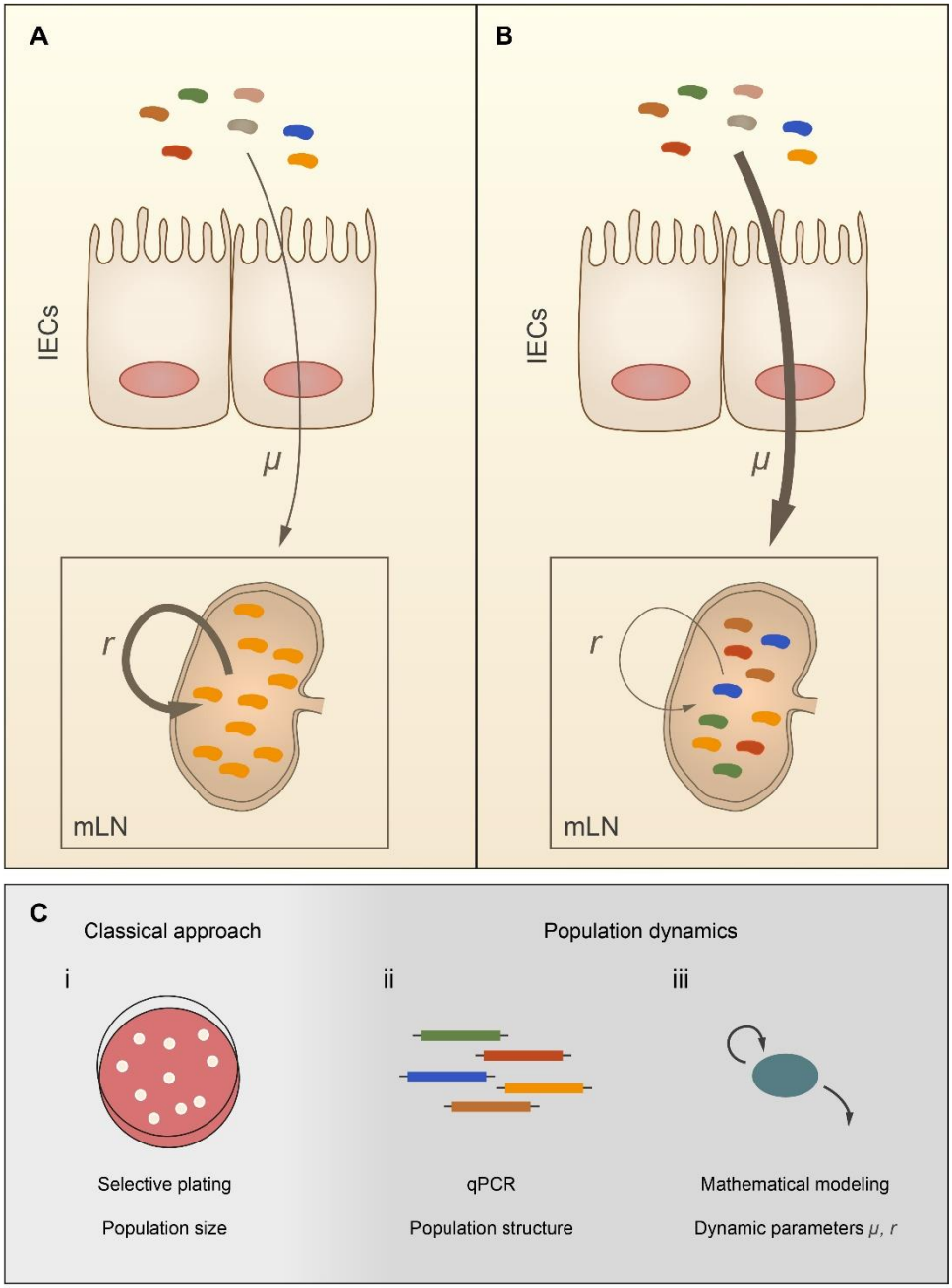

Figure S1 ***Schematic overview of the experimental approach****: The use of genetically tagged* S. Tm *for the quantitation of population dynamics during oral infection. Scenario* ***A*** *(low migration rate (*μ*), high net replication rate (*r*, integration of replication and clearance within the mLN)) and scenario* ***B*** *(high migration rate (*μ*) and low net replication in the mLN (*r*)) can result in the same pathogen loads in the mLN, and can therefore not be differentiated by conventional selective plating as shown in* ***C*** *(classical approach). Notably, using tagged WITS strains (represented by the different colors), analysis of tag-distribution within the mLN by qPCR provides information of the population structure and makes differentiation of the two scenarios possible. Mathematical modeling allows precise quantification of the contribution of the dynamic parameters* μ *and* r *to the total pathogen population within the mLN.*

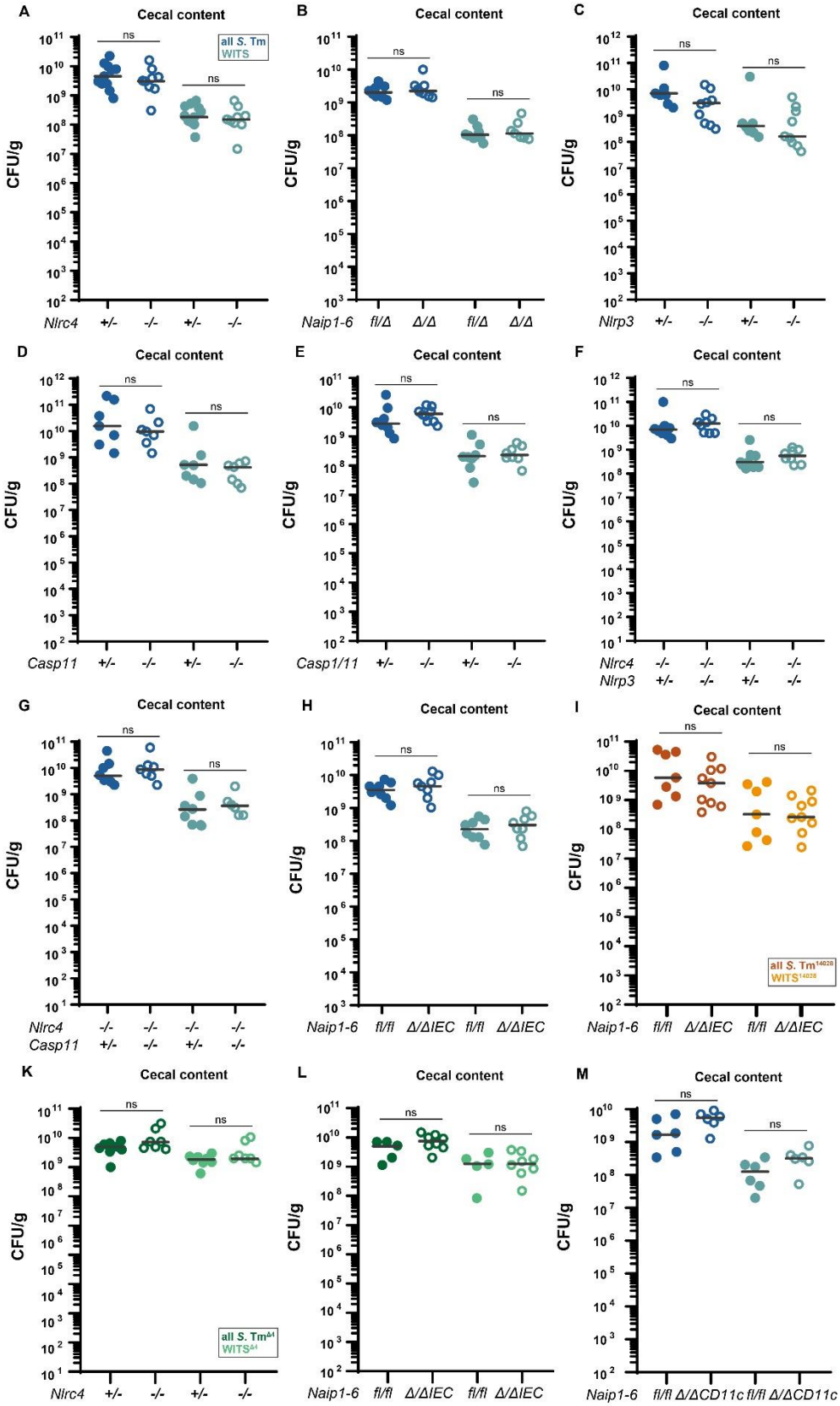

Figure S2 ***Deletion of inflammasome components does not alter luminal S. Tm colonization****. S. Tm cecal luminal counts (CFU/gram cecal content) in* ***A*** Nlrc4$^{+/-}$ *(circles) and* Nlrc4$^{-/-}$ *(open circles) mice shown in Figure 1A* ***B*** Naip1-6$^{\Delta/fl}$ *(circles) and* Naip1-6$^{\Delta/\Delta}$ *(open circles) mice shown in Figure 1E* ***C*** Nlrp3$^{+/-}$ *(circles) and* Nlrp3$^{-/-}$ *(open*

circles) mice shown in Figure 2A-B and S3A ***D*** Casp11$^{+/-}$ *(circles) and* Casp11$^{-/-}$ *(open circles) mice shown in Figure 2A-B and S3B* ***E*** Casp1/11$^{+/-}$ *(circles) and* Casp1/11$^{-/-}$ *(open circles) mice shown in Figure 2A-B and S3C* ***F*** Nlrc4$^{-/-}$ Nlrp3$^{+/-}$ *(circles) and* Nlrc4$^{-/-}$Nlrp3$^{-/-}$ *(open circles) mice shown in Figure 2C-D and S3D* ***G*** Nlrc4$^{-/-}$Casp11$^{+/-}$ *(circles) and* Nlrc4$^{-/-}$Casp11$^{-/-}$ *(open circles) mice shown in Figure 2C-D and S3E* ***H*** Naip1-6$^{fl/fl}$ *(circles) and* Naip1-6$^{\Delta/\Delta IEC}$ *(open circles) mice shown in Figure 3A* ***I*** Nlrc4$^{+/-}$ *(circles) and* Nlrc4$^{-/-}$ *(open circles) mice infected with* S. *Tm$^{\Delta 4}$ shown in Figure 3B* ***K*** Naip1-6$^{fl/fl}$ *(circles) and* Naip1-6$^{\Delta/\Delta IEC}$ *(open circles) mice infected with* S. *Tm$^{\Delta 4}$ shown in Figure 3C* ***L*** Naip1-6$^{fl/fl}$ *(circles) and* Naip1-6$^{\Delta/\Delta IEC}$ *(open circles) mice infected with* S. *Tm^{14028} shown in Figure S5A* ***M*** Naip1-6$^{fl/fl}$ *(circles) and* Naip1-6$^{\Delta/\Delta CD11c}$ *(open circles) mice shown in Figure S5B. Depicted are counts of all* S. *Tm (dark blue, selected for with Streptomycin, green for* S. *Tm$^{\Delta 4}$, selected for with Streptomycin; brown* S. *Tm^{14028}, selected for with Kanamycin) and specifically of the WITS (light blue for WITS, light green for WITS$^{\Delta 4}$, selected for with Kanamycin; orange for WITS^{14028}, selected for with Chloramphenicol). Each circle represents one mouse. Combined data of at least three independent experiments (see respective main figures). Grey line: Median. Statistical analysis: Mann-Whitney-U Test,* p*-values indicated, ns:* $p \geq 0.05$.

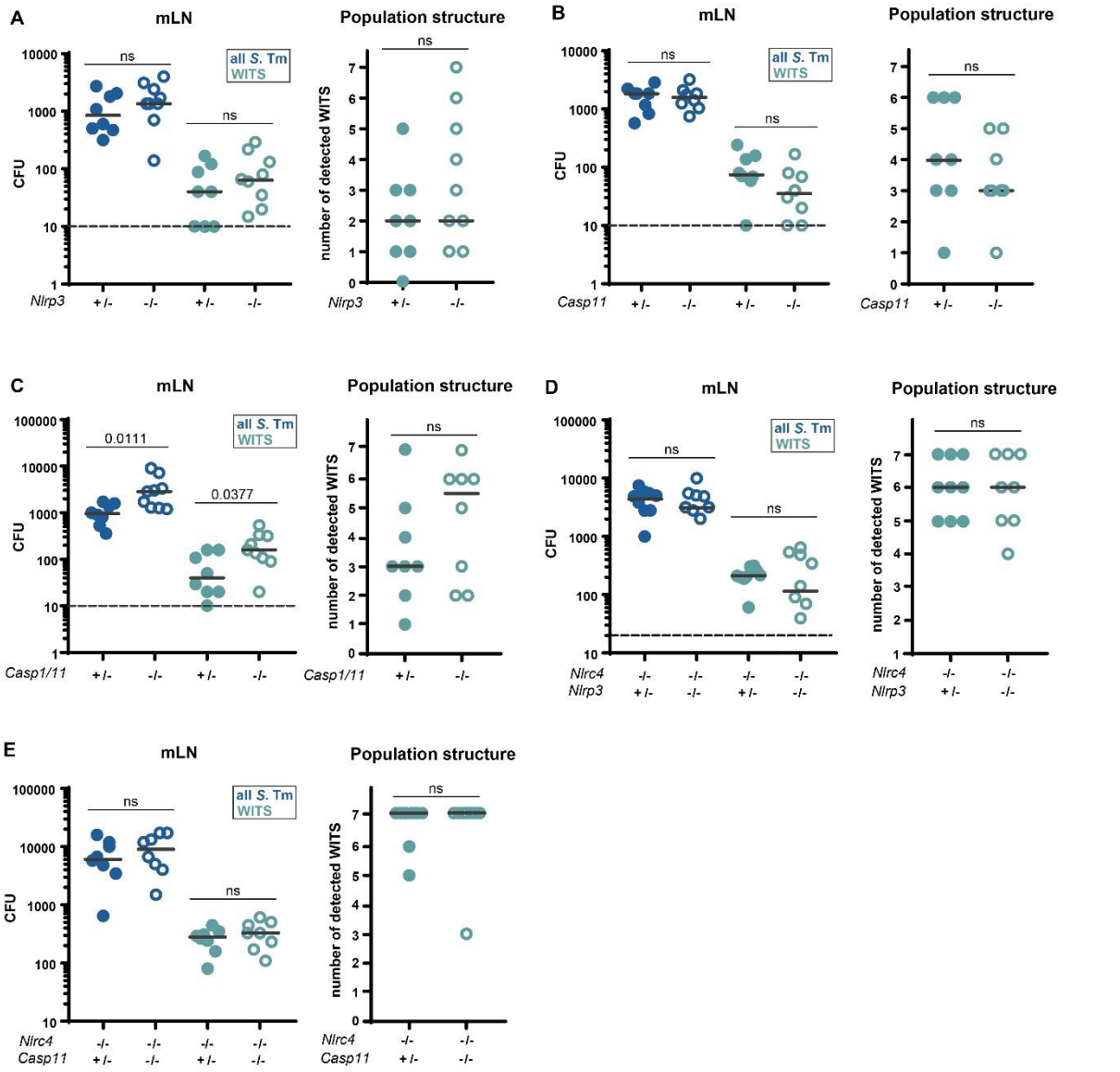

Figure S3 ***NLRP3 and Caspase-11 do not contribute to restriction of systemic* S. *Tm spread during oral infection, while Caspase-1 is partially involved****. Streptomycin pretreated mice were orally infected with 5x10^7 CFU* S. *Tm.* S. *Tm counts in the mLN at 24 hpi are independent of NLRP3 (**A**,* Nlrp3$^{+/-}$ *(circles) and* Nlrp3$^{-/-}$ *(open circles)) and Caspase-11 (**B**,* Casp11$^{+/-}$ *(circles) and* Casp11$^{-/-}$ *(open circles)). Caspase-1 partially contributed to restriction of mLN loads (**C**,* Casp1/11$^{+/-}$ *(circles) and* Casp1/11$^{-/-}$ *(open circles)). Even in absence of NLRC4, NLRP3 (**D**,* Nlrc4$^{-/-}$Nlrp3$^{+/-}$ *(circles) and* Nlrc4$^{-/-}$Nlrp3$^{-/-}$ *(open circles)) and Caspase-11 (**E**,* Nlrc4$^{-/-}$Casp11$^{+/-}$ *(circles) and* Nlrc4$^{-/-}$Casp11$^{-/-}$ *(open circles)) are not involved in restriction of mLN colonization. Depicted are counts of all* S. *Tm (dark blue, selected for with Streptomycin) and specifically of the WITS (light blue, selected for with Kanamycin, 5% of the inoculum) (A-E, left panels). A-E, right panels: Number of WITS tags detected in mLN of mice which are shown in the left panels. Only mice with detectable WITS in the mLN (plating) were included in the analysis, remaining samples were set to 0. Each circle represents one mouse. Combined data of at least three independent experiments (see respective main figures). Dotted line: detection limit. Grey line: Median. Statistical analysis: Mann-Whitney-U Test,* p*-values indicated, ns:* p ≥ 0.05.

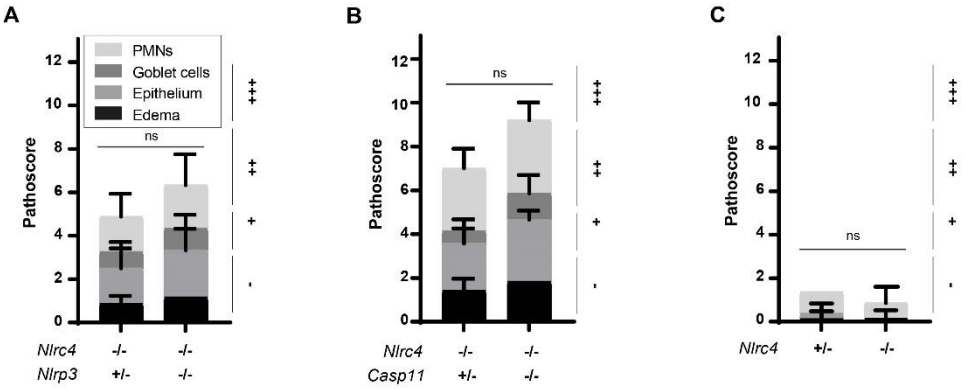

Figure S4 ***Histopathological analysis.*** *Histopathological scores of cecae of* ***A*** Nlrc4$^{-/-}$Nlrp3$^{+/-}$ *(n=8) and* Nlrc4$^{-/-}$ Nlrp3$^{-/-}$ *(n=6) mice shown in Fig S3D,* ***B*** Nlrc4$^{-/-}$Casp11$^{+/-}$ *(n=7) and* Nlrc4$^{-/-}$Casp11$^{-/-}$ *(n=6) mice shown in Fig S3E and* ***C*** *of* Nlrc4$^{+/-}$ *(n=8) and* Nlrc4$^{-/-}$ *(n=7) mice infected with* S. *Tm$^{\Delta 4}$ shown in Fig 3B. H&E stained sections were scored for submucosal edema, epithelial integrity, goblet cell loss and PMN infiltration. Symbols on the right indicate inflammatory states from "-", no inflammation, to "+++", strongly inflamed. Statistical analysis: Two-way ANOVA with Tukey`s correction, ns:* $p \geq 0.05$.

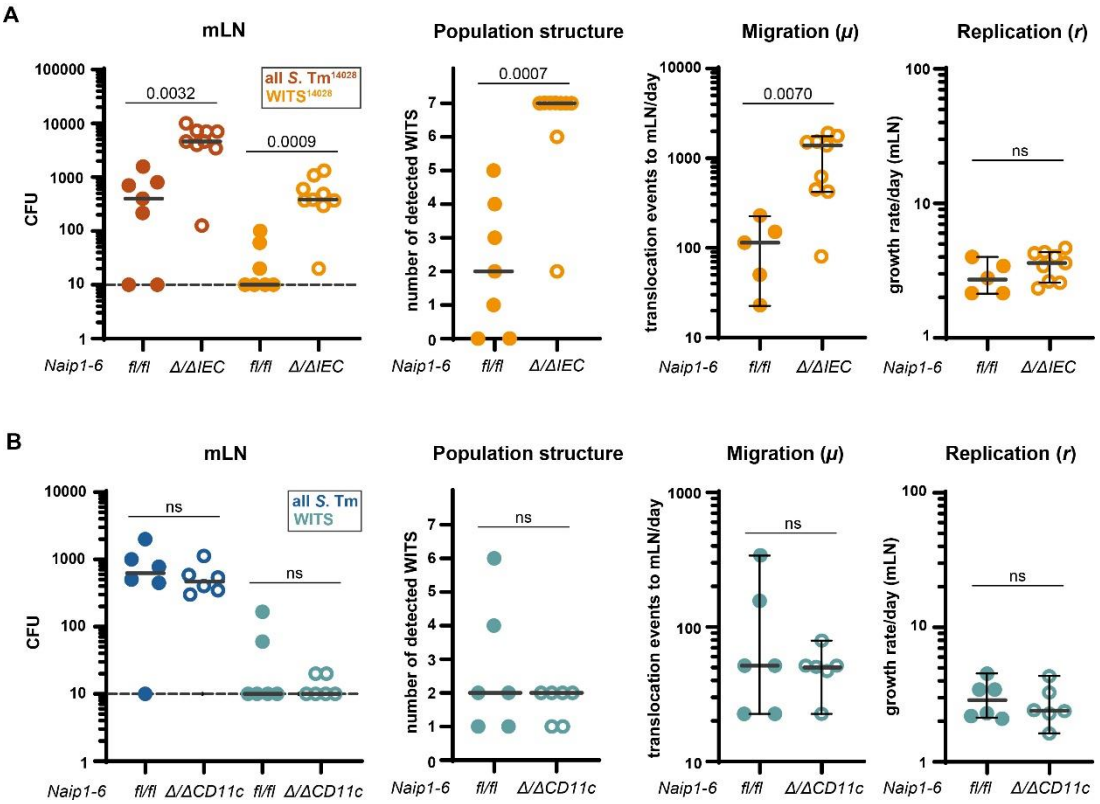

Figure S5 ***DC NAIP/NLRC4 is dispensable for restriction of S. Tm mLN loads. A*** *Kanamycin pretreated mice were orally infected with 5x10^7 CFU S. Tm^{14028}. Streptomycin pretreated mice were orally infected with 5x10^7 CFU S. Tm. S. Tm counts in the mLN at 24 hpi, number of WITS tags in the mLN, S. Tm migration rate μ to the mLN were increased in* Naip1-6$^{Δ/ΔIEC}$ *mice (open circles) compared to* Naip1-6$^{fl/fl}$ *littermates (circles), whereas the replication rate r was not affected. Depicted are counts of all S. Tm (brown, selected for with Kanamycin) and specifically of the WITS (orange, selected for with Chloramphenicol, 5% of the inoculum).* ***B*** *S. Tm counts in the mLN at 24 hpi, number of WITS tags in the mLN, S. Tm migration rate μ to the mLN, and replication rate r within the mLN were not altered in* Naip1-6$^{Δ/ΔCD11c}$ *mice (open circles) compared to* Naip1-6$^{fl/fl}$ *littermates (circles). Depicted are counts of all S. Tm (dark blue, selected for with Streptomycin) and specifically of the WITS (light blue, selected for with Kanamycin, 5% of the inoculum). Each circle represents one mouse. Combined data of two (A) or five (B) independent experiments. Dotted line: detection limit. Grey line: Median, for μ and r, 95%-Confidence Intervals are indicated. Statistical analysis: Mann-Whitney-U Test, p-values indicated, ns: p ≥ 0.05.*

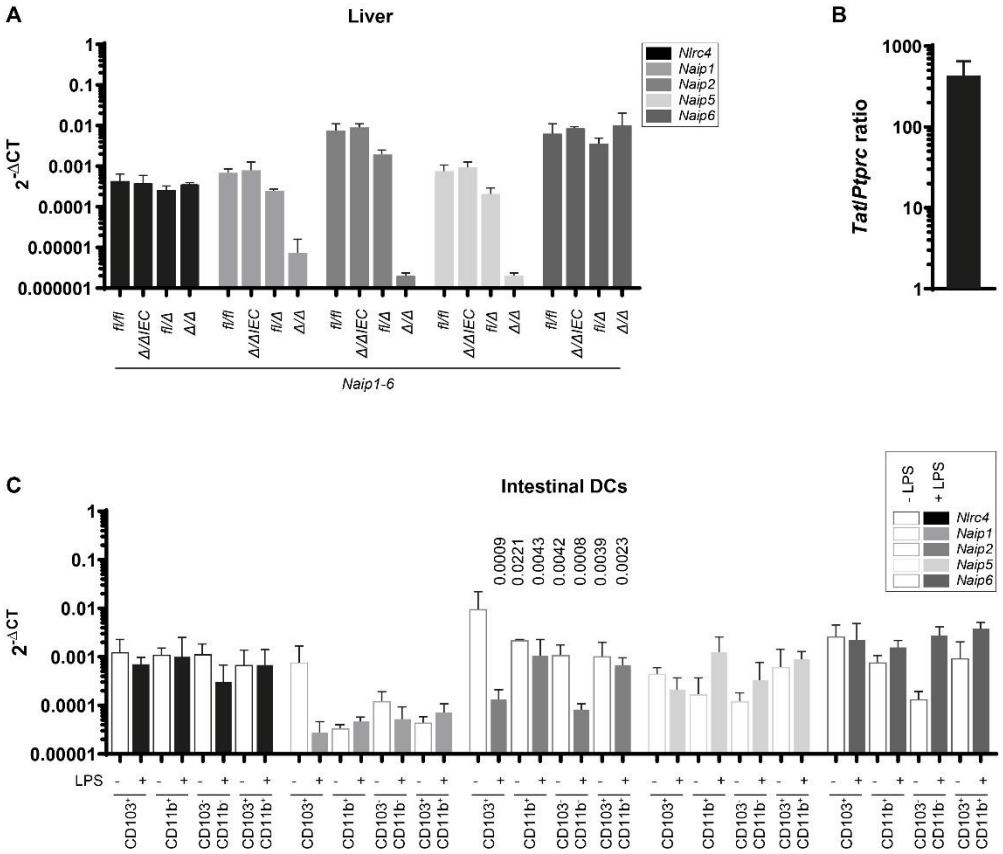

Figure S6 ***NAIP/NLRC4 inflammasome components are expressed at low levels in non-barrier, non-lymphoid tissues, and in intestinal DCs. A*** Naip/Nlrc4 *transcripts can be detected at low levels in liver tissue. Quantification of transcript expression for* Nlrc4, Naip1, Naip2, Naip5 *and* Naip6 *in the liver of* Naip1-6$^{fl/fl}$, Naip1-6$^{\Delta/\Delta IEC}$, Naip1-6$^{fl/\Delta}$ *and* Naip1-6$^{\Delta/\Delta}$ *mice depicted as* $2^{-\Delta CT}$ *values. Expression levels were normalized to* Actb. ***B*** *For the samples depicted in A, expression levels of* Tat *as hepatocyte marker, and* Ptprc*, as a marker for immune cells, were compared to estimate the relative contribution of both cell types to the transcripts within the respective tissue.* ***C*** *Intestinal DCs express low levels of* Naip/Nlrc4*. This expression is not increased upon exposure to the pro-inflammatory stimulus LPS. Quantification of transcript expression for* Nlrc4, Naip1, Naip2, Naip5 *and* Naip6 *in sorted DCs from the cecum of PBS ("-")- or 5 µg LPS ("+")-injected wild type mice (1h after injection) depicted as* $2^{-\Delta CT}$ *values. Expression levels were normalized to* Actb*. n=3. Mean and standard deviation plotted. Statistical analysis: two-way ANOVA with Tukey`s correction.* p*-values indicated in B in comparison to PBS-treated CD103$^+$ DCs.*

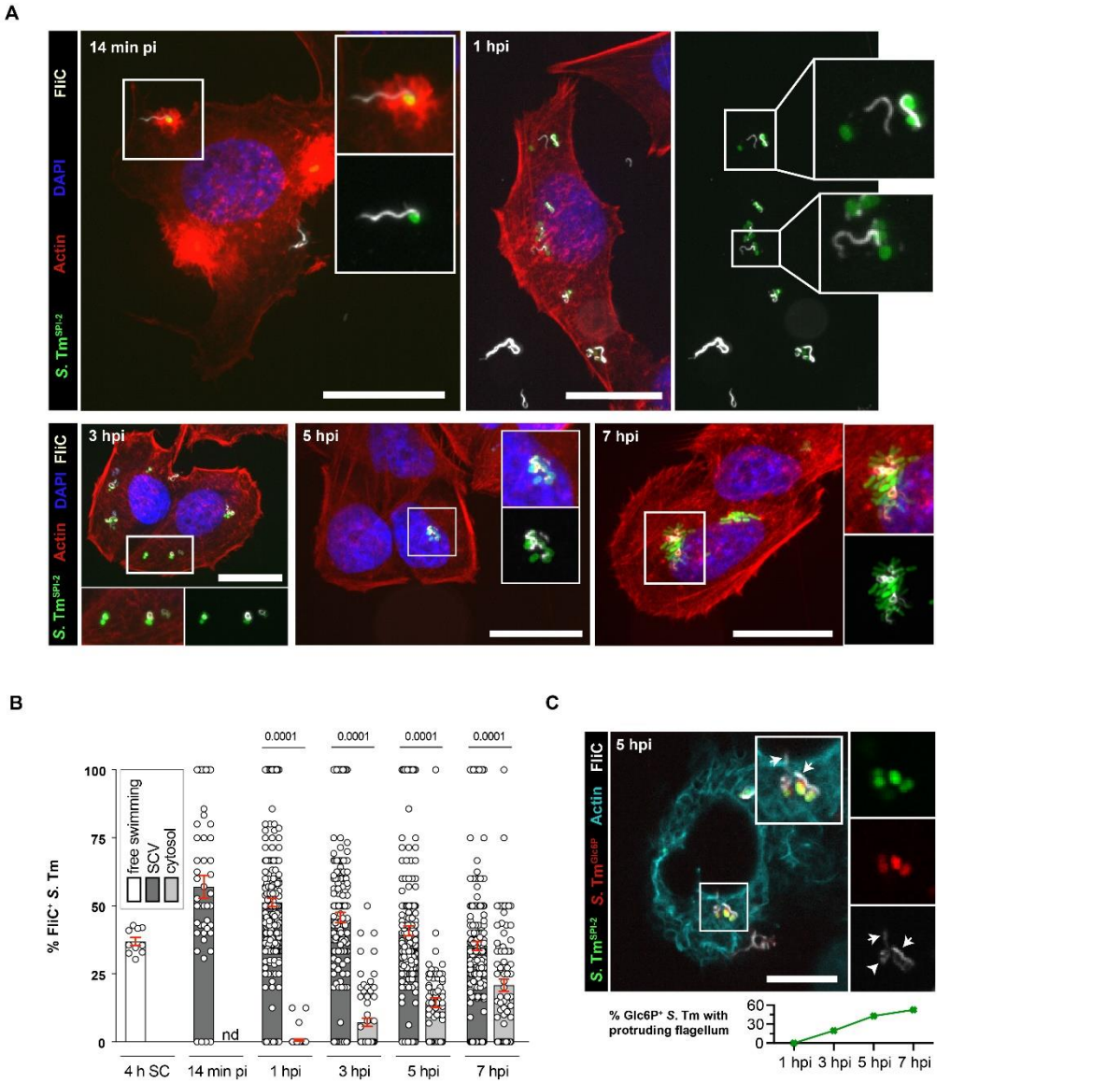

Figure S7 ***S. Tm carries flagella during invasion, within the SCV, and inside the host cell cytosol. A*** *Flagellated S. Tm can be detected during early HeLa cell invasion (14 mpi, $n^{total\ S.\ Tm}$=370) and persist until later infection times (1 hpi, $n^{total\ S.\ Tm}$=2443; 3 hpi, $n^{total\ S.\ Tm}$=1328); 5 hpi, $n^{total\ S.\ Tm}$=1403; 7 hpi, $n^{total\ S.\ Tm}$=1596).* ***B*** *Over the time course of HeLa cell infection, a subpopulation of flagellated S. Tm escaped from the SCV compartment (dark grey) to the cytosol (light grey). The fraction of flagellated S. Tm in the inoculum ("4 h SC", white) provides a baseline of flagella expression. Data is depicted as mean and SEM. Quantifications are based on immunofluorescence staining for FliC and the use of different fluorescent reporter constructs (SCV, pssaG-GFPmut2 for SPI-2-GFP (S. $Tm^{SPI\text{-}2\text{-}GFP}$); cytosol, pCK100 for Glc6P-mCherry (S. $Tm^{localizer}$)).* ***C*** *S. Tm carrying protruding flagella are found in the cytosol more frequently as the infection progresses ($n^{total\ Gl6P+\ flagellated\ S.\ Tm}$=638). White arrows, elongated flagella; white arrowheads, flagella coiled around S. Tm. Scale bars, 20 μm.*

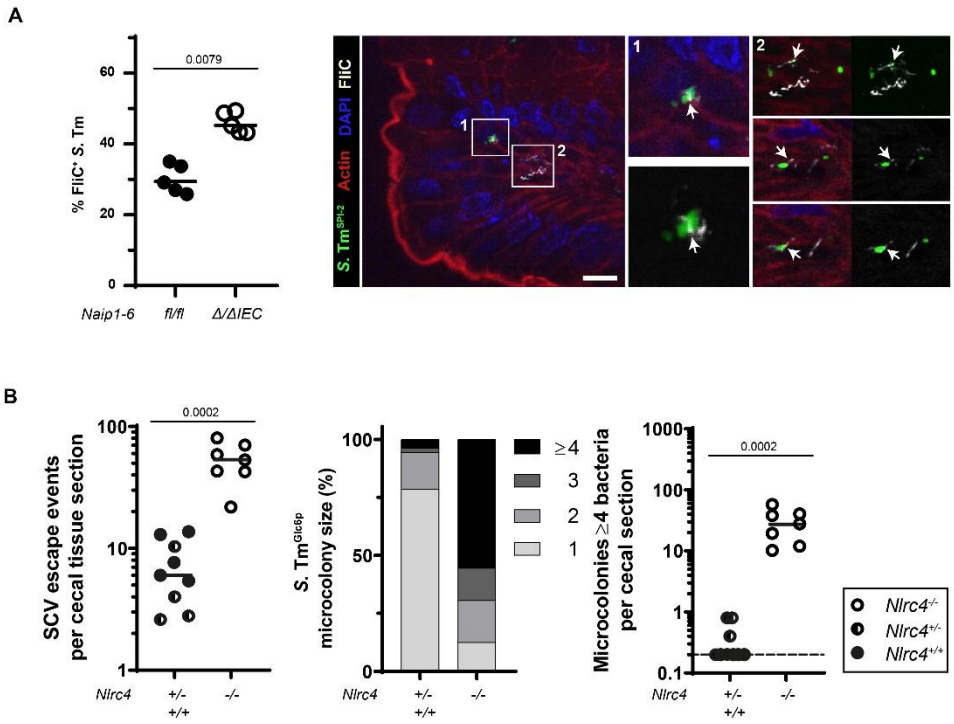

Figure S8 ***The relative abundance of flagellated S. Tm within IECs is restricted by NAIP/NLRC4. A*** *IEC-specific deletion of NAIP1-6 (Naip1-6$^{\Delta/\Delta IEC}$; open circles; $n^{total\ S.\ Tm}$=776) leads to an increase of flagellated S. Tm at 12 hpi within the cecal mucosa (Naip1-6$^{fl/fl}$; circles; $n^{total\ S.\ Tm}$=238). Quantifications are based on immunofluorescence staining for FliC.* ***B*** *This correlates with an increase in cytosolic S. Tm at 18 hpi within IECs of* Nlrc4$^{-/-}$ *mice (open circles) compared to* Nlrc4$^{+/-}$ *littermates (half-closed circles) and wild type mice (*Nlrc4$^{+/+}$*, circles) as quantified by counting of S. Tm$^{Glc6p\text{-}mCherry}$ in fluorescently labelled cecal tissue sections. Black bar, median. Statistical analysis, Mann-Whitney-U Test, p-value indicated. Scale bar, 10 µm.*

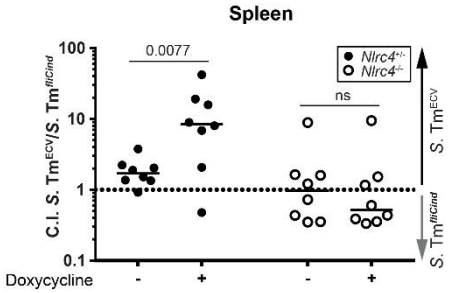

Figure S9 ***When FliC expression in phagocytes is forced, NAIP/NLRC4 restricts*** **S. *Tm* within the spleen.** Nlrc4$^{+/-}$ *(circles) and* Nlrc4$^{-/-}$ *(open circles) mice were iv infected with* 10^4 *CFU of a 1:1 mix of* S. Tm^{ECV} *and* S. $Tm^{fliCind}$*. At 17 hpi, 100 µl PBS ("-", control) or 0.8 mg Doxycycline in 100 µl PBS ("+") were iv injected to induce FliC expression. Induction of FliC expression leads to NLRC4-dependent elimination of* S. *Tm. The competitive index (C.I.) was normalized to the relative abundance of the two strains in the inoculum. The dotted line indicates a C.I. of 1, where none of the strains has an advantage. A C.I. > 1, indicates an advantage for* S. Tm^{ECV}*, a C.I. < 1 an advantage for* S. $Tm^{fliCind}$*. Each circle represents one mouse. Combined data of three independent experiments. Statistical analysis: Two-way ANOVA with Tukey`s correction,* p*-values indicated, ns*: p ≥ *0.05.*

CHAPTER 5 - GERM-FREE AND MICROBIOTA-ASSOCIATED MICE YIELD SMALL INTESTINAL EPITHELIAL ORGANOIDS WITH EQUIVALENT AND ROBUST TRANSCRIPTOME/PROTEOME EXPRESSION PHENOTYPES.

Annika Hausmann[1], Giancarlo Russo[2], Jonas Grossmann[2], Mirjam Zünd[1], Gerald Schwank[3], Ruedi Aebersold[4], Yansheng Liu[4, 5], Mikael E. Sellin[1, 6], Wolf-Dietrich Hardt[1]

Author affiliations:

[1]Institute of Microbiology, Department of Biology, ETH Zurich, Zurich, Switzerland
[2]Functional Genomics Center Zurich, University of Zurich, Zurich, Switzerland
[3]Institute of Pharmacology and Toxicology, University Zurich, Zurich, Switzerland
[4]Institute of Systems Biology, Department of Biology, ETH Zurich, Zurich, Switzerland
[5]Department of Pharmacology, Cancer Biology Institute, Yale University School of Medicine, West Haven, CT, 06516, USA
[6]Science for Life Laboratory, Department of Medical Biochemistry and Microbiology, Uppsala University, Uppsala, Sweden

Author contributions:

AH and MES prepared samples. YL performed proteomic experiments. GR, JG and AH performed data analysis. MZ and GS provided technical support. AH, YL, RA, MES and WDH designed experiments. AH, MES and WDH designed the study and wrote the manuscript. All authors read, amended and approved the manuscript.

Intestinal epithelial organoids established from gut tissue have become a widely used research tool. However, it remains unclear how environmental cues, divergent microbiota composition and other sources of variation before, during and after establishment confound organoid properties, and how these properties relate to the original tissue. While environmental influences cannot be easily addressed in human organoids, mice offer a controlled assay-system. Here, we probed the effect of donor microbiota differences, previously identified as a confounding factor in murine *in vivo* studies, on organoids. We analyzed the proteomes and transcriptomes of primary organoid cultures established from two colonized and one germ-free mouse colony of C57BL/6J genetic background, and compared them to their tissue of origin and commonly used cell lines. While an imprint of microbiota-exposure was observed on the proteome of epithelial samples, the long-term global impact of donor microbiota on organoid expression patterns was negligible. Instead, stochastic culture-to-culture differences accounted for a moderate variability between independently established organoids. Integration of transcriptome and proteome datasets revealed an organoid-typic expression signature comprising 14 transcripts and 10 proteins that distinguished organoids across all donors from murine epithelial cell lines and fibroblasts and closely mimicked expression patterns in the gut epithelium. This included the inflammasome components ASC, *Naip1-6*, *Nlrc4*, and *Caspase-1*, which were highly expressed in all organoids compared to the reference cell line m-IC_{c12} or mouse embryonic fibroblasts. Taken together, these results reveal that the donor microbiota has little effect on the organoid phenotype and suggest that organoids represent a more suitable culture model than immortalized cell lines, in particular for studies of intestinal epithelial inflammasomes.

Published in Cellular Microbiology, 13.01.2020

INTRODUCTION

Epithelia constitute essential barriers that protect the inner organs of the body, facilitate uptake and secretion, and coordinate immune responses (Allaire et al., 2018). Consequently, their biology has received significant attention. Due to the difficulty of keeping primary epithelial cells in culture, mechanistic studies of epithelial cell biology and physiology have traditionally relied on epithelial cell lines – transformed cultures established from carcinomas or produced by introducing oncogenes (Bens et al., 1996; Fogh and Trempe, 1975; Fogh et al., 1977; Scherer et al., 1953). Cell lines are easy to grow, can be maintained in culture indefinitely, and allow flexible genetic and pharmacological manipulation. However, the transferability of results to the *in vivo* scenario is often limited (Antoni et al., 2015; Ben-David et al., 2018; Niepel et al., 2019). This can be explained by poor mimicking of the complexity and interconnectedness inherent to epithelia *in vivo* (Antoni et al., 2015), the disruptive effects of cellular transformation and the gradual accumulation of genetic anomalies during prolonged culture (Ben-David et al., 2018; Foulke-Abel et al., 2014; Liu et al., 2019). Therefore, new, more stable and possibly more representative experimental models are needed.

Gut epithelial organoids offer an attractive alternative. Protocols for culturing and differentiation of primary blood-derived cell types have existed for decades (Sallusto and Lanzavecchia, 1994; Stone and Takemoto, 1970). More recently, the cumulative knowledge of the signals that maintain stem cells, drive epithelial cell growth and promote differentiation has allowed analogous protocols to be developed also for epithelia from humans and mice. This progress has been driven by studies of the gut stem cell niche (Sato and Clevers, 2013; Sato et al., 2009; Stappenbeck and Virgin, 2016). Embedding of extracted intestinal epithelial stem cells in a matrix overlaid with a growth factor-enriched culture medium (containing e.g. Wnt, Noggin, EGF, R-spondin) (Sato and Clevers, 2013; Sato et al., 2011) results in the outgrowth of three-dimensional primary epithelial structures – so called intestinal epithelial organoids (hereafter simply referred to as “organoids”). These organoids comprise a single layer of epithelial cells, with their apical side oriented towards a central lumen, while the basal side faces the extracellular matrix. In further similarity to the intact gut, organoids feature crypt invaginations harboring the stem cell compartment (Sato and Clevers, 2013). These stem cells divide and give rise to epithelial cell precursors, which differentiate into paneth cells, enteroendocrine cells, goblet cells and enterocytes, hence recapitulating much of the complexity of co-existing cell types in the gut mucosa (Foulke-Abel et al., 2014; Sato et al., 2011). For these reasons, organoids have since their conception become a widely used and realistic model to study the role of intestinal epithelial cells in e.g. gut physiology (Almeqdadi et al., 2019; Gunasekara et al., 2018; Williamson et al., 2018), cancer biology (Drost et al., 2015; Tuveson and Clevers, 2019), pharmacology (Takahashi, 2019; Walsh et al., 2016), and infectious disease (Chapter 1) (Co et al., 2019; Foulke-Abel et al., 2014; Sun, 2017; Zhang et al., 2014). It appears conceivable that organoids over time will replace traditional cell lines as the main tissue culture model of choice for mechanistic studies. However, it has remained unclear if the donor gut environment, in particular microbiota exposure, affects the organoid phenotype. These factors are difficult to control in organoids derived from human donors. To address the influence of the donor microbiota on organoid cultures, we have here compared organoids from well-controlled colonies of genetically identical mice, either germ-free or colonized with two different microbiotas.

The role of previous microbiota exposure on organoid cultures is particularly interesting, as the gut epithelium is constantly exposed to signals from environmental substances and intestinal microbes (Allaire et al., 2018). The microbiota can profoundly impact diverse aspects of epithelial physiology, including autophagy, mucus production and antimicrobial defense mechanisms (Benjamin et al., 2013; Chen et al., 2018; Jakobsson et al., 2015). Certain microbiota members even influence intestinal epithelial stem cell numbers and their proliferative capacity *in vivo* (Lee et al., 2018; Pan et al., 2018; Reedy et al., 2019; Savage et al., 1981; Sommer and Bäckhed, 2016; Stecher et al., 2006). As a result, the non-equal microbiota composition between separately kept mouse lines represents a major confounding factor in studies of how host genetics affect gut physiology and disease (Chapter 1) (Mamantopoulos et al., 2017, 2018; Robertson et al., 2019; Stappenbeck and Virgin, 2016).

Especially in the fields of gut inflammation and infection biology, the necessity for littermate-controlled *in vivo* experiments to normalize for such microbiota effects has become pressingly evident (Mamantopoulos et al., 2018).

The stem cell-containing crypts that make up the starting-material for intestinal epithelial organoids derive directly from this complex *in vivo* niche (Sato and Clevers, 2013). This raises the question whether environmental/microbial stimuli within the donor animal impact the long-term phenotype of established organoid cultures, e.g. by epigenetic mechanisms (Foster and Medzhitov, 2009) and whether experiments in genetically modified murine organoids require wild-type littermate-derived control organoid cultures. Moreover, the organoid establishment procedure itself might impose bottlenecks and promote drifts between independently generated cultures that could affect the long-term phenotype. Hence, the impact of *in vivo* environmental factors, the amplitude and causes of organoid culture variability, and the possible implications for experimental reproducibility remain poorly understood. This complicates the interpretation and comparability of results obtained in this emerging tissue culture model.

To assess reproducibility, faithful recapitulation of responses to relevant biological stimuli and stability towards confounding factors, we generated multiple independent organoid cultures from intestinal epithelial crypts of genetically identical mice housed in two distinct specific pathogen-free (SPF) facilities and one germ-free (GF) facility. By combining proteomics and transcriptomics, we compared the global expression profiles of the organoid cultures among each other, to their tissue of origin, and to widely used epithelial cell line and fibroblast models. Strikingly, organoids established from germ-free or colonized mice exhibited basal expression profiles that co-cluster together, rather than forming separate subgroups. Instead, the modest variability in expression between organoid cultures could be traced to stochastic sources during establishment and in-culture maintenance. Also, the specific expression program induced by a defined stimulus – low-dose TNF – appeared similar between organoid cultures from germ-free and colonized animals, but differed markedly from TNF-induced changes in a transformed intestinal epithelial cell line. Finally, our work uncovered an organoid expression signature that highlights significant expression of inflammasome signaling components in the primary intestinal epithelium, which is not detectable in commonly used cell lines.

RESULTS

PROTEOME PROFILES OF INDEPENDENTLY ESTABLISHED ORGANOID CULTURES REVEAL A LIMITED IMPACT OF THE DONOR'S MICROBIOTA

A tissue culture model should ideally exhibit limited variability and recapitulate the properties of the corresponding *in vivo* tissue. We have focused on murine intestinal epithelial organoids, as these provide an easily accessible system which allows precise control for impacts of the microbiota and the genetic background of the host. Using this system, we assessed reproducibility from genetically identical animals with the same life history, reared in the presence or the absence of a microbiota. Proteins carry most cellular functions and are tightly associated to specific phenotypes (Aebersold and Mann, 2016). Thus, as a start, we used proteome profiling to systematically probe the main sources of variability among intestinal epithelial organoid cultures and to address the relatedness of organoids to the gut epithelium.

To assess the effects of different microbiota exposures, we chose C57BL/6J wild-type mice which were bred in parallel for >2 years (>10 generations) in two separate SPF facilities featuring two different microbiotas (SR and SE), and one germ-free facility (GF). Organoid cultures were established from the jejunum of three 8-12 weeks old cohoused male littermate mice from each facility. During organoid establishment, samples corresponding to whole intestinal (distal jejunum; contains epithelium, lamina propria and submucosa) tissue (Tissue), and the

isolated epithelial fraction (Epithelium) were also collected (Figure S1). To avoid batch-to-batch medium variation, all organoid cultures were maintained using commercially available reagents (see material and methods) purchased in bulk. Organoid cultures were grown to purity, cryopreserved in liquid nitrogen, revived and grown to passage 5-8 before sample collection (Organoid, see Methods). This sample set allowed us to probe the relatedness between primary intestinal epithelial cells and the corresponding organoids, and to assess the source(s) of inter-sample variability in the absence of genetic diversity. As reference samples, we employed an immortalized murine small intestinal epithelial cell line (m-IC_{c12} (Bens et al., 1996)). Mouse embryonic fibroblasts (MEF; C57BL/6 mesodermal origin) were chosen as an outgroup representing primary cells from a different mouse organ. Using SWATH mass spectrometry (SWATH-MS) (Aebersold and Mann, 2016; Gillet et al., 2012; Liu et al., 2015, 2019; Williams et al., 2016), a proteomic data acquisition method that generates highly reproducible datasets between multiple samples, randomized sample processing, and downstream analysis in OpenSWATH (Röst et al., 2014, 2016), we were able to reproducibly quantify 3653 Swissprot murine proteins (i.e., 3,331 unique proteins matching to the transcriptomics data below) across the entire sample set. Analysis of technical SWATH-MS replicates confirmed a minimal variability stemming from the proteomics procedure itself (average Pearson correlation between technical replicates: 0.999).

Input from luminal microbiota, ingested chemicals and food particles may have profound effects on epithelial cell physiology and may imprint long-lasting characteristics, e.g. by epigenetic processes (Allaire et al., 2018; Lotz et al., 2006; Pan et al., 2018). We addressed whether such environmental conditions at the site-of-origin affected global proteome profiles within the sample set. In the unsupervised clustering, all three epithelium samples from the germ-free facility (Epithelium_GF_I-III) co-clustered in a separate subgroup from the epithelium samples of the six SPF facility mice (Epithelium_SR_I-III, _SE_I-III) (Figure 1A). While the distances were small, these results are consistent with some impact of microbiota and/or other environmental stimuli on global epithelial cell protein expression within the gut. In contrast, the corresponding organoid samples (Organoid_GF_I-III, _SR_I-III and _SE_I-III) were found to cluster essentially at random among each other (Figure 1A). Hence, source(s) of variation during establishment, cryopreservation, thawing, or continuous passaging appear to overshadow any impact of *in vivo* environment memory on the quantitative organoid proteome profiles.

Furthermore, the unsupervised clustering of the entire SWATH-MS data set revealed that the organoid samples clustered together with the epithelium (average Pearson correlation: 0.527) and gut tissue sample groups (average Pearson correlation 0.595) (Figure 1A). The m-IC_{c12} epithelial cell line sample group clustered further away in the dendrogram, and in fact was placed closer to the cultured MEFs than to either the organoid or epithelium sample groups (Figure 1A). Unsupervised clustering based on the top 100 proteins (as ranked by variance across all samples) instead of all proteins resulted in essentially identical results (Figure S2A). Moreover, a principal component analysis of the proteomes placed the organoid, the epithelium cell preparation (enriched for epithelial cells, see Methods for details), and tissue samples in proximity to each other along the main principal component (PC) 1 axis of variation, with the m-IC_{c12} and MEF samples at the opposing end of the axis (PC1 accounting for 57.34 % of the variation, Figure 1B and Figure S2B). The PC2 axis clearly resolved the organoid group from both epithelium and tissue (PC2 explained 26.58 % of the variation, Figure 1B and Figure S2B). Hence, we conclude that stable small intestinal epithelial organoid cultures exhibit a distinct proteome profile, which shows appreciable similarity to the gut epithelium *in vivo*, and is largely unaffected by the gut microbiota of the tissue donor.

To gauge the level of experimental noise, we next assessed the variability in protein expression between replicates within each sample group (measured as dispersion coefficient; i.e. standard deviation divided by the mean, in percent). As expected, the two reference cell lines (m-IC_{c12} and MEF) displayed a low variability between replicate samples (disp. coeff. of 13.27 % and 11.77%, respectively) (Table 1). A somewhat higher

variability was noted across biological replicates within the tissue (disp. coeff. 19.73 %) and epithelium (disp. coeff. 19.70 %) sample groups. By comparison, the variability within the organoid sample group was lower than within the epithelial and tissue sample groups (disp. coeff. 16.12 %) (Table 1). Two of the organoid subgroups even displayed a variability close to the one of the m-IC_{c12} sample group (disp. coeff. Organoid_SR 13.58 %; Organoid_SE 17.08 %; Organoid_GF 14.93 %) (Table 1 and 2). Considering that each organoid sample stems from a unique establishment, cryopreservation, revival, and ~3-4 additional weeks in separate culture, this degree of variability can be considered modest, and close to the variability noted for homogenous cell line cultures (m-IC_{c12} and MEF). Moreover, the variability within the tissue and epithelium samples is higher than within the organoid sample group, indicating that environmental cues influencing mouse-to-mouse variations may be partially eliminated in culture.

group	Dispersion coefficient (%)
Organoid	16.12
Tissue	19.73
Epithelium	19.7
m-IC_{c12}	13.27
MEF	11.77

Table 1 ***Dispersion coefficient of the different sample groups*****.**

group	Dispersion coefficient (%)
Organoid_SR	13.58
Organoid_SE	17.08
Organoid_GF	14.93

Table 2 ***Dispersion coefficient of the different organoid groups.***

Taken together, we conclude i) that murine small intestinal epithelial organoids exhibit a distinct proteome profile; ii) which resembles that of the *in vivo* epithelium more closely than an immortalized epithelial cell line; iii) that *in vivo* environmental factors including previous exposure to microbiota in the murine gut have a negligible impact on the global proteome of organoids; and iv) that the inter-sample variability between independent organoid cultures is only modestly higher than for commonly used cell lines.

CONTRASTING STOCHASTIC ORGANOID CULTURE VARIATION TO THE IMPACT OF A PHYSIOLOGICAL STIMULUS

In a next step, we sought to contrast the stochastic variation between independently established organoid cultures to the impact of a subtle physiological stimulus. For this purpose, we stimulated organoids with the cytokine Tumor Necrosis Factor (TNF) (5 ng/ml, 8h), known to induce a defined gene expression program in epithelial cells. Notably, we chose a low TNF concentration which would induce a distinct pro-inflammatory response rather than cell death (Janes et al., 2006; Vlantis et al., 2016). This treatment led to the significant up- or down-regulation of 15 proteins in the organoid sample group, including upregulation of typical marker proteins such as Nfkb2 (Mukherjee et al., 2017) (Figure S3A, Table S1).

Again, the global unsupervised clustering was used to assess the relative impact of stochastic culture-to-culture variability and TNF-induced changes. Notably, TNF-treated organoid samples (_T) clustered among the

untreated samples instead of forming a separate subgroup in the dendrogram (Figure 2A). A principal component analysis similarly revealed that all 18 organoid samples, irrespective of TNF-treatment, formed one mixed group placed at the opposing end of the PC1 axis from the m-IC_{c12} and MEF reference samples (Figure 2B). These data suggest a larger impact of stochastic or sample-to-sample variability (as shown in Figure 1A-B), than of subtle TNF stimulation upon the entire organoid proteome (Figure 2A-B).

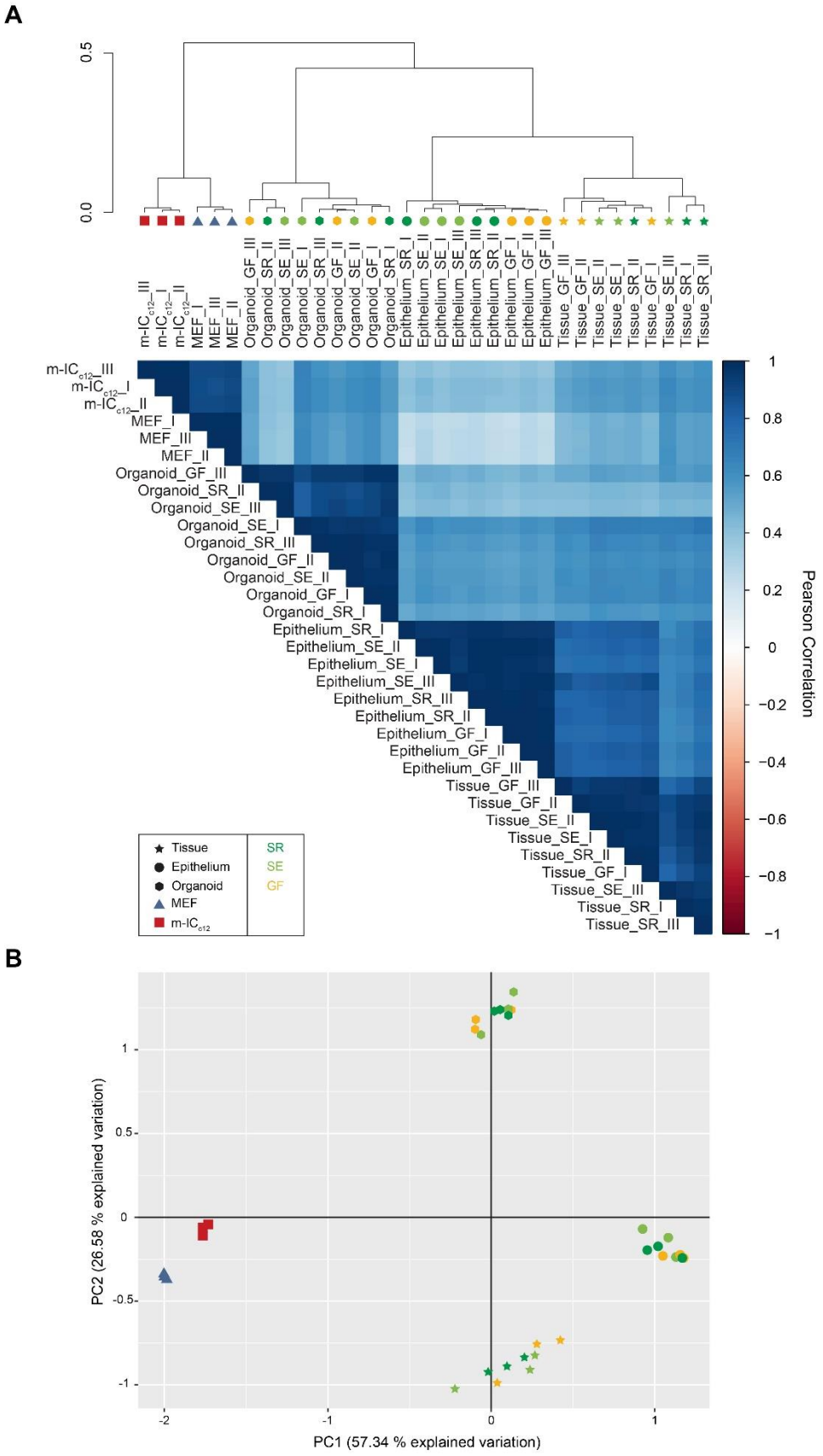

Figure 1 ***Donor microbiota minimally impacts the global protein expression pattern of small intestinal epithelial organoid cultures. A*** *Unsupervised hierarchical clustering analysis of the proteome data set including tissue (Tissue_I-III, star symbol), epithelial cell-enriched fraction (Epithelium_I-III, circle symbol) and organoid (Organoid_I-III, hexagon*

symbol) samples from mice raised in SPF facility 1 (_SR, dark green), SPF facility 2 (_SE, light green) or the germ-free facility (_GF, yellow), as well as MEF (MEF_I-III, blue triangle symbol) and m-IC_{c12} cell (m-IC_{c12}_I-III, red square symbol) samples. Correlation matrix depicts Pearson correlation values between indicated samples. ***B*** *Principal component analysis of the proteome data set as described in A.*

To complement the proteome data, an identical analysis was also conducted at the transcriptomic level by Illumina HiSeq 4000 sequencing (Figure 2C-D), which has a higher sensitivity for low-abundance targets. We detected and mapped on average $4.26x10^7$ reads per sample. TNF treatment induced significant up- or down-regulation of 316 out of 15698 total transcripts (Figure S3B, Table S2). Among these are previously described TNF-target genes, including *Nfkb2*, *Tnfaip3*, *C3* and *Relb* (Mukherjee et al., 2017; Sheerin et al., 1997; Vlantis et al., 2016; Zhao et al., 2015). Again, neither unsupervised clustering nor a principle component analysis of the whole transcriptomes resolved the TNF-treated organoid samples from the untreated sample group (Figure 2C-D). In fact, 5 out of 9 TNF-treated samples clustered closest to their non-treated counterparts (see e.g. Organoid_SE_I and Organoid_SE_I_T; Figure 2C). This is well in line with the subtle, physiological nature of the TNF stimulus employed in our experiment, in analogy to a typical specific biochemical perturbation, which is expected to affect only a very small set of selected genes in epithelial cells (Janes et al., 2006; Vlantis et al., 2016). Similar conclusions could be drawn both at the proteome and transcriptome level when the analysis was redone for the 100 proteins/transcripts contributing most to variation (Figure S4A-D). Hence, stochastic variability between separate organoid cultures has a stronger impact on the global expression pattern than the defined alteration of 15/3331 (0.45%) proteins and 316/15698 (2.01%) transcripts through low-level TNF stimulation.

ROBUST INDUCTION OF A TNF-INDUCED GENE EXPRESSION PROGRAM IN ORGANOIDS FROM DIFFERENTIALLY COLONIZED MICE

The data above reveal a modestly elevated variability in baseline organoid gene expression, as compared to cultured cell lines (Figure 1-2). For an experimental model system to be useful, another key aspect is the ability to respond reproducibly to a given stimulus. To assess this, we estimated the similarity in specific gene expression changes induced by TNF stimulation, comparing the panel of transcripts significantly altered by TNF across organoids of different origin, i.e. from the germ-free facility (mean of Organoid_GF) and the two SPF facilities (means of Organoid_SR and Organoid_SE; "Organoid_SPF"). This analysis revealed that the organoids derived from germ-free mice responded to TNF with a robust degree of similarity to those derived from SPF mice (R^2=0.563, Figure 3A). This implies that neither prior *in vivo* stem cell exposure/non-exposure to gut microbes, nor variability in the organoid production process, imprint differences that may preclude interpretation of the small intestinal organoid responses to the prototypical stimulus TNF.

Traditionally, cultured cell lines have been used as a proxy for studies of cell signaling and gene expression regulation in the gut epithelium. We next compared the specific gene expression changes induced by TNF stimulation in m-IC_{c12} cells versus SPF organoids. The correlation between significantly regulated transcripts was here considerably lower (Figure 3B, R^2=0.206). In fact, the vast majority of transcripts significantly up or down-regulated in either the m-IC_{c12} or the organoid group failed to show a corresponding behavior in the other group (Figure 3B). We conclude that the gene expression changes induced by a physiological stimulus may vary substantially between an intestinal epithelial cell line and primary epithelial organoids from the same species. The variability in response between organoids from germ-free and SPF mice, by contrast, appears more modest.

A

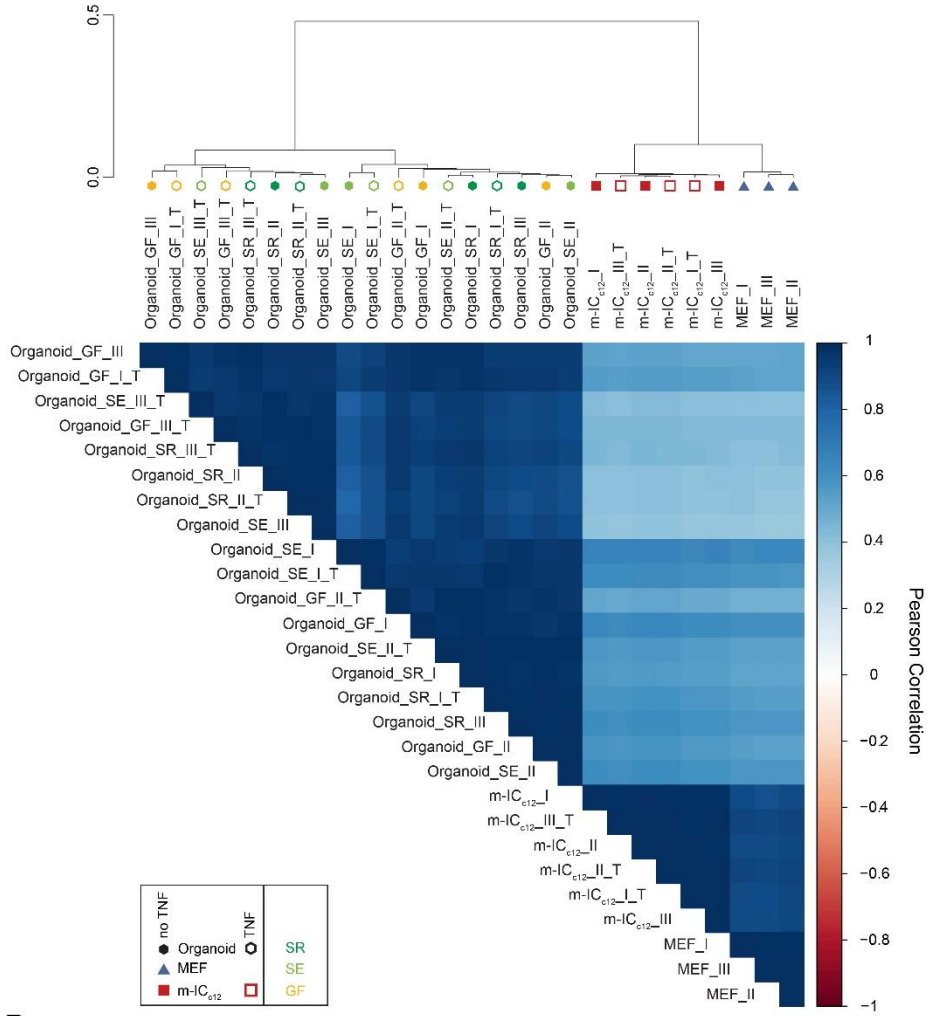
0.5
0.0
Organoid_GF_III
Organoid_GF_I_T
Organoid_SE_III_T
Organoid_GF_III_T
Organoid_SR_III_T
Organoid_SR_II
Organoid_SR_II_T
Organoid_SE_III
Organoid_SE_I
Organoid_SE_I_T
Organoid_GF_II_T
Organoid_GF_I
Organoid_SE_II_T
Organoid_SR_I
Organoid_SR_I_T
Organoid_SR_III
Organoid_GF_II
Organoid_SE_II
m-IC$_{c12}$_I
m-IC$_{c12}$_III_T
m-IC$_{c12}$_II
m-IC$_{c12}$_II_T
m-IC$_{c12}$_I_T
m-IC$_{c12}$_III
MEF_I
MEF_III
MEF_II
Pearson Correlation
1
0.8
0.6
0.4
0.2
0
−0.2
−0.4
−0.6
−0.8
−1
no TNF
TNF
Organoid
MEF
m-IC$_{c12}$
SR
SE
GF

B

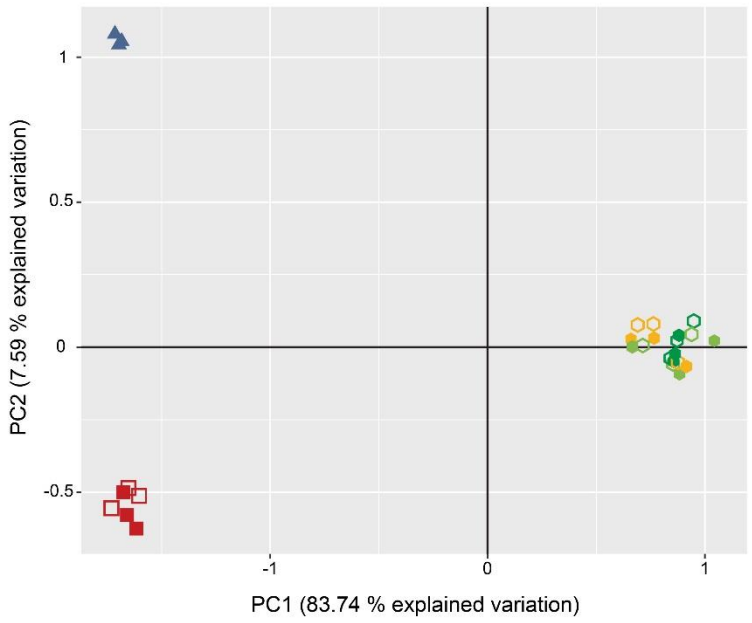
1
0.5
0
-0.5
-1
0
1
PC2 (7.59 % explained variation)
PC1 (83.74 % explained variation)

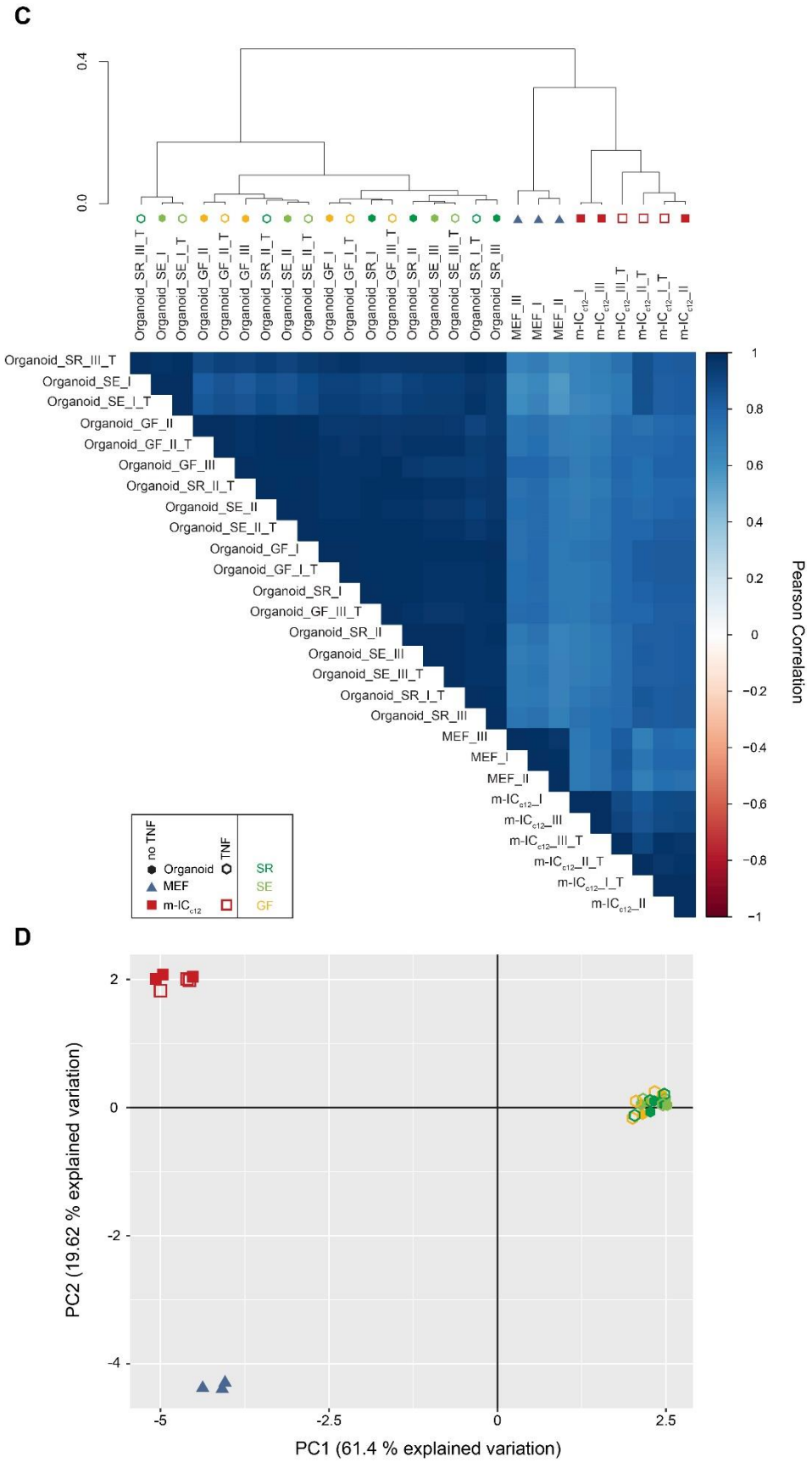

Figure 2 ***Stochastic variability between separate organoid cultures has a stronger impact on global gene expression than a defined, physiological stimulus. A*** *Unsupervised hierarchical clustering analysis of the proteome data set*

including untreated (closed symbols) and TNF-treated (5 ng/ml, 8h; open symbols;_T) organoid (Organoid_I-III, hexagon symbol) samples from mice raised in SPF facility 1 (_SR, dark green), SPF facility 2 (_SE, light green) or the germ-free facility (_GF, yellow), as well as MEF (MEF_I-III, blue triangle symbol) and m-IC$_{c12}$ cell (m-IC$_{c12}$_I-III, red square symbol) samples. Correlation matrix depicts Pearson correlation values between indicated samples. ***B*** *Principal component analysis of the proteome data set as described in A.* ***C*** *Unsupervised hierarchical clustering analysis of the transcriptome data set for the samples described in A. D Principal component analysis of the transcriptome data set as described in C.*

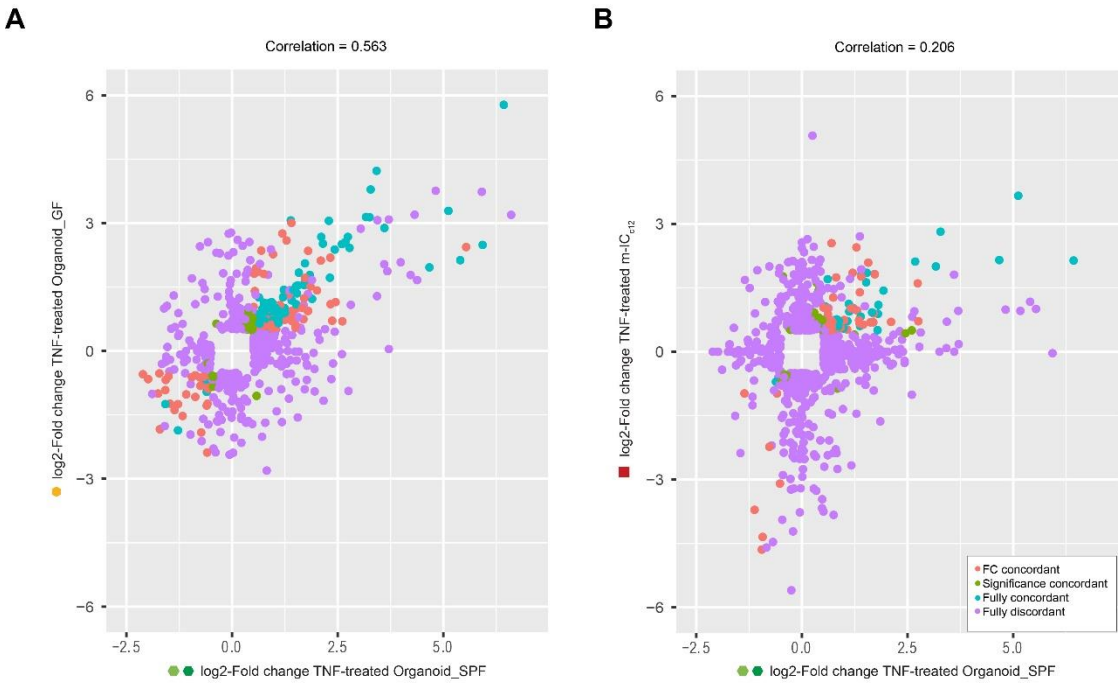

Figure 3 ***The TNF-induced transcriptional response of organoids from germ-free and colonized mice shows robust correlation. A*** *Correlation plot of TNF-induced changes in germ-free mouse derived organoids (y-axis, Organoid_GF) plotted against TNF-induced changes in SPF-derived organoids (x-axis, Organoid_SPF).* ***B*** *Correlation plot of TNF-induced changes in m-IC$_{c12}$ cells (y-axis, m-IC$_{c12}$) plotted against TNF-induced changes in SPF-derived organoids (x-axis, Organoid_SPF). Shown are fully concordant hits (blue), hits concordant in fold change (FC; red), hits concordant in p-value (green) and fully disconcordant hits (purple). Cut-offs: genes with log2 ratio <-0.5 or >0.5 and p-value <0.05 in at least one of the sample groups.*

A SMALL SET OF TRANSCRIPTS AND PROTEINS DEFINE AN ORGANOID-TYPIC EXPRESSION SIGNATURE

When applying unsupervised clustering to proteomes and transcriptomes of only the cultured cell sample groups (i.e. Organoids, m-IC$_{c12}$ cells and MEFs), we again found that in both cases, PC1 (explaining 83.56%/61.27% of the variation) clearly distinguished the organoid group from the other samples (S5A-B). PC2 (explaining 8.2%/19.13% of the variation) defined a smaller variance distance between MEFs and m-IC$_{c12}$ sample groups (S5A-B). This allowed investigation of the transcripts and proteins which define an organoid-typic expression signature.

As a starting point, we performed an integrative analysis of the transcriptome and proteome data sets, using the DIABLO framework of the CRAN package mixOmics (Rohart et al., 2017). The correlation between up- or downregulated proteins and their corresponding transcripts was high when comparing the organoid group to the MEF and m-IC$_{c12}$ groups (R^2=0.719) (Figure S5C). We identified 14 transcripts and 10 proteins that

distinguished an organoid expression signature. Herein, the expression levels of 9 transcripts (*Ena*, *Ankrd1*, *Dusp14*, *Dmwd*, *Il7*, *Amotl2*, *Evc2*, *Wwtr1-202* and *Trim35*) and 5 proteins (Capn2, Myg1, Lgals1, Bcat1 and ASC/Pycard) contributed to PC1. Expression levels of 5 transcripts (*Q8R164*, *Hs6st1*, *Sigirr*, *Map3k21* and *Pdlim1*) and 5 proteins (Coa3, Eml2, Rdh11, Selenbp1 and Krt18) defined PC2 (Figure S5D, 4A-B, Table S3). Generally, expression levels of most transcripts and proteins within a PC positively correlated with each other (Figure 4A). The variables associated with the main PC1 were upregulated in the MEF and m-IC_{c12} groups compared to the organoids. Here, ASC provided a notable exception, with substantially higher protein levels in organoids than in both MEFs and m-IC_{c12} cells (Figure 4B). The transcripts/proteins that defined PC2 showed moderate expression in organoids, upregulated levels in m-IC_{c12} cells and low expression in MEFs. Only the *Pdlim1* transcript behaved inversely between the MEF and m-IC_{c12} groups (Figure 4B).

To test if the identified organoid signature agreed with expression levels in the gut epithelium, we reassessed expression of the 10 protein hits (Figure 4) in the entire proteome data set, i.e. including also the tissue and epithelium sample groups (Figure S6). Strikingly, these identifier proteins showed highly similar expression levels in the epithelium samples and in organoids (Figure S6). Expression levels in whole intestinal tissue, which contains a mix of epithelial cells and multiple other cell types, appeared less similar. Finally, MEFs and m-IC_{c12} samples formed a separate outgroup also in this comparison (Figure S6). Hence, we have uncovered a small set of transcripts and proteins that constitute a physiologically relevant small intestinal epithelial organoid signature.

Interestingly, the signature included high expression of the inflammasome-scaffold protein ASC (apoptotic speck-like protein) (Figure 4B) (Richards et al., 2001). Inflammasomes mediate responses to pathogen- (PAMP) or damage-associated patterns (DAMP) by activation of Caspase-1 or Caspase-11, resulting in the release of active IL18 and/or IL1β, as well as induction of cell death (Broz, 2019). To probe whether additional inflammasome signaling components were also highly expressed specifically in organoids, we revisited the transcriptome data set. Strikingly, m-IC_{c12} cells and MEFs showed low or undetectable expression levels for all inflammasome components analyzed here (Figure 5). By contrast, organoids specifically expressed high levels of the NAIP/NLRC4 inflammasome components *Naip1*, *2*, *5*, *6* and *Nlrc4*, as well as *Asc*, *Nlrp6*, and *Caspase-1*. The expression of *Caspase-11* and *Gsdmd* could be induced by TNF in organoids, whereas *Gsdme* and *Nlrp3* transcripts were not detectably expressed in any of the analyzed sample groups. Finally, the pro-apoptotic proteases *Caspase-3* and *-8* were expressed at similar levels across organoids and m-IC_{c12} cells.

Taken together, these data suggest that intestinal epithelial organoids from differentially colonized donors exhibit a shared expression signature, which encompasses significant expression of inflammasome signaling components.

A

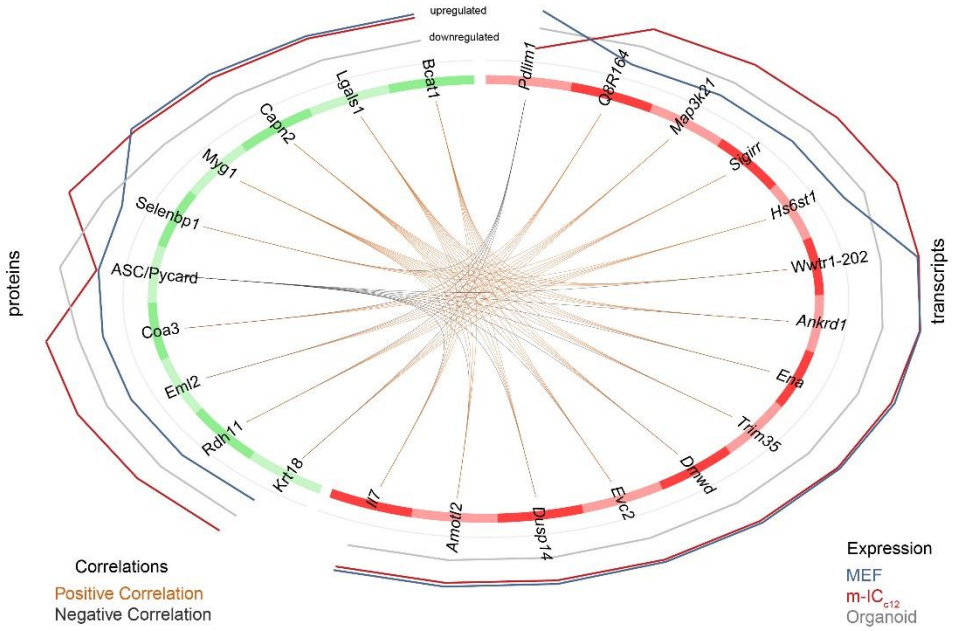

B

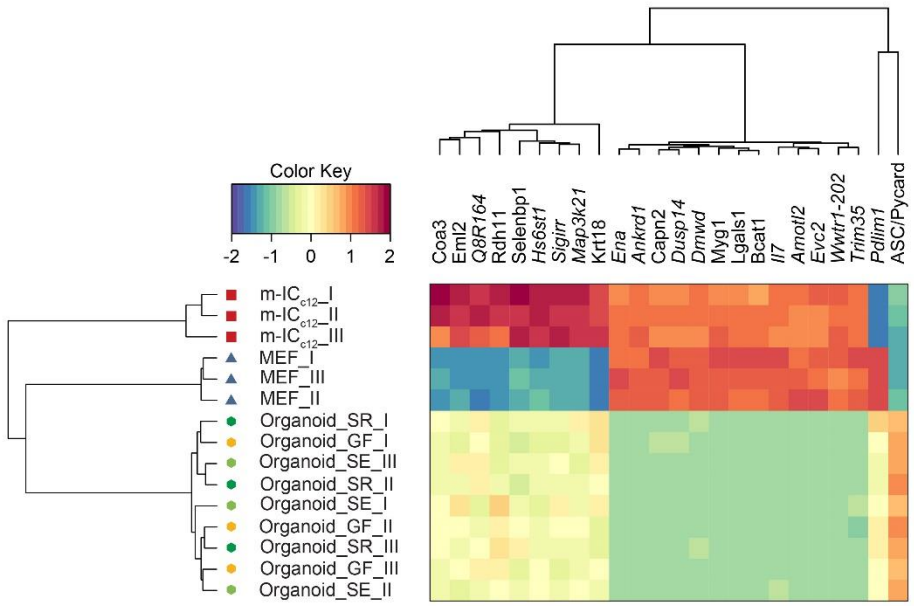

Figure 4 ***Identification of an organoid-typic expression signature by integrative analysis. A*** *Circos plot depicting the correlation of expression levels of the identified transcripts and proteins within the three analyzed sample groups (Organoid (grey line), MEF (blue line) and m-IC$_{c12}$ (red line)).* ***B*** *Unsupervised hierarchical clustering analysis and expression heat map of the identified transcripts and proteins shown in A for Organoid (Organoid_I-III, hexagon symbol) samples from mice raised in SPF facility 1 (_SR, dark green), SPF facility 2 (_SE, light green) or the germ-free facility (_GF, yellow), as well as MEFs (MEF_I-III, blue triangle symbol) and m-IC$_{c12}$ cell (m-IC$_{c12}$_I-III, red square symbol) samples.*

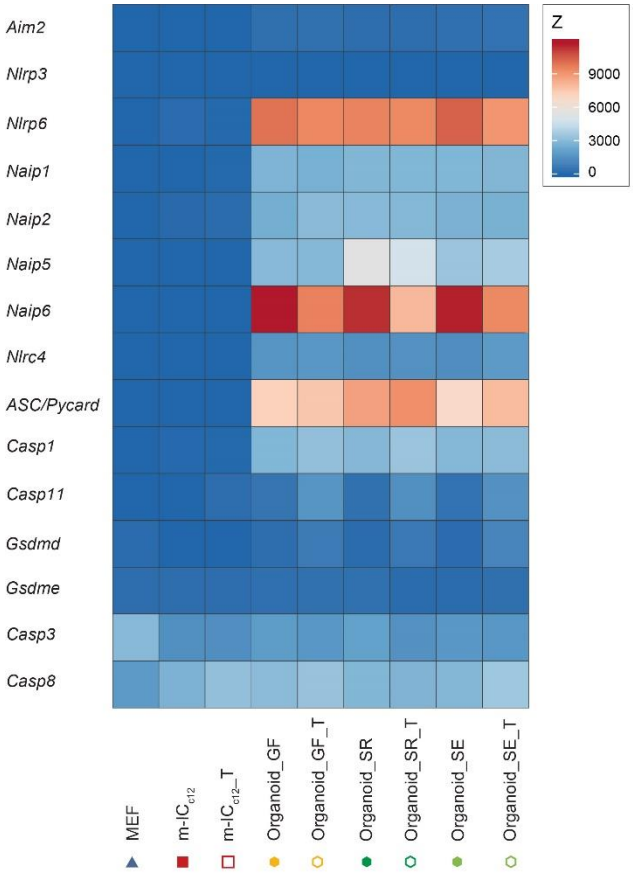

Figure 5 ***Inflammasome components are highly expressed in organoids compared to m-IC$_{c12}$ cells and fibroblasts.*** *Heat map depicting expression levels of several inflammasome components in untreated or TNF-treated (_T) organoids (Organoid_I-III, hexagon symbol) samples from mice raised in SPF facility 1 (_SR, dark green), SPF facility 2 (_SE, light green) or the germ-free facility (_GF, yellow), as well as untreated or TNF-treated (_T) m-IC$_{c12}$ cell (m-IC$_{c12}$_I-III, red square symbol) and MEF (MEF_I-III, blue triangle symbol) samples.*

DISCUSSION

Our work validates that murine small intestinal organoids are an experimental system with a robust expression pattern that resembles the phenotype of the homeostatic intestinal epithelium (Janeckova et al., 2019; Lindeboom et al., 2018). Importantly, our work extends previous data by demonstrating that this phenotype is largely independent from exposure with SPF microbiota. This is in contrast to *in vivo* studies, in which microbiota divergence between separately held mouse lines can affect a range of physiological functions and lead to non-reproducible results (Mamantopoulos et al., 2017, 2018; Robertson et al., 2019; Stappenbeck and Virgin, 2016). Even extensive co-housing appears insufficient to fully homogenize the gut microbiota and its impact between previously separated animals (Robertson et al., 2019). Donor-derived microbial cues in organoids grown in culture for ≥5 passages do not globally overshadow other sources of experimental variability. In line with this, organoids from SPF and GF donor mice showed a robust degree of concordance with respect to transcripts induced by low concentrations of the cytokine TNF. Littermate controls (which share the same microbiota) are a prerequisite for the accurate interpretation of *in vivo* gut biology data from knockout or transgenic animals. However, we here found that organoid experimentation may not require such littermate controls, as organoids from mouse colonies with or without microbiota yielded equivalent expression phenotypes. Notably, this applies to organoids cultured for ≥5 passages. It is likely that microbiota imprints are detectable in earlier passages (Janeckova et al., 2019).

The observed culture-to-culture variation in expression profiles may stem from bottleneck effects during early organoid establishment and/or adaptation to the culture conditions. In addition, the differentiation state and cell type composition of organoids is highly sensitive to the concentration of growth factors provided in the culture medium (e.g. Noggin, R-spondin, and EGF), or produced by the organoids themselves (e.g. Wnt3a) (Farin et al., 2016; van der Flier and Clevers, 2009; Kim et al., 2014; Lehmann et al., 2019; Lindeboom et al., 2018; Sato et al., 2009). Fluctuation of these, often unstable, proteinaceous factors provides another plausible source of culture-to-culture variability. While the exact impact of these and potentially other causes remain to be examined, the net effect is a moderately higher variation in expression (~1.5-fold increased dispersion coefficient for the proteome) among organoid cultures compared to the herein used reference cell lines. Considering that organoids more accurately mimic the overall expression patterns of the gut epithelium (this study), faithfully recapitulate the epithelial cell type composition of the intact gut, and in contrast to cell lines retain genetic stability over time (Ben-David et al., 2018; Liu et al., 2019; Sato and Clevers, 2013; Sato et al., 2009), organoids nevertheless appear vastly superior to classical cell line models for predicting physiological responses in the intestinal epithelium.

Combined, our findings have implications for experimentation in intestinal epithelial organoids. As mentioned above, littermate control organoids appear oblivious, as microbiota differences between tissue donors do not confound the analyzed global organoid phenotypes. Instead, the moderately elevated culture-to-culture variability may warrant larger experimental samples sizes overall to reliably detect subtle phenotypes. Finally, key findings should be validated in independently established organoid cultures from additional tissue donors to ensure reproducibility of results. It should be noted that these conclusions are strictly valid only for the small intestinal epithelial organoids of inbred specified pathogen free mice, as analyzed in this study. We cannot exclude that persisting microbiota effects would be more pronounced in colon organoids, due to higher microbial exposure within this gut region *in vivo*. Nor do our data refute that some specific organoid signaling pathways can be affected by the tissue donor's microbial status, especially during early culture passages (Janeckova et al., 2019) or in cases of pathobiont exposure. Human interindividual variation also exceeds that of genetically inbred animals, which has repercussions for experimental design in patient-derived organoids (Cristobal et al., 2017).

By integration of the transcriptome and the proteome datasets, we were able to identify a physiologically relevant organoid-typic expression signature, distinguishing the full set of organoid cultures across all three SPF/GF mouse colonies from the reference cell lines. Interestingly, this signature highlighted high expression of ASC, a central scaffolding protein for inflammasome signaling pathways (Richards et al., 2001). Our follow-up analysis extended this finding to also encompass the transcripts for a range of other inflammasome receptors (e.g. *Naip1, 2, 5, 6, Nlrc4*), inflammatory caspases (e.g. *Caspase-1*) and downstream executors (e.g. *GsdmD*), which all exhibited high expression in organoids and low to undetectable expression in epithelial cell line m-IC_{c12} and fibroblast reference cells. Importantly, high expression of these inflammasome components in epithelial cells were reported previously (Chapter 4) (Winsor et al., 2019), further indicating that organoids more realistically represent the *in vivo* situation. The differential regulation of inflammasome components upon exposure to the pro-inflammatory cytokine TNF likely represents a preparation of epithelial cells to microbial exposure. Upon sensing of PAMPs or DAMPs, inflammasomes drive acute pro-inflammatory and anti-microbial responses (Broz and Dixit, 2016). However, earlier studies have also implicated e.g. ASC, NAIPs, NLRP3, and NLRP6 as tumor suppressors (Allam et al., 2015; Allen et al., 2010; Das et al., 2006; Normand et al., 2011). A hallmark feature of inflammasome activation is the prompt induction of cell death machinery in the activated cell (Aglietti et al., 2016; Kayagaki et al., 2011; Knodler et al., 2010, 2014; Miao et al., 2010; Rauch et al., 2017; Richards et al., 2001; Sellin et al., 2014; Shi et al., 2015). It therefore seems conceivable that upon transformation/immortalization of epithelial cell lines, there would be a strong selective pressure to lose or downregulate inflammasome pathway components and thereby dampen cell death effects. By contrast,

organoids grown under optimal conditions retain expression also of such potential tumor suppressor genes. Notably, with regard to the widely discussed reciprocal interactions between microbiota and inflammasomes in the gut (Mamantopoulos et al., 2017; Robertson et al., 2019; Seo et al., 2015; Winsor et al., 2019), the expression of inflammasome components appears unaffected by the donor microbiota in small intestinal epithelial organoids. Thus, compared to classical tissue culture cell lines, organoids should be more realistic models to study the function of epithelial inflammasomes.

While the impact and mechanisms of inflammasome signaling in typical immune cells (e.g. macrophages, dendritic cells) have been thoroughly documented (Boyden and Dietrich, 2006; Franchi et al., 2006; Mariathasan et al., 2004; Martinon et al., 2006; Miao et al., 2006), the importance of intestinal epithelial inflammasomes in tissue homeostasis and defense has become evident only recently (Allam et al., 2015; Harrison et al., 2015; Knodler et al., 2010, 2014; Nowarski et al., 2015; Rauch et al., 2017; Sellin et al., 2014; Winsor et al., 2019). Tumor-derived or immortalized cell lines have traditionally been used as proxies for molecular studies in intestinal epithelia, which may in part explain why intestinal epithelial inflammasomes have for long been overlooked. We anticipate that the transition into primary organoids as the tissue culture models of choice will reshape our understanding of these and other physiological signaling circuits in the gut mucosa and beyond.

ACKNOWLEDGEMENTS

We thank the Hardt, Sellin and Aebersold labs for discussions and input, and Miguel Cuenca, Shinichi Sunagawa, the Functional Genomics Center Zürich, as well as the RCHCI and EPIC animal facilities, for their support. YL was supported by Pilot Grants from Yale Cancer Systems Biology Symposium and Yale Cancer Center, Yale University. MES was supported by the Swedish Research Council (2015-00635, 2018-02223) and the Swedish Foundation for Strategical Research (ICA16-0031). WDH was supported by the Swiss National Science 635 Foundation (SNF) (310030_53074 and 310030B_173338/1). The authors declare no conflicts of interests.

Disclosure

The authors declare no conflicts of interest.

METHODS

Mice

Animal experiments were approved by the Kantonales Verterinäramt Zürich, Switzerland under the license number 193/2016 and performed in accordance with ethical and legal requirements. C57BL/6 mice were kept under specific and opportunistic pathogen-free (SPF) conditions in individually ventilated cages either in the Rodent Center HCI (RCHCI, "SR") or in the ETH Phenomics Center (EPIC, "SE") (ETH Zurich, Switzerland). Germ free C57BL/6 mice were kept in isolators at ETH EPIC (“GF”). Mice derived from one facility were cohoused littermates, male and 8-12 weeks old at the time of experimentation.

Murine organoid culture establishment and maintenance

For organoid establishment, mice were euthanized and the small intestine isolated. Fat and vessels were removed. A ~5 cm piece of the distal jejunum was collected, washed three times in 1 ml Phosphate Buffered Saline (PBS)/0.01% Bovine Serum Albumin (BSA) and a ~2x2mm piece snap frozen in liquid nitrogen for later analysis of whole tissue (“Tissue”). The remaining tissue was opened longitudinally and washed in PBS to remove content and mucus. Subsequently, the tissue was minced and washed thoroughly in ice-cold PBS,

followed by 15 min incubation in Gentle Dissociation Reagent (Stemcell Technologies) on a rocking table at room-temperature. Intestinal crypts were sequentially extracted by four rounds of mechanical shearing in PBS/0.1% BSA. Typically, the first and second fraction contained differentiated epithelial cells, whereas the third and fourth fraction were enriched for stem cell-containing crypts. After filtration through a 70µm cell strainer, parts of fractions 1-4 were pooled, washed with PBS/0.1% BSA, pelleted (300g, 5min, 4°C) and half of the sample was snap frozen in liquid nitrogen for analysis of primary epithelial cells ("Epithelium"). The remaining half of fractions three and four were embedded into 50µl Matrigel (Chemie Brunschwig) domes and kept in complete Intesticult medium (Stemcell Technologies) at 37°C, 5% CO_2. After 3-4 days of culturing, the best-looking wells were selected for propagation. Complete Intesticult medium was replaced every 3-4 days. Organoids were subcultured every 5-7 days by mechanical shearing in Gentle Dissociation Reagent and re-embedding in 50µl Matrigel domes at a 1:2 to 1:4 splitting ratio. Stable organoid cultures were cryopreserved at passage (P) 2-4 in complete medium supplemented with 10% Dimethyl Sulfoxide (DMSO). For experimentation, cryopreserved organoids were thawed, maintained in culture as above for at least two weeks and used for experimentation at P5-8.

Cell line culture and maintenance

Mouse Embryonic Fibroblasts (MEFs) were maintained in DMEM-Glutamax supplemented with 10 % heat-inactivated Fetal Calf Serum (FCS) and 0.05 mg/ml Streptomycin at 37°C, 5% CO_2. M-ICc12 cells were cultured in DMEM/F12 supplemented with 5µg/ml human Insulin, 50nM Dexamethasone, 60nM Sodium selenite, 5µg/ml Bovine Apo-Transferrin, 1nM Triiodthyronin, 40µg/ml EGF, 20µM HEPES and 2.5% heat-inactivated FCS at 37°C, 5% CO_2.

TNF treatment and harvesting of organoid and cell line samples

For TNF treatment, the medium was removed and replaced by the respective culture medium supplemented with 5ng/ml murine TNF (Preprotech). For untreated controls, the medium was exchanged. After 8h, the medium was removed. Organoids (P5-8) were incubated with Gentle Dissociation Reagent for 1min to dissolve the Matrigel, but not the organoids. After pipetting up and down 10 times, extracted organoids were transferred to Eppendorf tubes (pre-coated over night with PBS/0.01% BSA), washed in cold PBS/0.01% BSA and spun down (5min at 300g, 4°C). The supernatant was discarded and the pellets snap frozen in liquid nitrogen for later analysis ("Organoids"). MEFs and m-ICc12 cells were washed with pre-warmed PBS and incubated for 3 (MEFs) or 12 (m-IC_{c12} cells) min with gentle dissociation reagent at 37°C. Subsequently, cells were detached from the bottom of the flask with the help of a cell scraper, pelleted by centrifugation (300g, 5min, 4°C) and the supernatant was removed. Pellets were washed with PBS/0.01% BSA, transferred to Eppendorf tubes (pre-coated with PBS/0.01% BSA), spun down (300 g, 5min, 4°C) and subsequently snap frozen in liquid nitrogen for later analysis.

RNA sequencing

Snap frozen cell/organoid pellets were lysed with the QIAShredder columns (Qiagen) according to manufacturer`s instructions. RNA was isolated with the Qiagen RNeasy Micro Kit including a DNA digestion step. Subsequently, RNA concentration was assessed on a Qubit Fluorometer (Invitrogen) using a Qubit™ RNA HS Assay Kit and samples were loaded on a Fragment Analyzer (Advanced Analytical, DNF-471-0500 Standard Sensitivity RNA Analysis Kit (15nt)) to determine RNA quality. RNA samples were diluted to 20 ng/ml for RNA sequencing and frozen at -80°C. Samples were

processed with the TruSeq RNA sample Prep Kit v2 (Illumina, Inc, California, USA). RNA samples (100-1000 ng) were polyA-enriched, reverse-transcribed into double-stranded cDNA and fragmented followed by end-repair, polyadenylation and ligation of TruSeq adapters containing multiplex-indices. Subsequently, fragments containing TruSeq adapters were selectively enriched by PCR and quality and quantity of the enriched libraries were analyzed using a Qubit 1.0 fluorometer and the Caliper GX LabChip® GX (Caliper Life Sciences, Inc., USA). The libraries were normalized to 10 nM in Tris-Cl 10 mM, pH8.5 with 0.1% Tween 20. Cluster generation was performed with TruSeq PR Cluster Kit (Illumina, Inc, California, USA) using 10 pM of the pooled normalized libraries on the cBOT. Sequencing was performed using the TruSeq SBS Kit HS4000 (Illumina, Inc, California, USA) on an Illumina HiSeq 4000 single end 125 bp. The transcriptome data set was uploaded to the GEO data base (Accession number GSE140703).

Proteome analysis

All the biological samples were suspended in 10M Urea with complete protease inhibitor cocktail (Roche) and ultrasonically lysed in a VialTweeter device (Hielscher-Ultrasound Technology), as previously described (Collins et al., 2017; Liu et al., 2019). The mixtures were centrifuged at 21,000 g for 1 hour and the supernatant protein amount was quantified by Bio-Rad protein assay. Protein samples were reduced by 10mM Tris-(2-carboxyethyl)-phosphine (TCEP) for 1 hour at 37°C and 20 mM iodoacetamide (IAA) in the dark for 45 minutes at room temperature. All the samples were further diluted by 1:6 (v/v) with 100 mM NH_4HCO_3 and were digested with sequencing-grade porcine trypsin (Promega) at a protease/protein ratio of 1:25 overnight at 37°C. The amount of the purified peptides was determined using Nanodrop ND-1000 (Thermo Scientific) and 1.5 µg peptides were injected per a LC-MS run. The peptide samples were stored in -80°C before measurment.

An SCIEX 5600 TripleTOF mass spectrometer was interfaced with an Eksigent NanoLC. Peptides were directly injected onto a 20-cm PicoFrit emitter (New Objective, self-packed to 20 cm), and then separated using a 90-min gradient at a flow rate of 300 nL/min (Gillet et al., 2012; Liu et al., 2019). For shotgun sequencing mode, MS1 spectra were collected in the range 360–1,460 m/z with 250ms per scan. The 20 most intense precursors triggered MS2 spectra were collected (50–2,000 m/z for 100 ms). For SWATH mode, 64-variable window schema was used (Collins et al., 2017; Liu et al., 2019; Ludwig et al., 2018). A dwell time of 50 ms was used for all MS2 scans after a survey MS1 scan of 250 ms, resulting in a duty cycle of ~3.45 s.

OpenSWATH (Röst et al., 2014) was used to identify peptides from all SWATH maps with statistical control at 1% FDR and then to align between SWATH maps using a novel TRIC with requantification option enabled (TRansfer of Identification Confidence) (Röst et al., 2016). Because we had nine samples for tissue and epithelium type of samples analyzed in this dataset (18 samples for organoid type), to further increase the protein confidence, only those peptide signals identified in more than eight samples were accepted for protein identification and quantification. To quantify the protein abundance levels across samples, we used the Top3 method (Grossmann et al., 2010; Liu et al., 2015; Ludwig et al., 2012; Williams et al., 2016). The quantitative protein matrix was rounded to the full integer value for further analysis. The input for the downstream analysis of the protein expression data was the matrix obtained by applying TMM-normalization to the raw count matrix. The proteome data set was uploaded to the PRIDE database (project ID PXD016339).

Data analysis

RNA sequencing

Reads were quality-checked with FastQC. Sequencing adapters were removed with Trimmomatic (Bolger et al., 2014) and reads were hard-trimmed by 5 bases at the 3' end. Successively, reads at least 20 bases long, and with an overall average phred quality score greater than 10 were aligned to the reference genome and transcriptome of Mus musculus (FASTA and GTF files, respectively, downloaded from GRCm38, Release 91) with STAR v2.5.1 (Dobin et al., 2013) with default settings for single end reads. Distribution of the reads across genomic isoform expression was quantified using the R package GenomicRanges (Lawrence et al., 2013) from Bioconductor Version 3.0.

Differential Expression

Differentially expressed genes and proteins were identified using the R package edgeR (Robinson et al., 2010) from Bioconductor Version 3.0, using a generalised linear model (glm) and Quasi-likelihood (QL) F-test coupled with a Trimmed Means of M-values (TMM) normalization. In a differential expression analyses, a gene is marked as DE if it possesses the following characteristics: 1) at least 10 counts in at least half of the samples in one group (*above background noise* criterion, genes not meeting this criterion are marked as *absent*); 2) p <= 0.05; 3) log2 (fold change) >= 0.5.

Transcriptomics - Proteomics integration

The integration of the Transcriptomics and the Proteomics data was performed using the Diablo framework (Singh et al., 2019) from the CRAN package mixOmics (Rohart et al., 2017). Briefly, 3 components are chosen based on an initial fitting (function mixOmics::block.splsda) and on a 5-Mfold, 30 repeats evaluation (function mixOmics::perf). Successively, a list of subset variables was run through a 5-Mfold, 30 repeats tuning step (function mixOmics::tune.block.splsda) using centroids distance to select the optimal subset of variables for the final model.

Data availability

The mass spectrometry proteomics data have been deposited to the ProteomeXchange Consortium via the PRIDE (Perez-Riverol et al., 2019) partner repository with the dataset identifier PXD016339.

The transcriptomics data have been deposited to the GEO repository (Edgar et al., 2002) with the dataset identifier GSE140703.

REFERENCES

Aebersold, R., and Mann, M. (2016). Mass-spectrometric exploration of proteome structure and function. Nature *537*, 347–355.

Aglietti, R.A., Estevez, A., Gupta, A., Ramirez, M.G., Liu, P.S., Kayagaki, N., Ciferri, C., Dixit, V.M., and Dueber, E.C. (2016). GsdmD p30 elicited by caspase-11 during pyroptosis forms pores in membranes. Proc. Natl. Acad. Sci. U.S.A. *113*, 7858–7863.

Allaire, J.M., Crowley, S.M., Law, H.T., Chang, S.-Y., Ko, H.-J., and Vallance, B.A. (2018). The Intestinal Epithelium: Central Coordinator of Mucosal Immunity. Trends in Immunology *39*, 677–696.

Allam, R., Maillard, M.H., Tardivel, A., Chennupati, V., Bega, H., Yu, C.W., Velin, D., Schneider, P., and Maslowski, K.M. (2015). Epithelial NAIPs protect against colonic tumorigenesis. J. Exp. Med. *212*, 369–383.

Allen, I.C., TeKippe, E.M., Woodford, R.-M.T., Uronis, J.M., Holl, E.K., Rogers, A.B., Herfarth, H.H., Jobin, C., and Ting, J.P.-Y. (2010). The NLRP3 inflammasome functions as a negative regulator of tumorigenesis during colitis-associated cancer. J. Exp. Med. *207*, 1045–1056.

Almeqdadi, M., Mana, M.D., Roper, J., and Yilmaz, Ö.H. (2019). Gut organoids: mini-tissues in culture to study intestinal physiology and disease. Am. J. Physiol., Cell Physiol. *317*, C405–C419.

Antoni, D., Burckel, H., Josset, E., and Noel, G. (2015). Three-dimensional cell culture: a breakthrough in vivo. Int J Mol Sci *16*, 5517–5527.

Ben-David, U., Siranosian, B., Ha, G., Tang, H., Oren, Y., Hinohara, K., Strathdee, C.A., Dempster, J., Lyons, N.J., Burns, R., et al. (2018). Genetic and transcriptional evolution alters cancer cell line drug response. Nature *560*, 325–330.

Benjamin, J.L., Sumpter, R., Levine, B., and Hooper, L.V. (2013). Intestinal epithelial autophagy is essential for host defense against invasive bacteria. Cell Host Microbe *13*, 723–734.

Bens, M., Bogdanova, A., Cluzeaud, F., Miquerol, L., Kerneis, S., Kraehenbuhl, J.P., Kahn, A., Pringault, E., and Vandewalle, A. (1996). Transimmortalized mouse intestinal cells (m-ICc12) that maintain a crypt phenotype. Am. J. Physiol. *270*, C1666-1674.

Bolger, A.M., Lohse, M., and Usadel, B. (2014). Trimmomatic: a flexible trimmer for Illumina sequence data. Bioinformatics *30*, 2114–2120.

Boyden, E.D., and Dietrich, W.F. (2006). Nalp1b controls mouse macrophage susceptibility to anthrax lethal toxin. Nat. Genet. *38*, 240–244.

Broz, P. (2019). Recognition of Intracellular Bacteria by Inflammasomes. Microbiol Spectr *7*.

Broz, P., and Dixit, V.M. (2016). Inflammasomes: mechanism of assembly, regulation and signalling. Nat. Rev. Immunol. *16*, 407–420.

Chen, B., Ni, X., Sun, R., Zeng, B., Wei, H., Tian, Z., and Wei, H. (2018). Commensal Bacteria-Dependent CD8αβ+ T Cells in the Intestinal Epithelium Produce Antimicrobial Peptides. Front. Immunol. *9*.

Co, J.Y., Margalef-Català, M., Li, X., Mah, A.T., Kuo, C.J., Monack, D.M., and Amieva, M.R. (2019). Controlling Epithelial Polarity: A Human Enteroid Model for Host-Pathogen Interactions. Cell Reports *26*, 2509-2520.e4.

Collins, B.C., Hunter, C.L., Liu, Y., Schilling, B., Rosenberger, G., Bader, S.L., Chan, D.W., Gibson, B.W., Gingras, A.-C., Held, J.M., et al. (2017). Multi-laboratory assessment of reproducibility, qualitative and quantitative performance of SWATH-mass spectrometry. Nat Commun *8*, 291.

Cristobal, A., van den Toorn, H.W.P., van de Wetering, M., Clevers, H., Heck, A.J.R., and Mohammed, S. (2017). Personalized Proteome Profiles of Healthy and Tumor Human Colon Organoids Reveal Both Individual Diversity and Basic Features of Colorectal Cancer. Cell Rep *18*, 263–274.

Das, P.M., Ramachandran, K., Vanwert, J., Ferdinand, L., Gopisetty, G., Reis, I.M., and Singal, R. (2006). Methylation mediated silencing of TMS1/ASC gene in prostate cancer. Mol. Cancer *5*, 28.

Dobin, A., Davis, C.A., Schlesinger, F., Drenkow, J., Zaleski, C., Jha, S., Batut, P., Chaisson, M., and Gingeras, T.R. (2013). STAR: ultrafast universal RNA-seq aligner. Bioinformatics *29*, 15–21.

Drost, J., van Jaarsveld, R.H., Ponsioen, B., Zimberlin, C., van Boxtel, R., Buijs, A., Sachs, N., Overmeer, R.M., Offerhaus, G.J., Begthel, H., et al. (2015). Sequential cancer mutations in cultured human intestinal stem cells. Nature *521*, 43–47.

Edgar, R., Domrachev, M., and Lash, A.E. (2002). Gene Expression Omnibus: NCBI gene expression and hybridization array data repository. Nucleic Acids Res. *30*, 207–210.

Farin, H.F., Jordens, I., Mosa, M.H., Basak, O., Korving, J., Tauriello, D.V.F., de Punder, K., Angers, S., Peters, P.J., Maurice, M.M., et al. (2016). Visualization of a short-range Wnt gradient in the intestinal stem-cell niche. Nature *530*, 340–343.

van der Flier, L.G., and Clevers, H. (2009). Stem cells, self-renewal, and differentiation in the intestinal epithelium. Annu. Rev. Physiol. *71*, 241–260.

Fogh, J., and Trempe, G. (1975). New Human Tumor Cell Lines. In Human Tumor Cells in Vitro, J. Fogh, ed. (Boston, MA: Springer US), pp. 115–159.

Fogh, J., Wright, W.C., and Loveless, J.D. (1977). Absence of HeLa cell contamination in 169 cell lines derived from human tumors. J. Natl. Cancer Inst. *58*, 209–214.

Foster, S.L., and Medzhitov, R. (2009). Gene-specific control of the TLR-induced inflammatory response. Clin. Immunol. *130*, 7–15.

Foulke-Abel, J., In, J., Kovbasnjuk, O., Zachos, N.C., Ettayebi, K., Blutt, S.E., Hyser, J.M., Zeng, X.-L., Crawford, S.E., Broughman, J.R., et al. (2014). Human enteroids as an ex-vivo model of host–pathogen interactions in the gastrointestinal tract. Exp Biol Med (Maywood) *239*, 1124–1134.

Franchi, L., Amer, A., Body-Malapel, M., Kanneganti, T.-D., Özören, N., Jagirdar, R., Inohara, N., Vandenabeele, P., Bertin, J., Coyle, A., et al. (2006). Cytosolic flagellin requires Ipaf for activation of caspase-1 and interleukin 1β in salmonella-infected macrophages. Nat Immunol *7*, 576–582.

Gillet, L.C., Navarro, P., Tate, S., Röst, H., Selevsek, N., Reiter, L., Bonner, R., and Aebersold, R. (2012). Targeted data extraction of the MS/MS spectra generated by data-independent acquisition: a new concept for consistent and accurate proteome analysis. Mol. Cell Proteomics *11*, O111.016717.

Grossmann, J., Roschitzki, B., Panse, C., Fortes, C., Barkow-Oesterreicher, S., Rutishauser, D., and Schlapbach, R. (2010). Implementation and evaluation of relative and absolute quantification in shotgun proteomics with label-free methods. J Proteomics *73*, 1740–1746.

Gunasekara, D.B., DiSalvo, M., Wang, Y., Nguyen, D.L., Reed, M.I., Speer, J., Sims, C.E., Magness, S.T., and Allbritton, N.L. (2018). Development of Arrayed Colonic Organoids for Screening of Secretagogues Associated with Enterotoxins. Anal. Chem. *90*, 1941–1950.

Harrison, O.J., Srinivasan, N., Pott, J., Schiering, C., Krausgruber, T., Ilott, N.E., and Maloy, K.J. (2015). Epithelial-derived IL-18 regulates Th17 cell differentiation and Foxp3$^+$ Treg cell function in the intestine. Mucosal Immunology *8*, 1226–1236.

Jakobsson, H.E., Rodríguez-Piñeiro, A.M., Schütte, A., Ermund, A., Boysen, P., Bemark, M., Sommer, F., Bäckhed, F., Hansson, G.C., and Johansson, M.E. (2015). The composition of the gut microbiota shapes the colon mucus barrier. EMBO Reports *16*, 164–177.

Janeckova, L., Kostovcikova, K., Svec, J., Stastna, M., Strnad, H., Kolar, M., Hudcovic, T., Stancikova, J., Tureckova, J., Baloghova, N., et al. (2019). Unique Gene Expression Signatures in the Intestinal Mucosa and Organoids Derived from Germ-Free and Monoassociated Mice. Int J Mol Sci *20*.

Janes, K.A., Gaudet, S., Albeck, J.G., Nielsen, U.B., Lauffenburger, D.A., and Sorger, P.K. (2006). The Response of Human Epithelial Cells to TNF Involves an Inducible Autocrine Cascade. Cell *124*, 1225–1239.

Kayagaki, N., Warming, S., Lamkanfi, M., Vande Walle, L., Louie, S., Dong, J., Newton, K., Qu, Y., Liu, J., Heldens, S., et al. (2011). Non-canonical inflammasome activation targets caspase-11. Nature *479*, 117–121.

Kim, T.-H., Li, F., Ferreiro-Neira, I., Ho, L.-L., Luyten, A., Nalapareddy, K., Long, H., Verzi, M., and Shivdasani, R.A. (2014). Broadly permissive intestinal chromatin underlies lateral inhibition and cell plasticity. Nature *506*, 511–515.

Knodler, L.A., Vallance, B.A., Celli, J., Winfree, S., Hansen, B., Montero, M., and Steele-Mortimer, O. (2010). Dissemination of invasive Salmonella via bacterial-induced extrusion of mucosal epithelia. Proc. Natl. Acad. Sci. U.S.A. *107*, 17733–17738.

Knodler, L.A., Crowley, S.M., Sham, H.P., Yang, H., Wrande, M., Ma, C., Ernst, R.K., Steele-Mortimer, O., Celli, J., and Vallance, B.A. (2014). Noncanonical inflammasome activation of caspase-4/caspase-11 mediates epithelial defenses against enteric bacterial pathogens. Cell Host Microbe *16*, 249–256.

Lawrence, M., Huber, W., Pagès, H., Aboyoun, P., Carlson, M., Gentleman, R., Morgan, M.T., and Carey, V.J. (2013). Software for computing and annotating genomic ranges. PLoS Comput. Biol. *9*, e1003118.

Lee, Y.-S., Kim, T.-Y., Kim, Y., Lee, S.-H., Kim, S., Kang, S.W., Yang, J.-Y., Baek, I.-J., Sung, Y.H., Park, Y.-Y., et al. (2018). Microbiota-Derived Lactate Accelerates Intestinal Stem-Cell-Mediated Epithelial Development. Cell Host & Microbe *24*, 833-846.e6.

Lehmann, R., Lee, C.M., Shugart, E.C., Benedetti, M., Charo, R.A., Gartner, Z., Hogan, B., Knoblich, J., Nelson, C.M., and Wilson, K.M. (2019). Human organoids: a new dimension in cell biology. MBoC *30*, 1129–1137.

Lindeboom, R.G., van Voorthuijsen, L., Oost, K.C., Rodríguez-Colman, M.J., Luna-Velez, M.V., Furlan, C., Baraille, F., Jansen, P.W., Ribeiro, A., Burgering, B.M., et al. (2018). Integrative multi-omics analysis of intestinal organoid differentiation. Molecular Systems Biology *14*, e8227.

Liu, Y., Buil, A., Collins, B.C., Gillet, L.C.J., Blum, L.C., Cheng, L.-Y., Vitek, O., Mouritsen, J., Lachance, G., Spector, T.D., et al. (2015). Quantitative variability of 342 plasma proteins in a human twin population. Mol. Syst. Biol. *11*, 786.

Liu, Y., Mi, Y., Mueller, T., Kreibich, S., Williams, E.G., Van Drogen, A., Borel, C., Frank, M., Germain, P.-L., Bludau, I., et al. (2019). Multi-omic measurements of heterogeneity in HeLa cells across laboratories. Nat. Biotechnol. *37*, 314–322.

Lotz, M., Gütle, D., Walther, S., Ménard, S., Bogdan, C., and Hornef, M.W. (2006). Postnatal acquisition of endotoxin tolerance in intestinal epithelial cells. J. Exp. Med. *203*, 973–984.

Ludwig, C., Claassen, M., Schmidt, A., and Aebersold, R. (2012). Estimation of absolute protein quantities of unlabeled samples by selected reaction monitoring mass spectrometry. Mol. Cell Proteomics *11*, M111.013987.

Ludwig, C., Gillet, L., Rosenberger, G., Amon, S., Collins, B.C., and Aebersold, R. (2018). Data-independent acquisition-based SWATH-MS for quantitative proteomics: a tutorial. Mol. Syst. Biol. *14*, e8126.

Mamantopoulos, M., Ronchi, F., Van Hauwermeiren, F., Vieira-Silva, S., Yilmaz, B., Martens, L., Saeys, Y., Drexler, S.K., Yazdi, A.S., Raes, J., et al. (2017). Nlrp6- and ASC-Dependent Inflammasomes Do Not Shape the Commensal Gut Microbiota Composition. Immunity *47*, 339-348.e4.

Mamantopoulos, M., Ronchi, F., McCoy, K.D., and Wullaert, A. (2018). Inflammasomes make the case for littermate-controlled experimental design in studying host-microbiota interactions. Gut Microbes *9*, 374–381.

Mariathasan, S., Newton, K., Monack, D.M., Vucic, D., French, D.M., Lee, W.P., Roose-Girma, M., Erickson, S., and Dixit, V.M. (2004). Differential activation of the inflammasome by caspase-1 adaptors ASC and Ipaf. Nature *430*, 213–218.

Martinon, F., Pétrilli, V., Mayor, A., Tardivel, A., and Tschopp, J. (2006). Gout-associated uric acid crystals activate the NALP3 inflammasome. Nature *440*, 237–241.

Miao, E.A., Alpuche-Aranda, C.M., Dors, M., Clark, A.E., Bader, M.W., Miller, S.I., and Aderem, A. (2006). Cytoplasmic flagellin activates caspase-1 and secretion of interleukin 1β via Ipaf. Nat Immunol *7*, 569–575.

Miao, E.A., Leaf, I.A., Treuting, P.M., Mao, D.P., Dors, M., Sarkar, A., Warren, S.E., Wewers, M.D., and Aderem, A. (2010). Caspase-1-induced pyroptosis is an innate immune effector mechanism against intracellular bacteria. Nat. Immunol. *11*, 1136–1142.

Mukherjee, T., Chatterjee, B., Dhar, A., Bais, S.S., Chawla, M., Roy, P., George, A., Bal, V., Rath, S., and Basak, S. (2017). A TNF-p100 pathway subverts noncanonical NF-κB signaling in inflamed secondary lymphoid organs. EMBO J. *36*, 3501–3516.

Niepel, M., Hafner, M., Mills, C.E., Subramanian, K., Williams, E.H., Chung, M., Gaudio, B., Barrette, A.M., Stern, A.D., Hu, B., et al. (2019). A Multi-center Study on the Reproducibility of Drug-Response Assays in Mammalian Cell Lines. Cell Systems *9*, 35-48.e5.

Normand, S., Delanoye-Crespin, A., Bressenot, A., Huot, L., Grandjean, T., Peyrin-Biroulet, L., Lemoine, Y., Hot, D., and Chamaillard, M. (2011). Nod-like receptor pyrin domain-containing protein 6 (NLRP6) controls epithelial self-renewal and colorectal carcinogenesis upon injury. Proc. Natl. Acad. Sci. U.S.A. *108*, 9601–9606.

Nowarski, R., Jackson, R., Gagliani, N., de Zoete, M.R., Palm, N.W., Bailis, W., Low, J.S., Harman, C.C.D., Graham, M., Elinav, E., et al. (2015). Epithelial IL-18 Equilibrium Controls Barrier Function in Colitis. Cell *163*, 1444–1456.

Pan, W.-H., Sommer, F., Falk-Paulsen, M., Ulas, T., Best, P., Fazio, A., Kachroo, P., Luzius, A., Jentzsch, M., Rehman, A., et al. (2018). Exposure to the gut microbiota drives distinct methylome and transcriptome changes in intestinal epithelial cells during postnatal development. Genome Medicine *10*, 27.

Perez-Riverol, Y., Csordas, A., Bai, J., Bernal-Llinares, M., Hewapathirana, S., Kundu, D.J., Inuganti, A., Griss, J., Mayer, G., Eisenacher, M., et al. (2019). The PRIDE database and related tools and resources in 2019: improving support for quantification data. Nucleic Acids Res. *47*, D442–D450.

Rauch, I., Deets, K.A., Ji, D.X., von Moltke, J., Tenthorey, J.L., Lee, A.Y., Philip, N.H., Ayres, J.S., Brodsky, I.E., Gronert, K., et al. (2017). NAIP-NLRC4 Inflammasomes Coordinate Intestinal Epithelial Cell Expulsion with Eicosanoid and IL-18 Release via Activation of Caspase-1 and -8. Immunity *46*, 649–659.

Reedy, A.R., Luo, L., Neish, A.S., and Jones, R.M. (2019). Commensal microbiota-induced redox signaling activates proliferative signals in the intestinal stem cell microenvironment. Development *146*.

Richards, N., Schaner, P., Diaz, A., Stuckey, J., Shelden, E., Wadhwa, A., and Gumucio, D.L. (2001). Interaction between pyrin and the apoptotic speck protein (ASC) modulates ASC-induced apoptosis. J. Biol. Chem. *276*, 39320–39329.

Robertson, S.J., Lemire, P., Maughan, H., Goethel, A., Turpin, W., Bedrani, L., Guttman, D.S., Croitoru, K., Girardin, S.E., and Philpott, D.J. (2019). Comparison of Co-housing and Littermate Methods for Microbiota Standardization in Mouse Models. Cell Rep *27*, 1910-1919.e2.

Robinson, M.D., McCarthy, D.J., and Smyth, G.K. (2010). edgeR: a Bioconductor package for differential expression analysis of digital gene expression data. Bioinformatics *26*, 139–140.

Rohart, F., Gautier, B., Singh, A., and Lê Cao, K.-A. (2017). mixOmics: An R package for 'omics feature selection and multiple data integration. PLoS Comput. Biol. *13*, e1005752.

Röst, H.L., Rosenberger, G., Navarro, P., Gillet, L., Miladinović, S.M., Schubert, O.T., Wolski, W., Collins, B.C., Malmström, J., Malmström, L., et al. (2014). OpenSWATH enables automated, targeted analysis of data-independent acquisition MS data. Nat. Biotechnol. *32*, 219–223.

Röst, H.L., Sachsenberg, T., Aiche, S., Bielow, C., Weisser, H., Aicheler, F., Andreotti, S., Ehrlich, H.-C., Gutenbrunner, P., Kenar, E., et al. (2016). OpenMS: a flexible open-source software platform for mass spectrometry data analysis. Nat. Methods *13*, 741–748.

Sallusto, F., and Lanzavecchia, A. (1994). Efficient presentation of soluble antigen by cultured human dendritic cells is maintained by granulocyte/macrophage colony-stimulating factor plus interleukin 4 and downregulated by tumor necrosis factor alpha. J. Exp. Med. *179*, 1109–1118.

Sato, T., and Clevers, H. (2013). Primary mouse small intestinal epithelial cell cultures. Methods Mol. Biol. *945*, 319–328.

Sato, T., Vries, R.G., Snippert, H.J., van de Wetering, M., Barker, N., Stange, D.E., van Es, J.H., Abo, A., Kujala, P., Peters, P.J., et al. (2009). Single Lgr5 stem cells build crypt-villus structures in vitro without a mesenchymal niche. Nature *459*, 262–265.

Sato, T., van Es, J.H., Snippert, H.J., Stange, D.E., Vries, R.G., van den Born, M., Barker, N., Shroyer, N.F., van de Wetering, M., and Clevers, H. (2011). Paneth cells constitute the niche for Lgr5 stem cells in intestinal crypts. Nature *469*, 415–418.

Savage, D.C., Siegel, J.E., Snellen, J.E., and Whitt, D.D. (1981). Transit time of epithelial cells in the small intestines of germfree mice and ex-germfree mice associated with indigenous microorganisms. Appl Environ Microbiol *42*, 996–1001.

Scherer, W.F., Syverton, J.T., and Gey, G.O. (1953). Studies on the propagation in vitro of poliomyelitis viruses. IV. Viral multiplication in a stable strain of human malignant epithelial cells (strain HeLa) derived from an epidermoid carcinoma of the cervix. J. Exp. Med. *97*, 695–710.

Sellin, M.E., Müller, A.A., Felmy, B., Dolowschiak, T., Diard, M., Tardivel, A., Maslowski, K.M., and Hardt, W.-D. (2014). Epithelium-intrinsic NAIP/NLRC4 inflammasome drives infected enterocyte expulsion to restrict Salmonella replication in the intestinal mucosa. Cell Host Microbe *16*, 237–248.

Seo, S.-U., Kamada, N., Muñoz-Planillo, R., Kim, Y.-G., Kim, D., Koizumi, Y., Hasegawa, M., Himpsl, S.D., Browne, H.P., Lawley, T.D., et al. (2015). Distinct Commensals Induce Interleukin-1β via NLRP3 Inflammasome in Inflammatory Monocytes to Promote Intestinal Inflammation in Response to Injury. Immunity *42*, 744–755.

Sheerin, N.S., Zhou, W., Adler, S., and Sacks, S.H. (1997). TNF-alpha regulation of C3 gene expression and protein biosynthesis in rat glomerular endothelial cells. Kidney Int. *51*, 703–710.

Shi, J., Zhao, Y., Wang, K., Shi, X., Wang, Y., Huang, H., Zhuang, Y., Cai, T., Wang, F., and Shao, F. (2015). Cleavage of GSDMD by inflammatory caspases determines pyroptotic cell death. Nature *526*, 660–665.

Singh, A., Shannon, C.P., Gautier, B., Rohart, F., Vacher, M., Tebbutt, S.J., and Lê Cao, K.-A. (2019). DIABLO: an integrative approach for identifying key molecular drivers from multi-omics assays. Bioinformatics *35*, 3055–3062.

Sommer, F., and Bäckhed, F. (2016). Know your neighbor: Microbiota and host epithelial cells interact locally to control intestinal function and physiology. Bioessays *38*, 455–464.

Stappenbeck, T.S., and Virgin, H.W. (2016). Accounting for reciprocal host-microbiome interactions in experimental science. Nature *534*, 191–199.

Stecher, B., Paesold, G., Barthel, M., Kremer, M., Jantsch, J., Stallmach, T., Heikenwalder, M., and Hardt, W.-D. (2006). Chronic Salmonella enterica Serovar Typhimurium-Induced Colitis and Cholangitis in Streptomycin-Pretreated Nramp1+/+ Mice. Infection and Immunity *74*, 5047–5057.

Stone, L.B., and Takemoto, K.K. (1970). Transformation of Mouse Macrophages by Simian Virus 40. J Virol *6*, 621–627.

Sun, J. (2017). Intestinal organoid as an in vitro model in studying host-microbial interactions. Front. Biol. *12*, 94–102.

Takahashi, T. (2019). Organoids for Drug Discovery and Personalized Medicine. Annual Review of Pharmacology and Toxicology *59*, 447–462.

Tuveson, D., and Clevers, H. (2019). Cancer modeling meets human organoid technology. Science *364*, 952–955.

Vlantis, K., Wullaert, A., Polykratis, A., Kondylis, V., Dannappel, M., Schwarzer, R., Welz, P., Corona, T., Walczak, H., Weih, F., et al. (2016). NEMO Prevents RIP Kinase 1-Mediated Epithelial Cell Death and Chronic Intestinal Inflammation by NF-κB-Dependent and -Independent Functions. Immunity *44*, 553–567.

Walsh, A.J., Cook, R.S., Sanders, M.E., Arteaga, C.L., and Skala, M.C. (2016). Drug response in organoids generated from frozen primary tumor tissues. In Scientific Reports, p.

Williams, E.G., Wu, Y., Jha, P., Dubuis, S., Blattmann, P., Argmann, C.A., Houten, S.M., Amariuta, T., Wolski, W., Zamboni, N., et al. (2016). Systems proteomics of liver mitochondria function. Science *352*, aad0189.

Williamson, I.A., Arnold, J.W., Samsa, L.A., Gaynor, L., DiSalvo, M., Cocchiaro, J.L., Carroll, I., Azcarate-Peril, M.A., Rawls, J.F., Allbritton, N.L., et al. (2018). A High-Throughput Organoid Microinjection Platform to Study Gastrointestinal Microbiota and Luminal Physiology. Cell Mol Gastroenterol Hepatol *6*, 301–319.

Winsor, N., Krustev, C., Bruce, J., Philpott, D.J., and Girardin, S.E. (2019). Canonical and noncanonical inflammasomes in intestinal epithelial cells. Cell. Microbiol. e13079.

Zhang, Y.-G., Wu, S., Xia, Y., and Sun, J. (2014). Salmonella-infected crypt-derived intestinal organoid culture system for host-bacterial interactions. Physiol Rep *2*.

Zhao, Z., Hou, X., Yin, X., Li, Y., Duan, R., Boyce, B.F., and Yao, Z. (2015). TNF Induction of NF-κB RelB Enhances RANKL-Induced Osteoclastogenesis by Promoting Inflammatory Macrophage Differentiation but also Limits It through Suppression of NFATc1 Expression. PLoS ONE *10*, e0135728.

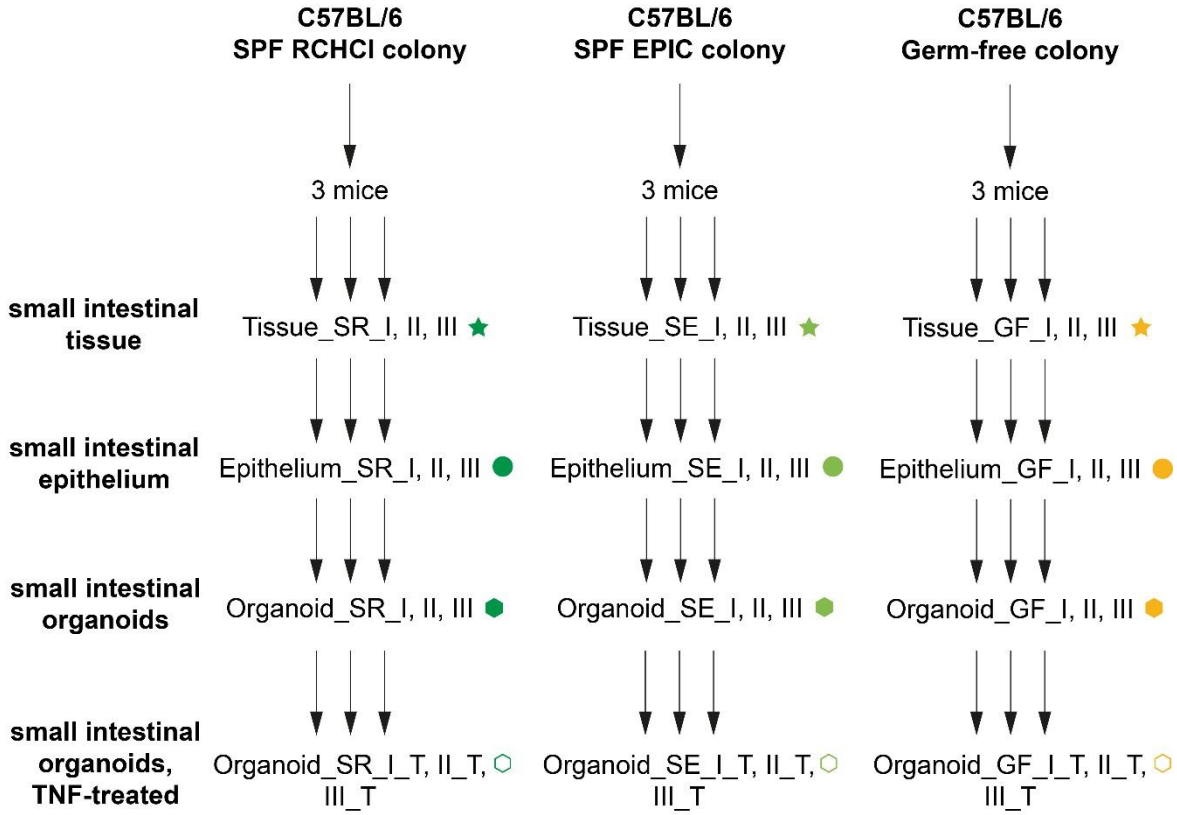

Figure S1 ***Sample workflow of primary samples.*** *Tissue: distal jejunum; contains epithelium, lamina propria and submucosa. Epithelium: epithelial cell-enriched fraction.*

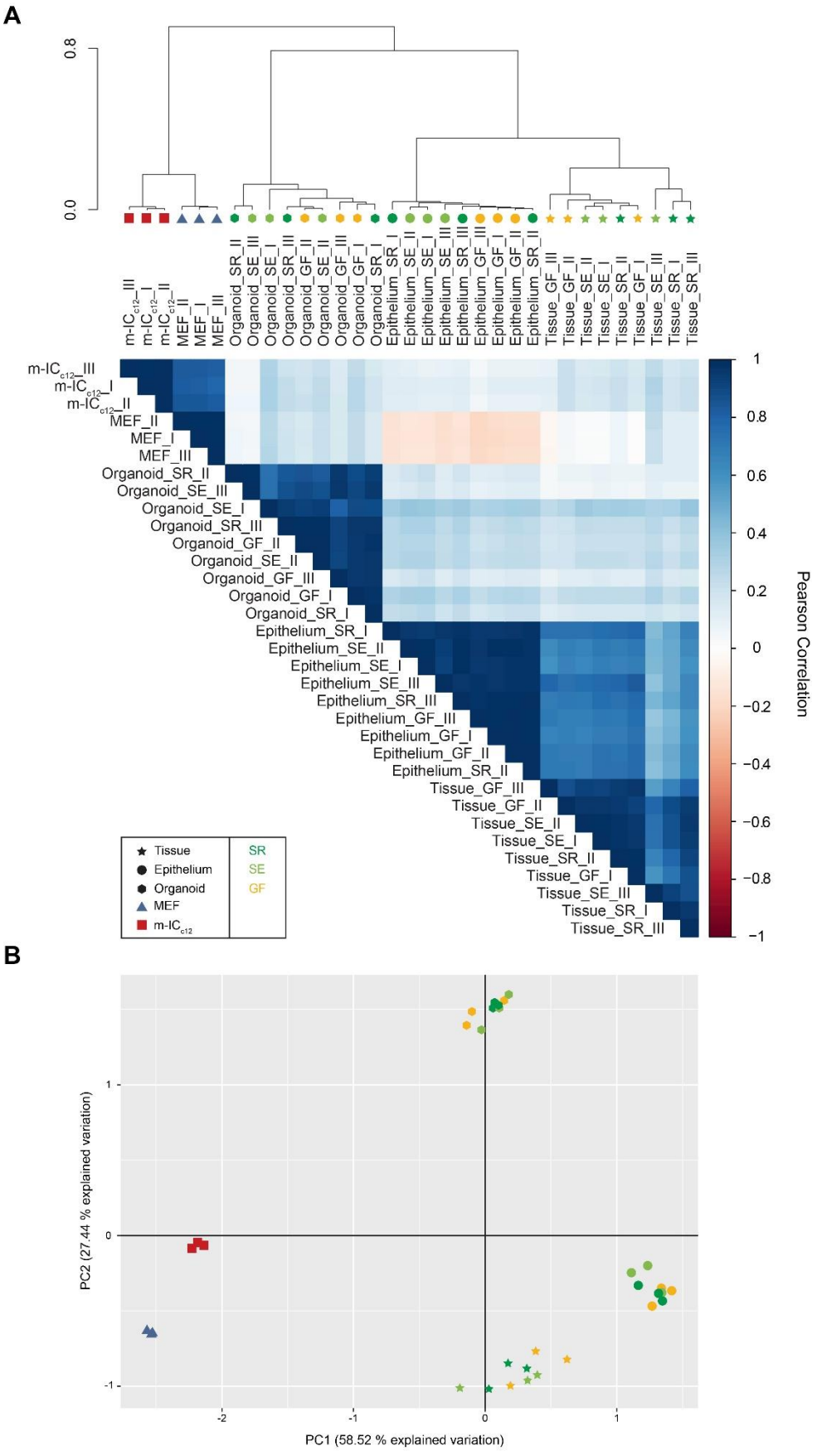

Figure S2 ***Organoid samples cluster among each other, independent of donor microbiota. A*** *Unsupervised hierarchical clustering analysis of the top 100 hits, as ranked by variance across all the samples, of the*

proteome data set including tissue (Tissue_I-III, star symbol), epithelial cell-enriched fraction (Epithelium_I-III, circle symbol), organoid (Organoid_I-III, hexagon symbol) samples from mice raised in SPF facility 1 (_SR, dark green), SPF facility 2 (_SE, light green) or the germ-free facility (_GF, yellow), as well as MEFs (MEF_I-III, blue triangle symbol) and m-IC$_{c12}$ cell (m-IC$_{c12}$_I-III, red square symbol) samples. Correlation matrix depicts Pearson correlation values between indicated samples. ***B*** *Principal component analysis of the proteome data set as described in A.*

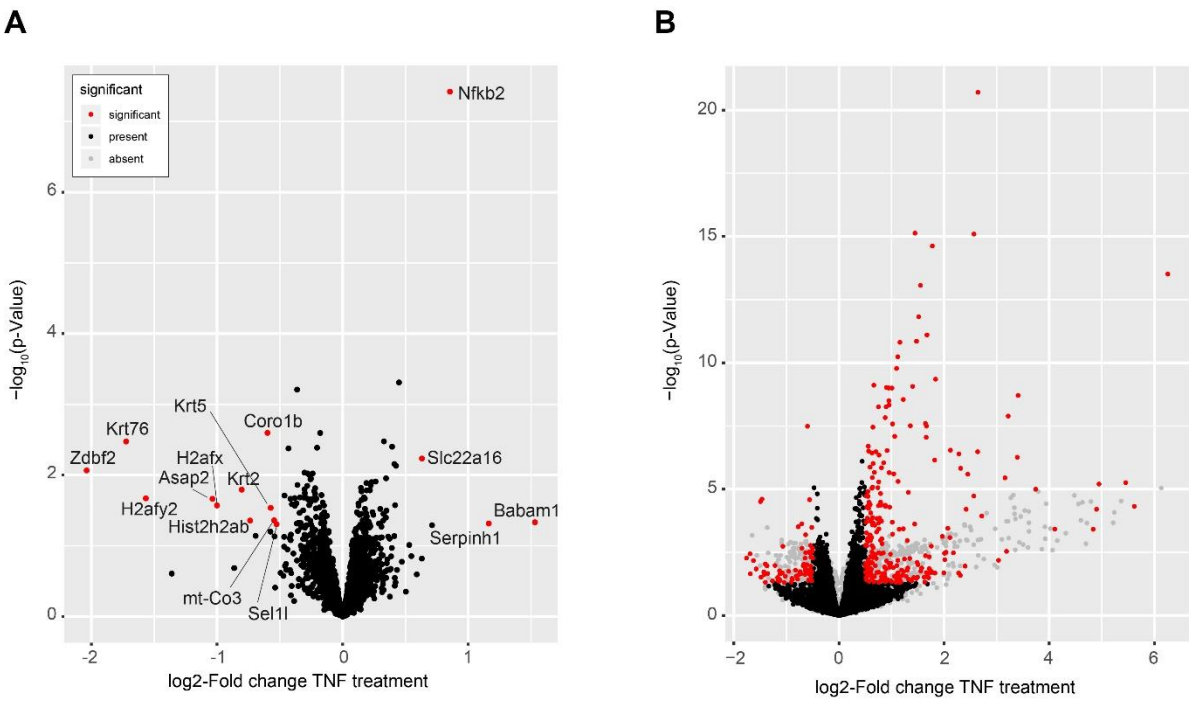

Figure S3 ***TNF-induced target expression in organoids. A*** *Volcano plot showing TNF-induced protein changes in the organoid sample group.* ***B*** *Volcano plot showing TNF-induced transcript changes in the organoid sample group. Red dots: siginificant. Differential expression cut-offs: log2 ratio <-0.5 or >0.5 and p-value <0.05.*

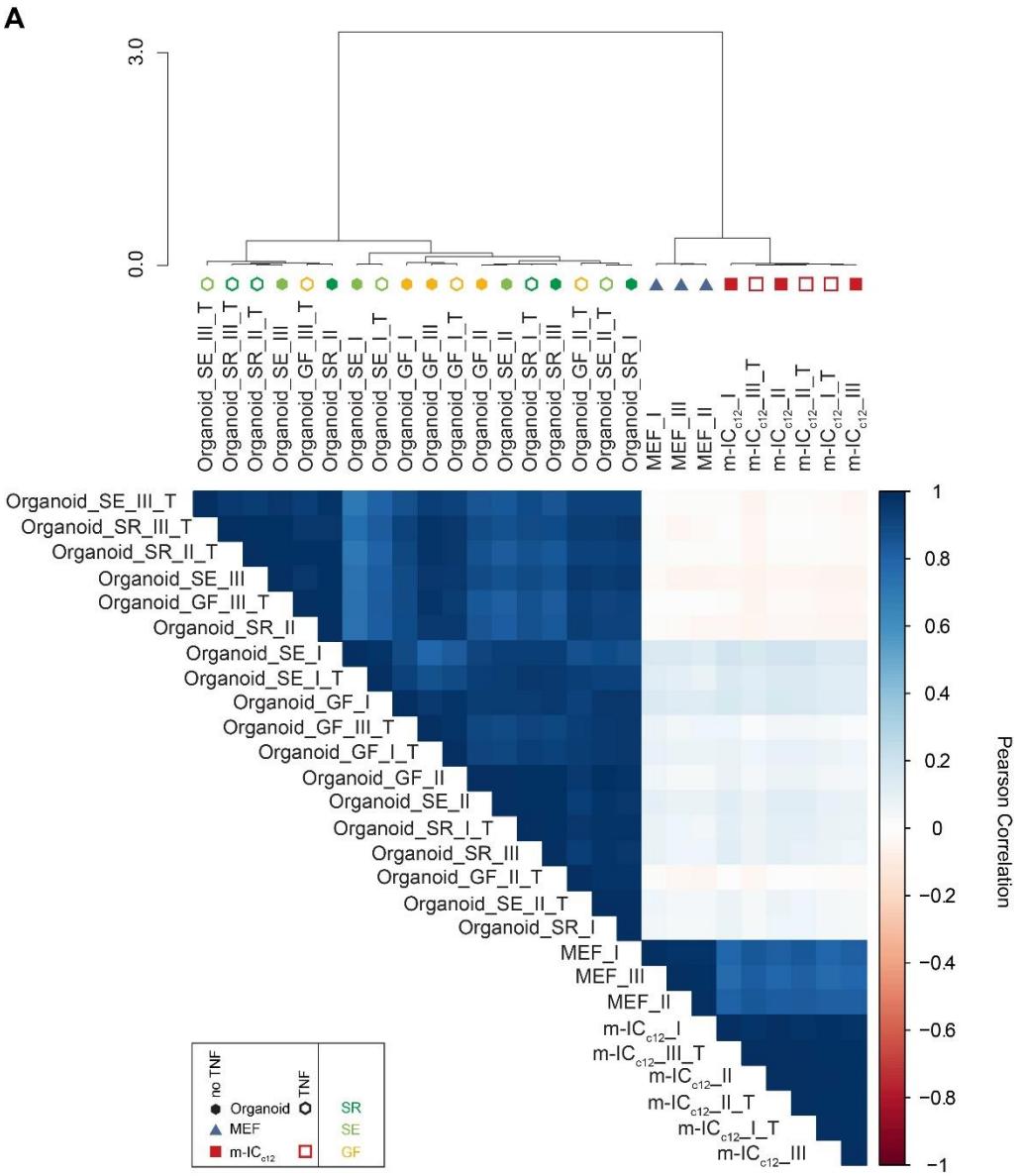
A
3.0
0.0
Organoid_SE_III_T
Organoid_SR_III_T
Organoid_SR_II_T
Organoid_SE_III
Organoid_GF_III_T
Organoid_SR_II
Organoid_SE_I
Organoid_SE_I_T
Organoid_GF_I
Organoid_GF_III
Organoid_GF_I_T
Organoid_GF_II
Organoid_SE_II
Organoid_SR_I_T
Organoid_SR_III
Organoid_GF_II_T
Organoid_SE_II_T
Organoid_SR_I
MEF_I
MEF_III
MEF_II
m-IC$_{c12}$_I
m-IC$_{c12}$_III_T
m-IC$_{c12}$_II
m-IC$_{c12}$_II_T
m-IC$_{c12}$_I_T
m-IC$_{c12}$_III
1
0.8
0.6
0.4
0.2
0
−0.2
−0.4
−0.6
−0.8
−1
Pearson Correlation
no TNF
TNF
Organoid
MEF
m-IC$_{c12}$
SR
SE
GF

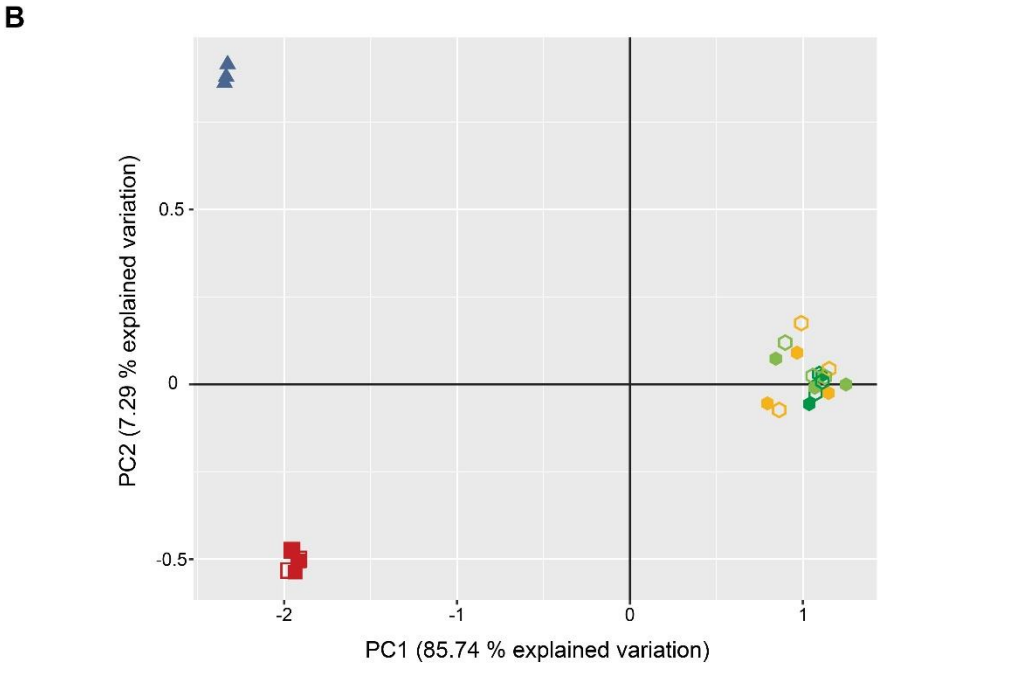
B
PC2 (7.29 % explained variation)
0.5
0
-0.5
-2
-1
0
1
PC1 (85.74 % explained variation)

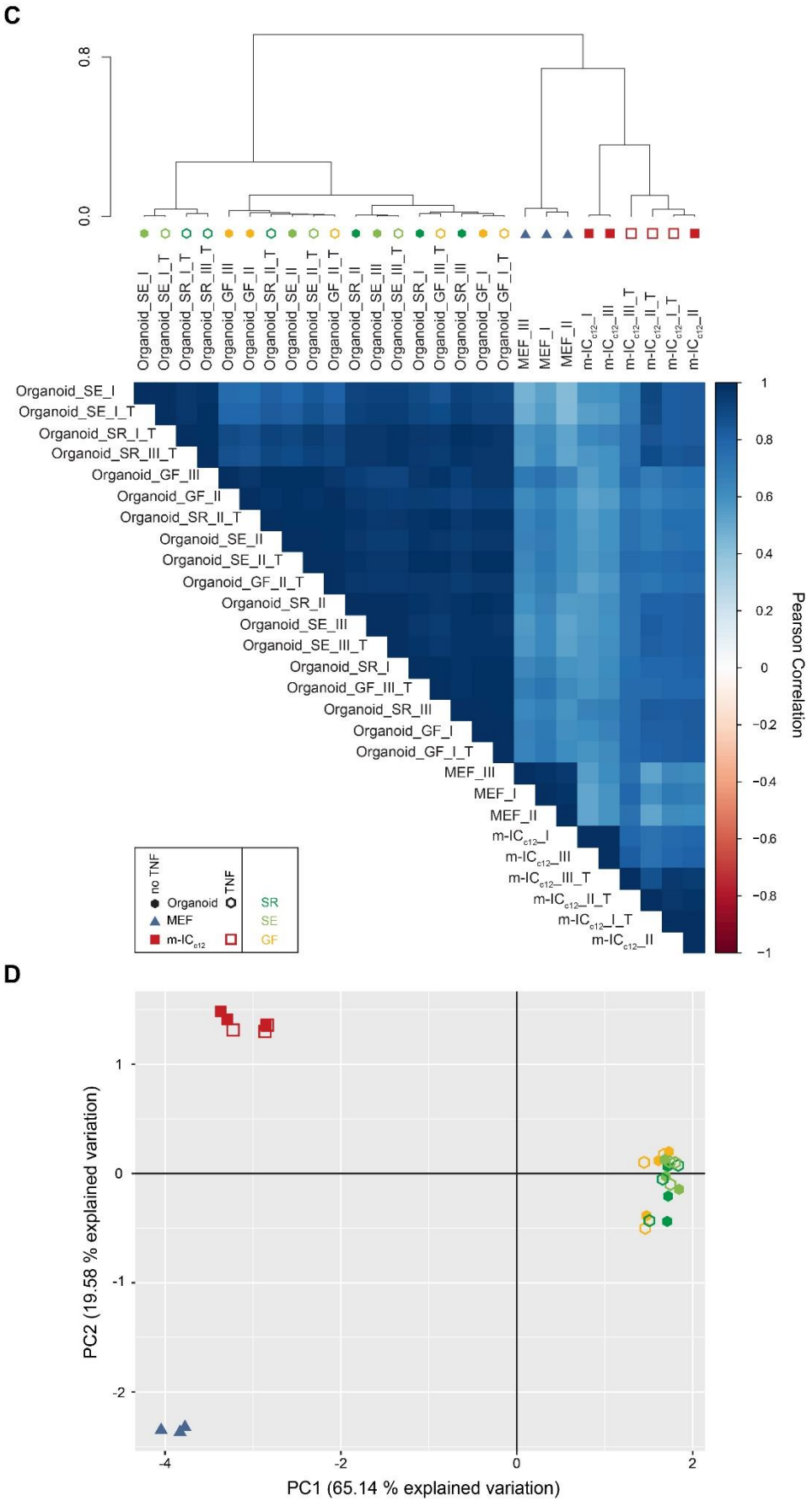

Figure S4 ***Stochastic variation overshadows low dose TNF-induced expression changes in organoids. A*** *Unsupervised hierarchical clustering analysis of the top 100 hits, as ranked by variance across all the samples, of*

the proteome data set including untreated (closed symbols) and TNF-treated (5 ng/ml, 8h; open symbols; _T) organoid (Organoid_I-III, hexagon symbol) samples from mice raised in SPF facility 1 (_SR, dark green), SPF facility 2 (_SE, light green) or the germ-free facility (_GF, yellow), as well as MEFs (MEF_I-III, blue triangle symbol) and m-IC_{c12} cell (m-IC_{c12}_I-III, red square symbol) samples. Correlation matrix depicts Pearson correlation values between indicated samples. ***B*** *Principal component analysis of the proteome data set as described in A.* ***C*** *Unsupervised hierarchical clustering analysis of the top 100 hits, as ranked by variance across all the samples, of the transcriptome data set for the samples described in A.* ***D*** *Principal component analysis of the proteome data set as described in C.*

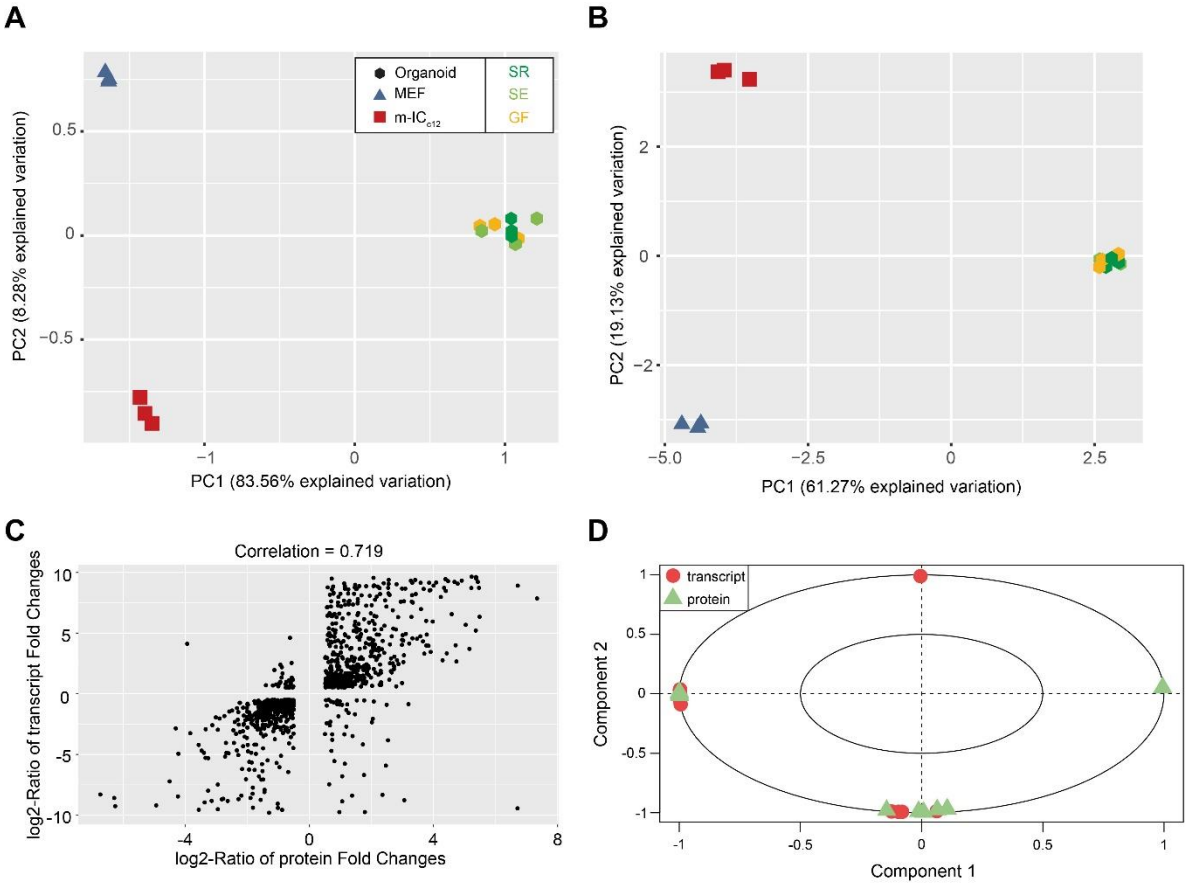

Figure S5 ***Integration of proteome and transcriptome data sets. A*** *Principal component analysis of the proteome data for the three cultured sample groups of organoids (Organoid_I-III, hexagon symbol) from mice raised in SPF facility 1 (_SR, dark green), SPF facility 2 (_SE, light green) or the germ-free facility (_GF, yellow), MEFs (MEF_I-III, blue triangle symbol) and m-IC$_{c12}$ cells (m-IC$_{c12}$_I-III, red square symbol).* ***B*** *Principal component analysis of the sample set as described in A.* ***C*** *Correlation plot of log2 ratio of transcript fold changes between the Organoid sample group and m-IC$_{c12}$ and MEF cells (y-axis) and the log2 ratio of protein fold changes between the Organoid sample group and m-IC$_{c12}$ and MEF cells (x-axis).* ***D*** *Circle plot indicating the hits identified in the proteome - transcriptome integration as variables of PC1 and PC2 described in Figure 4 and Table S3.*

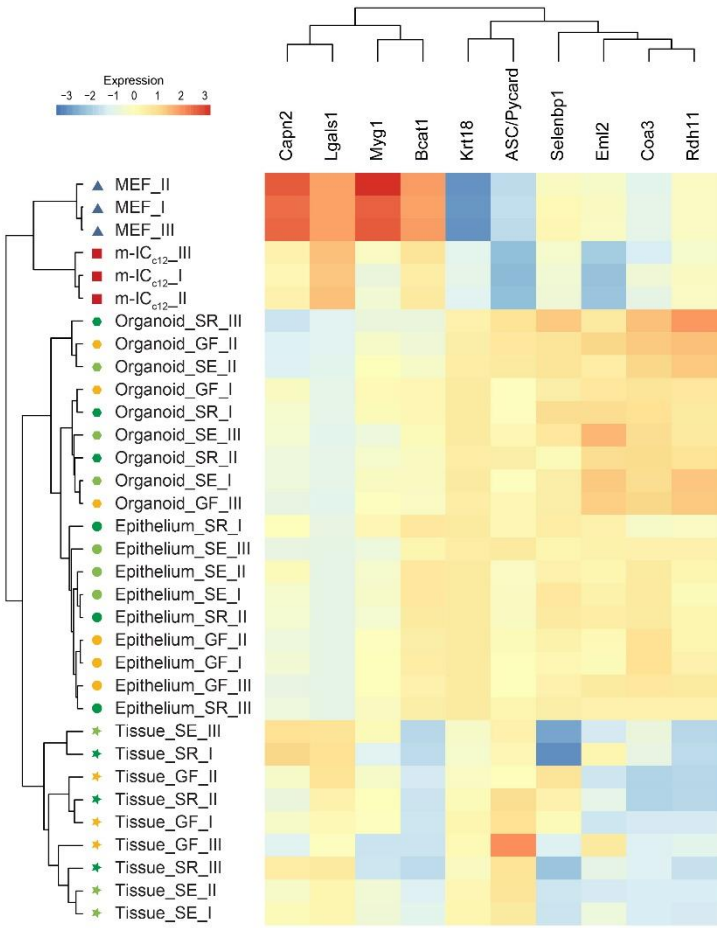

Figure S6 ***Organoid identifier proteins exhibit a similar expression pattern in freshly harvested primary epithelial cells and organoids****. Unsupervised hierarchical clustering analysis and expression heat map of identifier proteins described in Figure 4 for organoid (Organoid_I-III, hexagon symbol), epithelial cell-enriched fraction (Epithelium_I-III, circle symbol) and tissue samples (Tissue_I-III, star symbol) from mice raised in SPF facility 1 (_SR, dark green), SPF facility 2 (_SE, light green) or the germ-free facility (_GF, yellow), as well as MEFs (MEF_I-III, blue triangle symbol) and m-IC$_{c12}$ cell (m-IC$_{c12}$_I-III, red square symbol) samples.*

Table S1 ***Significant hits of proteome analysis of TNF-treated organoids compared to untreated organoids.*** *Differential expression cut-offs: log2 ratio <-0.5 or >0.5 and* p-*value <0.05.*

gene_id	gene_name	*p*-Value	FDR	log2 Ratio
ENSMUSG00000025225	Nfkb2	3.78E-08	0.000126	0.8538
ENSMUSG00000019834	Slc22a16	0.005833	0.9966	0.6306
ENSMUSG00000031820	Babam1	0.0464	0.9966	1.53
ENSMUSG00000070436	Serpinh1	0.04827	0.9966	1.163
ENSMUSG00000024835	Coro1b	0.002535	0.9966	-0.5986
ENSMUSG00000075402	Krt76	0.003355	0.9966	-1.723
ENSMUSG00000027520	Zdbf2	0.008595	0.9966	-2.037
ENSMUSG00000064201	Krt2	0.01611	0.9966	-0.8037
ENSMUSG00000020086	H2afy2	0.02131	0.9966	-1.567
ENSMUSG00000052632	Asap2	0.02165	0.9966	-1.037
ENSMUSG00000049932	H2afx	0.02693	0.9966	-1
ENSMUSG00000061527	Krt5	0.02902	0.9966	-0.5723
ENSMUSG00000064358	mt-Co3	0.0435	0.9966	-0.545
ENSMUSG00000063689	Hist2h2ab	0.04384	0.9966	-0.7368
ENSMUSG00000020964	Sel1l	0.04943	0.9966	-0.5253

Table S2 ***Significant hits of transcriptome analysis of TNF-treated organoids compared to untreated organoids.*** *Differential expression cut-offs: log2 ratio <-0.5 or >0.5 and* p-*value <0.05.*

Identifier	gene_name	pValue	fdr	log2 Ratio
ENSMUSG00000021025	Nfkbia	1.96E-21	2.36E-17	2.643
ENSMUSG00000039395	Mreg	7.48E-16	3.27E-12	1.444
ENSMUSG00000006519	Cyba	8.13E-16	3.27E-12	2.57
ENSMUSG00000025225	Nfkb2	2.39E-15	7.21E-12	1.776
ENSMUSG00000024164	C3	3.08E-14	7.43E-11	6.255
ENSMUSG00000037033	Clca3b	8.72E-14	1.75E-10	1.551
ENSMUSG00000019850	Tnfaip3	1.53E-12	2.63E-09	1.518
ENSMUSG00000033538	Casp4	7.89E-12	1.19E-08	1.674
ENSMUSG00000002983	Relb	1.40E-11	1.87E-08	1.476
ENSMUSG00000029810	Tmem176b	1.55E-11	1.87E-08	1.159
ENSMUSG00000029860	Zyx	5.75E-11	6.30E-08	1.12
ENSMUSG00000024308	Tapbp	1.66E-10	1.67E-07	1.097
ENSMUSG00000030017	Reg3g	4.43E-10	4.11E-07	1.837
ENSMUSG00000060802	B2m	7.70E-10	6.63E-07	0.6629
ENSMUSG00000053175	Bcl3	8.62E-10	6.71E-07	1.402
ENSMUSG00000023367	Tmem176a	9.48E-10	6.71E-07	0.9019
ENSMUSG00000020400	Tnip1	9.91E-10	6.71E-07	0.942
ENSMUSG00000042349	Ikbke	1.00E-09	6.71E-07	1.007
ENSMUSG00000037405	Icam1	1.98E-09	1.26E-06	3.407
ENSMUSG00000032359	Ctsh	2.85E-09	1.72E-06	1.224
ENSMUSG00000028654	Mycl	3.21E-09	1.84E-06	0.9469
ENSMUSG00000056313	1810011O10Rik	4.66E-09	2.56E-06	0.9572
ENSMUSG00000029334	Prkg2	5.51E-09	2.79E-06	0.8964
ENSMUSG00000037820	Tgm2	5.55E-09	2.79E-06	0.749
ENSMUSG00000016283	H2-M2	1.28E-08	6.19E-06	3.22
ENSMUSG00000041025	Iffo2	1.50E-08	6.95E-06	0.8805
ENSMUSG00000028262	Clca3a2	2.54E-08	1.13E-05	1.646
ENSMUSG00000030413	Pglyrp1	2.63E-08	1.13E-05	1.021
ENSMUSG00000018899	Irf1	3.11E-08	1.28E-05	1.359
ENSMUSG00000022575	Gsdmd	3.21E-08	1.28E-05	1.665
ENSMUSG00000079197	Psme2	3.54E-08	1.34E-05	0.647
ENSMUSG00000032000	Birc3	8.26E-08	3.02E-05	1.059
ENSMUSG00000009248	Ascl2	8.87E-08	3.14E-05	1.659
ENSMUSG00000001123	Lgals9	1.98E-07	6.83E-05	0.557
ENSMUSG00000017167	Cntnap1	2.90E-07	9.71E-05	2.121
ENSMUSG00000019320	Noxo1	2.99E-07	9.73E-05	0.9149
ENSMUSG00000038235	F11r	3.13E-07	9.93E-05	0.5615
ENSMUSG00000007659	Bcl2l1	3.29E-07	0.000101	0.7022
ENSMUSG00000020826	Nos2	3.35E-07	0.000101	2.637
ENSMUSG00000030681	Mvp	3.69E-07	0.000109	0.6259
ENSMUSG00000035226	Rims4	4.07E-07	0.000117	2.282

ENSMUSG00000030303	Far2	4.53E-07	0.000127	0.7602
ENSMUSG00000024401	Tnf	5.56E-07	0.000152	3.393
ENSMUSG00000022026	Olfm4	7.14E-07	0.000191	1.818
ENSMUSG00000023044	Csad	9.11E-07	0.000234	0.8508
ENSMUSG00000039304	Tnfsf10	9.65E-07	0.000242	0.6533
ENSMUSG00000020422	Tns3	1.36E-06	0.000334	0.5912
ENSMUSG00000034487	Kdelc2	1.44E-06	0.000347	0.809
ENSMUSG00000039232	Stx11	1.50E-06	0.000354	2.314
ENSMUSG00000021998	Lcp1	2.17E-06	0.000502	0.6725
ENSMUSG00000041895	Wipi1	2.22E-06	0.000505	0.9529
ENSMUSG00000018648	Dusp14	2.47E-06	0.000552	1.041
ENSMUSG00000024610	Cd74	2.59E-06	0.000568	2.452
ENSMUSG00000027359	Slc27a2	3.54E-06	0.000761	0.6323
ENSMUSG00000026166	Ccl20	3.64E-06	0.000769	3.16
ENSMUSG00000094439	Gm21969	4.96E-06	0.00103	1.127
ENSMUSG00000020806	Rhbdf2	5.22E-06	0.001067	0.7538
ENSMUSG00000037798	Mat1a	5.55E-06	0.001097	5.456
ENSMUSG00000031722	Hp	6.31E-06	0.001227	4.945
ENSMUSG00000040128	Pnrc1	8.23E-06	0.00153	0.641
ENSMUSG00000031365	Zfp275	8.87E-06	0.001596	0.7372
ENSMUSG00000029859	Epha1	9.17E-06	0.001603	0.628
ENSMUSG00000031257	Nox1	1.02E-05	0.001736	3.741
ENSMUSG00000055447	Cd47	1.24E-05	0.002076	0.5491
ENSMUSG00000021662	Arhgef28	1.35E-05	0.002206	1.32
ENSMUSG00000026321	Tnfrsf11a	1.51E-05	0.002363	0.7921
ENSMUSG00000028191	Bcl10	1.87E-05	0.002781	0.5152
ENSMUSG00000034205	Loxl2	1.89E-05	0.002785	2.565
ENSMUSG00000013643	Lypd8	1.94E-05	0.002823	0.5518
ENSMUSG00000035929	H2-Q4	3.27E-05	0.00443	0.7935
ENSMUSG00000029093	Sorcs2	3.32E-05	0.004445	0.572
ENSMUSG00000067219	Nipal1	4.10E-05	0.005318	0.5932
ENSMUSG00000074211	Sdhaf1	4.30E-05	0.005488	0.8026
ENSMUSG00000032849	Abcc4	4.33E-05	0.005488	0.8816
ENSMUSG00000038781	Stap2	4.43E-05	0.005565	0.5554
ENSMUSG00000040964	Arhgef10l	4.53E-05	0.005633	0.748
ENSMUSG00000030895	Hpx	4.80E-05	0.005906	5.618
ENSMUSG00000002980	Bcam	4.89E-05	0.00596	0.8846
ENSMUSG00000054256	Msi1	5.14E-05	0.006199	0.9636
ENSMUSG00000026421	Csrp1	5.22E-05	0.006232	0.5291
ENSMUSG00000021277	Traf3	5.73E-05	0.006639	0.562
ENSMUSG00000022868	Ahsg	6.20E-05	0.006894	4.898
ENSMUSG00000074896	Ifit3	6.23E-05	0.006894	2.419
ENSMUSG00000047030	Spata2	8.78E-05	0.009449	0.6066
ENSMUSG00000073599	Ecscr	0.000115	0.0119	2.717
ENSMUSG00000042129	Rassf4	0.000133	0.0136	0.6378

ENSMUSG00000056025	Clca3a1	0.000141	0.01424	0.7752
ENSMUSG00000031897	Psmb10	0.000142	0.01431	0.54
ENSMUSG00000039349	C130074G19Rik	0.000146	0.01446	0.7215
ENSMUSG00000015085	Entpd2	0.000168	0.01616	0.6092
ENSMUSG00000055652	Klhl25	0.000186	0.0174	0.8074
ENSMUSG00000056919	Cep162	0.000186	0.0174	0.6066
ENSMUSG00000052512	Nav2	0.000202	0.01854	0.5137
ENSMUSG00000062210	Tnfaip8	0.000203	0.01855	1.015
ENSMUSG00000074195	Clca4b	0.000215	0.01947	0.7542
ENSMUSG00000031790	Mmp15	0.000222	0.02001	0.649
ENSMUSG00000037613	Tnfrsf23	0.000238	0.02078	1.442
ENSMUSG00000004446	Bid	0.000259	0.02243	0.6363
ENSMUSG00000038301	Snx10	0.000271	0.02334	0.678
ENSMUSG00000034685	Fam171a2	0.000356	0.02923	2.072
ENSMUSG00000051439	Cd14	0.000372	0.03026	1.222
ENSMUSG00000021062	Rab15	0.000376	0.03044	0.759
ENSMUSG00000032554	Trf	0.000382	0.03066	4.106
ENSMUSG00000026832	Cytip	0.000386	0.03071	1.145
ENSMUSG00000029368	Alb	0.000387	0.03071	4.837
ENSMUSG00000023247	Guca2a	0.000499	0.03808	0.7168
ENSMUSG00000033721	Vav3	0.000538	0.04051	0.5233
ENSMUSG00000025780	Itih5	0.000609	0.04535	1.018
ENSMUSG00000024411	Aqp4	0.000649	0.04741	0.5947
ENSMUSG00000002997	Prkar2b	0.000748	0.05396	1.964
ENSMUSG00000033819	Ppp1r16a	0.000809	0.0573	0.6127
ENSMUSG00000027333	Smox	0.000819	0.05739	0.6195
ENSMUSG00000057751	Megf6	0.000831	0.05759	2.109
ENSMUSG00000044469	Tnfaip8l1	0.000888	0.06116	0.5484
ENSMUSG00000052485	Tmem171	0.000911	0.06237	0.8172
ENSMUSG00000040296	Ddx58	0.001067	0.07042	0.7906
ENSMUSG00000030748	Il4ra	0.001073	0.07042	0.5319
ENSMUSG00000018920	Cxcl16	0.001075	0.07042	1.298
ENSMUSG00000022587	Ly6e	0.001091	0.0707	0.5958
ENSMUSG00000068015	Lrch1	0.001153	0.07379	0.5537
ENSMUSG00000026278	Bok	0.001436	0.08719	0.8222
ENSMUSG00000046879	Irgm1	0.001673	0.09974	0.5054
ENSMUSG00000038387	Rras	0.001694	0.09974	0.6253
ENSMUSG00000029811	Aoc1	0.001742	0.1006	0.5298
ENSMUSG00000041653	Pnpla3	0.001812	0.104	1.757
ENSMUSG00000022885	St6gal1	0.002056	0.1146	0.6507
ENSMUSG00000028001	Fga	0.002923	0.1474	3.187
ENSMUSG00000045441	Gprin3	0.003042	0.1522	0.6268
ENSMUSG00000029445	Hpd	0.003198	0.1549	2.038
ENSMUSG00000032978	Guca2b	0.003225	0.1552	0.7565
ENSMUSG00000036931	Nfkbid	0.003334	0.1583	0.8465

ENSMUSG00000003617	Cp	0.003376	0.159	2.178
ENSMUSG00000021725	Parp8	0.003448	0.1605	2.009
ENSMUSG00000016382	Pls3	0.0036	0.1644	0.802
ENSMUSG00000030340	Scnn1a	0.00373	0.1672	0.9791
ENSMUSG00000000732	Icosl	0.003745	0.1672	0.6621
ENSMUSG00000010307	Tmem86a	0.003839	0.1702	0.69
ENSMUSG00000027583	Zbtb46	0.004344	0.1864	1.645
ENSMUSG00000060206	Zfp462	0.004713	0.1972	0.5985
ENSMUSG00000034855	Cxcl10	0.004744	0.1972	1.718
ENSMUSG00000020941	Map3k14	0.005074	0.2044	0.6467
ENSMUSG00000027907	S100a11	0.005496	0.2123	0.711
ENSMUSG00000024349	Tmem173	0.005557	0.2127	1.345
ENSMUSG00000042532	Golga7b	0.005906	0.2232	1.244
ENSMUSG00000029561	Oasl2	0.006137	0.2298	2.014
ENSMUSG00000037349	Nudt22	0.006325	0.2339	0.56
ENSMUSG00000030074	Gxylt2	0.006494	0.2394	1.119
ENSMUSG00000079015	Serpina1c	0.006631	0.2437	3.034
ENSMUSG00000026494	Kif26b	0.006994	0.2473	0.905
ENSMUSG00000018347	Zkscan6	0.007474	0.256	0.5684
ENSMUSG00000002985	Apoe	0.008063	0.267	1.487
ENSMUSG00000052837	Junb	0.008111	0.2679	0.6307
ENSMUSG00000063354	Slc39a4	0.008194	0.2699	0.5625
ENSMUSG00000071847	Apcdd1	0.008221	0.2701	0.6074
ENSMUSG00000050777	Tmem37	0.008727	0.2801	0.9821
ENSMUSG00000019122	Ccl9	0.008815	0.2801	0.9549
ENSMUSG00000030595	Nfkbib	0.008882	0.2803	0.503
ENSMUSG00000029101	Rgs12	0.009277	0.2866	0.5665
ENSMUSG00000080316	Spaca6	0.009717	0.2958	1.502
ENSMUSG00000005413	Hmox1	0.01067	0.3147	1.099
ENSMUSG00000061751	Kalrn	0.01069	0.3147	0.6938
ENSMUSG00000024990	Rbp4	0.01107	0.3201	2.397
ENSMUSG00000026399	Cd55	0.01174	0.3323	0.5039
ENSMUSG00000032596	Uba7	0.01217	0.3388	0.8677
ENSMUSG00000090639	Gm20425	0.01231	0.3403	0.9649
ENSMUSG00000038213	Tapbpl	0.01242	0.3419	0.5276
ENSMUSG00000041390	Mdfic	0.01295	0.3516	1.034
ENSMUSG00000026193	Fn1	0.01307	0.3533	1.309
ENSMUSG00000060402	Chst8	0.01322	0.3544	1.574
ENSMUSG00000026380	Tfcp2l1	0.01347	0.3578	0.5946
ENSMUSG00000017652	Cd40	0.01403	0.3679	1.718
ENSMUSG00000002083	Bbc3	0.01446	0.3754	0.8958
ENSMUSG00000027712	Anxa5	0.01454	0.3754	0.6169
ENSMUSG00000025212	Sfxn3	0.01468	0.3782	0.5624
ENSMUSG00000014599	Csf1	0.01604	0.3955	1.301
ENSMUSG00000049807	Arhgap23	0.01623	0.3969	1.192

ENSMUSG00000035606	Ky	0.01661	0.4013	1.737
ENSMUSG00000055172	C1ra	0.01754	0.4098	1.559
ENSMUSG00000051022	Hs3st1	0.01801	0.4141	0.5559
ENSMUSG00000029380	Cxcl1	0.01841	0.4166	1.232
ENSMUSG00000020462	Cfap36	0.01876	0.417	0.5473
ENSMUSG00000021257	Angel1	0.01892	0.417	0.6013
ENSMUSG00000036390	Gadd45a	0.01933	0.417	0.5038
ENSMUSG00000044626	Liph	0.01935	0.417	0.5213
ENSMUSG00000024042	Sik1	0.01954	0.417	0.7569
ENSMUSG00000027358	Bmp2	0.01979	0.4179	0.7226
ENSMUSG00000027995	Tlr2	0.01985	0.4179	1.781
ENSMUSG00000037921	Ddx60	0.01995	0.419	1.663
ENSMUSG00000076441	Ass1	0.0203	0.4203	1.728
ENSMUSG00000005681	Apoa2	0.02039	0.4203	1.997
ENSMUSG00000026676	Ccdc3	0.02093	0.4251	1.119
ENSMUSG00000021373	Cap2	0.02095	0.4251	2.278
ENSMUSG00000017211	Gsdma2	0.02098	0.4251	1.827
ENSMUSG00000068452	Duox2	0.02157	0.4257	0.8692
ENSMUSG00000029449	Rhof	0.02163	0.4257	0.8374
ENSMUSG00000024018	Ccdc167	0.02207	0.4258	0.5658
ENSMUSG00000033540	Idua	0.023	0.4328	0.5686
ENSMUSG00000030409	Dmpk	0.02376	0.4387	0.8308
ENSMUSG00000036052	Dnajb5	0.02407	0.4409	0.5602
ENSMUSG00000023947	Nfkbie	0.0243	0.4421	1.107
ENSMUSG00000000276	Dgke	0.02468	0.4429	0.6062
ENSMUSG00000023186	Vwa5a	0.02486	0.4441	0.547
ENSMUSG00000019737	Syne4	0.02491	0.4441	1.126
ENSMUSG00000026715	Serpinc1	0.02579	0.4484	2.308
ENSMUSG00000051314	Ffar2	0.02611	0.4504	1.202
ENSMUSG00000053192	Mllt11	0.02646	0.4525	0.5508
ENSMUSG00000019832	Rab32	0.02717	0.4574	0.6673
ENSMUSG00000034701	Neurod1	0.02764	0.4615	0.6651
ENSMUSG00000016262	Sertad4	0.0279	0.4625	1.275
ENSMUSG00000021509	Slc25a48	0.02821	0.4628	1.056
ENSMUSG00000015396	Cd83	0.02865	0.4666	0.8742
ENSMUSG00000011832	Evi5l	0.02869	0.4666	0.8083
ENSMUSG00000069581	Tspear	0.02875	0.4666	1.686
ENSMUSG00000031292	Cdkl5	0.02916	0.4687	0.6742
ENSMUSG00000032717	Mdfi	0.03046	0.4824	1.494
ENSMUSG00000044337	Ackr3	0.0307	0.4832	1.622
ENSMUSG00000041849	Card6	0.03113	0.4862	0.5137
ENSMUSG00000039328	Rnf122	0.03151	0.4877	1.13
ENSMUSG00000016206	H2-M3	0.03178	0.489	1.425
ENSMUSG00000040026	Saa3	0.03212	0.4896	1.706
ENSMUSG00000047501	Cldn4	0.03353	0.4996	0.6282

ENSMUSG00000036036	Zfp57	0.03413	0.5036	1.469
ENSMUSG00000020654	Adcy3	0.03599	0.5135	1.316
ENSMUSG00000044991	1110034G24Rik	0.03674	0.5182	0.868
ENSMUSG00000043424	Eif3j2	0.03809	0.5266	0.9233
ENSMUSG00000024778	Fas	0.03811	0.5266	0.8207
ENSMUSG00000025743	Sdc3	0.03864	0.5299	1.351
ENSMUSG00000040329	Il7	0.03873	0.5299	1.159
ENSMUSG00000023009	Nckap5l	0.03884	0.5299	1.094
ENSMUSG00000070407	Hs3st3b1	0.03886	0.5299	0.5216
ENSMUSG00000018411	Mapt	0.042	0.5435	0.9817
ENSMUSG00000061762	Tac1	0.04214	0.5435	0.7987
ENSMUSG00000054598	9130230L23Rik	0.04227	0.5438	1.382
ENSMUSG00000037001	Zfp39	0.04321	0.5475	0.7912
ENSMUSG00000001946	Esam	0.04418	0.5535	0.8953
ENSMUSG00000026200	Glb1l	0.04493	0.5589	0.9997
ENSMUSG00000033022	Cdo1	0.04518	0.5595	0.5758
ENSMUSG00000046694	Fam46b	0.04615	0.5635	1.178
ENSMUSG00000026712	Mrc1	0.04617	0.5635	1.161
ENSMUSG00000009378	Slc16a12	0.0466	0.5635	0.8853
ENSMUSG00000049690	Nckap5	0.04696	0.5656	0.6614
ENSMUSG00000003505	Psg18	0.04764	0.5716	1.631
ENSMUSG00000071178	Serpina1b	0.0489	0.5718	1.158
ENSMUSG00000048232	Fbxo10	0.04894	0.5718	1.085
ENSMUSG00000017405	Nek8	0.04977	0.5727	0.7558
ENSMUSG00000026784	Pdss1	3.28E-08	1.28E-05	-0.5979
ENSMUSG00000047517	Dmbt1	2.48E-05	0.003514	-1.464
ENSMUSG00000024900	Cpt1a	2.63E-05	0.00369	-0.5603
ENSMUSG00000052496	Pkdrej	3.09E-05	0.004234	-1.493
ENSMUSG00000006642	Tcf23	0.000237	0.02078	-0.708
ENSMUSG00000090626	Tex9	0.000312	0.02627	-0.7758
ENSMUSG00000041886	Macc1	0.000331	0.02748	-0.5181
ENSMUSG00000043252	Tmem64	0.000642	0.04717	-0.6349
ENSMUSG00000020838	Slc6a4	0.001683	0.09974	-0.542
ENSMUSG00000043639	Rbm20	0.001828	0.1044	-1.067
ENSMUSG00000050379	Sep.06	0.002166	0.1183	-0.7066
ENSMUSG00000047221	Fam185a	0.002172	0.1183	-0.5033
ENSMUSG00000043587	Pxylp1	0.002943	0.1478	-0.5052
ENSMUSG00000015533	Itga2	0.003084	0.1536	-0.5656
ENSMUSG00000032313	AI118078	0.003277	0.1562	-0.6357
ENSMUSG00000021223	Papln	0.003492	0.1616	-0.5441
ENSMUSG00000053783	1700016K19Rik	0.003621	0.1647	-1.695
ENSMUSG00000029335	Bmp3	0.004997	0.2022	-0.534
ENSMUSG00000052373	Mpp3	0.004997	0.2022	-0.524
ENSMUSG00000006641	Slc5a6	0.00533	0.2107	-0.5012
ENSMUSG00000021589	Rhobtb3	0.005398	0.2111	-0.6485

ENSMUSG00000042213	Zfand4	0.005436	0.2114	-1.76
ENSMUSG00000025348	Itga7	0.006772	0.2444	-1.627
ENSMUSG00000037681	Esyt3	0.009232	0.2863	-1.399
ENSMUSG00000030513	Pcsk6	0.009389	0.2883	-0.6695
ENSMUSG00000031919	Tmed6	0.009672	0.2952	-0.6136
ENSMUSG00000036231	Agr3	0.01056	0.3137	-1.216
ENSMUSG00000005677	Nr1i3	0.01075	0.3147	-0.6804
ENSMUSG00000030124	Lag3	0.01078	0.3148	-1.368
ENSMUSG00000025464	Paox	0.01112	0.3206	-0.5384
ENSMUSG00000048186	Bend7	0.01264	0.3463	-0.6381
ENSMUSG00000030491	Tdrd12	0.01452	0.3754	-1.575
ENSMUSG00000042367	Gjb3	0.01558	0.3896	-0.5446
ENSMUSG00000026389	Steap3	0.01592	0.3945	-0.5848
ENSMUSG00000079588	Tmem182	0.01622	0.3969	-0.8281
ENSMUSG00000032315	Cyp1a1	0.01649	0.4	-0.6433
ENSMUSG00000019124	Scrn1	0.01715	0.4066	-1.13
ENSMUSG00000019975	Ikbip	0.01788	0.4137	-0.9574
ENSMUSG00000037279	Ovol2	0.01856	0.4166	-0.7376
ENSMUSG00000002799	Jag2	0.01905	0.417	-0.5158
ENSMUSG00000070287	Slc35g2	0.01916	0.417	-1.429
ENSMUSG00000004328	Hif3a	0.0196	0.4175	-0.5978
ENSMUSG00000059493	Nhs	0.02047	0.4205	-1.081
ENSMUSG00000069713	4933406P04Rik	0.02203	0.4258	-1.352
ENSMUSG00000021684	Pde8b	0.02224	0.4277	-0.7249
ENSMUSG00000044067	Gpr22	0.0224	0.4287	-1.689
ENSMUSG00000034472	Rasd2	0.02278	0.4328	-1.121
ENSMUSG00000024805	Pcgf5	0.0232	0.4357	-0.5576
ENSMUSG00000001062	Vps9d1	0.02352	0.4373	-0.5527
ENSMUSG00000022696	Sidt1	0.02369	0.4382	-0.7596
ENSMUSG00000096910	Zfp955b	0.02405	0.4409	-0.6451
ENSMUSG00000047990	C2cd4a	0.02463	0.4429	-1.423
ENSMUSG00000021752	Kctd6	0.027	0.4565	-0.5354
ENSMUSG00000018239	Zcchc10	0.02754	0.4613	-0.8145
ENSMUSG00000048279	Sacs	0.02804	0.4625	-1.019
ENSMUSG00000024770	Lipn	0.03053	0.4824	-1.484
ENSMUSG00000014602	Kif1a	0.0314	0.4877	-1.165
ENSMUSG00000027420	Bfsp1	0.03421	0.5036	-0.8975
ENSMUSG00000018340	Anxa6	0.0358	0.5126	-0.7861
ENSMUSG00000051721	BC068281	0.03711	0.5206	-0.8884
ENSMUSG00000030498	Gas2	0.03835	0.5272	-0.5654
ENSMUSG00000058773	Hist1h1b	0.03957	0.5329	-1.12
ENSMUSG00000020658	Efr3b	0.0399	0.5341	-0.5802
ENSMUSG00000004558	Ndrg2	0.04084	0.5369	-0.524
ENSMUSG00000075033	Nxpe3	0.04114	0.5385	-1.163
ENSMUSG00000018486	Wnt9b	0.0425	0.5451	-1.268

ENSMUSG00000036430	Tbcc	0.04314	0.5475	-0.517
ENSMUSG00000028541	B4galt2	0.04386	0.5519	-1.137
ENSMUSG00000035678	Tnfsf9	0.04835	0.5718	-0.9066
ENSMUSG00000004654	Ghrhr	0.04856	0.5718	-1.401
ENSMUSG00000104043	Gm6525	0.04987	0.5727	-1.045

Table S3: *List of hits for Component 1 and 2 shown in Figure 4 and S5.*

Component 1	**Component 2**
Capn2	Coa3
Myg1	Eml2
Lgasl1	Rdh11
Bcat1	Selenbp1
Pycard	Krt18
Ena	*Q8R164*
Ankrd1	*Hs6st1*
Dusp14	*Sigirr*
Dmwd	*Map3k21*
Il7	*Pdlim1*
Amotl2	
Evc2	
Wwtr1-202	
Trim35	

CHAPTER 6 - DISCUSSION

The content of this chapter was partially adapted (as indicated) from the following manuscripts:

The Interplay between *Salmonella enterica* Serovar Typhimurium and the Intestinal Mucosa during Oral Infection

Annika Hausmann[1] and Wolf-Dietrich Hardt[1]

Author Affiliations:

[1]Institute of Microbiology, D-BIOL, ETH Zurich, Zurich, Switzerland

Author Contributions:

AH and WDH designed the scope of the review. AH wrote the manuscript with corrections and suggestions by WDH.

Published in Microbiology Spectrum, 05.04.2019. Doi: 10.1128/microbiolspec.BAI-0004-2019

Sections adapted from that manuscript are clearly indicated with "adapted from Hausmann and Hardt, Microbiology Spectrum 2019"

and

Elucidating Host-Microbe Interactions *in vivo* by Studying Population Dynamics Using Neutral Genetic Tags

Annika Hausmann[1] and Wolf-Dietrich Hardt[1]

Author Affiliations:

[1]Institute of Microbiology, D-BIOL, ETH Zurich, Zurich, Switzerland

Author Contributions:

AH designed the scope of the review with input by WDH. AH wrote the manuscript with corrections and suggestions by WDH.

Published in Immunology, 15.09.2020. Doi: 10.1111/imm.13266

Sections adapted from that manuscript are clearly indicated with "adapted from Hausmann and Hardt, Immunology 2020"

PRRS AND BACTERIAL SENSING IN THE INTESTINAL MUCOSA

TLR4

TLR4 is the extracytosolic receptor for LPS. It is widely expressed on immune cells. The role of intestinal epithelial TLR4 in sensing of bacterial LPS however is controversial. The data presented in Chapter 3 of this thesis conclusively suggest that the intestinal epithelium of adult mice does not sense LPS via TLR4, at least under homeostatic conditions. This appears in contrast to studies reporting TLR4 expression in IECs (Hornef et al., 2002, 2003; Kayisoglu et al., 2020; Price et al., 2018). Importantly, and partially in line with our observations, some of these studies fail to observe LPS-induced upregulation of NFκB target genes in organoids of the small intestine, and report only very moderate expression of single target genes upon stimulation of colon organoids (Kayisoglu et al., 2020; Price et al., 2018). This indicates that the expression of TLR4 does not imply its functionality as a rule.

Several factors modulate the reactivity of cells to TLR4 stimuli: i) The expression of TLR4 itself, ii) the regulation of TLR4 downstream signaling and iii) the expression of TLR4 co-receptor molecules. While the actual epithelial expression of TLR4 under homeostatic conditions remains to be resolved, modulation of cellular reactivity by regulating downstream signaling and/or co-receptor expression would explain discrepancies between epithelial TLR4 gene and/or protein expression, but no or only very low epithelial activation upon LPS stimulation (Kayisoglu et al., 2020; Price et al., 2018). In line with this, we cannot fully exclude low-level TLR4 expression on IECs, but do not detect direct epithelial NFκB activation upon LPS treatment (Chapter 3). Stimulation with NFκB signaling inducing cytokines like TNF (Chapter 3 and 5) reveal that IECs are generally able to induce full blown NFκB activation, indicating that potential mechanisms interfering with epithelial TLR4 signaling would have to be located upstream of NFκB activation. Finally, the expression of the TLR4 co-receptors LBP, CD14 and MD2 modulates cellular sensitivity to LPS. A recent study showed that intestinal epithelial organoids express low levels of TLR4 co-receptors in comparison to gastric organoids, which are sensitive to LPS (Kayisoglu et al., 2020). In addition to limited expression of TLR4 in IECs, it would therefore be conceivable that low expression levels of CD14 and LBP under homeostatic conditions contribute to epithelial insensitivity to LPS stimulation. Notably, the supplementation of soluble CD14 augmented the sensitivity of endothelial cells to LPS (Haziot et al., 1993). Likewise, besides an upregulated expression of TLR4, the increased production of these soluble co-receptors, e.g. in the inflamed mucosa, could potentially increase epithelial LPS sensitivity.

Finally, technical biases can influence the induction of downstream responses upon LPS treatment. Organoids frequently serve as a model to specifically study epithelial responses to PAMPs. To date it is unknown whether organoids recapitulate epithelial TLR4 expression patterns *in vivo*. Furthermore, the LPS employed in stimulation studies usually derives from *E. coli* expression systems and can therefore potentially be contaminated by other PAMPs (Takeuchi and Akira, 2010). The thorough testing of LPS purity in *Tlr4*$^{-/-}$ mice is therefore a crucial control to exclude the confounding activation of further PRRs.

In conclusion, our data, partially in line with previous studies (Günther et al., 2015; Kayisoglu et al., 2020; Price et al., 2018), suggest that the epithelium functions as an inert barrier with regard to LPS sensing under homeostatic conditions. Instead, we have identified a CD11b^{+} CD103^{-} MP subset, which stretches out in the intercrypt lamina propria and is characterized by specifically early TNF production in response to LPS stimulation (~20 min.p.inj.). This subset thereby activates localized NFκB signaling in the IECs of its adjacent crypts to induce antibacterial programs. This model of indirect activation of IECs upon LPS sensing has interesting implications for the tunability of antibacterial responses. i) The epithelial inertness to LPS, which is an abundant molecule in the intestinal lumen, prevents overactivation. Complementary,

the presence of LPS in the lamina propria is usually associated with bacterial translocation and/or barrier dysfunction. The spatial segregation of TLR4 expression within the mucosa thus provides a mechanism of differentiating a homeostatic LPS signal from threat-associated LPS. Similar spatial segregation patterns were described for other TLRs (Lee et al., 2006). ii) The indirect activation of IECs could have interesting potential consequences for signal propagation and the adjustment of antibacterial responses to the intensity of a bacterial trigger (Figure 1). According to this model, the accidental, isolated translocation of a commensal bacterium would result in sensing by the sentinel MP, which induces a local response resulting in strengthening of the epithelial barrier at the site of bacterial intrusion. Notably, this response triggers local barrier reinforcement through the induction of epithelial innate immune effectors such as secretion of mucus (Leppkes et al., 2014), C3 and AMPs (Chapter 1). Besides, it results in epithelial chemokine secretion. The direct epithelial immune effectors might be especially relevant in mediating quick protection against low-level threats while avoiding exaggerated inflammatory responses. By contrast, the infection with an invasive enteropathogen induces activation of multiple crypts, which ultimately results in a tissue-level response (Chapter 3). While the contribution to this response per activated IEC likely remains equal compared to the upper scenario, the tissue wide epithelial activation results in signal amplification. Accordingly, the transition from localized chemokine production by a small fraction of IECs to full-blown epithelial chemokine production might represent a threshold, which needs to be overcome to induce efficient influx of immune cells and might thereby function as a switch for tipping the mucosal balance towards inflammation.

The indirect activation of a distinct area of IECs could therefore present an important regulatory mechanism, which functions as a rheostat for sensing of the intensity of a bacterial threat and the initiation of appropriate downstream responses. The relevance of this signaling pathway in tuning antibacterial responses in the mucosa in relation to a bacterial insult however remains to be tested experimentally.

This modulatory role of $CD11b^{+}$ $CD103^{-}$ sentinel MPs would be in line with the defined nature of its TNF response. TNF production occurs extremely fast (~20 min.p.inj.) upon LPS exposure and starts to drop again as early as 1 h.p.inj.. It will be interesting to decipher how this fast and defined response is regulated. TNF production in macrophages is tuned by suppression of translation of *Tnf* mRNA (Beutler et al., 1986; Han et al., 1990). The presence of pre-transcribed RNA, allowing fast production of TNF upon a bacterial stimulus, might specifically characterize the identified subset and further specify its role as a sentinel cell.

Overshooting NFκB signaling in the intestinal mucosa can induce chronic inflammation. The quick termination of pro-inflammatory signals to avoid overstimulation is crucial for intestinal homeostasis (Karrasch et al., 2007; Maloy and Powrie, 2011). IL10 controls MP responses to TLR stimuli (Monteleone et al., 2008). It will be important to elucidate if/how IL10 regulates the TNF production by sentinel MPs. Ablation of IL10 signaling might allow prolonged TNF production and thereby an enlargement of the epithelial activation foci, as well as potential activation of further immune cells.

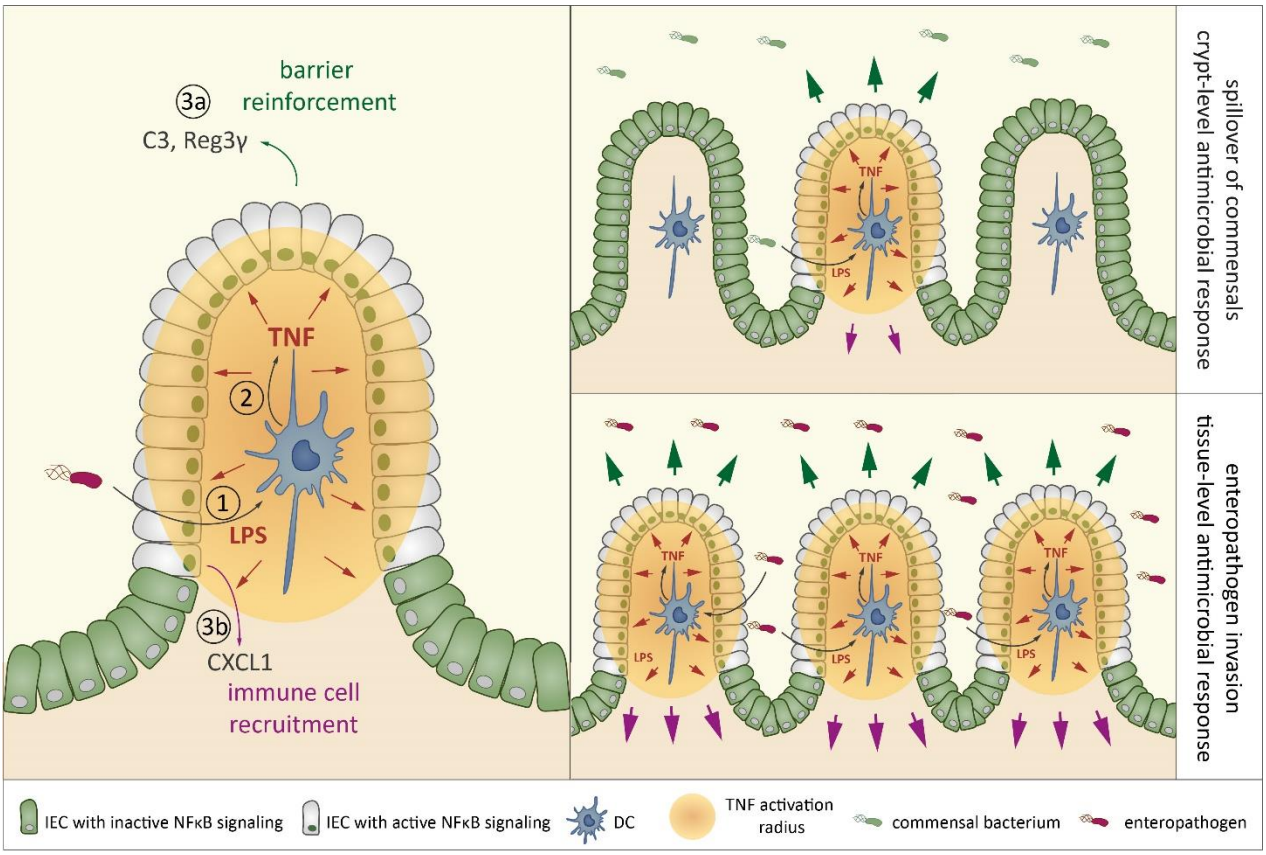

Figure 1 ***Proposed model of local versus tissue-wide activation.*** *LPS sensing by CD11b$^+$ CD103$^-$ sentinel MP (1) triggers TNF secretion (2), which induces epithelial NFκB activation. This leads to epithelial secretion of direct effectors involved in barrier reinforcement (e.g. C3, Reg3γ; 3a; green arrows) and indirect effectors like chemokines, which recruit immune cells to the mucosa (e.g. CXCL1; 3b; purple arrows).*

The TLR-MyD88-NFκB axis is central for the regulation of intestinal homeostasis. Both overactivation (Dheer et al., 2016; Vereecke et al., 2010, 2014) and depletion (Chassaing et al., 2014; Ii et al., 2012; Rakoff-Nahoum et al., 2004; Vlantis et al., 2016) of one or several of its components can induce IBD. The regulatory mechanisms that maintain the delicate balance of NFκB signaling in the intestinal mucosa remain incompletely understood. Specifically, the contribution of specific cell types to signaling circuits requires further studies. It will be relevant to investigate the role of the here identified CD11b$^+$ CD103$^-$ sentinel MPs as a gatekeeper of homeostatic and inflammatory responses to bacterial stimulation, also in the context of aberrant responses to commensals as observed in IBD.

Another important topic of future work will be whether the activation of the CD11b$^+$ CD103$^-$ sentinel MPs via TLR4 relies fully on the presence of bacteria in the lamina propria, or if these cells also engage in the direct sampling of the intestinal lumen (Niess et al., 2005), e.g. to detect bacteria which penetrated the inner mucus layer.

NAIP/NLRC4

The NAIP/NLRC4 inflammasome induces defense mechanisms upon sensing of bacterial flagella and TTSS-1. NAIP/NLRC4 has been characterized thoroughly in immune cells. Yet, the role of epithelial NAIP/NLRC4

in pathogen defenses became evident only recently (Knodler et al., 2014; Rauch et al., 2017; Sellin et al., 2014, 2015). Many mucosal pathogens rely on reaching the mucosal tissue and/or attaching/invading (in)to it with the help of flagella and the TTSS-1 (Hapfelmeier et al., 2008; Nordlander et al., 2014; Stecher et al., 2004). Consequently, the downregulation or mutation of these PAMPs for immune evasion often results in decreased virulence of these pathogens (Tenthorey et al., 2017). This creates a dilemma for enteropathogens between dependence on virulence factor expression and recognition of those factors by the immune system of the host, and ideally positions IECs for the sensing of these PAMPs via NAIP/NLRC4. In line with this, expression of *Naip/Nlrc4* is specifically high in IECs compared to professional immune cells (Chapter 4). Furthermore, the work presented in Chapter 4 of this thesis emphasizes the relevance of epithelial NAIP/NLRC4 during early oral infection with *S*. Tm beyond the intestinal mucosa. The expulsion of infected enterocytes restricts the migration of pathogen cells to the mLN, and thereby controls systemic pathogen loads during early infection. Importantly, immune cell NAIP/NLRC4 does not contribute to the control of early systemic *S*. Tm loads. This is at least in part attributable to *S*. Tm gene expression modulation, which downregulates PAMPS and thereby promotes the evasion of NAIP/NLRC4 recognition.

To date it remains unclear how exactly cytosolic NAIP/NLRC4 senses intracellular *S*. Tm, which often reside within the SCV. Surprisingly, we observe that *S*. Tm regularly carries flagella within the SCV, instead of shedding them before host cell invasion (Chapter 4). It remains unclear whether these assembled flagella directly contribute to NAIP/NLRC4 detection upon cytosolic escape, or whether NAIP/NLRC4 activation is rather triggered by flagellar subunits which are secreted into the cytosol via TTSS-1 (Sun et al., 2007). Deciphering this will be an important aim of future work.

The wiring of infection-induced cell death pathways downstream of inflammasome activation is highly flexible and redundant in macrophages (Doerflinger et al., 2020). It remains unclear to which degree this applies to other cell types, as cell death induction upon infection has distinct consequences depending on the infected cell type. Neutrophils, for example, appear to be specifically resistant to NLRC4-induced cell death, which contributes to maintenance of inflammasome-independent effector functions during infection (Chen et al., 2014). Similarly, IECs provide specific non-inflammasome related immune functions such as forming a physical barrier to protect from bacterial translocation. Consequently, epithelial infection-induced cell death needs to be coordinated to maintain tissue integrity. Given the distinct roles of different cell types in the context of infections, a cell type-specific wiring of cell death pathways according to the localization and function of these cell types is therefore likely. The details of epithelial inflammasome-induced cell death wiring and its manifestations are highly relevant for a better understanding of tissue responses to infections, and should be addressed in future studies.

Mucosal IL18 has ambiguous functions in the intestinal mucosa. On the one hand, IECs constitutively express IL18, which contributes to homeostasis maintenance. Epithelial IL18 production protects from colitis by driving T_{reg}-cell function in the intestine and suppressing T helper 17-cell differentiation (Harrison et al., 2015). In addition, IL18 induces regenerative responses in IECs via induction of IL22 (Lo et al., 2019; Muñoz et al., 2015; Pickert et al., 2009). On the other hand, NAIP/NLRC4-mediated IL18-activation contributes to the induction of early inflammation in *S*. Tm infection (Müller et al., 2016; Sellin et al., 2018). Interestingly, this IL18-activation is not required for early restriction of *S*. Tm loads (Sellin et al., 2014). In line with its pro-inflammatory properties during enteropathogen infection, IBD patients display elevated IL18 levels (Monteleone et al., 1999; Pizarro et al., 1999). In conclusion, the role of IL18 is highly complex and context dependent. It will be relevant to gain a more detailed understanding of the contributions of IL18 to acute and chronic inflammation. This applies to NAIP/NLRC4-activated IL18. In

contrast to the involvement of NAIP/NLRC4 and IL18 in the early induction of inflammation, there is collective evidence for its role in the control of longterm inflammatory responses. Specifically, *Nlrc4*$^{-/-}$ mice display exacerbated inflammation at later time points during enteropathogen infection or colitis induction via dextrane sulfate sodium (Carvalho et al., 2012; Nordlander et al., 2014). Given the homeostatic functions of IL18, it will be relevant to investigate its involvement in the induction of negative feedback loops or regeneration, which might contribute to the termination of pro-inflammatory responses. Dissecting pro- and anti-inflammatory properties of IL18 will yield valuable information about its contribution to the regulation of tissue homeostasis.

Regulation of bacterial sensing in the intestinal mucosa - It is about where you are, not who you are

The innate immune system relies on PRRs for the recognition of PAMPs. These PAMPs are however present on both pathogens and commensals. This results in a detection problem especially in the intestinal mucosa, which is constantly in contact with the commensal microbiota in the intestinal lumen. It therefore remains incompletely understood how the innate immune system in the intestinal mucosa differentiates between pathogenic and commensal bacteria.

Several regulatory entities exist to ensure a peaceful coexistence between commensals and their hosts. Many of these entities, such as the mucus layer and AMPs, collaborate to keep the microbiota in the intestinal lumen, at a safe distance from the mucosa (Chapter 1). By contrast, numerous enteropathogens have evolved strategies for host invasion. Conclusively, invasiveness is one feature that distinguishes pathogenic from commensal bacteria.

Two innate defense mechanisms analyzed in this thesis employ this feature of invasiveness to differentiate between pathogens and commensals. In both cases, the expression of PRRs is restricted to compartments of the intestinal mucosa that are usually bacteria-free. i) The inertness of IECs and, at the same time, the reactivity of CD11b^{+} CD103^{-} sentinel MPs to LPS specifically allows the detection of gram-negative bacteria that translocated into the lamina propria (Chapter 3). ii) Epithelial equipment with NAIP/NLRC4 enables specific detection of intracellular or epithelium-attached bacteria (Chapter 4). Specific compartments of the intestinal mucosa, such as the lamina propria or the host cell cytosol, are inherently bacteria-free. A change of this status therefore represents a perturbance of the physiological state and signals the need for adjustment by mounting protective responses. In conclusion, the presented defense mechanisms define bacteria as harmless or dangerous according to their localization (in combination with specific PAMP expression). For this reason, physiologically bacteria-free compartments are well equipped with PRRs, while compartments in which high PAMP concentrations are physiological, such as the luminal surface of the intestinal epithelium, are inert to these PAMPs. Notably, this applies to the PRRs analyzed in this thesis, TLR4 and NAIP/NLRC4, and remains to be assessed for others.

Given the detrimental effect of immune overactivation in the intestinal mucosa, the two defense mechanisms presented here employ control mechanisms to prevent the induction of inappropriate responses and tissue damage: The signal transmission of CD11b^{+} CD103^{-} sentinel MPs is locally restricted and could thereby allow adjusting antibacterial responses to the intensity of a bacterial stimulus in a modular fashion (Figure 1; Chapter 3). The expulsion of infected IECs by NAIP/NLRC4 is cell-intrinsic and strictly regulated to ensure maintenance of tissue integrity (Rauch et al., 2017; Sellin et al., 2014).

The regulation of PRR expression on IECs is especially intriguing, given their anatomical location in close contact to the microbes in the intestinal lumen. The loading with intracellular sensors exploits their specific suitability for the detection of invasive bacteria (Chapter 4). Besides this suitability for detection of invasion-associated PAMPs by NAIP/NLRC4, the reliance of IECs on intracellular instead of extracellular PRRs might also represent a mechanism that allows screening for microbial presence while avoiding the risk of overstimulation by extracellular PRRs on the luminal surface.

Taken together, the presented data show that responses to bacterial exposure require coordinated tissue reactions. Herein, cells of non-hematopoietic origin play an important role in the coordination and execution of homeostatic surveillance and antibacterial defenses. The contributions of these "non-immune cells" to immune responses only starts to emerge. Dissecting the involvement of cells of non-hematopoietic origin will therefore be an essential step towards understanding tissue responses during acute and chronic inflammation.

VIRULENCE FACTOR EXPRESSION TO EVADE/MODULATE IMMUNE RESPONSES

(partially adapted from Hausmann and Hardt, Microbiology Spectrum 2019)

The coevolution between pathogens and their hosts results in a fine-tuned, reciprocal relationship. The race of adapting to improved immune defenses or virulence strategies lead to the development of a tight regulation of virulence factor expression for well-adapted pathogens and evasion-"proof" host immune defenses. The recognition of the *S*. Tm flagella and TTSS-1 during oral infection by NAIP/NLRC4 presents an interesting example of this coevolution (Chapter 4).

As outlined above, *S*. Tm rapidly downregulates these PAMPs upon entry into the intestinal mucosa of the host in an attempt to circumvent immune detection. This downregulation is fast and occurs during the transition from the epithelium to the lamina propria (Chapter 4). This swift adaptation of PAMP expression highlights the relevance of evasion from detection by phagocytes for the enteropathogen. Indeed, *S. enterica* specifically evolved flagellar downregulation upon host cell entry (Ilyas et al., 2018). Consequently, despite detectable expression of *Naip/Nlrc4* in immune cells, they are unable to sense *S*. Tm via NAIP/NLRC4 (Chapter 4).

Epithelial recognition can however not be completely avoided, as flagella and TTSS-1 are imperative for epithelial invasion. This has a couple of interesting implications for the impact of epithelial NAIP/NLRC4 on the lifestyle of *S*. Tm in the cecal mucosa. *S*. Tm brings the flagellum, a potent trigger of the NAIP/NLRC4 inflammasome, into the host cell. While the largest fraction of these cells resides within the SCV - shielded by the SCV membrane from the cytosolic NLR sensors - a small fraction of flagella-carrying *S*. Tm localizes in the cytosol. It remains to be shown whether a fully assembled flagellum can trigger NAIP/NLRC4 activation. Nonetheless, the flagellar presence is likely associated with the presence of monomeric flagella subunits, which are potent activators of NAIP/NLRC4 (Miao et al., 2006). It therefore seems counterintuitive that *S*. Tm carries flagella in vicinity of the cytosolic NAIP sensors. Furthermore, the fraction of flagella-carrying *S*. Tm within the host cell cytosol seems to increase over time. This indicates that *S*. Tm indeed upregulates SPI-1 (which is associated with flagella expression) intracellularly in preparation for a reinfection cycle upon expulsion of the infected IEC, as proposed by Laughlin et al. (Laughlin et al., 2014) (Chapter 1). Herein the flagellum could serve a double role in i) inducing expulsion of the infected IEC via NAIP/NLRC4 to release *S*. Tm into the intestinal lumen and ii) preparing *S*. Tm to swim towards the intestinal mucosa for a second round of infection. Whether these reinfection cycles really occur *in vivo* remains to be investigated.

The high prevalence of FliC$^+$ (flagella$^+$) *S*. Tm in the intestinal epithelium compared to the fast downregulation of flagella and TTSS-1 upon transition into the lamina propria poses the intriguing question which cues regulate these differences, and whether they are directly linked to invasion kinetics. Detailed studies addressing the dwelling time of *S*. Tm within different IEC compartments will help to elaborate which subpopulations express flagella within IECs *in vivo*, and how this is regulated. Nonetheless, the epithelium of *Naip1-6*$^{\Delta IEC}$ mice harbors significantly more cytosolic FliC$^+$ *S*. Tm compared to their wild type littermate controls, indicating that NAIP/NLRC4 is proficient in restricting epithelial FliC$^+$ *S*. Tm (Chapter 4). Cytosolic *S*. Tm have free access to cytosolic nutrients, which enables them to hyperreplicate (Knodler et al., 2010). In line with this, *Naip1-6*$^{\Delta IEC}$ mice harbored more cytosolic microcolonies than their wild type littermate controls. This indicates that FliC$^+$ *S*. Tm escape the SCV and attempt cytosolic hyperreplication, which NAIP/NLRC4 restricts in wild type mice, likely by the expulsion of the infected cell (Rauch et al., 2017; Sellin et al., 2014).

Taken together these data indicate that, besides relying on the expression of PAMPs recognized by epithelial NAIP/NLRC4 for invasion, *S*. Tm might actually provoke epithelial sensing by NAIP/NLRC4 to a certain extent. By contrast, NAIP/NLRC4 sensing by immune cells is strictly avoided. Previous studies indicate a supportive role of inflammation in *S*. Tm colonization. *S*. Tm has evolved strategies to overcome inflammatory responses, whereas the microbiota is highly affected by it. Consequently, inflammation maintains an open gut luminal niche for *S*. Tm to bloom in (Stecher et al., 2007). Given the involvement of NAIP/NLRC4 in triggering early inflammation during infection (Sellin et al., 2014), it is conceivable that flagella-induced activation of epithelial NAIP/NLRC4 might contribute to the establishment of *S*. Tm in the intestinal lumen. This is difficult to address in the streptomycin mouse model, in which the microbiota is cleared by antibiotic treatment before infection. Studying the early infection kinetics in *Nlrc4*$^{-/-}$ mice in the presence of a microbiota, for example in low-complexity microbiota or Oligo mice (Brugiroux et al., 2016; Maier et al., 2013), might shed further light on this.

As outlined above, pathogens rely on PAMP expression at certain stages of the infection and are therefore not always able to downregulate their expression to avoid the induction of detrimental host responses. This might explain why several enteropathogenic bacteria employ TTSS effector proteins to inhibit the host's innate immune response (Chapter 1).

Numerous *S*. Tm TTSS effectors exist and may well contribute to dampening the host's mucosal innate response. The analysis of virulence factors for their role in controlling inflammasome activation will be relevant for an improved understanding of enteropathogen infection and might shed light on discrepancies in studies reporting the involvement of different inflammasome components in host defense (Chapter 4). However, demonstrating virulence factor function *in vivo* might be challenging for several reasons. Due to redundant activities, one will have to test mutants with reduced effector protein repertoires in a trial-and-error type of approach. Also, fine-tuning of the mouse infection model will be crucial to decipher immune-modulation during particular steps of the gut tissue infection process. It should be noted that the classical streptomycin mouse model might be sub-optimal, as invading pathogen loads increase very sharply by 6-10h of infection, which leads to prodigal inflammation (and may cover up more subtle TTSS effector phenotypes) by 10-12h of infection (Barthel et al., 2003). More benign gut infection kinetics, as observed in mice with a low-complexity gut microbiota, might help to resolve this issue (Maier et al., 2013). Finally, it remains unclear, whether some *S*. Tm TTSS effectors work only in specific hosts. This is particularly pressing, as *S*. Tm is a broad host range pathogen and the emergence of new epidemic clones occurs in their zoonotic animal reservoirs, i.e. chicken, swine and cattle.

RECENT ADVANCES IN THE ANALYSIS OF HOST-MICROBE INTERACTION

INTESTINAL EPITHELIAL ORGANOIDS

Intestinal organoids become increasingly important as a tool to study epithelial responses. The data presented in Chapter 5 of this thesis further validates organoids as an overall reproducible model, which recapitulates the tissue of origin and exhibits robustness to environmental cues. Importantly, the impact of the microbiota of SPF microbiota-associated donors on global organoid gene and protein expression was negligible, refuting the requirement of littermate control organoids. It remains to be shown whether disease-associated microbiota signatures, e.g. implicated in colitis development, imprint on intestinal epithelial stem cells and thereby affect organoid cultures.

Our data indicate a moderate variability in the responsiveness to TNF between different organoid cultures (Chapter 5). It will be important to address the sources of organoid culture-to-culture variability to improve reproducibility of organoid experimentation, and its suitability as an experimental model. One major confounding factor in intestinal organoid maintenance is its dependence on matrigel. Matrigel is a hetergenous mix of extracellular matrix proteins, which is produced by a mouse sarcoma cell line (Kleinman et al., 1986). Batch-to-batch variations and incomplete knowledge of the molecular composition of matrigel may therefore impact the reproducibility of organoid experiments. The recent development of a defined hydrogel matrix (Broguiere et al., 2018) promises to resolve this issue. Systematic studies on the effect of further culture-to-culture variations, e.g. organoid density, on organoid phenotypes will help to further improve reproducibility.

Another hurdle for the use of organoids in infection studies is their growth in 3D spheres. The lumen of these spheres mimics the luminal epithelial interface, which is the main entry site for invasive enteropathogens. It is however not easy to access experimentally in spheroid organoids. Recent techniques for the seeding of organoids into monolayers make experimental manipulation and the control of host cell numbers easier (Liu et al., 2019).

Experimental validation of organoid suitability as a model in combination with the constant improvement of culturing techniques will further solidify the importance of organoids as a model system.

MMMS AND NEUTRAL GENETIC TAGS TO STUDY POPULATION DYNAMICS

(adapted from Hausmann and Hardt, Immunology 2020)

Population dynamics approaches employing neutral genetic tags in combination with MMMs help to dissect the complex, dynamic relations underlying host-microbe interactions. Strategies exist for the analysis of bacterial and host population dynamics and will be discussed below.

POPULATION DYNAMICS APPROACHES TO STUDY HOST-PATHOGEN INTERACTIONS

S. Tm infections in mice have served as an important model for developing MMMs in the context of genetic tag dynamics, i.e. for describing the infection dynamics and identifying critical host barriers during infection. Here, we focus on an MMM describing *S*. Tm migration from the intestinal lumen to the mLN during oral infection (quantified as migration events per day) (Figure 2A, wild type mouse, ~300 bacterial cells/day migrate to the mLN (Kaiser et al., 2013)). By combining population dynamics approaches with mouse knock out lines, *S*. Tm migration heavily depends on CCR7-mediated migration of immune cells from the lamina propria to the mLN (Figure 2B, scenario i: *CCR7*$^{-/-}$ mouse). The application of this model to

infections with mutant *S*. Tm also revealed a role for inflammation in restriction of bacterial replication in the mLN (Figure 2B, scenario ii) (Kaiser et al., 2013). Recently, we have extended the application of the above-described model to identify the cell type responsible for NAIP/NLRC4-mediated restriction of *S*. Tm infection of the mLN. While epithelial NAIP/NLRC4 is highly relevant for the control of *S*. Tm loads within the epithelium (Rauch et al., 2017; Sellin et al., 2014), immune cell NAIP/NLRC4 can also be involved in bacterial restriction (Carvalho et al., 2012; Franchi et al., 2006; Lara-Tejero et al., 2006). It remained unclear, whether *S*. Tm loads in the mLN of NAIP/NLRC4 deficient mice were increased due to an impaired antibacterial response at the epithelial level, or due to the inability of immune cells to restrict intracellular *S*. Tm replication via NAIP/NLRC4. Assessing migration to the mLN and replication rates of *S*. Tm within the mLN, we could exclude NAIP/NLRC4 mediated restriction of bacterial replication within immune cells in the mLN. Much rather, we identified NAIP/NLRC4 as a critical migration barrier for *S*. Tm on their way to the mLN, protecting from increased systemic spread. The combination of this modeling approach with cell-type specific knock out mice revealed that NAIP/NLRC4 within the gut epithelium controls *S*. Tm migration to systemic compartments (Figure 2B, scenario iii: *Naip1-6*$^{\Delta IEC}$ mouse), while immune cell NAIP/NLRC4 is dispensable for controlling bacterial loads during early infection (Chapter 4).

Similarly, the elegant combination of genetic barcodes with mouse and bacterial knockout strains deciphered transmission routes of *Listeria monocytogenes* (*L. monocytogenes*) within and between hosts (Zhang et al., 2017). The comparison of the genetic (barcode) relatedness of bacterial subpopulations in spleen and liver revealed distinct initial founding events of organ subpopulations during early infection, and bacterial exchange between these organs via the bloodstream during later stages of the infection. Surprisingly, and in contrast to previous assumptions, this analysis revealed the gall bladder as the main reservoir for fecal host-to-host transmission (Zhang et al., 2017).

Taken together, the above-described examples illustrate the great potential of population dynamics and mathematical modeling in identification of critical host barriers and prediction of intervention strategies during bacterial infections. This approach is especially powerful in combination with experimentation on host and bacterial knock out strains to pinpoint critical interactions for pathogen restriction during different disease stages and/or transmission at the molecular and cellular level.

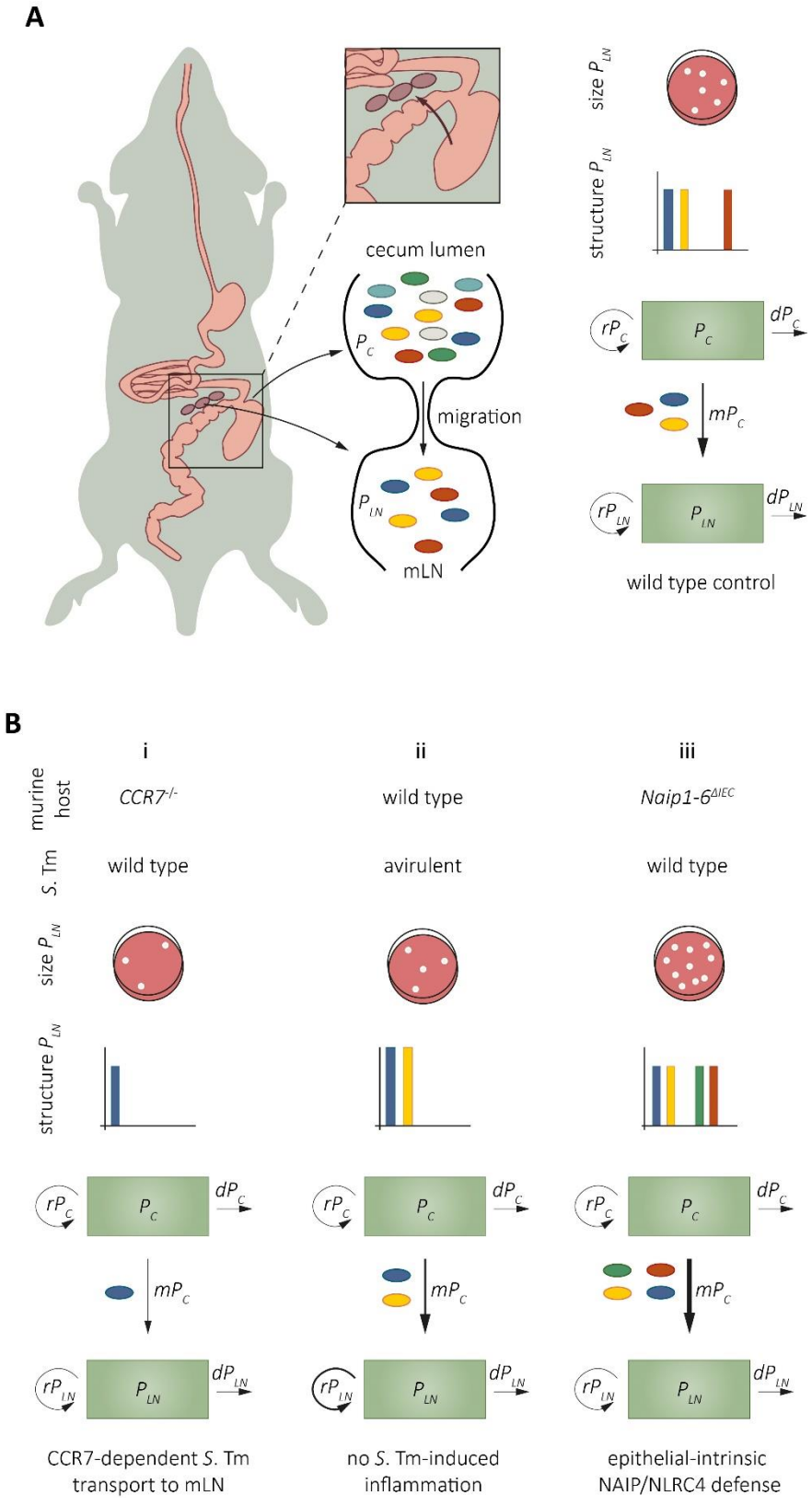

Figure 2 ***A*** *Schematic of S. Tm migration from the cecal lumen to the mLN during oral infection (left panel). ~300 S. Typhimurium cells per day migrate from the cecal lumen to the mLN during oral infection (wild type mouse, right panel), contributing to the bacterial mLN population* P_{LN} *as described by the compartmental model shown in Chapter 1 (Kaiser et al., 2013). Compared to*

the population in the cecum (~10^9 S. Tm cells/g content) this number is small. The migration to the mLN thus represents a bottleneck, which only a small number of bacteria can pass. In conclusion, genetic diversity (different colors, see also graphs "structure P_{LN}") of the mLN population (P_{LN}) is reduced in comparison to the cecal population (P_C) (middle panel). Using the size and structure of P_{LN} as input for the MMM enables calculation of m *and* r *of* P_{LN}. ***B*** *Migration of* S. *Tm to the mLN (*m*) is reduced in the absence of CCR7 (scenario i,* $CCR7^{-/-}$ *mouse) (Kaiser et al., 2013). Replication of* S. *Tm within the mLN (*rP_{LN}*) is controlled by* S. *Tm-induced inflammation (scenario ii, infection with an* S. *Tm mutant which is unable to trigger early inflammation) (Kaiser et al., 2013). Migration of* S. *Tm to the mLN (*m*) is increased in the absence of NAIP/NLRC4-mediated expulsion of infected epithelial cells (scenario iii,* $Naip1\text{-}6^{\Delta IEC}$ *mouse) (Chapter 4).*

POPULATION DYNAMICS APPROACHES TO STUDY HOST-MICROBIOTA INTERACTIONS

Similar to host-pathogen relationships, host-microbiota interactions are highly complex and dynamic. Deciphering the kinetics of microbiota colonization, response to perturbations and behavior in disease conditions holds the key to assessment of the role of microbiota members in these scenarios and to manipulation of microbiota contributions to disease development. Quantitative and causal microbiota analysis is facing three major challenges: i) the difficulty to conclude a precise, overarching definition of "the" microbiota, ii) the difficulty to culture and therefore manipulate a large fraction of typical microbiota members and iii) the complexity of interactions within the microbiota community and with its host. In the past years, approaches were developed to tackle these challenges. Defined murine microbiota consortia enable studies of community interactions and contributions of specific strains to phenotypes (Brugiroux et al., 2016; Maier et al., 2013; Stecher et al., 2010). Studies on culturable microbiota members such as *Escherichia coli* (*E. coli*) and *Bacteroides thetaiotaomicron* (Cremer et al., 2016; Oliveira et al., 2020), as well as longitudinal studies on microbiota composition (Furman et al., 2020; Ji et al., 2020) have shed light on general concepts of intestinal colonization and interspecies competition. Despite these efforts, to date most studies modelling microbial community dynamics are based on *in vitro* or *in silico* systems (Arnoldini et al., 2018; Labarthe et al., 2019), general patterns extracted from sequencing data (Inamine et al., 2018; Marino et al., 2014), or analysis of the microbiota as a metaorganism (Wotzka et al., 2019) (see Table 1 for a summary of selected *in vivo* studies). These studies are fundamental in gaining a basic understanding of the formation of community structures and can potentially be extended to perturbation scenarios and disease settings. Precise quantification and identification of causalities *in vivo* on a species/strain level and in specific intestinal niches however remains difficult. In the future, it will therefore be extremely valuable to implement precise quantitative setups offered by population dynamics using genetic barcodes in the field of host-microbiota interactions. Experimental models of defined microbiota, in which the community members are known (Brugiroux et al., 2016; Maier et al., 2013), will be an essential tool in this context. Specifically combining defined microbiota models with neutral genetic barcoding tools as described above for host-pathogen interaction analysis will be a powerful approach to decipher those intricate interactions.

Table 1 ***Studies analyzing microbiota population dynamics*** **in vivo.** *bp = base pairs, n.a. = not applicable.*

Bacterium	Method	Number of unique identifiers	Analyzed parameters	Main finding	Reference
E. coli, *Klebsiella michiganensis* (*K. michiganensis*)	fluorescent proteins	2	intestinal colonization	*K. michiganensis* provides colonization resistance against *E. coli*	(Oliveira et al., 2020)
E. coli	fluorescent proteins	2	niche competition in intestinal colonization	Horizontal gene transfer promotes niche adaptation	(Frazão et al., 2019)
Microbiota	16S sequencing, qPCR quantification	n.a.	replication and death rate of microbiota exposed to bile salts	Diet-evoked increased bile salt concentrations perturb microbiota composition and lead to decreased colonization resistance to *S*. Tm	(Wotzka et al., 2019)
Several microbiota members (mouse)	qPCR (16S)	n.a.	replication rate, interstrain interactions	colonization dynamics in the murine intestine	(Marino et al., 2014)
Several microbiota members (fruitfly)	plating	n.a.	transition time through intestine, intraintestinal replication and death rate	colonization dynamics in the intestine of *Drosophila melanogaster*	(Inamine et al., 2018)

STUDYING HOST RESPONSE DYNAMICS *IN VIVO*

The abstraction of complex scenarios by MMMs will help to gain a more refined and holistic understanding of the processes underlying host responses to microbe exposure. This approach is especially valuable in complementation to traditional approaches including single knock out/transgenic mouse models. To extend current knowledge, it will be helpful to broaden the application of the available tools to further cell types and models. The analysis of myeloid populations, for example, is highly complicated by the vast plasticity of this cell group, overlapping marker expression, and longevity of specific subpopulations (Guilliams et al., 2014; Joeris et al., 2017). The Confetti construct (Chapter 2) has contributed to deciphering dynamics of regional turnover, contribution of bone marrow-derived precursors, and response to insults of brain microglia (Tay et al., 2017) and mucosal DCs (Cabeza-Cabrerizo et al., 2019). The number of markers required for cell type identification however complicates straightforward characterization of myeloid cell subsets involved in tissue homeostasis and immune responses. Recently developed inducible barcoding tools like the CARLIN mouse (Bowling et al., 2020), which allow read-out of barcodes and high resolution cell type identification via single cell transcriptomics in parallel, have great potential in this context: i) the higher resolution due to a higher variety of barcodes allows more refined tracing of lineage dynamics during development and in the adult, and ii) the induction of barcode labeling before, during, or after pathogen exposure or disease conditions can reveal contributions of different (myeloid) cell subsets to immune responses. Thus, *in vivo* labeling strategies in combination with MMMs holds promise for dissecting reciprocal, dynamic relationships underlying host-microbe interactions.

DRAWBACKS AND OUTLOOK

Combining MMMs with experiments using genetic tagging techniques holds great potential for deciphering the intricate dynamics underlying host-microbe interactions. A couple of aspects however need to be considered for the application of this approach. One critical factor is the number of unique tags used in an experiment. This determines the sensitivity for bottleneck detection. The detection of wide bottlenecks requires the use of large tag libraries (Abel et al., 2015a; Zhang et al., 2017), which can be achieved by genetic barcoding (Abel et al., 2015b). The calculation of population bottlenecks with the help of genetic barcodes relies on the assumption that the fitness of each barcoded cell is equal in the given conditions, as they are isogenic. This assumption however is often an over-simplification, i.e. when phenotypic heterogeneity occurs within bacterial subpopulations. Thereby, different cells carrying identical barcodes may express different virulence factors in a stochastic fashion and thereby interact differentially with host cells. Thus, also isogenic bacteria might feature fitness differences. In scenarios with a low variety of barcodes (i.e., a high number of cells/barcode), population averages might equal this effect out. In scenarios in which a high variety of barcodes is used (i.e., a low number of cells/barcode), phenotypical diversity of isogenic organisms might however skew genetic barcode distribution. Besides that, especially when working with large barcode libraries that are randomly inserted, great care needs to be taken to exclude fitness effects by the insertion. Finally, while barcoding strategies allow large scale analysis of populations, they require dissociation of the tissue. Thus, spatial resolution in these approaches is lost. This caveat could be overcome by combining barcoding strategies with fluorescence in situ hybridization of the barcodes. Finally, detailed a priori knowledge about the experimental system is required for setting up MMMs, which makes this method unsuitable for new and/or understudied experimental setups.

Taken together, we see potential in extending the use of neutral barcodes to further fields, especially for i) microbiota members in the context of defined microbiota models and ii) a variety of host cells, e.g. the myeloid immune cell compartment to decipher the contribution of certain cell subsets to responses to microbial triggers. For the analysis of host cells, *in vivo* labeling approaches (Bowling et al., 2020; Spanjaard et al., 2018; Sun et al., 2014; Weber et al., 2016) (Chapter 2) prove especially useful, as they allow studying population dynamics in the absence of strong technically induced disturbances. These approaches hold promise to facilitate deciphering the complexity of host-microbe interaction and help to reveal contributions of different immune effectors.

Recent advances in sequencing technology provide a platform for cost efficient, high throughput read out of genetic barcodes. The introduction of barcodes which can be quantified by next generation sequencing techniques relieves constraints on the number of tags that can be used in an experiment, allowing the introduction of large barcode libraries and high-resolution quantification of population parameters. By tagging of host cells and bacteria with distinct barcodes, sequencing techniques in combination with MMMs enable analysis of large-scale population interaction dynamics within one host. Combined with single cell RNA sequencing (Bowling et al., 2020), this experimental setup promises to provide information about host-pathogen interaction at single cell level e.g. in the context of intracellular infections.

FINAL CONCLUSIONS

(partially adapted from Hausmann and Hardt, Microbiology Spectrum, 2019)

The innate immune system of the intestinal mucosa mounts protective responses against enteropathogens, while tolerating the commensal microbiota in the lumen. A common pathogen-associated feature is invasiveness. The expression of the PRRs TLR4 and NAIP/NLRC4 is restricted to mucosal compartments (or intracellular sites), which are physiologically devoid of bacteria (Chapter 3 and 4). Pathogenic bacteria, by contrast, often target these compartments for protection from luminal immune effectors, access to nutrients and migration to distant body sites. Given their localization, TLR4 and NAIP/NLRC4 therefore specifically screen for invasive bacteria, and mount protective responses against them.

S. Tm faces a variety of challenges and environments during the infection cycle. A cardinal dilemma is created by the host's innate immune system, which detects key virulence factors essential for infection. The pathogen employs two general strategies to avoid elimination, i.e. controlling the innate immune response and stage-specific adaptation of the gene expression profile (Chapter 4), leading to a phenotypic heterogeneity of the infecting population.

The host response against *S*. Tm infection is similarly multifaceted. Different cell types within the infected tissue cooperate to fight the infection. As described above, IECs emerge as central players in this defense. Indeed, the epithelial-intrinsic expulsion of infected IECs is the most potent host defense mechanism during the first 12-18h of oral *S*. Tm infection identified so far. It protects local, but also systemic sites from increased *S*. Tm loads (Chapter 4). On top of that, complex interaction networks as well as the development of organotypic features like the mucus layer require the interplay of different cell types in a specific microenvironment, imposing a major challenge on *in vitro* culture.

Taken together, in the early phase of gut tissue invasion by *S*. Tm there seems to be i) a need for expression of certain virulence factors required for invasion and ii) initiation of an inflammatory host response by factors crucial or supportive for invasion. This host response is quite effective and reduces pathogen tissue loads by as much as ~100-fold. However, this defense is not purely beneficial for the host, as it imposes tissue damage, delays remission of the inflamed mucosa, fuels gut luminal pathogen blooms and suppresses regrowth of the microbiota, thereby allowing prolonged inhabitation of the intestinal lumen by the pathogen (Dolowschiak et al., 2016; Miki et al., 2017; Stecher and Hardt, 2008; Wotzka et al., 2017). In conclusion, inflammation triggered by the bacterium is a double-edged sword for the host, especially when dealing with well-adapted pathogens like *S*. Tm.

The complexity of the system highlights the importance of analyzing host-pathogen interactions *in vivo* in the organs of an infected host. Cell culture models have great value for detailed analysis of molecular signaling mechanisms. However, immortalized cell lines are unlikely to represent a realistic model for short-lived IECs. Intestinal organoids (Sato et al., 2009) serve as a more realistic model, especially for studies focusing on cell death (Chapter 5). Nevertheless, the relevance of mechanisms discovered *in vitro* can only be fully verified in animal models.

The usage of genetically modified bacteria facilitates the real-time analysis of the interaction between host and pathogen. Fluorescent reporters enable monitoring the localization or gene expression by the bacterium during different stages of infection, quantification of replication (Claudi et al., 2014) or probing for environmental conditions such as oxygen levels (Nomata and Hisabori, 2018), reactive oxygen species (Schürmann et al., 2017) or pH (Morimoto et al., 2016). In combination with intravital microscopy, these

fluorescent reporters provide a powerful tool to decipher real-time dynamics of host-pathogen interaction (Kreibich and Hardt, 2015). In the future, epitope-tag surface display might further expand the repertoire of techniques for scrutinizing the heterogeneity of the pathogen-host interaction at the single cell level (Curkić et al., 2016). Finally, barcoded bacteria or host cells in combination with mathematical modeling allow the analysis of population dynamics and determination of bottlenecks throughout the infection (Kaiser et al., 2013) (Chapter 2 and 4). The combination of single cell approaches with population dynamics has great potential.

For comparability and interpretability of *in vivo* data, the use of littermate controls in *S*. Tm infections is crucial, as the microbiota composition can influence *S*. Tm infection kinetics (Kaiser et al., 2012) (Chapter 4). This will be of particular importance when using new gnotobiotic mouse models, which allow for slow gut luminal pathogen growth and realistic stimulation kinetics of the host's defenses (Brugiroux et al., 2016; Maier et al., 2013). Such models may hold the key for deciphering the *in vivo* function of the numerous *S*. Tm virulence factors and host immune effectors. These approaches will likely decipher mechanisms which are of broad general relevance also for other pathogens, as well as the interactions of the host with its microbiota.

REFERENCES

Abel, S., zur Wiesch, P.A., Chang, H.-H., Davis, B.M., Lipsitch, M., and Waldor, M.K. (2015a). STAMP: Sequence tag-based analysis of microbial population dynamics. Nat Methods *12*, 223–226.

Abel, S., Wiesch, P.A. zur, Davis, B.M., and Waldor, M.K. (2015b). Analysis of Bottlenecks in Experimental Models of Infection. PLOS Pathogens *11*, e1004823.

Arnoldini, M., Cremer, J., and Hwa, T. (2018). Bacterial growth, flow, and mixing shape human gut microbiota density and composition. Gut Microbes 1–8.

Barthel, M., Hapfelmeier, S., Quintanilla-Martínez, L., Kremer, M., Rohde, M., Hogardt, M., Pfeffer, K., Rüssmann, H., and Hardt, W.-D. (2003). Pretreatment of Mice with Streptomycin Provides a Salmonella enterica Serovar Typhimurium Colitis Model That Allows Analysis of Both Pathogen and Host. Infect Immun *71*, 2839–2858.

Beutler, B., Krochin, N., Milsark, I.W., Luedke, C., and Cerami, A. (1986). Control of cachectin (tumor necrosis factor) synthesis: mechanisms of endotoxin resistance. Science *232*, 977–980.

Bowling, S., Sritharan, D., Osorio, F.G., Nguyen, M., Cheung, P., Rodriguez-Fraticelli, A., Patel, S., Yuan, W.-C., Fujiwara, Y., Li, B.E., et al. (2020). An Engineered CRISPR-Cas9 Mouse Line for Simultaneous Readout of Lineage Histories and Gene Expression Profiles in Single Cells. Cell.

Broguiere, N., Isenmann, L., Hirt, C., Ringel, T., Placzek, S., Cavalli, E., Ringnalda, F., Villiger, L., Züllig, R., Lehmann, R., et al. (2018). Growth of Epithelial Organoids in a Defined Hydrogel. Advanced Materials *30*, 1801621.

Brugiroux, S., Beutler, M., Pfann, C., Garzetti, D., Ruscheweyh, H.-J., Ring, D., Diehl, M., Herp, S., Lötscher, Y., Hussain, S., et al. (2016). Genome-guided design of a defined mouse microbiota that confers colonization resistance against Salmonella enterica serovar Typhimurium. Nat Microbiol *2*, 16215.

Cabeza-Cabrerizo, M., van Blijswijk, J., Wienert, S., Heim, D., Jenkins, R.P., Chakravarty, P., Rogers, N., Frederico, B., Acton, S., Beerling, E., et al. (2019). Tissue clonality of dendritic cell subsets and emergency DCpoiesis revealed by multicolor fate mapping of DC progenitors. Sci Immunol *4*.

Carvalho, F.A., Nalbantoglu, I., Aitken, J.D., Uchiyama, R., Su, Y., Doho, G.H., Vijay-Kumar, M., and Gewirtz, A.T. (2012). Cytosolic flagellin receptor NLRC4 protects mice against mucosal and systemic challenges. Mucosal Immunol *5*, 288–298.

Chassaing, B., Ley, R.E., and Gewirtz, A.T. (2014). Intestinal epithelial cell toll-like receptor 5 regulates the intestinal microbiota to prevent low-grade inflammation and metabolic syndrome in mice. Gastroenterology *147*, 1363-1377.e17.

Chen, K.W., Groß, C.J., Sotomayor, F.V., Stacey, K.J., Tschopp, J., Sweet, M.J., and Schroder, K. (2014). The neutrophil NLRC4 inflammasome selectively promotes IL-1β maturation without pyroptosis during acute Salmonella challenge. Cell Rep *8*, 570–582.

Claudi, B., Spröte, P., Chirkova, A., Personnic, N., Zankl, J., Schürmann, N., Schmidt, A., and Bumann, D. (2014). Phenotypic variation of Salmonella in host tissues delays eradication by antimicrobial chemotherapy. Cell *158*, 722–733.

Cremer, J., Segota, I., Yang, C., Arnoldini, M., Sauls, J.T., Zhang, Z., Gutierrez, E., Groisman, A., and Hwa, T. (2016). Effect of flow and peristaltic mixing on bacterial growth in a gut-like channel. Proc Natl Acad Sci USA *113*, 11414–11419.

Curkić, I., Schütz, M., Oberhettinger, P., Diard, M., Claassen, M., Linke, D., and Hardt, W.-D. (2016). Epitope-Tagged Autotransporters as Single-Cell Reporters for Gene Expression by a Salmonella Typhimurium wbaP Mutant. PloS One *11*, e0154828.

Dheer, R., Santaolalla, R., Davies, J.M., Lang, J.K., Phillips, M.C., Pastorini, C., Vazquez-Pertejo, M.T., and Abreu, M.T. (2016). Intestinal Epithelial Toll-Like Receptor 4 Signaling Affects Epithelial Function and Colonic Microbiota and Promotes a Risk for Transmissible Colitis. Infect. Immun. *84*, 798–810.

Doerflinger, M., Deng, Y., Whitney, P., Salvamoser, R., Engel, S., Kueh, A.J., Tai, L., Bachem, A., Gressier, E., Geoghegan, N.D., et al. (2020). Flexible Usage and Interconnectivity of Diverse Cell Death Pathways Protect against Intracellular Infection. Immunity.

Dolowschiak, T., Mueller, A.A., Pisan, L.J., Feigelman, R., Felmy, B., Sellin, M.E., Namineni, S., Nguyen, B.D., Wotzka, S.Y., Heikenwalder, M., et al. (2016). IFN-γ Hinders Recovery from Mucosal Inflammation during Antibiotic Therapy for Salmonella Gut Infection. Cell Host Microbe *20*, 238–249.

Franchi, L., Amer, A., Body-Malapel, M., Kanneganti, T.-D., Özören, N., Jagirdar, R., Inohara, N., Vandenabeele, P., Bertin, J., Coyle, A., et al. (2006). Cytosolic flagellin requires Ipaf for activation of caspase-1 and interleukin 1β in salmonella-infected macrophages. Nat Immunol *7*, 576–582.

Frazão, N., Sousa, A., Lässig, M., and Gordo, I. (2019). Horizontal gene transfer overrides mutation in Escherichia coli colonizing the mammalian gut. Proc. Natl. Acad. Sci. U.S.A. *116*, 17906–17915.

Furman, O., Shenhav, L., Sasson, G., Kokou, F., Honig, H., Jacoby, S., Hertz, T., Cordero, O.X., Halperin, E., and Mizrahi, I. (2020). Stochasticity constrained by deterministic effects of diet and age drive rumen microbiome assembly dynamics. Nat Commun *11*, 1904.

Guilliams, M., Ginhoux, F., Jakubzick, C., Naik, S.H., Onai, N., Schraml, B.U., Segura, E., Tussiwand, R., and Yona, S. (2014). Dendritic cells, monocytes and macrophages: a unified nomenclature based on ontogeny. Nature Reviews Immunology *14*, 571–578.

Günther, C., Buchen, B., He, G.-W., Hornef, M., Torow, N., Neumann, H., Wittkopf, N., Martini, E., Basic, M., Bleich, A., et al. (2015). Caspase-8 controls the gut response to microbial challenges by Tnf-α-dependent and independent pathways. Gut *64*, 601–610.

Han, J., Brown, T., and Beutler, B. (1990). Endotoxin-responsive sequences control cachectin/tumor necrosis factor biosynthesis at the translational level. J. Exp. Med. *171*, 465–475.

Hapfelmeier, S., Müller, A.J., Stecher, B., Kaiser, P., Barthel, M., Endt, K., Eberhard, M., Robbiani, R., Jacobi, C.A., Heikenwalder, M., et al. (2008). Microbe sampling by mucosal dendritic cells is a discrete, MyD88-independent step in DeltainvG S. Typhimurium colitis. J. Exp. Med. *205*, 437–450.

Harrison, O.J., Srinivasan, N., Pott, J., Schiering, C., Krausgruber, T., Ilott, N.E., and Maloy, K.J. (2015). Epithelial-derived IL-18 regulates Th17 cell differentiation and Foxp3^{+} Treg cell function in the intestine. Mucosal Immunology *8*, 1226–1236.

Haziot, A., Rong, G.W., Silver, J., and Goyert, S.M. (1993). Recombinant soluble CD14 mediates the activation of endothelial cells by lipopolysaccharide. J. Immunol. *151*, 1500–1507.

Hornef, M.W., Frisan, T., Vandewalle, A., Normark, S., and Richter-Dahlfors, A. (2002). Toll-like receptor 4 resides in the Golgi apparatus and colocalizes with internalized lipopolysaccharide in intestinal epithelial cells. J. Exp. Med. *195*, 559–570.

Hornef, M.W., Normark, B.H., Vandewalle, A., and Normark, S. (2003). Intracellular recognition of lipopolysaccharide by toll-like receptor 4 in intestinal epithelial cells. J. Exp. Med. *198*, 1225–1235.

Ii, W.A.R., Sakamoto, K., and Leifer, C.A. (2012). TLR9 is important for protection against intestinal damage and for intestinal repair. Sci Rep *2*, 574.

Ilyas, B., Mulder, D.T., Little, D.J., Elhenawy, W., Banda, M.M., Pérez-Morales, D., Tsai, C.N., Chau, N.Y.E., Bustamante, V.H., and Coombes, B.K. (2018). Regulatory Evolution Drives Evasion of Host Inflammasomes by Salmonella Typhimurium. Cell Rep *25*, 825-832.e5.

Inamine, H., Ellner, S.P., Newell, P.D., Luo, Y., Buchon, N., and Douglas, A.E. (2018). Spatiotemporally Heterogeneous Population Dynamics of Gut Bacteria Inferred from Fecal Time Series Data. MBio *9*.

Ji, B.W., Sheth, R.U., Dixit, P.D., Tchourine, K., and Vitkup, D. (2020). Macroecological dynamics of gut microbiota. Nat Microbiol *5*, 768–775.

Joeris, T., Müller-Luda, K., Agace, W.W., and Mowat, A.M. (2017). Diversity and functions of intestinal mononuclear phagocytes. Mucosal Immunol *10*, 845–864.

Kaiser, P., Diard, M., Stecher, B., and Hardt, W.-D. (2012). The streptomycin mouse model for Salmonella diarrhea: functional analysis of the microbiota, the pathogen's virulence factors, and the host's mucosal immune response. Immunol. Rev. *245*, 56–83.

Kaiser, P., Slack, E., Grant, A.J., Hardt, W.-D., and Regoes, R.R. (2013). Lymph node colonization dynamics after oral Salmonella Typhimurium infection in mice. PLoS Pathog. *9*, e1003532.

Karrasch, T., Kim, J.-S., Muhlbauer, M., Magness, S.T., and Jobin, C. (2007). Gnotobiotic IL-10−/−;NF-κBEGFP Mice Reveal the Critical Role of TLR/NF-κB Signaling in Commensal Bacteria-Induced Colitis. The Journal of Immunology *178*, 6522–6532.

Kayisoglu, O., Weiss, F., Niklas, C., Pierotti, I., Pompaiah, M., Wallaschek, N., Germer, C.-T., Wiegering, A., and Bartfeld, S. (2020). Location-specific cell identity rather than exposure to GI microbiota defines many innate immune signalling cascades in the gut epithelium. Gut gutjnl-2019-319919.

Kleinman, H.K., McGarvey, M.L., Hassell, J.R., Star, V.L., Cannon, F.B., Laurie, G.W., and Martin, G.R. (1986). Basement membrane complexes with biological activity. Biochemistry *25*, 312–318.

Knodler, L.A., Vallance, B.A., Celli, J., Winfree, S., Hansen, B., Montero, M., and Steele-Mortimer, O. (2010). Dissemination of invasive Salmonella via bacterial-induced extrusion of mucosal epithelia. Proc. Natl. Acad. Sci. U.S.A. *107*, 17733–17738.

Knodler, L.A., Crowley, S.M., Sham, H.P., Yang, H., Wrande, M., Ma, C., Ernst, R.K., Steele-Mortimer, O., Celli, J., and Vallance, B.A. (2014). Noncanonical inflammasome activation of caspase-4/caspase-11 mediates epithelial defenses against enteric bacterial pathogens. Cell Host Microbe *16*, 249–256.

Kreibich, S., and Hardt, W.-D. (2015). Experimental approaches to phenotypic diversity in infection. Curr. Opin. Microbiol. *27*, 25–36.

Labarthe, S., Polizzi, B., Phan, T., Goudon, T., Ribot, M., and Laroche, B. (2019). A mathematical model to investigate the key drivers of the biogeography of the colon microbiota. Journal of Theoretical Biology *462*, 552–581.

Lara-Tejero, M., Sutterwala, F.S., Ogura, Y., Grant, E.P., Bertin, J., Coyle, A.J., Flavell, R.A., and Galán, J.E. (2006). Role of the caspase-1 inflammasome in Salmonella typhimurium pathogenesis. Journal of Experimental Medicine *203*, 1407–1412.

Laughlin, R.C., Knodler, L.A., Barhoumi, R., Payne, H.R., Wu, J., Gomez, G., Pugh, R., Lawhon, S.D., Bäumler, A.J., Steele-Mortimer, O., et al. (2014). Spatial segregation of virulence gene expression during acute enteric infection with Salmonella enterica serovar Typhimurium. MBio *5*, e00946-00913.

Lee, J., Mo, J.-H., Katakura, K., Alkalay, I., Rucker, A.N., Liu, Y.-T., Lee, H.-K., Shen, C., Cojocaru, G., Shenouda, S., et al. (2006). Maintenance of colonic homeostasis by distinctive apical TLR9 signalling in intestinal epithelial cells. Nat. Cell Biol. *8*, 1327–1336.

Leppkes, M., Roulis, M., Neurath, M.F., Kollias, G., and Becker, C. (2014). Pleiotropic functions of TNF-α in the regulation of the intestinal epithelial response to inflammation. Int Immunol *26*, 509–515.

Liu, Y., Mi, Y., Mueller, T., Kreibich, S., Williams, E.G., Van Drogen, A., Borel, C., Frank, M., Germain, P.-L., Bludau, I., et al. (2019). Multi-omic measurements of heterogeneity in HeLa cells across laboratories. Nat. Biotechnol. *37*, 314–322.

Lo, B.C., Shin, S.B., Canals Hernaez, D., Refaeli, I., Yu, H.B., Goebeler, V., Cait, A., Mohn, W.W., Vallance, B.A., and McNagny, K.M. (2019). IL-22 Preserves Gut Epithelial Integrity and Promotes Disease Remission during Chronic Salmonella Infection. J. Immunol. *202*, 956–965.

Maier, L., Vyas, R., Cordova, C.D., Lindsay, H., Schmidt, T.S.B., Brugiroux, S., Periaswamy, B., Bauer, R., Sturm, A., Schreiber, F., et al. (2013). Microbiota-derived hydrogen fuels Salmonella typhimurium invasion of the gut ecosystem. Cell Host Microbe *14*, 641–651.

Maloy, K.J., and Powrie, F. (2011). Intestinal homeostasis and its breakdown in inflammatory bowel disease. Nature *474*, 298–306.

Marino, S., Baxter, N.T., Huffnagle, G.B., Petrosino, J.F., and Schloss, P.D. (2014). Mathematical modeling of primary succession of murine intestinal microbiota. PNAS *111*, 439–444.

Miao, E.A., Alpuche-Aranda, C.M., Dors, M., Clark, A.E., Bader, M.W., Miller, S.I., and Aderem, A. (2006). Cytoplasmic flagellin activates caspase-1 and secretion of interleukin 1β via Ipaf. Nat Immunol *7*, 569–575.

Miki, T., Goto, R., Fujimoto, M., Okada, N., and Hardt, W.-D. (2017). The Bactericidal Lectin RegIIIβ Prolongs Gut Colonization and Enteropathy in the Streptomycin Mouse Model for Salmonella Diarrhea. Cell Host Microbe *21*, 195–207.

Monteleone, G., Trapasso, F., Parrello, T., Biancone, L., Stella, A., Iuliano, R., Luzza, F., Fusco, A., and Pallone, F. (1999). Bioactive IL-18 expression is up-regulated in Crohn's disease. J. Immunol. *163*, 143–147.

Monteleone, I., Platt, A.M., Jaensson, E., Agace, W.W., and Mowat, A.M. (2008). IL-10-dependent partial refractoriness to Toll-like receptor stimulation modulates gut mucosal dendritic cell function. Eur. J. Immunol. *38*, 1533–1547.

Morimoto, Y.V., Kami-ike, N., Miyata, T., Kawamoto, A., Kato, T., Namba, K., and Minamino, T. (2016). High-Resolution pH Imaging of Living Bacterial Cells To Detect Local pH Differences. MBio *7*, e01911-16.

Müller, A.A., Dolowschiak, T., Sellin, M.E., Felmy, B., Verbree, C., Gadient, S., Westermann, A.J., Vogel, J., LeibundGut-Landmann, S., and Hardt, W.-D. (2016). An NK Cell Perforin Response Elicited via IL-18 Controls Mucosal Inflammation Kinetics during Salmonella Gut Infection. PLoS Pathog. *12*, e1005723.

Muñoz, M., Eidenschenk, C., Ota, N., Wong, K., Lohmann, U., Kühl, A.A., Wang, X., Manzanillo, P., Li, Y., Rutz, S., et al. (2015). Interleukin-22 induces interleukin-18 expression from epithelial cells during intestinal infection. Immunity *42*, 321–331.

Niess, J.H., Brand, S., Gu, X., Landsman, L., Jung, S., McCormick, B.A., Vyas, J.M., Boes, M., Ploegh, H.L., Fox, J.G., et al. (2005). CX3CR1-mediated dendritic cell access to the intestinal lumen and bacterial clearance. Science *307*, 254–258.

Nomata, J., and Hisabori, T. (2018). Development of heme protein based oxygen sensing indicators. Sci Rep *8*.

Nordlander, S., Pott, J., and Maloy, K.J. (2014). NLRC4 expression in intestinal epithelial cells mediates protection against an enteric pathogen. Mucosal Immunol *7*, 775–785.

Oliveira, R.A., Ng, K.M., Correia, M.B., Cabral, V., Shi, H., Sonnenburg, J.L., Huang, K.C., and Xavier, K.B. (2020). Klebsiella michiganensis transmission enhances resistance to Enterobacteriaceae gut invasion by nutrition competition. Nature Microbiology *5*, 630–641.

Pickert, G., Neufert, C., Leppkes, M., Zheng, Y., Wittkopf, N., Warntjen, M., Lehr, H.-A., Hirth, S., Weigmann, B., Wirtz, S., et al. (2009). STAT3 links IL-22 signaling in intestinal epithelial cells to mucosal wound healing. J Exp Med *206*, 1465–1472.

Pizarro, T.T., Michie, M.H., Bentz, M., Woraratanadharm, J., Smith, M.F., Foley, E., Moskaluk, C.A., Bickston, S.J., and Cominelli, F. (1999). IL-18, a novel immunoregulatory cytokine, is up-regulated in Crohn's disease: expression and localization in intestinal mucosal cells. J. Immunol. *162*, 6829–6835.

Price, A.E., Shamardani, K., Lugo, K.A., Deguine, J., Roberts, A.W., Lee, B.L., and Barton, G.M. (2018). A Map of Toll-like Receptor Expression in the Intestinal Epithelium Reveals Distinct Spatial, Cell Type-Specific, and Temporal Patterns. Immunity *49*, 560-575.e6.

Rakoff-Nahoum, S., Paglino, J., Eslami-Varzaneh, F., Edberg, S., and Medzhitov, R. (2004). Recognition of commensal microflora by toll-like receptors is required for intestinal homeostasis. Cell *118*, 229–241.

Rauch, I., Deets, K.A., Ji, D.X., von Moltke, J., Tenthorey, J.L., Lee, A.Y., Philip, N.H., Ayres, J.S., Brodsky, I.E., Gronert, K., et al. (2017). NAIP-NLRC4 Inflammasomes Coordinate Intestinal Epithelial Cell Expulsion with Eicosanoid and IL-18 Release via Activation of Caspase-1 and -8. Immunity *46*, 649–659.

Sato, T., Vries, R.G., Snippert, H.J., van de Wetering, M., Barker, N., Stange, D.E., van Es, J.H., Abo, A., Kujala, P., Peters, P.J., et al. (2009). Single Lgr5 stem cells build crypt-villus structures in vitro without a mesenchymal niche. Nature *459*, 262–265.

Schürmann, N., Forrer, P., Casse, O., Li, J., Felmy, B., Burgener, A.-V., Ehrenfeuchter, N., Hardt, W.-D., Recher, M., Hess, C., et al. (2017). Myeloperoxidase targets oxidative host attacks to Salmonella and prevents collateral tissue damage. Nat Microbiol *2*, 16268.

Sellin, M.E., Müller, A.A., Felmy, B., Dolowschiak, T., Diard, M., Tardivel, A., Maslowski, K.M., and Hardt, W.-D. (2014). Epithelium-intrinsic NAIP/NLRC4 inflammasome drives infected enterocyte expulsion to restrict Salmonella replication in the intestinal mucosa. Cell Host Microbe *16*, 237–248.

Sellin, M.E., Maslowski, K.M., Maloy, K.J., and Hardt, W.-D. (2015). Inflammasomes of the intestinal epithelium. Trends Immunol. *36*, 442–450.

Sellin, M.E., Müller, A.A., and Hardt, W.-D. (2018). Consequences of Epithelial Inflammasome Activation by Bacterial Pathogens. J. Mol. Biol. *430*, 193–206.

Spanjaard, B., Hu, B., Mitic, N., Olivares-Chauvet, P., Janjuha, S., Ninov, N., and Junker, J.P. (2018). Simultaneous lineage tracing and cell-type identification using CRISPR-Cas9-induced genetic scars. Nat. Biotechnol. *36*, 469–473.

Stecher, B., and Hardt, W.-D. (2008). The role of microbiota in infectious disease. Trends Microbiol. *16*, 107–114.

Stecher, B., Hapfelmeier, S., Müller, C., Kremer, M., Stallmach, T., and Hardt, W.-D. (2004). Flagella and chemotaxis are required for efficient induction of Salmonella enterica serovar Typhimurium colitis in streptomycin-pretreated mice. Infect. Immun. *72*, 4138–4150.

Stecher, B., Robbiani, R., Walker, A.W., Westendorf, A.M., Barthel, M., Kremer, M., Chaffron, S., Macpherson, A.J., Buer, J., Parkhill, J., et al. (2007). Salmonella enterica serovar typhimurium exploits inflammation to compete with the intestinal microbiota. PLoS Biol. *5*, 2177–2189.

Stecher, B., Chaffron, S., Käppeli, R., Hapfelmeier, S., Freedrich, S., Weber, T.C., Kirundi, J., Suar, M., McCoy, K.D., Mering, C. von, et al. (2010). Like Will to Like: Abundances of Closely Related Species Can Predict Susceptibility to Intestinal Colonization by Pathogenic and Commensal Bacteria. PLOS Pathogens *6*, e1000711.

Sun, J., Ramos, A., Chapman, B., Johnnidis, J.B., Le, L., Ho, Y.-J., Klein, A., Hofmann, O., and Camargo, F.D. (2014). Clonal dynamics of native haematopoiesis. Nature *514*, 322–327.

Sun, Y.-H., Rolán, H.G., and Tsolis, R.M. (2007). Injection of Flagellin into the Host Cell Cytosol by Salmonella enterica Serotype Typhimurium. J. Biol. Chem. *282*, 33897–33901.

Takeuchi, O., and Akira, S. (2010). Pattern Recognition Receptors and Inflammation. Cell *140*, 805–820.

Tay, T.L., Mai, D., Dautzenberg, J., Fernández-Klett, F., Lin, G., Sagar, Datta, M., Drougard, A., Stempfl, T., Ardura-Fabregat, A., et al. (2017). A new fate mapping system reveals context-dependent random or clonal expansion of microglia. Nature Neuroscience *20*, 793–803.

Tenthorey, J.L., Haloupek, N., López-Blanco, J.R., Grob, P., Adamson, E., Hartenian, E., Lind, N.A., Bourgeois, N.M., Chacón, P., Nogales, E., et al. (2017). The structural basis of flagellin detection by NAIP5: A strategy to limit pathogen immune evasion. Science *358*, 888–893.

Vereecke, L., Sze, M., Guire, C.M., Rogiers, B., Chu, Y., Schmidt-Supprian, M., Pasparakis, M., Beyaert, R., and van Loo, G. (2010). Enterocyte-specific A20 deficiency sensitizes to tumor necrosis factor–induced toxicity and experimental colitis. J Exp Med *207*, 1513–1523.

Vereecke, L., Vieira-Silva, S., Billiet, T., van Es, J.H., Mc Guire, C., Slowicka, K., Sze, M., van den Born, M., De Hertogh, G., Clevers, H., et al. (2014). A20 controls intestinal homeostasis through cell-specific activities. Nat Commun *5*, 5103.

Vlantis, K., Wullaert, A., Polykratis, A., Kondylis, V., Dannappel, M., Schwarzer, R., Welz, P., Corona, T., Walczak, H., Weih, F., et al. (2016). NEMO Prevents RIP Kinase 1-Mediated Epithelial Cell Death and Chronic Intestinal Inflammation by NF-κB-Dependent and -Independent Functions. Immunity *44*, 553–567.

Weber, T.S., Dukes, M., Miles, D.C., Glaser, S.P., Naik, S.H., and Duffy, K.R. (2016). Site-specific recombinatorics: in situ cellular barcoding with the Cre Lox system. BMC Systems Biology *10*, 43.

Wotzka, S.Y., Nguyen, B.D., and Hardt, W.-D. (2017). Salmonella Typhimurium Diarrhea Reveals Basic Principles of Enteropathogen Infection and Disease-Promoted DNA Exchange. Cell Host Microbe *21*, 443–454.

Wotzka, S.Y., Kreuzer, M., Maier, L., Arnoldini, M., Nguyen, B.D., Brachmann, A.O., Berthold, D.L., Zünd, M., Hausmann, A., Bakkeren, E., et al. (2019). Escherichia coli limits Salmonella Typhimurium infections after diet shifts and fat-mediated microbiota perturbation in mice. Nature Microbiology *4*, 2164–2174.

Zhang, T., Abel, S., Abel Zur Wiesch, P., Sasabe, J., Davis, B.M., Higgins, D.E., and Waldor, M.K. (2017). Deciphering the landscape of host barriers to Listeria monocytogenes infection. Proc. Natl. Acad. Sci. U.S.A. *114*, 6334–6339.

ACKNOWLEDGEMENTS

The past five years were a (largely) very fun and exciting journey. Many people were part of it - for this, I would like to thank:

*Wolf-Dietrich Hardt letting me be part of the Hardt Lab. Thank you, Wolf, for all of your support and input. It was a great experience to have the freedom to explore and find my own path. At the same time, I always felt supported by you. I really appreciated this combination of freedom and security, which made it possible for me to learn much more than I would have imagined. It was great to learn from your enthusiasm for science (and *Salmonella*) and your approaches to scientific enigmas.

*Mikael Sellin for his extremely valuable support throughout my PhD. I am thankful that you included me in scientific endeavors early on, and it was an incredibly rewarding experience to learn from your systematic approach to experimentation and writing. Besides that, I am deeply grateful for all the time you dedicated to discuss manuscripts, collaborations and experimental difficulties with me while setting up your own group. It was a great and fun experience to work with you. Your enthusiasm and optimism helped me to navigate through challenging passages during this journey.

*Roman Spörri and Kevin Maloy for inspiring hours of discussions and valuable input during the committee meetings. I am especially grateful for the continuous scientific and moral immunological support by Roman Spörri.

*Petra Geiser, Toshihiro Nakamura, Dorothée Berthold, Giverny Ganz and Dejan Malcic, for their hard work, dedication and enthusiasm during their Master projects with me. Similarly, I am grateful to Limay Beron, who worked with me during her apprenticeship in the lab. I truly enjoyed the fun (and less fun) hours in the lab with all of you. Thank you for your impressive experimental and conceptual input to the projects. I am incredibly proud of your developments during your time in the lab and very thankful for everything you taught me during these experiences.

*the current and former Hardt workers. Thanks for providing such a fun, friendly and supportive environment to work in. Having colleagues like you made the last years so much fun. I wouldn`t want to miss any of the fun aperos, barbeques, hikes, SOLA runs, Fondue nights and Höngger games we had. I am especially grateful to Boas Felmy for making my start in the lab so smooth, to Manja Barthel for her continuous support, to Bidong Nguyen for providing entertainment during endless hours in the lab and to Emma Slack for her input and for being a great role model for women in science.

*the members of the Oxenius, Slack and Sallusto groups for fun times in and outside of the lab, and for generously sharing equipment, reagents and experiences.

*the various collaborators who contributed to the work presented in this thesis. Good collaborations can catapult a project forward, which was especially the case for our work with Desirée Böck (Pilhofer lab) and Leo Kunz (Schroeder lab). I am deeply thankful for their dedication, reliability and hard work.

*the staff of the Institute of Microbiology and the EPIC/RCHCI. I highly appreciate the well organized, structured and reliable organization of the institute and the animal facilities. Thank you creating an environment in which it is not necessary to worry about logistics and implementation of science.

*my friends. Thank you for living the beautiful sides of Switzerland and other places in the world with me. Your support was invaluable to relax, recharge and get distracted from work. Thank you for all the fun times and experiences!

*meine Familie. Danke dass ihr immer an mich glaubt. Vielen Dank für das Zuhören und die Ratschläge in schwierigen Zeiten, und für die tollen guten Zeiten, Feiern, Unternehmungen und Spielerunden zusammen!

*Fede. Thanks for being by my side throughout this journey. I am deeply grateful for the reminders to enjoy life outside the lab, for the encouragement, inspiration and the shared experiences. You made this journey truly special.